POLYMER GRAFTING ONTO CELLULOSE

POLYMER GRAFTING ONTO CELLULOSE

By
XIAO WU B. Eng. M. Eng.

A Thesis Submitted to the School of Graduate Studies
in Partial Fulfilment of the Requirements
for the Degree of Doctor of Philosophy

McMaster University

Doctor of Philosophy (2023) McMaster University
(Chemical Engineering) Hamilton, Ontario

TITLE: Polymer Grafting onto Cellulose

AUTHOR: Xiao Wu
B.Eng. (Ocean University of China, China)
M.Eng. (University of Chinese Academy of Sciences, China)

SUPERVISOR: Dr. Robert H. Pelton

NUMBER OF PAGES: ix, 171

Lay Abstract

Canada has extensive forest coverage, accounting for 9% of the global forested land. The abundant tree resource makes the pulp and paper industry vital to the Canadian economy, contributing an annual average of $8.4 billion to the GDP from 2009 to 2019. Canada ranks among the leading global wood pulp exporters, showing an export value of $7.7 billion in 2021. Wood pulp is the raw material for manufacturing paper products such as tissues and printing paper. Although Canada pulps are a premium product, there are opportunities to impart unique properties to market pulps. My thesis focuses on the strategies to modify the surface properties of wood pulp at the end of the pulp manufacturing process. I have investigated the feasibility of modifying the wood pulp fibres by grafting polymers onto their surfaces. Additionally, I have extended the work to include cellulose nanofibres, an emerging new material. The alteration of surface properties expands the potential applications of these fibres across various fields.

Abstract

The proposed work investigates the potential utilization of poly (ethylene-*alt*-maleic anhydride) (PEMA) as linkers for grafting alkane and PEG chains onto cellulosic fibres. Alkyl-amines and PEG-amines were introduced on the PEMA backbone, forming comb polymers. These comb polymers can be grafted onto cellulose with as low as 12-14% anhydride moieties remaining. The investigation is structured into three main sections as follows:

The behaviour of comb polymers in aqueous solutions was investigated. Specifically, PEMAc-alkyl exhibited a pH-induced conformation transition, primarily influenced by the alkyl chain length. In the case of alkyl chains ranging from 6 to 10 carbons, the comb polymers exhibited a hypercoil to expanded coil transition with increasing pH. Notably, comb polymers with pendant decyl (C10) chains formed stable unimolecular nanogels at pH of 7-9, and this behaviour remained insensitive to the degree of substitution (DS) in the range of 25-75%.

PEMAc derivatives were grafted onto bleached softwood pulp fibres through an aqueous impregnation method. High yields (>90%) were achieved when polymer dosages were below 13 g/kg (dry polymer/dry fibre) for PEMAc-alkyl and 38 g/kg for PEMAc-PEG The maximum wet tensile index (WTImax) of the grafted pulp sheets fit in a power-law model represented as $WTI_{max} \sim \beta \Gamma_{ru}^{0.54–0.62}$. However, at high polymer doses, the WTI_{max} values deviated from the model due to the lubricating effect of the ungrafted polymers.

PEMAc and its derivatives were grafted onto cellulose nanofibrils (CNF) using DMAP-catalyzed esterification in acetone. High yields were obtained when the PEMA dosages were below 0.125 g/g (dry polymer/dry CNF). Aggregated structures, consisting of individualized nanofibrils, microribbons, and flocs, were formed in acetone first and then preserved by the grafted polymer. Changes in polymer dosage and DS influenced the floc content. The structure of microribbons was affected by the DS values of PEMA-PEG3 derivatives, with helical structures observed for DS values below 75% and flat structures when DS values exceeded 75%.

Acknowledgments

First and foremost, I would like to express my deepest gratitude to my supervisor, Dr. Robert Pelton, for his invaluable support, guidance, and mentorship throughout my research journey. Working under his guidance has been a privilege and a profound learning experience. His profound insights into interfacial science and adept presentation skills have indelibly impacted my academic pursuits. The knowledge I have acquired under his guidance will undoubtedly shape my future career. His exceptional expertise and unwavering enthusiasm have been a constant source of inspiration, motivating me to achieve my best. I appreciate his kindness and patience in both academic and personal spheres.

I would like to thank my supervisory committee members, Prof. Jose M Moran-Mirabal and Prof. Heather Sheardown, for their insightful feedback and enlightening discussions. Their contributions have significantly enriched my research and provided valuable guidance. I am immensely grateful to our laboratory manager, Mr. Doug Keller, and administrative secretary, Ms. Sally Watson, for their continuous support and assistance during my research.

I would like to thank Dr. Mouhanad Babi and Dr. João Pedro Bronze de Firmino from the Centre for Advanced Light Microscopy (CALM) at McMaster. for their expertise in microscopy imaging, which has been instrumental in advancing my research. Their help and guidance have been truly invaluable.

I would like to thank my summer students who contributed valuable time and effort to this research: Elizabeth Lee, Zhen Hu, Annika Culhane, and Kashaf Amir. Their dedication and hard work have significantly contributed to the progress of my research.

I would like to thank my colleagues: Dr. Emil Gustafsson, Dr. Hongfeng Zhang, Dr. Dong Yang, Dr. Ayodele Fatona, Dr. Gaoyin He, and Abdollah Karami for their technical support and collaborative efforts on my work. I am equally thankful to Prof. Raja Ghosh, Dr. Marcia Reid, Dr. Lina Liu, Dr. Dialia Ritaine, Yue Su, Wenjuan Yang, Abdelrahman Award, Mrunal Ingawale, and Yating Xu for their technical assistance and support during my experiments.

Lastly, I would like to thank my parents for their unending love, encouragement, and support throughout my academic journey. Their love and support are my greatest blessings, and I am truly grateful for everything they have done for me.

Table of Contents

List of Abbreviations and Symbols

AFM	Atomic force microscopy
AKD	Alkyl ketene dimer
ASA	Alkenyl succinic acid anhydride
ATRP	Atom transfer radical polymerization
CLSM	Confocal laser scanning microscopy
CMC	Carboxymethylcellulose
CNC	Cellulose nanocrystal
CNF	Cellulose nanofibril
CSC	Cellulose synthase complex
CTC	Charge-transfer complex
DLS	Dynamic light scattering
DMAP	4-Dimethylamine pyridine
DMF	Dimethylformamide
DP	Degree of polymerization
GGM	Galactoglucomannans
HOMO	Highest occupied molecular orbital
LUMO	Lowest occupied molecular orbital
MCC	Microcrystalline cellulose
MFC	Micro-fibrillated cellulose
NMR	Nuclear magnetic resonance
PAA	Polyacrylic acid
PAE	Polyamideamine-epichlorohydrin
PAH	Poly (allylamine hydrochloride)
PCL	Poly (ε-caprolactone)
PDADMAC	Poly (diallyldimethylammonium chloride)
PDI	Polydispersity index
PDMAEMA	Poly (2-(dimethylamino)ethyl methacrylate)
PEC	Polyelectrolyte complex

PEG	Polyethylene glycol
PEGDA	Polyethylene glycol diacrylate
PEI	Poly (ethylene imine)
PEMA	Poly (ethylene-*alt*-maleic anhydride)
PEMAc	Poly (ethylene-*alt*-maleic acid)
PLA	Poly (lactic acid)
PMA	Poly (maleic anhydride)
POEGMA	Poly (oligoethylene glycol methacrylate)
POMA	Poly (octadecene-alt-maleic anhydride)
PPMA	Poly (propylene-alt-maleic anhydride)
PSMA	Poly (styrene-co-maleic anhydride)
PSS	Poly (sodium 4-styrene sulfonate)
PVA	Poly (vinyl alcohol)
RAFT	Reversible addition–fragmentation chain transfer polymerization
SEM	Scanning electron microscopy
SOMO	Singly occupied molecular orbital
TEA	Triethylamine
TEM	Transmission electron microscopy
TEMPO	2,2,6,6-Tetramethyl-1-piperidinyloxy
TOCNF	TEMPO oxidized cellulose nanofibril
XRD	X-ray diffraction

Chapter 1

Introduction and Objectives

Canada ranks as the world's third-largest forested country, having a substantial 9% share of the global forested area. Plenty of forestry resources contribute a noteworthy$25.2 billion to the nominal GDP. The forestry sector comprises three primary components: in-forest activity, pulp and paper product manufacturing, and wood product manufacturing, constituting 15%, 28%, and 57% of forestry earnings in 2021 respectively.[1] Softwood lumber and softwood pulp are two major forestry products, with over 60% of these products being exported annually. This robust export activity positions Canada as a major global softwood lumber and pulp producer.[2]

Wood is composed of cellulose, lignin, and other polysaccharides, such as hemicellulose. Cellulose, the primary wood component, accounts for roughly 50% of wood's dry weight. Lignin, a class of cross-linked phenolic compounds, presents colours ranging from yellow to dark brown. In wood pulp production, lignin is typically removed as waste through a process known as pulping, which can be categorized into mechanical and chemical methods.[3] Mechanical pulping involves grinding or refining processes conducted at elevated temperatures, but it incurs significantly higher energy consumption than chemical pulping.[4] Wood chips are cooked with either alkaline or sulphite in chemical pulping to soften the wood and extract fibres.

After pulping, washing, screening, and bleaching are performed to obtain clean wood pulp fibres. These fibres typically range from 50-100 μm in width and 1-2 mm in length, varying among tree species. Fibres from softwoods like spruces and pines are long and robust, yielding excellent mechanical properties, while hardwood fibres, although shorter, are more opaque and smoother.[5] Different types of pulp fibres find application in specific products, such as softwood pulp for paper boxes and packages, and hardwood pulp for printing paper and tissues.[6] Chemical additives are employed to modify pulp and paper properties, extending their utility in areas like filtration, clinical diagnosis, and device substrates.[7]

Wood pulp fibres could be split into smaller fibre units called cellulose nanofibrils through a defibrillation step.[8] The cellulose nanofibrils exhibit widths between 1-100 nm and lengths spanning several micrometres.[9] The nanoscale size confers cellulose nanofibrils with a high surface area, robust mechanical properties, and customizable optical attributes, rendering them useful as reinforcements in polymer composites, filters in high-performance separation units, and flexible substrates for biomedical, electronic, and optical devices.[10-12]

Despite the development of products from pulp fibres and cellulose nanofibrils in paper sheets, the inherent hydrophilicity and limited reactive sites of cellulose surfaces constrain their applications relative to synthetic polymers.[13] This limitation prompts surface modification to broaden their potential uses and alter their properties. In some instances, multiple types of molecules are necessary to achieve the desired effect, making surface modification a multifaceted process involving several steps.

This thesis summarizes my efforts to develop a versatile platform for cellulose fibre surface modification. By taking advantage of the plenty of anhydride moieties, PEMA serves as both carriers and anchors to immobilize target molecules on the cellulose surface. This chapter includes a literature review to comprehend the structure of diverse cellulosic materials, grafting chemistry, and comparisons with alternative surface modification methods. It also introduces the hierarchical structure of cellulose, cellulose modification chemistry, maleic copolymers, hydrophobically modified cellulose, and PEG-modified cellulose.

1.1 Hierarchical Structure of Cellulose

1.1.1 Cellulose in Wood

Wood presents a complex hierarchical structure, as depicted in **Figure 1- 1**.[14] The transverse section of a tree reveals growth ring structures representing each year of growth. The cellular tissues, comprising multiple layers of cell walls, serve functions in water transportation, metabolism, and structural support. The cell wall consists of distinct regions: the middle lamella (*M*), the primary cell wall (*P*), and the outer layers (S_1) and the middle (S_2) and inner (S_3) layers of the secondary wall. Lignin skeletons and pectin primarily support the intercellular layers (*M&P*), while the secondary walls consist of cellulose and other polysaccharides like xylan and galactoglucomannans (GGM).[5] Cellulose, a key component in the secondary cell wall, forms bundles and lamellas of elementary fibrils within the amorphous matrix of hemicellulose and lignin.[13]

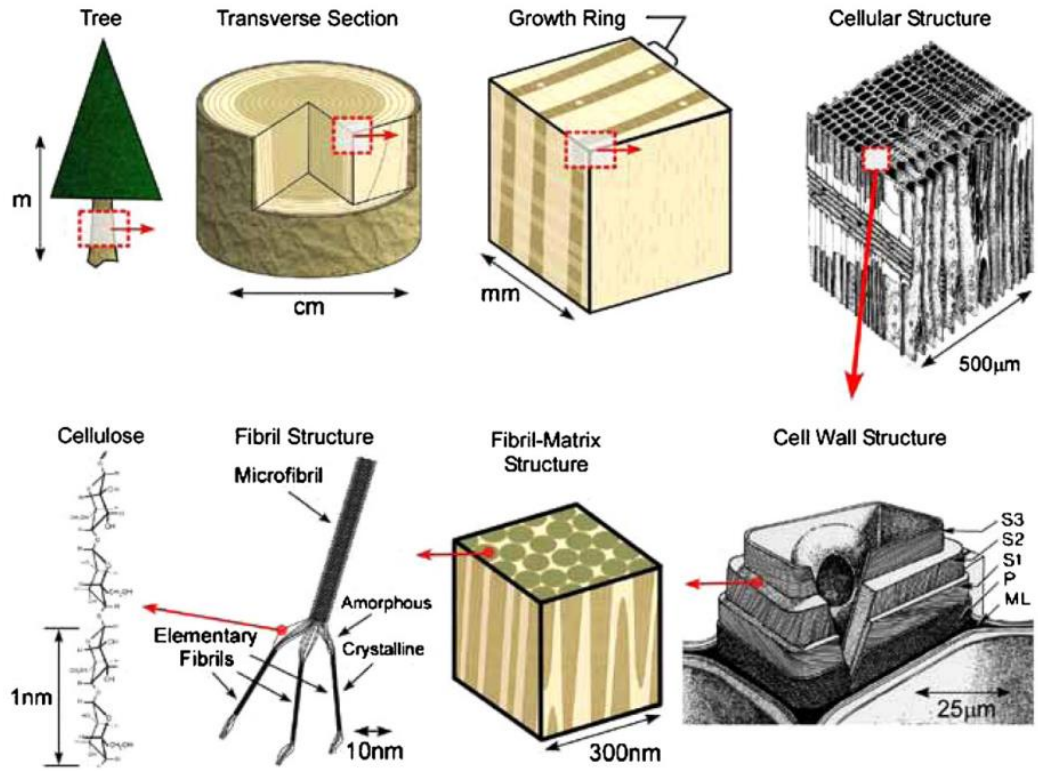

Figure 1- 1 Hierarchical structure of cellulose in wood. Reprinted from Postek et al.[15]

Cellulose is a linear homopolymer of β-D-glucose units at the molecular level, connected by β-1-4 glycosidic bonds. Native cellulose from plants, algae, and bacteria exhibits a degree of polymerization (DP) ranging from 1000 to 30000.[16] Each glucose unit along the cellulose macromolecular chains is rotated 180°, forming a flat ribbon conformation that measures 0.3 nm in width and varies in length from 500-15000 nm, depending on the DP.[17] In nature, cellulose is synthesized by the cellulose synthase complex (CSC) and assembles into elementary fibrils.[18] The biosynthesis of cellulose and cellulose synthase exhibits variation among different species.[19]

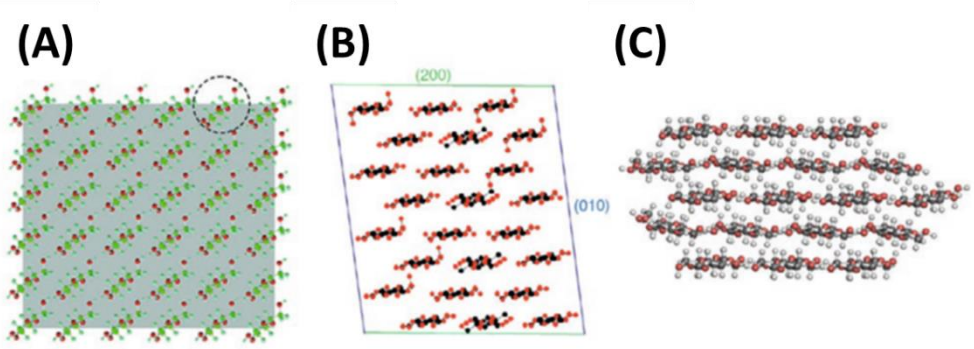

Figure 1-2 (A) 6×6 chain model of cellulose. (B) 6×4 chain model. (C) 18-chain model (in 34443 form). Reprinted from Heise et al.[10]

In high plants like trees, cellulose elementary fibrils are generated by the rosette-shaped CSC module in the plasma membrane of the cell wall. These elementary fibrils consist of multiple cellulose macromolecular chains.[20] However, the exact number of cellulose chains in an elementary fibril is a matter of debate. Initial studies suggested 36 chains (**Figure 1-2**A) based on the structure of the cellulose synthase enzyme. [21, 22] A 24-chain structure was later proposed by Jarvis et al., as shown in **Figure 1-2**B.[23] Other models, like the 18-chain structure proposed by Kubicki et al. (**Figure 1-2**C), have also been suggested.[24] Recent research has indicated that the CSC comprises six groups of 3 enzymatic units. Despite ongoing debates, there is a growing consensus in favor of the 18-cellulose chain model, which is widely applied in molecular dynamic simulations and utilized to explain the effects of chemical modifications on elementary fibrils.[25-27]

1.1.2 Structural Order of Cellulose

Each elementary fibril comprises ordered and disordered domains. The ordered domains, referred to as crystalline regions, give rise to cellulose nanocrystals (CNC). Native cellulose exhibits crystallinity levels measured by X-ray diffraction ranging from 50-80%.[28] Disordered domains, previously assumed to be 25-50 nm long in amorphous states, were later found to be much smaller, measuring only 1-2 nm through neutron scattering testing.[29, 30] This discovery contradicted the old model, aligning with atomic force microscopy (AFM) observations where disordered domains are seen as periodic kinks.

Cellulose crystalline structures are classified as various types of allomorphs, cellulose I, II, III_I, III_{II}, IV_I, and IV_{II}. Thermal and chemical treatments lead to transformations of cellulose into these allomorphs.[31] Native cellulose typically exhibits the crystalline structure of cellulose I, which further has two sub-allomorphs known as I_α and I_β. Cellulose I_α features triclinic unit cells in the crystal structure, while cellulose I_β features monoclinic unit cells.[14] The cellulose I_α is the staple form in primitive species such as

algae, bacteria, and tunicates. Both cellulose I_α and I_β exist in high plants, and the ratio of I_α to I_β is related to the tree species and cell wall types.[32]

Chirality is another intriguing property found in the crystalline domains of cellulose. Twisted structures on cellulose fibrils exist at both the nanoscale and microscale, arising from the chirality of cellulose macromolecules. Each glucose unit has chiral centers for carbons 1 to 5 in the glucopyranose ring, with carbon 6 being the only exception, connecting to the primary alcohol in glucose.[33] Cellulose microfibrils extracted from algae exhibit a periodically twisted right-handed structure.[34] Additionally, free CNC in water exhibit continuous right-handed twists, observed through cryo-TEM and electron diffraction. These CNC display sharp twists alternated with long flat segments after drying.[35] A natural evaporation process induces the self-assembly of CNC, creating nematic liquid crystal films.[36] Within these films, CNC with right-handed chirality assemble into left-handed twisted helices, generating circularly polarized (CP) light. These films exhibit iridescent colors when the wavelength of reflective light falls within the visible spectrum. The reflective light's color can be controlled by adjusting the film's pitch size and refractive index, following Bragg's law.[11]

1.1.3 Cellulosic Fibres from Wood

After the pulping process, the fibril matrix is transformed into hollow cellulose fibres, commonly referred to as pulp fibres (**Figure 1-3**A). The pulp fibres usually are 20-50 μm in width and up to several millimetres in length. The pulp fibres are negatively charged because of carboxylate groups originating from the hemicelluloses such as xylan.[16] These carboxylate groups create binding sites for certain paper-making additives through both physical adsorption and chemical reactions. Electron microscopy investigations of the pulp fibre surface reveal a porous morphology. The structural arrangement of these pores impacts fibre cell wall thickness, influencing water retention ratios, and the flexibility of fibres when immersed in water.[37] The drying of pulp fibres results in the irreversible collapse or shrinkage of these porous morphologies, leading to a phenomenon known as hornification.[38] Hornification causes the closure of the fibre lumen, which is the hollow

void inside the fibres.

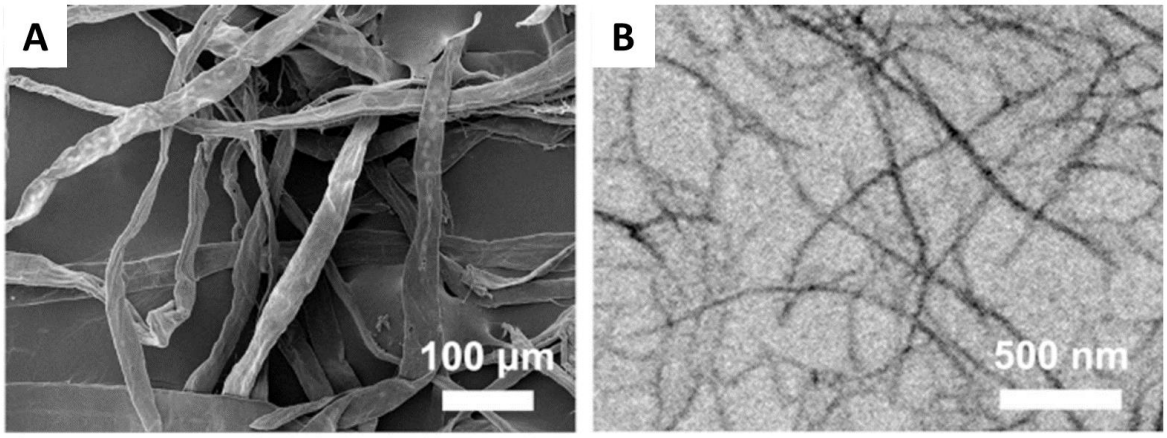

Figure 1-3 (A) SEM image of bleached softwood kraft pulp fibres. Morphology of cellulose fibres examined by SEM. (B) TEM image of CNF after homogenization treatment. Reprinted from Li et al.[39]

The ultrastructure characterization of the wood cell wall reveals that the S2 layer, where most of the cellulose is embedded, consists of helically wound microfibrils.[40] This analogous structure is retained in pulp fibres extracted from the wood cell wall. Mechanical methods are employed to treat pulp fibres, disassembling the bundled microfibrils within the cell walls, thereby generating micro-fibrillated cellulose (MFC).[9] As shown in **Figure 1-3**B, the fibrils in MFC exhibit high aspect ratios, ranging from 5-200 nm in width and 100-225 µm in length. Due to the nanoscale cross-section of MFC, these fibrils are also known as cellulose nanofibrils (CNF).

Various mechanical isolation techniques are employed during the defibrillation process, including refining, microfluidization, grinding, homogenization, cryo crushing, and ultrasonication.[41] Multiple passes are executed to achieve diverse nanofibril content, referred to as the fine grade. However, high energy consumption is a significant limiting factor in MFC production, as the fine grade is directly proportional to energy consumption. Efforts to reduce energy consumption involve pretreatments, such as alkaline-acid hydrolysis, enzymatic treatments, and chemical treatments, performed before the defibrillation step.[42] Hydrolysis in HCl or NaOH solutions at mild temperatures cleaves the linkages within the fibril matrix, solubilizing lignin and hemicelluloses. Enzymatic and chemical treatments partially soften the pulp fibres, effectively lowering energy consumption. In chemical treatments, approaches like 2,2,6,6-tetramethyl-1-piperidinyloxy (TEMPO)-triggered oxidation and carboxymethylation are commonly employed. These methods not only produce small nanofibrils with lengths below one µm and widths below 5 nm but also introduce negatively charged carboxyl groups, ensuring good water dispersibility. Interestingly,

pristine CNF bearing few charges have a strong tendency to agglomerate, forming fibril bundles.[43] The agglomeration is likely associated with hydrogen bonding due to the high surface area and abundance of hydroxyl groups on the CNF surface.

Other types of cellulosic fibres, previously mentioned, include cellulose nanocrystals (CNC). CNC are prepared from cellulose through acid hydrolysis. During this process, all the disordered domains are eliminated, resulting in rod-like crystalline sections with 3-50 nm in diameter and 50-1160 nm in length. CNC possess high crystallinity, exceeding 75%, as detected through wide-angle X-ray scattering (WAXS). The high crystallinity and rigid structure make CNC extensively employed in reinforcement applications, hydrogels, aerogels, and photonic materials.[44]

1.2 Approaches for Cellulose Modification

Although cellulose is the most abundant bioresource and has applications in various fields, its lack of hydrophobicity and versatile physical properties limits its engineering applications. To enhance the value of cellulosic materials and enable the production of high-value-added products, it becomes essential to conduct modifications that endow cellulose with new features and functions. These modification strategies can be categorized into two main approaches: physical and chemical modifications.[42] This section provides a comprehensive overview of both physical and chemical modification methods.

1.2.1 Physical Adsorption

Physical adsorption stands as the simplest surface modification method, often performed in aqueous solutions. This approach involves the binding of positively charged polymers or small molecules to cellulose, facilitated by ionic interactions with the carboxylate groups present on the cellulose surface. The effectiveness of this step is influenced by the charge density of both the polymers and cellulose, as well as the ionic strength of the aqueous solution. Various polyelectrolytes and molecules carrying positive charges, primarily derived from different types of amine groups, are shown in **Figure 1-4**.

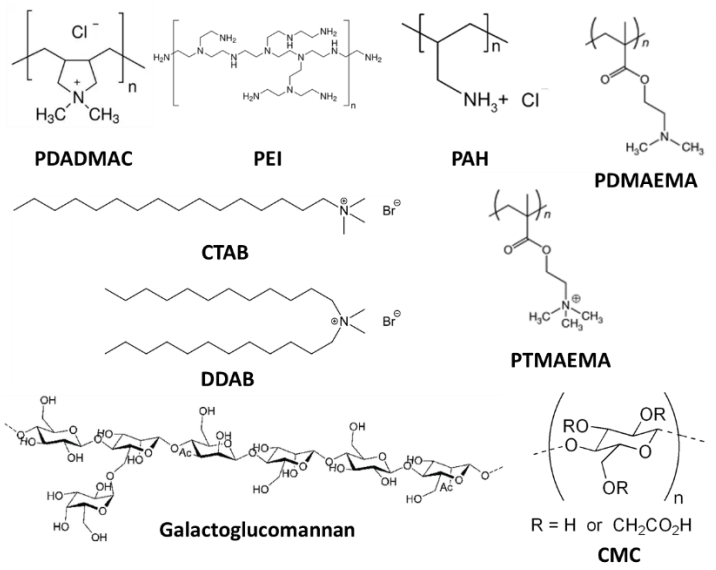

Figure 1-4 Typical molecules and macromolecules can adsorb on cellulose.

It's noteworthy that amines display pH-sensitive charge content, with more amines being positively charged at lower pH. Therefore, the solution pH significantly affects the adsorption isotherm and the conformation of the adsorbed polymers. At lower pH levels, attached polymers exhibit more expanded conformations than those adsorbed at higher pH levels.[45]

The maximum adsorption capacity for polyelectrolytes is constrained by monolayer deposition. However, this limitation can be overcome by employing advanced strategies, such as layer-by-layer adsorption and making complexes. Wagberg et al. introduced the layer-by-layer assembly of polyelectrolytes on both pulp fibre[46] and cellulose nanofibril surfaces.[47] This method involved the adsorption of cationic polyelectrolytes (e.g., poly(diallyldimethylammonium chloride) (PDADMAC), poly(ethylene imine) (PEI), and poly(allylamine hydrochloride) (PAH)) followed by the adsorption of anionic polyelectrolytes (e.g., poly(sodium 4-styrene sulfonate) (PSS)). By repeating these steps, approximately ten polyelectrolyte layers were ultimately deposited onto the cellulose nanofibril surface. The thickness of this polyelectrolyte multilayer could be controlled by adjusting the ionic strength of the water.[48]

Polyelectrolyte complexes (PEC), formed by mixing cationic and anionic polyelectrolytes, provide colloidal stable systems for modifying cellulose surfaces. Balancing the charges yields positively charged complexes that can be adsorbed onto pulp fibres as additives to enhance paper dry and wet strength. For example, complexes formed by mixing cationic polyamide-amine epichlorohydrin (PAE) with anionic carboxymethylcellulose (CMC) proved effective as additives for paper products.[49-51] The

addition of these complexes resulted in even greater enhancement of paper dry tensile strength than achieved through mechanical beating alone. Additionally, PECs can also be adsorbed onto CNF surfaces for surface modifications. Galvan et al. developed complexes by mixing anionic xylan or polyacrylic acid (PAA) with cationic PAH or chitosan.[52] All types of PEC were used to functionalize cellulose nanofibrils or lignocellulose nanofibrils.[53] The modified nanofibrils as additives in paper-making significantly improve the mechanical properties of paper sheets.[54]

In addition to electrostatic attraction, non-ionic polymers can be adsorbed onto cellulose surfaces through van der Waals interactions, hydrogen bonds, or specific affinities to cellulose. Lindström et al. described a method for adsorbing carboxymethylcellulose (CMC) onto pulp fibres with the aid of calcium ions and mild heat.[55] Polyethylene glycol (PEG)-derivatized CMC (CMC-g-PEG) exhibited abilities similar to the original CMC, and it was adsorbed onto CNF films at pH 4.5. The grafted films swelled at pH 7.5, and the grafted CMC-g-PEG reduced inter-fibril friction, resulting in good compatibility in composites.[56] Polysaccharides like xyloglucans and galactoglucomanans (GGM) could also be adsorbed onto cellulose.[57] Specifically, synthesized amphiphilic GGM exhibited a strong affinity for CNF derived from hardwood pulp fibres, with attachment being irreversible.[58] The robust association is possibly related to the mannan-mannan interactions since hardwood contains more hemicelluloses than softwood.

1.2.2 Oxidation

At the molecular level, oxidation of cellulose introduces charges and reactive sites, broadening its potential applications. Among the most widely used methods, TEMPO (2,2,6,6-tetramethylpiperidine-1-oxyl) oxidation and periodate oxidation are most used. In TEMPO oxidation (**Figure 1-5**A), the key reagents include TEMPO, NaClO, and NaBr. Sodium hypochlorite converts TEMPO into a nitrosonium cation, which effectively oxidizes the alcohol at C6 to form a carboxyl group. The reoxidation of the nitrosonium cation is achieved by reduced hydroxylamine, with NaBr and NaClO triggering the regenerative process. This catalytic cycle leads to the continuous generation of carboxyl groups on the cellulose structure.[59] Notably, enzymes like laccase can also serve as co-oxidants in conjunction with TEMPO, resulting in a modified oxidation that introduces more aldehyde groups than carboxyl groups.[60, 61]

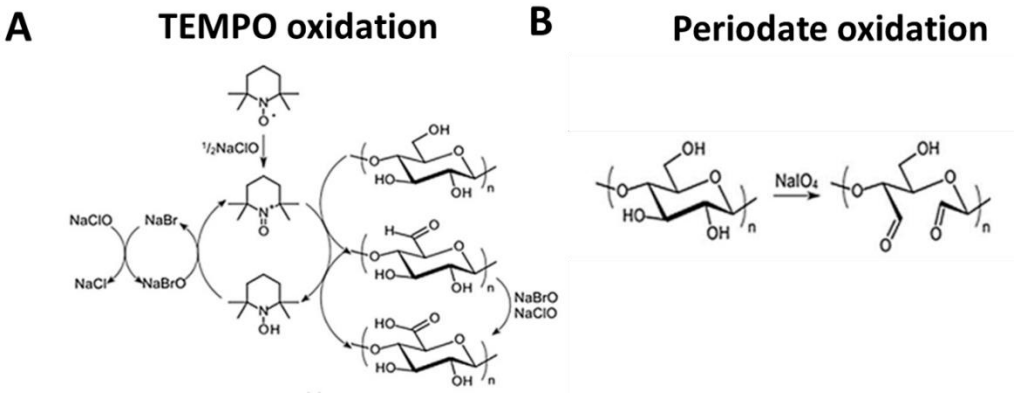

Figure 1-5 Different mechanisms of cellulose oxidation. (A) TEMPO oxidation. (B) Periodateoxidation.

Metaperiodate salts represent another effective oxidant that induces regioselective oxidation of hydroxyl groups at C2 and C3 of the glucose units (**Figure 1-5**B). This oxidation cleaves the C-C bond between C2 and C3, yielding two aldehyde groups. These aldehyde groups offer higher reactivity compared to hydroxyl and carboxyl groups, facilitating reactions with primary amines to form Schiff bases, or with alcohols to form hemiacetals and acetals. It introduces additional reactive sites for further cellulose modification. Furthermore, the generated aldehydes can be reduced to hydroxyl groups using $NaBH_4$ or oxidized into carboxyl groups using $NaClO_2$.[62, 63] Larsson et al. employed periodate oxidation as the pretreatment in producing CNF. The oxidized CNF were then reduced by $NaBH_4$ and processed through microfluidization to defibrillate the fibres. The oxidations led to glucopyranose ring opening, resulting in a significant reduction in cellulose crystallinity. Interestingly, the single nanofibril structure displayed a core-shell configuration, where a dense fibril core was enveloped by an amorphous alcohol shell. This unique fibril structure was found to contribute to the plasticity and mechanical properties of the CNF.[64] Liimatainen et al. developed dicarboxylic acid cellulose (DCC) by applying $NaClO_2$ after the periodate oxidation.[65]

1.2.3 Small Molecules Grafting

The grafting of molecules onto cellulose via chemical reactions primarily targets the hydroxyl groups in anhydroglucose units. **Figure 1-6** illustrates typical reactions that result in linkages with these hydroxyl groups, with the most common types being ester, ether, and urethane bonds.

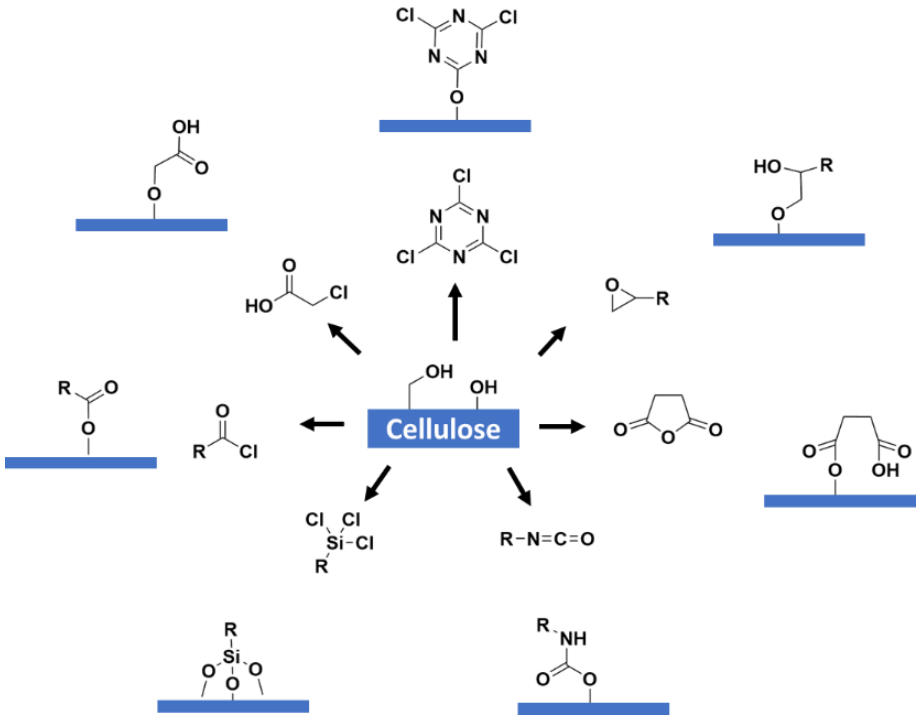

Figure 1-6 Chemistries for forming linkages with hydroxyl groups on cellulose.

Early on, chlorine-involved reactions found application in the textile industry for treating cotton fibres. Triazine molecules, owing to their three reactive arms, exhibit versatile capabilities in functionalizing cellulose surfaces. This feature allows for efficient derivatization, enhancing their conjugation with cellulose for surface modification. Chlorine-involved etherification and acetylation, using chlorine as a leaving group, are effective reactions for connecting hydroxyl groups. A well-known example is the carboxymethylation of cellulose, a process that introduces negative charges onto the cellulose surface.[48] In this reaction, cellulose fibres are first solvent-exchanged into alcohol, followed by the addition of monochloroacetic acid and NaOH. Monochloroacetic acid substitutes all hydroxyl groups in anhydroglucose units with the assistance of NaOH. However, many chlorine-involved reactions have limitations related to solvents.[66, 67] The reactions show high efficiency in organic solvents, but their yields decrease significantly when performed in water due to the quick hydrolysis of chlorine moieties, generating hydrochloric acid. Moreover, chlorine-containing chemicals can have harmful environmental impacts, leading to restrictions in certain industrial areas.

Esterification through acid or anhydride reactions produces less harmful byproducts, with water being the primary byproduct. However, the generated water can slow down the reaction and hydrolyze anhydrides. A similar solvent-exchange step is usually implemented in the initial stages to achieve high reaction yields, analogous to chlorine-

based reactions.[68] Direct esterification between acids and alcohols typically requires high energy input, such as extended heating or ultrasonication.[69, 70] In comparison, some multifunctional carboxylic acids, termed polycarboxylic acids, react with alcohols at much lower temperatures. Yang et al. have found that polycarboxylic acids, shown in **Figure 1-7**, can cross-link cotton cellulose at moderately high temperatures (110 °C).[71] Sodium hypophosphite (NaH_2PO_2) or monobasic sodium phosphate (NaH_2PO_4) are catalysts to provide the cured cotton fibres with high mechanical strength.[72] The reaction mechanism, as interpreted by infrared spectroscopy, involves the formation of five-membered or six-membered cyclic anhydride intermediates under the curing conditions, followed by a reaction with the hydroxyl groups on the cotton fibres.[73-75]

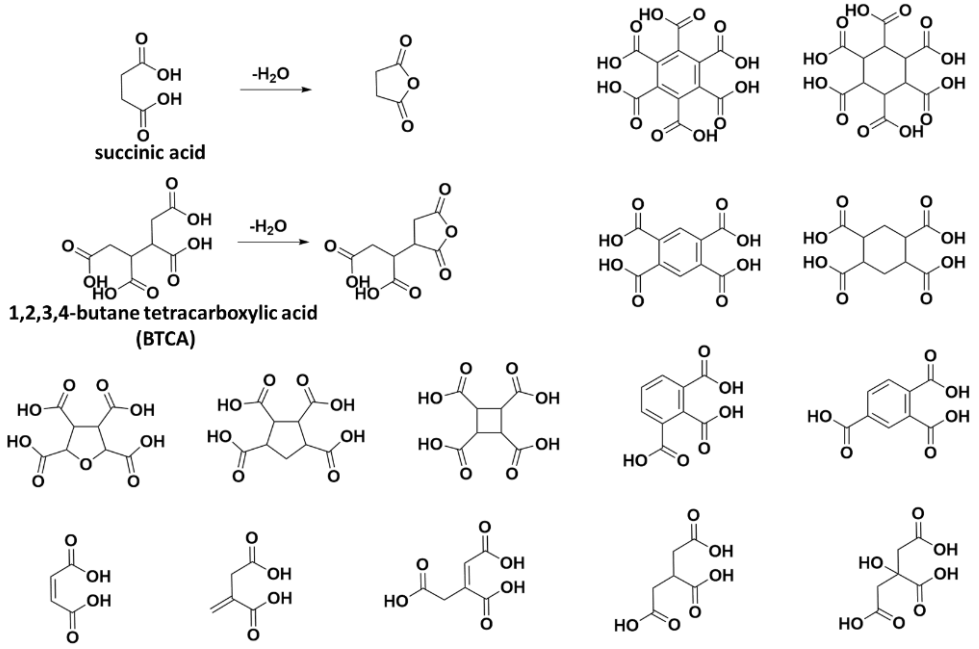

Figure 1-7 Polycarboxylic acids crosslinking cotton fibres.

Other reactive moieties such as epoxy,[76] isocyanate,[77] and silane[78] are also employed for cellulose modification. However, these moieties also face solvent challenges, as they are sensitive to water. As green chemistry gains attention, there is a growing trend toward replacing chemicals that are incompatible with aqueous solutions.

1.2.4 Polymer Grafting

Polymer grafting on cellulose offers several advantages over molecule grafting, as it allows for the incorporation of multiple functions within one single macromolecule. This approach significantly alters the physical properties of cellulose, making it suitable for various purposes. The polymer grafting majorly happens on the cellulose surface, which differs from the molecule grafting. As shown in **Figure 1-8**, the approaches to achieving

polymer grafting on cellulose could be classified into three categories: (I) "grafting-to," (II) "grafting-from," and (III) "grafting-through."[79]

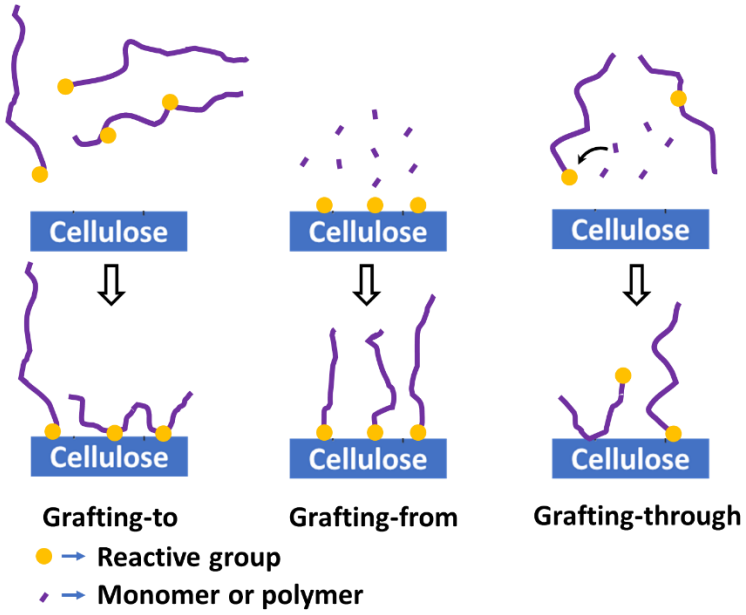

Figure 1-8 Schematic graphs showing different types of polymers grafting on cellulose.

The "grafting-to" approach involves attaching polymers to the cellulose surface through anchor groups. Covalent bonds are commonly used as anchors due to their stability in various environments. Anchor groups on the polymer chains can be monofunctional or multifunctional.[80] Monofunctional polymers are designed with a single anchor group at one end of the polymer chain, resulting in brush-like polymer chains on the cellulose surface.[81] However, monofunctional polymers have limited reactivity since grafting relies on a single reactive site.

Additionally, the crowding effect from attached polymer chains can hinder accessibility and reduce grafting density.[82] If multiple anchor groups from one chain react with cellulose, inter-cellulose cross-linking occurs during grafting. Hence, the anchoring reactions must be delicately controlled for the multifunctional polymer grafting on cellulose to suppress the cross-linking. One of the critical advantages of multifunctional polymer grafting is that it works efficiently for the direct elaboration of composites comprising cellulose.[83] Polymeric matrices such as polyurethane, epoxy resin, and polycaprolactone reinforced with nanocellulose could be rapidly fabricated through a "grafting-to" based cross-linking reaction.[84]

The "grafting-from" approach propagates polymer chains from the cellulose backbone, typically involving free radical polymerization. Free radical sites are initiated on the

cellulose backbone, often derived from hydroxyl groups. Monomers then link to these free radical sites, leading to the growth of brush-like polymer chains attached firmly to the cellulose surface.[79] Compared with the "grafting-to," the approach could provide higher grafting density that imparts distinct characteristics to the pristine cellulose. The free radical could be generated using persulfate salts, Fenton's reagents (Fe^{2+}+H_2O_2 system), and Ce (IV) ions.[85] However, the free radical polymerizations generally show low grafting yields due to significant interference from homopolymerization reactions.[86]

In contrast, living radical polymerizations, such as atom transfer radical polymerization (ATRP) and reversible addition–fragmentation chain transfer polymerization (RAFT), provide polymers of controlled molecular weight, polydispersity index (PDI), and composition. The mechanism of the living radical polymerizations is keeping partial radicals in "dormant" form. So, the chain termination is suppressed due to low concentrations of active radicals.[79] By taking advantage of living radical polymerizations, efficient grafting of poly(styrene) and acrylic polymers onto cellulose surfaces has been achieved. For instance, poly(butyl acrylate),[87] polymethyl acrylate (PMA),[88] and poly (glycidyl methacrylate) (PGMA)[89] was successfully attached to cellulose surface through the ATRP method. In contrast, poly (styrene)[90] and poly (dimethylamine ethyl methacrylate) (PDMAEMA)[91] were linked to cellulose via RAFT way. Well-defined polymers are introduced onto cellulose surfaces if the chain transfer agents and feed are selected tactfully.

The "grafting-through" approach is typically a copolymerization involving cellulose-based monomers. Cellulose is initially functionalized with a polymerizable group like vinyl and acrylic.[79] They employ the monomers in copolymerization with other monomers, resulting in cellulose-embedded copolymers. While this approach offers versatility, it is less commonly used for cellulose functionalization due to its more complex steps.

1.3 Maleic Anhydride Copolymers

Maleic anhydride copolymers are a series of copolymers obtained from the copolymerization of maleic anhydride and other olefinic monomers. These copolymers incorporate functional groups from the olefinic monomers[92] and can also undergo chemical reactions on the succinic moieties along the polymer chains, leading to maleic copolymer derivatives with multiple functional groups. Additionally, the reversible transformation between succinic anhydride and succinic acid,[93] triggered by introducing or removing water, adds to the versatility of these copolymers.

1.3.1 Synthesis of Maleic Anhydride Copolymer

The homopolymerization of maleic anhydride usually is difficult unless under high energy input, and the obtained poly (maleic anhydride) (PMA) has a low molecular

weight and broad molecular distribution.[94] Instead, the synthesis of maleic anhydride copolymers typically involves the copolymerization of maleic anhydride with various olefinic and acrylic monomers. The copolymerization process is facilitated by initiated free radicals. A wide range of monomers can be used, including ethylene, styrene, octadecene, butadiene, vinylpyrrolidone, methyl vinyl ether, and acrylic acid.[92]

The copolymerization tends to result in alternating copolymers, and several factors contribute to this alternated structure. The first is the tendency to form a charge-transfer complex (CTC) between electron-poor maleic anhydrides and electron-rich comonomers. Once the CTCs participate in the chain propagation, alternating copolymers are obtained. However, the CTC-based mechanism can not explain the fast kinetics of copolymerizations since CTC concentration in the systems is low due to the fast lifetime of CTCs.[95, 96]

Additionally, the molecular orbitals of free radicals derived from maleic anhydride play a crucial role. The free radical generated from maleic anhydride has an unpaired electron adjacent to the cyclic anhydride ring, which has a partially occupied p-orbital. The model leads to low energy in SOMO (singly occupied molecular orbital). Therefore, the HOMO (highest occupied molecular orbital) of the olefinic monomers becomes a crucial factor influencing the reaction.[92] In the example of copolymerization of styrene and maleic anhydride, the styrene monomers possess high-energy HOMO, facilitating the linkage formation with the SOMO of maleic anhydride radicals. Besides, the free radicals derived from styrene also have SOMO with high energy, linking with the LUMO of maleic anhydride monomers. In conclusion, the maleic anhydride and styrene tend to form alternating copolymers because of the orbital structure.

The steric hindrance is another factor impacting the monomer structure along the polymer chains. The steric hindrance influences the copolymerization rate and the configuration of anhydride moieties.[97] The effect of steric hindrance on copolymerization rate was observed when polymerizing maleic anhydride with isobutene, ethyl acrylate, and pentene.[98, 99] Furthermore, the steric hindrance also makes the anhydride configuration in the *trans*(threo) form (**Figure 1-9**A) rather than the *cis*(erythro) form (**Figure 1-9**B) since the threo forms are less sterically hindered. For instance, Komber measured the content of erythro and threo configuration in poly (ethylene-*alt*-maleic anhydride) (PEMA), giving 12% and 88% for the polymer synthesized at 60 ^{o}C and 14% and 86% for the poly (ethylene-*alt*-maleic acid) (PEMAc) after hydrolysis in water.[100]

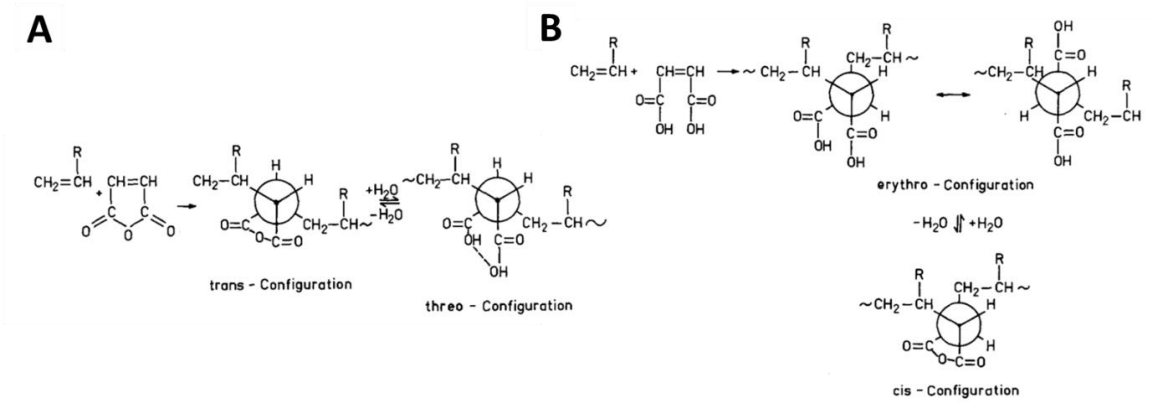

Figure 1-9 *Trans*(threo) (A) and *cis*(erythro) (B) of acid and anhydride form shown using the Newman projection. Reprinted from Rätzsch.[92]

The configuration, nevertheless, is affected by the synthetic route. Rätzsch et al. synthesized PEMAc through the copolymerization of maleic acid with half ester and ethylene and followed by cleavage of ester bonds, generating the same polymer structure as PEMAc. The ^{13}C-NMR spectra suggested a different result, in which 38% threo and 62% erythro were found.[101] The pKa values of diacids after hydrolysis and the reactivity of the succinic moieties are determined by different configurations. For example, two pairs of pKa values (4.1, 6.1 and 4.2, 6.8) for the diacids are detected from PEMAc arising from the erythro and threo forms, respectively.[100] The erythro form has a higher ring strain than the threo form. The erythro form is more reactive for ring-opening reactions with nucleophiles, while the threo form is easier to reform the cyclic anhydride rings.[102]

1.3.2 Derivatization of Maleic Anhydride Copolymers

Figure 1-10 illustrates three typical routes to functionalize maleic anhydride copolymers. The derivatizations commonly take advantage of the nucleophilic attack from nucleophiles such as alcohols, amines, and thiols on the anhydride moieties, which generates linkages like ester, amide, and thioester bonds.[103]

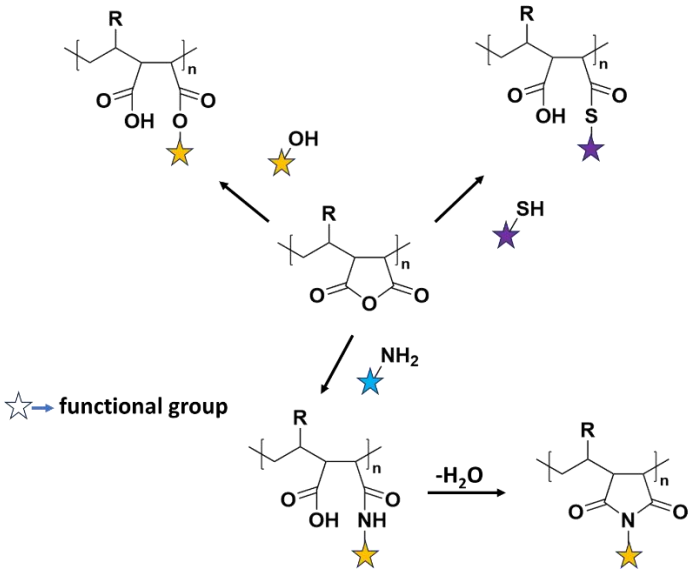

Figure 1-10 Derivatization ways of maleic anhydride copolymer.

The steric hindrance of the comonomers can impact the derivatization of anhydride moieties. During nucleophilic attack, both carbonyl groups of the anhydride can be involved in linkage formation, either on the carbonyl adjacent to the R group or on the one farther from the R group. Rätzsch et al. conclude that the ester bond linkages preferentially form from the carbonyl group far from the R group.[92] They tested the reactions of methanol with propylene/maleic anhydride (PPMA) copolymers and styrene/maleic anhydride (PSMA). The ^{13}C-NMR showed that 40% of ester bonds are formed adjacent to the methyl group in PPMA, while only 20% of ester bonds are formed adjacent to the phenyl group in PSMA.[104] Thus, the steric hindrance affects PEMA less because of the lack of pendant groups in the comonomers.

Primary amines are particularly effective nucleophiles, triggering rapid amidation of maleic moieties. The resulting amide bonds are stable, making them a popular choice for derivatizing maleic copolymers. Werner et al. developed a versatile platform using maleic copolymers to immobilize biomolecules. Copolymers, such as poly (octadecene-*alt*-maleic anhydride) (POMA),[105, 106] poly (propylene-*alt*-maleic anhydride) (PPMA),[107] poly (styrene-*alt*-maleic anhydride) (PSMA),[108] and poly (ethylene-*alt*-maleic anhydride) (PEMA),[109] are coated on the substrates and functionalized with amine molecules to modify surface properties and control cell adhesion. The primary amine-induced amidation is generally performed without adding any catalyst, thanks to the high pKa values of primary amines. Interestingly, the addition of fundamental catalysts like triethylamine (TEA) was found to reduce the derivatization yields for aliphatic amines, as reported by Hue et al.[110]

1.3.3 Properties of Derivatized Maleic Anhydride Copolymer

The introduction of Poly (ethylene glycol)s (PEGs) onto maleic copolymers, where comonomers include ethylene, styrene, and methyl vinyl ether, results in the creation of comb-like copolymers with pendant PEG chains. These PEG chains, acting as spacing agents, have the effect of lowering the glass transition temperature (T_g) of the copolymers. Besides, the PEG-modified poly (styrene-*alt*-maleic acid) displays thermal and pH-triggered phase transition in water.[111] Due to the complex formation between PEG and lithium salts, the modified copolymers are utilized as solid polymer electrolytes for lithium batteries.[112, 113] Additionally, these modified copolymers are employed in applications related to thermal energy storage, benefiting from their solid-solid phase transition behavior.[114]

Pendant alkyl groups on maleic copolymers induce a conformational transition in water, giving rise to a comb-like structure. In high-pH environments, the polymer chains take on a expanded coil conformation. In contrast, they form compact hypercoil under low pH conditions, attributed to the restricted movement of hydrophobic domains.[115] It is discovered that conformation transition occurs when the pendant alkyls are either directly linked with the polymer backbone or modified through anhydride groups.[116-118] The conformational transition has been confirmed through various techniques, including dynamic light scattering (DLS), pyrene fluorescent spectra, changes in viscosity, and potentiometric titration.[116, 119] The hypercoil conformation at low pH is facilitated by intramolecular interactions from the hydrophobic domains. At high pH, the copolymers tend to form unimolecular globules, stabilized by electrostatic repulsion resulting from the negatively charged carboxyl groups. The carbon number on the alkyl chain is another factor influencing the polymer conformation. For example, Poly (methyl vinyl ether-*co*-maleic acid) and poly(ethyl vinyl ether-*co*-maleic acid) containing one and two carbons on the alkyl don't display any hypercoil conformation even at low pH.[117, 120] Copolymers with alkyl chain lengths over ten carbons incline to maintain as globules under a wide pH range.[121] Copolymers with intermediate chain lengths exhibit a transition from hypercoil to expanded coil structure as the pH increases.[122]

1.3.4 PEMAc Grafted Wood Pulp

Owing to the reversible transformation between diacid and anhydride forms, PEMAc was demonstrated as an efficient grafting agent introducing carboxylate groups on pulp fibres by Zhang et al. PEMAc was selected from various maleic acid copolymers as it gave the highest charge density on the pulp fibres.[123] The grafting process is given in **Figure 1-11**. The polymer is obtained in anhydride form. The hydrolysis in water converts the polymers into diacid form giving PEMAc solutions. The polymer solutions are directly applied to the pulp fibres as sheets in an impregnation way. After curing the pulp sheets at

an elevated temperature (>100 °C), the PEMAc is fixed on the fibre surface via covalent bond linkages.

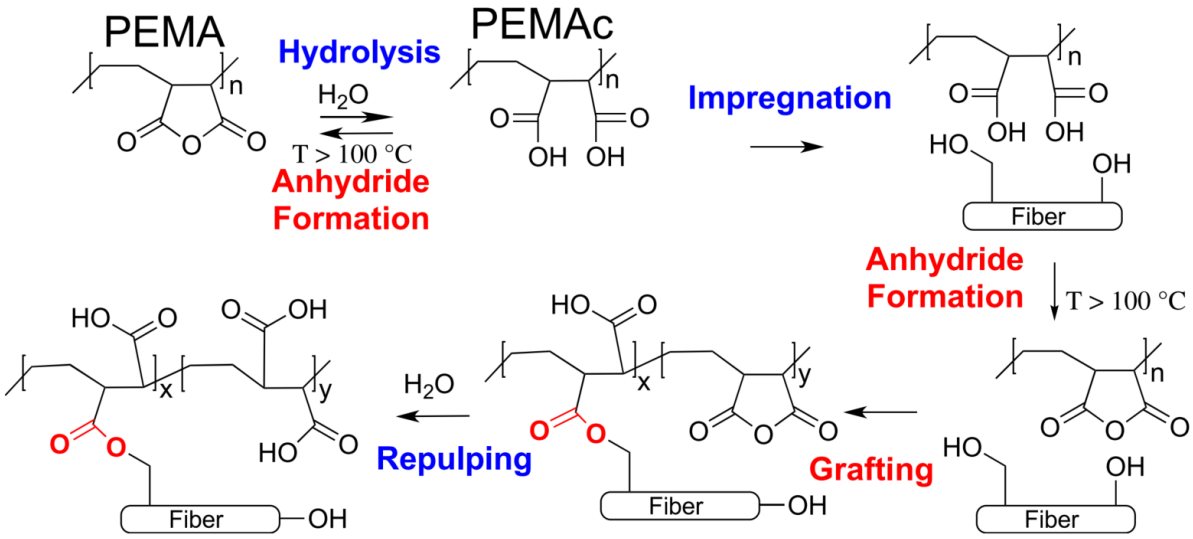

Figure 1-11 Illustration graph showing steps for PEMAc grafting on pulp fibres. Reprinted from Zhang et al.[124]

The pH of the polymer solutions and the curing temperature are critical factors in controlling the grafting yield and the wet strength of the cured pulp sheet. Chemical fixation manifests when the pH becomes low and neglectable at a pH above 8. It is indicated that the reformation of cyclic anhydrides needs at least one of the carboxyl groups to be protonated within the succinic unit.[124] The polymer solutions at pH four are selected as the ideal agent for pulp treatment since they always provide high grafting yields. The increased curing temperature dramatically improves the wet strength of pulp sheets if the impregnation is done with a pH 4 solution, which in turn makes the pulp sheets difficult to be disintegrated in water. Unlike the modification on the paper sheets, the modified pulp sheets must have good repulpability (re-dispersible in water) since the dry pulp sheets as feedstock in the paper-making process produce a homogeneous slurry generating even paper sheets.

To address the issue of repulping, a power-law model was designed to implement the grafting technique for industrial processes.[125] In the model, the wet tensile indices of the treated pulp sheets obey a power-law relationship with $\beta\Gamma$, where β is the conversion from diacid to anhydride form and Γ (meq/g) is the amount of PEMAc applied on pulp sheets. The power-law correlation enables the estimation of optimal curing conditions that provide high grafting yields and good repulpability. PEMAc grafted bleached and unbleached softwood pulps exhibit thermosetting properties due to the thermal-activated

anhydride reformation.[126] Moreover, reformed anhydride moieties offer reactive sites for further modifications, such as linking with alcohols and amines.

1.4 Hydrophobically Modified Cellulose

One of the potential applications for cellulose is used as packaging material. In contrast to conventional hydrophobic synthetic polymers such as polyethylene and polypropylene, which have low water and vapor permeability. Cellulosic materials inherently exhibit hydrophilicity due to abundant hydroxyl groups on their surfaces.[13, 16] The hydrophobicity of cellulose significantly impacts the substitution of synthetic polymers with cellulosic materials. When employing nanocelluloses as reinforcements, the compatibility with nonpolar polymeric matrices greatly influences composite mechanical properties.[14, 127] To enhance compatibility and prevent phase separation, essential hydrophobic modification is performed prior to mixing. Thus, rendering cellulosic materials hydrophobic becomes a critical objective for surface modification.[128] It is recognized that two primary strategies are employed to alter surface hydrophobicity: grafting nonpolar components onto the cellulose surface and morphology design involving the creation of micro- or nano-asperities. Chemical modification is the predominant way to increase cellulose surface hydrophobicity for cellulose fibres.

1.4.1 Paper Sizing

Paper-making process has always involved the essential task of imparting hydrophobic characteristics to the paper. The water-repelling properties are usually achieved by sizing operation at the wet-end stage of paper-making, aiming to minimize water adsorption.[129] This is done to fulfill various objectives, such as preventing ink smudging or deeply penetrating and maintaining the mechanical strength of cardboard under humid conditions. The most widely used paper-sizing chemicals include alkyl ketene dimer (AKD) and alkenyl succinic acid anhydride (ASA),[13] which are applied in emulsions to the fibre suspension or through the vapor phase.

AKD, with its four-membered lactone ring, reacts with the hydroxyl groups on cellulose, leading to covalent bonds that immobilize AKD on the cellulose surface and outwardly orientate the alkyl chains.[130, 131] The molecular level reactions make the grafting reaction efficient and confer paper with good resistance to both acid and alkaline penetrants, as well as some AKD-soluble organic solvents like tetrahydrofuran and chloroform. Similarly, ASA is anchored on the paper surface via esterification between the five-membered succinic anhydride and the hydroxyl groups. ASA, being water-insoluble, is typically formulated into emulsions. The emulsification involves mixing ASA in cationic starch using high-shear equipment. However, the emulsions are susceptible to hydrolysis, compromising the anhydride groups and leading to poor binding with paper.[132] Therefore, the ASA emulsions must be used within a short period to minimize hydrolysis.

1.4.2 Hydrophobically Modified Nanocellulose

Hydrophobic modification is also conducted on nanocellulose materials such as CNF and CNC. Following the hydrophobic modifications, nanocelluloses become compatible with synthetic polymers like polyethylene, polypropylene, polystyrene, polylactide, epoxy resin, and polyurethane.[127] As a result, they are employed as reinforcements in composite materials fabrication by taking advantage of their good compatibility, high surface area, and high aspect ratio. The long alkyl chains on the surface create physical entanglements with synthetic polymer chains, effectively strengthening the cellulose and polymeric matrix interface.

A simple method to increase surface hydrophobicity is to adsorb cationic surfactants onto the anionic CNF or CNC. Salajková et al.[133] and Yin et al.[134] demonstrated that quaternary ammonium salts bearing various hydrophobic groups (stearyl, benzyl, and diallyl) can attach to CNC surface. The amphiphilic salts were adsorbed onto the CNC surface under stirring, and excessive salts were removed by dialysis. After drying, the salts were firmly attached to the CNC, enhancing the contact angle of CNC films and providing good dispersibility in organic solvent, e.g., toluene. Shimizu et al. used quarternary ammonium salts to modify the TEMPO-oxidized CNF (TOCNF) films, increasing the contact angle to 100º.[135] Utsel et al. designed cationic amphiphilic block copolymers consisting of cationic poly (2-(dimethylamino)ethyl methacrylate) (PDMAEMA) with quaternary amines and hydrophobic blocks such as polystyrene[136] and poly (ε-caprolactone) (PCL).[137] The cationic block copolymers formed micelles in water, which were adsorbed and dried on the CNF surface. The copolymers, acting as compatibilizers, can be applied in aqueous solutions to enhance the hydrophobicity of CNF.

Chemical modifications generate strong covalent bonds connecting hydrophobic groups, ensuring resistance to a wide range of ionic strength and various solvents. Sizing agents like ASA have been modified on CNF surfaces to use them as reinforcements in polypropylene (PP) composites.[138] Li et al. developed a technique using 10-undecanoyl chloride to treat the CNF.[139] The hydrophobically modified CNF were applied as packaging materials, displaying low vapour permeability, high moisture resistance, and good mechanical properties. Additionally, hydrophobic polymers can be grafted onto nanocellulose surfaces. The two most widely used approaches are conducting the polymerization from the cellulose surface and directly mixing the reactive monomers with cellulose. PDMAEMA was grafted on CNF and CNC surfaces through a surface-initiated atom-transfer radical polymerization (ATRP).[140] The modified nanocellulose films showed high water contact angles (>130º). Alkyl bromides (C10-C18) were reacted on tertiary amines generating quaternary amines, which offered antibacterial properties to nano papers.[141] The direct mixing approach is a rapid way of preparing nanocellulose-involved composites. For instance, Auad et al. described an approach by directly mixing

the polyurethane with CNC in dimethylformamide (DMF), and the composites were fabricated through solvent casting.[142] Abushammala et al. produced CNC-reinforced polyurethane by reacting the CNC with alcohols and followed by reactions with 2, 4-toluene diisocyanate (TDI).[143] The CNF and CNC were also directly added into the extruder and embedded into polymer matrices such as polyethylene (PE), polypropylene (PP), poly (lactic acid) (PLA), poly (vinyl alcohol) (PVA), and polycaprolactone (PCL). However, the unavoidable agglomeration gave poor fibre distribution in polymeric matrices.[144]

1.5 PEG-modified Cellulose

Polyethylene glycol (PEG) is a linear polymer known for its excellent water solubility. It finds widespread applications in pharmaceutical and industrial fields as lubricants, dispersants, solvents, and surfactants. The oxygen in the ethylene glycol unit is an accepter for hydrogen bonding, resulting in strong hydrogen bonding and high-water binding capacity. The long PEG chains also introduce steric hindrance, preventing inter-fibril bonding. PEG ultimately find applications when incorporated with cellulosic materials, for example, in the production of paper-based devices and tuning interactions in nanocelluloses.

1.5.1 PEG Modified Paper

Paper-based analytical devices present promising solutions for point-of-care assays in biomedical diagnosis due to their advantages, including low cost, rapid responses, and eco-friendliness.[7] PEG-modified papers serve as suitable substrates compatible with various biomedical analytical techniques. Jeevarathinam et al. impregnated the paper with the PEG and infused the cationic dyes to fabricate a test paper sensitive to the negatively charged heparin.[145] PEG were used to balance the attraction between the dye and heparin. In the grafting process on paper substrates, PEG mostly act as inert spacers, allowing the introduction of ligands like various peptides and proteins. The support PEG layers provide the ligands with sufficient accessibility to the binders and have little disruption on the protein conformation.[146] In addition to serving as spacers, PEG display responsive phase behavior influenced by increased ionic strength. Yu et al. developed PEG-coated filter paper for monoclonal antibody selection in membrane separation.[147] Grafted PEG underwent phase separation under high anti-chaotropic salt concentrations, leading to the binding of PEG to antibodies through hydrophobic segments.

1.5.2 PEG Modified Nanocellulose

Steric interactions reduce inter-fibril bonding when PEG are directly mixed with CNC or CNF in water. For instance, PEG have been utilized as steric stabilizers to prevent the agglomeration of nanocelluloses. Mathew et al. demonstrated that PEG served as processing aids in making microcrystalline cellulose (MCC) reinforced poly (lactic acid) (PLA).[148] The presence of PEG improved the dispersion of MCC in the PLA matrix,

although the mechanical properties of the composites were not significantly enhanced. PEG were also employed as redispersing agents mixed and dried with CNF. After freeze-drying and heat drying, redispersibility was evaluated by measuring the change in hydrodynamic diameter.[149] Hydrodynamic diameter was reduced to the same value as never-dried CNF when 20 wt% PEG (1 kDa) was added. Yao et al. prepared PEG/CNC assembled chiral nematic films that displayed tunable colors. PEG intercalated into CNC layers after drying. Films with 20 wt% PEG (20 kDa) content exhibited reversible color changes from green to transparent as relative humidity increased from 50% to 100%.[150]

Hydrogen bonding between PEG and nanocelluloses occurs when embedding nanocelluloses into the PEG-involved nanocomposite hydrogels and films. Hydrogen bonding contributes to forming a three-dimensional network in nanocomposite hydrogels. Jiang et al. introduced CNC-reinforced poly(propylene carbonate)/PEG hydrogels.[151] The hydrogen bonding between the hydroxyl group on cellulose and the oxygen on PEG was detected by an infrared spectrometer. Mechanical properties of the hydrogels were improved by the addition of a small amount of CNC (0.3 wt%), suggesting a contribution from hydrogen bonding. Similar increased mechanical properties were observed when CNC were added as reinforcements to hydrogels obtained from cross-linked poly(oligoethylene glycol methacrylate) (POEGMA)[152] or PEG-diacrylate (PEGDA).[153] Additionally, Reid et al. introduced CNC-reinforced nanocomposite films without chemical cross-linking, demonstrating that PEG could bind with CNC surface, leading to a 60% increase in Young's modulus after CNC loading.[154]

Osmotic dehydration induced by PEG also tailors the inter-fibril interactions. Guccini et al. described an approach to trigger nematic ordering in carboxylated CNF suspensions by controlling PEG concentration.[155] When the PEG concentration exceeded 1 wt%, polarized light microscopy and small-angle X-ray scattering detected oriented nematic domains. High-concentration PEG solutions (10-25 wt%) were also used to create CNF hydrogels with tunable porosities.[156]

In summary, the overall goal of this project is to achieve cellulose modification using maleic copolymers by taking advantage of the reactivity of cyclic anhydride moieties. Among these copolymers, poly (ethylene-*alt*-maleic anhydride) (PEMA) has emerged as a prominent choice for the modification of pulp fibres. The numerous anhydride moieties along the polymer chain provide versatile sites for anchoring other molecules onto cellulose surfaces. Specifically, alkyl and PEG molecules have been selected as model molecules for examination due to the broad potential applications after modifications. Therefore, the thesis focuses on the modification of cellulosic surfaces, encompassing both pulp fibres and CNF, by utilizing PEMA as the linker for grafting alkyl and PEG chains onto the fibre surfaces. The research will involve the synthesis and investigation of PEMA derivatives containing pendant alkyl and PEG groups. Subsequently, these derivatives will be grafted onto bleached softwood pulp fibres and then onto CNF.

1.6 Objectives

The primary goal of this research is to assess the feasibility of utilizing PEMA to introduce molecules, such as alkyl and PEG chains, onto cellulose surfaces. In the grafting process, alkyl-amines and PEG-amines were modified on PEMA backbone and then grafted onto cellulosic fibres. The work documented in this thesis aims to achieve four main objectives.

1. To define the minimum number of anhydride moieties required for grafting PEMAc derivatives onto cellulose while ensuring high grafting yields.
2. To investigate the impact of derivatization on the behavior of the polymer in aqueous solutions, particularly in response to changes in pH.
3. To extend the application of the power-law model, previously used in PEMAc grafting, to the grafting of PEMAc derivatives.
4. To achieve the grafting of PEMAc and PEMAc derivatives onto cellulose nanofibrils.

1.7 Thesis Outline

This thesis consists of five chapters.

Chapter 1 provides a literature review of cellulose structure, cellulose surface modification, maleic copolymers, and the existing methods for grafting alkane and PEG onto the cellulose surface.

Chapter 2 investigates the behavior of hydrophobically modified PEMAc in aqueous solutions, particularly for the changes of polymer conformations with varying solution pH.

Chapter 3 describes the grafting of alkane- and PEG- modified PEMAc derivatives onto softwood bleached kraft pulp fibres. The grafting process employed an aqueous impregnation approach, and the power-law model was adapted to optimize the curing conditions and polymer dosages for PEMAc derivatives.

Chapter 4 proposes an approach for grafting PEMAc and its derivatives onto cellulose nanofibrils (CNF) in acetone. In the approach, the aggregated structures generated in acetone were preserved by grafted polymers. The various aggregated structures and their composition in the grafted CNF were investigated using the particle size measurements and imaging techniques.

Chapter 5 summarizes the contributions of this thesis.

References

(1) Gustafsson, S.; Mihranyan, A. Strategies for Tailoring the Pore-Size Distribution of Virus Retention Filter Papers. *ACS Appl Mater Interfaces* **2016**, *8* (22), 13759-13767. DOI: 10.1021/acsami.6b03093.

(2) Government of Canada. *Forest industry and trade*. https://natural-resources.canada.ca/our-natural-resources/forests/industry-and-trade/13305 (accessed 2023 May 15th).

(3) Bajpai, P.; Bajpai, P. Basic overview of pulp and paper manufacturing process. *Green chemistry and sustainability in pulp and paper industry* **2015**, 11-39.

(4) Höglund, H. Mechanical Pulping. In *Pulping Chemistry and Technology*, Walter de Gruyter GmbH, 2009; pp 57-90.

(5) Fengel, D.; Wegener, G. *Wood: chemistry, ultrastructure, reactions*; Walter de Gruyter GmbH, 2011.

(6) Bajpai, P.; Bajpai, P. Brief description of the pulp and papermaking process. *Biotechnology for pulp and paper processing* **2018**, 9-26.

(7) Tang, R. H.; Liu, L. N.; Zhang, S. F.; He, X. C.; Li, X. J.; Xu, F.; Ni, Y. H.; Li, F. A review on advances in methods for modification of paper supports for use in point-of-care testing. *Mikrochim Acta* **2019**, *186* (8), 521. DOI: 10.1007/s00604-019-3626-z.

(8) Stelte, W.; Sanadi, A. R. Preparation and characterization of cellulose nanofibres from two commercial hardwood and softwood pulps. *Industrial & engineering chemistry research* **2009**, *48* (24), 11211-11219.

(9) Klemm, D.; Kramer, F.; Moritz, S.; Lindstrom, T.; Ankerfors, M.; Gray, D.; Dorris, A. Nanocelluloses: a new family of nature-based materials. *Angew Chem Int Ed Engl* **2011**, *50* (24), 5438-5466. DOI: 10.1002/anie.201001273.

(10) Heise, K.; Kontturi, E.; Allahverdiyeva, Y.; Tammelin, T.; Linder, M. B.; Nonappa; Ikkala, O. Nanocellulose: Recent Fundamental Advances and Emerging Biological and Biomimicking Applications. *Adv Mater* **2021**, *33* (3), e2004349. DOI: 10.1002/adma.202004349.

(11) Tran, A.; Boott, C. E.; MacLachlan, M. J. Understanding the Self-Assembly of Cellulose Nanocrystals-Toward Chiral Photonic Materials. *Adv Mater* **2020**, *32* (41), e1905876. DOI: 10.1002/adma.201905876.

(12) Li, T.; Chen, C.; Brozena, A. H.; Zhu, J. Y.; Xu, L.; Driemeier, C.; Dai, J.; Rojas, O. J.; Isogai, A.; Wagberg, L.; et al. Developing fibrillated cellulose as a sustainable technological material. *Nature* **2021**, *590* (7844), 47-56. DOI: 10.1038/s41586-020-03167-7.

(13) Rojas, O. J. *Cellulose chemistry and properties: fibres, nanocelluloses and advanced materials*; Springer, 2016.

(14) Moon, R. J.; Martini, A.; Nairn, J.; Simonsen, J.; Youngblood, J. Cellulose nanomaterials review: structure, properties and nanocomposites. *Chem Soc Rev* **2011**, *40* (7), 3941-3994. DOI: 10.1039/c0cs00108b.

(15) Postek, M. T.; Vladár, A.; Dagata, J.; Farkas, N.; Ming, B.; Wagner, R.; Raman, A.; Moon, R. J.; Sabo, R.; Wegner, T. H.; et al. Development of the metrology and imaging of cellulose nanocrystals. *Measurement Science and Technology* **2011**, *22* (2). DOI: 10.1088/0957-0233/22/2/024005.

(16) Sjöström, E.; Westermark, U. Chemical composition of wood and pulps: basic constituents and their distribution. In *Analytical methods in wood chemistry, pulping, and papermaking*, Springer, 1999; pp 1-19.

(17) Zugenmaier, P. Conformation and packing of various crystalline cellulose fibres. *Progress in polymer science* **2001**, *26* (9), 1341-1417.

(18) Cosgrove, D. J. Re-constructing our models of cellulose and primary cell wall assembly. *Curr Opin Plant Biol* **2014**, *22*, 122-131. DOI: 10.1016/j.pbi.2014.11.001.

(19) Malcolm Jr, R.; Saxena, I. M. *Cellulose: molecular and structural biology: selected articles on the synthesis, structure, and applications of cellulose*; Springer Science & Business Media, 2007.

(20) Somerville, C. Cellulose synthesis in higher plants. *Annu Rev Cell Dev Biol* **2006**, *22*, 53-78. DOI: 10.1146/annurev.cellbio.22.022206.160206.

(21) Okita, Y.; Saito, T.; Isogai, A. Entire surface oxidation of various cellulose microfibrils by TEMPO-mediated oxidation. *Biomacromolecules* **2010**, *6* (11), 1696-1700.

(22) Ding, S.-Y.; Himmel, M. E. The maize primary cell wall microfibril: a new model derived from direct visualization. *Journal of agricultural and food chemistry* **2006**, *54* (3), 597-606.

(23) Fernandes, A. N.; Thomas, L. H.; Altaner, C. M.; Callow, P.; Forsyth, V. T.; Apperley, D. C.; Kennedy, C. J.; Jarvis, M. C. Nanostructure of cellulose microfibrils in spruce wood. *Proceedings of the National Academy of Sciences* **2011**, *108* (47), E1195-E1203.

(24) Kubicki, J. D.; Yang, H.; Sawada, D.; O'Neill, H.; Oehme, D.; Cosgrove, D. The shape of native plant cellulose microfibrils. *Scientific reports* **2018**, *8* (1), 13983.

(25) Nixon, B. T.; Mansouri, K.; Singh, A.; Du, J.; Davis, J. K.; Lee, J.-G.; Slabaugh, E.; Vandavasi, V. G.; O'Neill, H.; Roberts, E. M. Comparative structural and computational analysis supports eighteen cellulose synthases in the plant cellulose synthesis complex. *Scientific reports* **2016**, *6* (1), 28696.

(26) Oehme, D. P.; Downton, M. T.; Doblin, M. S.; Wagner, J.; Gidley, M. J.; Bacic, A. Unique aspects of the structure and dynamics of elementary I β cellulose microfibrils revealed by computational simulations. *Plant physiology* **2015**, *168* (1), 3-17.

(27) Terrett, O. M.; Lyczakowski, J. J.; Yu, L.; Iuga, D.; Franks, W. T.; Brown, S. P.; Dupree, R.; Dupree, P. Molecular architecture of softwood revealed by solid-state NMR. *Nature communications* **2019**, *10* (1), 4978.

(28) Ahvenainen, P.; Kontro, I.; Svedström, K. Comparison of sample crystallinity determination methods by X-ray diffraction for challenging cellulose I materials. *Cellulose* **2016**, *23* (2), 1073-1086.

(29) Nishiyama, Y.; Kim, U.-J.; Kim, D.-Y.; Katsumata, K. S.; May, R. P.; Langan, P. Periodic disorder along ramie cellulose microfibrils. *Biomacromolecules* **2003**, *4* (4), 1013-1017.

(30) Usov, I.; Nyström, G.; Adamcik, J.; Handschin, S.; Schütz, C.; Fall, A.; Bergström, L.; Mezzenga, R. Understanding nanocellulose chirality and structure–properties relationship at the single fibril level. *Nature communications* **2015**, *6* (1), 7564.

(31) Dufresne, A. *Nanocellulose: from nature to high performance tailored materials*; Walter de Gruyter GmbH, 2017.

(32) Seddiqi, H.; Oliaei, E.; Honarkar, H.; Jin, J.; Geonzon, L. C.; Bacabac, R. G.; Klein-Nulend, J. Cellulose and its derivatives: Towards biomedical applications. *Cellulose* **2021**, *28* (4), 1893-1931.

(33) Bu, L.; Himmel, M. E.; Crowley, M. F. The molecular origins of twist in cellulose I-beta. *Carbohydr Polym* **2015**, *125*, 146-152. DOI: 10.1016/j.carbpol.2015.02.023.

(34) Hanley, S. J.; Revol, J.-F.; Godbout, L.; Gray, D. G. Atomic force microscopy and transmission electron microscopy of cellulose from Micrasterias denticulata; evidence for a chiral helical microfibril twist. *Cellulose* **1997**, *4*, 209-220.

(35) Ogawa, Y. Electron microdiffraction reveals the nanoscale twist geometry of cellulose nanocrystals. *Nanoscale* **2019**, *11* (45), 21767-21774.

(36) Revol, J.-F.; Bradford, H.; Giasson, J.; Marchessault, R.; Gray, D. Helicoidal self-ordering of cellulose microfibrils in aqueous suspension. *International journal of biological macromolecules* **1992**, *14* (3), 170-172.

(37) Joutsimo, O. P.; Asikainen, S. Effect of fibre wall pore structure on pulp sheet density of softwood kraft pulp fibres. *BioResources* **2013**, *8* (2).

(38) Fernandes Diniz, J.; Gil, M.; Castro, J. Hornification—its origin and interpretation in wood pulps. *Wood Science and Technology* **2004**, *37*, 489-494.

(39) Li, Q.; Wang, A.; Long, K.; He, Z.; Cha, R. Modified Fenton Oxidation of Cellulose Fibres for Cellulose Nanofibrils Preparation. *ACS Sustainable Chemistry & Engineering* **2018**, *7* (1), 1129-1136. DOI: 10.1021/acssuschemeng.8b04786.

(40) Page, D.; El-Hosseiny, F.; Winkler, K. Behaviour of single wood fibres under axial tensile strain. *Nature* **1971**, *229* (5282), 252-253.

(41) Abdul Khalil, H. P.; Davoudpour, Y.; Islam, M. N.; Mustapha, A.; Sudesh, K.; Dungani, R.; Jawaid, M. Production and modification of nanofibrillated cellulose using various mechanical processes: a review. *Carbohydr Polym* **2014**, *99*, 649-665. DOI: 10.1016/j.carbpol.2013.08.069.

(42) Rol, F.; Belgacem, M. N.; Gandini, A.; Bras, J. Recent advances in surface-modified cellulose nanofibrils. *Progress in Polymer Science* **2019**, *88*, 241-264. DOI: 10.1016/j.progpolymsci.2018.09.002.

(43) Sinquefield, S.; Ciesielski, P. N.; Li, K.; Gardner, D. J.; Ozcan, S. Nanocellulose dewatering and drying: current state and future perspectives. *ACS Sustainable Chemistry & Engineering* **2020**, *8* (26), 9601-9615.

(44) Habibi, Y.; Lucia, L. A.; Rojas, O. J. Cellulose nanocrystals: chemistry, self-assembly, and applications. *Chemical reviews* **2010**, *110* (6), 3479-3500.

(45) Stockton, W.; Rubner, M. Molecular-level processing of conjugated polymers. 4. Layer-by-layer manipulation of polyaniline via hydrogen-bonding interactions. *Macromolecules* **1997**, *30* (9), 2717-2725.

(46) Wågberg, L. Polyelectrolyte adsorption onto cellulose fibres–A review. *Nordic Pulp & Paper Research Journal* **2000**, *15* (5), 586-597.

(47) Wågberg, L.; Erlandsson, J. The use of layer-by-layer self-assembly and nanocellulose to prepare advanced functional materials. *Advanced Materials* **2021**, *33* (28), 2001474.

(48) Wågberg, L.; Decher, G.; Norgren, M.; Lindström, T.; Ankerfors, M.; Axnäs, K. The build-up of polyelectrolyte multilayers of microfibrillated cellulose and cationic polyelectrolytes. *Langmuir* **2008**, *24* (3), 784-795.

(49) Bates, N. Polyamide-epichlorohydrin wet-strength resin. I. Retention by pulp. *Tappi Tech Ass Pulp Pap Indus* **1969**.

(50) Espy, H. H.; Rave, T. The mechanism of wet-strength development by alkaline-curing amino polymer-epichlorohydrin resins. *Tappi journal* **1988**, *71* (5), 133-137.

(51) Wågberg, L.; Bjőrklund, M. On the mechanism behind wet strength development in papers containing wet strength resins. *Nordic Pulp & Paper Research Journal* **1993**, *8* (1), 53-58.

(52) Mocchiutti, P.; Galván, M. V.; Peresin, M. S.; Schnell, C. N.; Zanuttini, M. A. Complexes of xylan and synthetic polyelectrolytes. Characterization and adsorption onto high quality unbleached fibres. *Carbohydrate polymers* **2015**, *116*, 131-139.

(53) Mocchiutti, P.; Schnell, C. N.; Rossi, G. D.; Peresin, M. S.; Zanuttini, M. A.; Galván, M. V. Cationic and anionic polyelectrolyte complexes of xylan and chitosan. Interaction with lignocellulosic surfaces. *Carbohydrate polymers* **2016**, *150*, 89-98.

(54) Schnell, C. N.; Tarrés, Q.; Galván, M. V.; Mocchiutti, P.; Delgado-Aguilar, M.; Zanuttini, M. A.; Mutjé, P. Polyelectrolyte complexes for assisting the application of lignocellulosic micro/nanofibres in papermaking. *Cellulose* **2018**, *25*, 6083-6092.

(55) Laine, J.; Lindström, T. Studies on topochemical modification of cellulosic fibres: Part 1. Chemical conditions for the attachment of carboxymethyl cellulose onto fibres. *Nordic Pulp & Paper Research Journal* **2000**, *15* (5), 520-526.

(56) Olszewska, A.; Junka, K.; Nordgren, N.; Laine, J.; Rutland, M. W.; Österberg, M. Non-ionic assembly of nanofibrillated cellulose and polyethylene glycol grafted carboxymethyl cellulose and the effect of aqueous lubrication in nanocomposite formation. *Soft Matter* **2013**, *9* (31). DOI: 10.1039/c3sm50578b.

(57) Eronen, P.; Österberg, M.; Heikkinen, S.; Tenkanen, M.; Laine, J. Interactions of structurally different hemicelluloses with nanofibrillar cellulose. *Carbohydrate Polymers* **2011**, *86* (3), 1281-1290. DOI: 10.1016/j.carbpol.2011.06.031.

(58) Lozhechnikova, A.; Dax, D.; Vartiainen, J.; Willfor, S.; Xu, C.; Osterberg, M. Modification of nanofibrillated cellulose using amphiphilic block-structured galactoglucomannans. *Carbohydr Polym* **2014**, *110*, 163-172. DOI: 10.1016/j.carbpol.2014.03.087.

(59) Isogai, A.; Saito, T.; Fukuzumi, H. TEMPO-oxidized cellulose nanofibres. *Nanoscale* **2011**, *3* (1), 71-85. DOI: 10.1039/c0nr00583e.

(60) Fu, Q.; Sutherland, A.; Gustafsson, E.; Ali, M. M.; Soleymani, L.; Pelton, R. Relating redox properties of polyvinylamine-g-TEMPO/laccase hydrogel complexes to cellulose oxidation. *Langmuir* **2017**, *33* (32), 7854-7861.

(61) Bragd, P.; Van Bekkum, H.; Besemer, A. TEMPO-mediated oxidation of polysaccharides: survey of methods and applications. *Topics in Catalysis* **2004**, *27*, 49-66.

(62) Larsson, P. A.; Berglund, L. A.; Wagberg, L. Ductile all-cellulose nanocomposite films fabricated from core-shell structured cellulose nanofibrils. *Biomacromolecules* **2014**, *15* (6), 2218-2223. DOI: 10.1021/bm500360c.

(63) Liimatainen, H.; Visanko, M.; Sirvio, J. A.; Hormi, O. E.; Niinimaki, J. Enhancement of the nanofibrillation of wood cellulose through sequential periodate-chlorite oxidation. *Biomacromolecules* **2012**, *13* (5), 1592-1597. DOI: 10.1021/bm300319m.

(64) Larsson, P. A.; Berglund, L. A.; Wågberg, L. Highly ductile fibres and sheets by core-shell structuring of the cellulose nanofibrils. *Cellulose* **2014**, *21*, 323-333.

(65) Liimatainen, H.; Ezekiel, N.; Sliz, R.; Ohenoja, K.; Sirvio, J. A.; Berglund, L.; Hormi, O.; Niinimaki, J. High-strength nanocellulose-talc hybrid barrier films. *ACS Appl Mater Interfaces* **2013**, *5* (24), 13412-13418. DOI: 10.1021/am4043273.

(66) Eyholzer, C.; Bordeanu, N.; Lopez-Suevos, F.; Rentsch, D.; Zimmermann, T.; Oksman, K. Preparation and characterization of water-redispersible nanofibrillated cellulose in powder form. *Cellulose* **2010**, *17*, 19-30.

(67) Eyholzer, C.; de Couraca, A. B.; Duc, F.; Bourban, P. E.; Tingaut, P.; Zimmermann, T.; Manson, J. A.; Oksman, K. Biocomposite hydrogels with carboxymethylated, nanofibrillated cellulose powder for replacement of the nucleus pulposus. *Biomacromolecules* **2011**, *12* (5), 1419-1427. DOI: 10.1021/bm101131b.

(68) Yan, Y.; Amer, H.; Rosenau, T.; Zollfrank, C.; Dörrstein, J.; Jobst, C.; Zimmermann, T.; Keckes, J.; Veigel, S.; Gindl-Altmutter, W.; et al. Dry, hydrophobic microfibrillated cellulose powder obtained in a simple procedure using alkyl ketene dimer. *Cellulose* **2016**, *23* (2), 1189-1197. DOI: 10.1007/s10570-016-0887-0.

(69) Espino-Perez, E.; Domenek, S.; Belgacem, N.; Sillard, C.; Bras, J. Green process for chemical functionalization of nanocellulose with carboxylic acids. *Biomacromolecules* **2014**, *15* (12), 4551-4560. DOI: 10.1021/bm5013458.

(70) Robles, E.; Izaguirre, N.; Dogaru, B.-I.; Popescu, C.-M.; Barandiaran, I.; Labidi, J. Sonochemical production of nanoscaled crystalline cellulose using organic acids. *Green Chemistry* **2020**, *22* (14), 4627-4639. DOI: 10.1039/d0gc01283a.

(71) Yang, C. Q. Infrared spectroscopy studies of the cyclic anhydride as the intermediate for the ester crosslinking of cotton cellulose by polycarboxylic acids. I. Identification of the cyclic anhydride intermediate. *Journal of Polymer Science Part A: Polymer Chemistry* **1993**, *31* (5), 1187-1193.

(72) Xiaohong, G.; Yang, C. Q. FTIR spectroscopy study of the formation of cyclic anhydride intermediates of polycarboxylic acids catalyzed by sodium hypophosphite. *Textile Research Journal* **2000**, *70* (1), 64-70.

(73) Yang, C. Q.; Wang, X. Formation of cyclic anhydride intermediates and esterification of cotton cellulose by multifunctional carboxylic acids: An infrared spectroscopy study. *Textile Research Journal* **1996**, *66* (9), 595-603.

(74) Yang, C. Q.; Wang, X. Infrared spectroscopy studies of the cyclic anhydride as the intermediate for the ester crosslinking of cotton cellulose by polycarboxylic acids. II. Comparison of different polycarboxylic acids. *Journal of Polymer Science Part A: Polymer Chemistry* **1996**, *34* (8), 1573-1580.

(75) Yang, C. Q.; Wang, X. Formation of five-membered cyclic anhydride intermediates by polycarboxylic acids: Thermal analysis and Fourier transform infrared spectroscopy. *Journal of applied polymer science* **1998**, *70* (13), 2711-2718.

(76) Tang, L.; Weder, C. Cellulose whisker/epoxy resin nanocomposites. *ACS Appl Mater Interfaces* **2010**, *2* (4), 1073-1080. DOI: 10.1021/am900830h.

(77) Siqueira, G.; Bras, J.; Dufresne, A. New process of chemical grafting of cellulose nanoparticles with a long chain isocyanate. *Langmuir* **2010**, *26* (1), 402-411. DOI: 10.1021/la9028595.

(78) Lu, T.; Jiang, M.; Jiang, Z.; Hui, D.; Wang, Z.; Zhou, Z. Effect of surface modification of bamboo cellulose fibres on mechanical properties of cellulose/epoxy composites. *Composites Part B: Engineering* **2013**, *51*, 28-34. DOI: 10.1016/j.compositesb.2013.02.031.

(79) Roy, D.; Semsarilar, M.; Guthrie, J. T.; Perrier, S. Cellulose modification by polymer grafting: a review. *Chem Soc Rev* **2009**, *38* (7), 2046-2064. DOI: 10.1039/b808639g.

(80) Mulyadi, A.; Deng, Y. Surface modification of cellulose nanofibrils by maleated styrene block copolymer and their composite reinforcement application. *Cellulose* **2016**, *23*, 519-528.

(81) Azzam, F.; Heux, L.; Putaux, J.-L.; Jean, B. Preparation by grafting onto, characterization, and properties of thermally responsive polymer-decorated cellulose nanocrystals. *Biomacromolecules* **2010**, *11* (12), 3652-3659.

(82) Moad, G.; Solomon, D. H. *The chemistry of radical polymerization*; Elsevier, 2006.

(83) Miao, C.; Hamad, W. Y. Cellulose reinforced polymer composites and nanocomposites: a critical review. *Cellulose* **2013**, *20*, 2221-2262.

(84) Mohanty, A. K.; Vivekanandhan, S.; Pin, J.-M.; Misra, M. Composites from renewable and sustainable resources: Challenges and innovations. *Science* **2018**, *362* (6414), 536-542.

(85) Kumar, M.; Gehlot, P. S.; Parihar, D.; Surolia, P. K.; Prasad, G. Promising grafting strategies on cellulosic backbone through radical polymerization processes–A review. *European polymer journal* **2021**, *152*, 110448.

(86) Littunen, K.; Hippi, U.; Johansson, L.-S.; Österberg, M.; Tammelin, T.; Laine, J.; Seppälä, J. Free radical graft copolymerization of nanofibrillated cellulose with acrylic monomers. *Carbohydrate polymers* **2011**, *84* (3), 1039-1047.

(87) Xiao, M.; Li, S.; Chanklin, W.; Zheng, A.; Xiao, H. Surface-initiated atom transfer radical polymerization of butyl acrylate on cellulose microfibrils. *Carbohydrate polymers* **2011**, *83* (2), 512-519.

(88) Carlmark, A.; Malmström, E. Atom transfer radical polymerization from cellulose fibres at ambient temperature. *Journal of the American Chemical Society* **2002**, *124* (6), 900-901.

(89) Nystrom, D.; Lindqvist, J.; Ostmark, E.; Antoni, P.; Carlmark, A.; Hult, A.; Malmstrom, E. Superhydrophobic and self-cleaning bio-fibre surfaces via ATRP and subsequent postfunctionalization. *ACS applied materials & interfaces* **2009**, *1* (4), 816-823.

(90) Roy, D.; Guthrie, J. T.; Perrier, S. Graft polymerization: Grafting poly (styrene) from cellulose via reversible addition− fragmentation chain transfer (RAFT) polymerization. *Macromolecules* **2005**, *38* (25), 10363-10372.

(91) Roy, D.; Knapp, J. S.; Guthrie, J. T.; Perrier, S. Antibacterial cellulose fibre via RAFT surface graft polymerization. *Biomacromolecules* **2008**, *9* (1), 91-99.

(92) Rätzsch, M. Alternating maleic anhydride copolymers. *Progress in polymer science* **1988**, *13* (4), 277-337.

(93) JOHNSON, D. New Applications for Poly (ethylene-alt-maleic anhydride). Durham University, 2010.

(94) Lang, J. L.; Pavelich, W.; Clarey, H. Homopolymerization of maleic anhydride. I. Preparation of the polymer. *Journal of Polymer Science Part A: General Papers* **1963**, *1* (4), 1123-1136.

(95) Rzaev, Z.; Bryksina, L.; Sadykh-Zade, S. Charge transfer complexes of maleic anhydride in radical homo-and copolymerization. In *Journal of Polymer Science: Polymer Symposia*, 1973; Wiley Online Library: Vol. 42, pp 519-529.

(96) Georgiev, G.; Konstantinov, K.; Kabaivanov, V. The role of the charge-transfer complex during the copolymerization of N-vinylpyrrolidone and maleic anhydride. *Macromolecules* **1992**, *25* (23), 6302-6308.

(97) Gaylord, N. g. Poly (maleic anhydride). *Journal of Macromolecular Science—Reviews in Macromolecular Chemistry* **1975**, *13* (2), 235-261.

(98) Rätzsch, M.; Arnold, M.; Steinert, V. Untersuchungen zur radikalischen Copolymerisation von 2, 4, 4-Trimethylpent-1-en und 2, 4, 4-Trimethylpent-2-en mit Maleinsäureanhydrid. *Acta polymerica* **1985**, *36* (1), 8-12.

(99) Arnold, M.; Rätzsch, M. The copolymerization of maleic anhydride with propene and isobutene. *Die Makromolekulare Chemie: Macromolecular Chemistry and Physics* **1986**, *187* (7), 1593-1596.

(100) Komber, H. The 1H and 13C NMR spectra of an alternating ethene/maleic anhydride copolymer and the corresponding acid and sodium salt. *Macromolecular Chemistry and Physics* **1995**, *196* (2), 669-678.

(101) Rätzsch, M.; Steinert, V.; Seiler, S.; Büttner, B. Thermisches Verhalten und Struktur von Copolymeren der Maleinsäure-bzw. Fumarsäurehalbester. *Acta polymerica* **1984**, *35* (5), 373-378.

(102) Eberson, L.; Welinder, H. Cyclic anhydrides. III. Equilibrium constants for the acid-anhydride equilibrium in aqueous solutions of certain vicinal diacids. *Journal of the American Chemical Society* **1971**, *93* (22), 5821-5826.

(103) Musa, O. M. Handbook of maleic anhydride based materials. *Springer* **2016**, *10*, 978-973.

(104) Rätzsch, M.; Schicht, G. Untersuchungen zur Kinetik der photoinitiierten Copolymerisation von Styrol mit Maleinsäureanhydrid. *Acta Polymerica* **1980**, *31* (7), 419-423.

(105) Renner, L.; Pompe, T.; Salchert, K.; Werner, C. Fibronectin displacement at polymer surfaces. *Langmuir* **2005**, *21* (10), 4571-4577.

(106) Salchert, K.; Streller, U.; Pompe, T.; Herold, N.; Grimmer, M.; Werner, C. In vitro reconstitution of fibrillar collagen type I assemblies at reactive polymer surfaces. *Biomacromolecules* **2004**, *5* (4), 1340-1350.

(107) Pompe, T.; Kobe, F.; Salchert, K.; Jørgensen, B.; Oswald, J.; Werner, C. Fibronectin anchorage to polymer substrates controls the initial phase of endothelial cell adhesion. *Journal of Biomedical Materials Research Part A: An Official Journal of The Society for Biomaterials, The Japanese Society for Biomaterials, and The Australian Society for Biomaterials and the Korean Society for Biomaterials* **2003**, *67* (2), 647-657.

(108) Pompe, T.; Renner, L.; Grimmer, M.; Herold, N.; Werner, C. Functional films of maleic anhydride copolymers under physiological conditions. *Macromolecular bioscience* **2005**, *5* (9), 890-895.

(109) Pompe, T.; Zschoche, S.; Herold, N.; Salchert, K.; Gouzy, M.-F.; Sperling, C.; Werner, C. Maleic anhydride copolymers a versatile platform for molecular biosurface engineering. *Biomacromolecules* **2003**, *4* (4), 1072-1079.

(110) Rätzsch, M.; Hue, N. T. Die umsetzung von aliphatischen aminen mit copolymeren des maleinsäureanhydrids. *Acta Polymerica* **1979**, *30* (2), 93-97.

(111) Yin, X.; Stöver, H. D. Thermosensitive and pH-sensitive polymers based on maleic anhydride copolymers. *Macromolecules* **2002**, *35* (27), 10178-10181.

(112) Rietman, E.; Kaplan, M. Single-ion conductivity in comblike polymers. *Journal of Polymer Science Part C: Polymer Letters* **1990**, *28* (6), 187-191.

(113) Qi, L.; Lin, Y.; Wang, F. Characterization and ionic conductivity of an amorphous comblike polymer II: Based on ethylene–maleic anhydride copolymer backbone with monoethyl ether of poly (ethylene glycol) of MW= 550 as side chain. *European polymer journal* **1999**, *35* (5), 789-793.

(114) Sarı, A.; Bicer, A.; Alkan, C. Thermal energy storage characteristics of poly (styrene-co-maleic anhydride)-graft-PEG as polymeric solid–solid phase change materials. *Solar Energy Materials and Solar Cells* **2017**, *161*, 219-225.

(115) Tonge, S.; Tighe, B. Responsive hydrophobically associating polymers: a review of structure and properties. *Advanced drug delivery reviews* **2001**, *53* (1), 109-122.

(116) Hu, Y.; Smith, G. L.; Richardson, M. F.; McCormick, C. L. Water soluble polymers. 74. pH responsive microdomains in labeled n-octylamide-substituted poly (sodium maleate-alt-ethyl vinyl ethers): synthesis, steady-state fluorescence, and nonradiative energy transfer studies. *Macromolecules* **1997**, *30* (12), 3526-3537.

(117) Dubin, P.; Strauss, U. P. Hydrophobic hypercoiling in copolymers of maleic acid and alkyl vinyl ethers. *The Journal of Physical Chemistry* **1967**, *71* (8), 2757-2759.

(118) Dubin, P. L.; Strauss, U. P. Hydrophobic bonding in alternating copolymers of maleic acid and alkyl vinyl ethers. *The Journal of Physical Chemistry* **1970**, *74* (14), 2842-2847.

(119) Sauvage, E.; Plucktaveesak, N.; Colby, R. H.; Amos, D.; Antalek, B.; Schroeder, K.; Tan, J. Amphiphilic maleic acid-containing alternating copolymers—2. Dilute solution characterization by light scattering, intrinsic viscosity, and PGSE NMR spectroscopy. *Journal of Polymer Science Part B: Polymer Physics* **2004**, *42* (19), 3584-3597.

(120) Qiu, Q.; Lou, A.; Somasundaran, P.; Pethica, B. Intramolecular association of poly (maleic acid/octyl vinyl ether) in aqueous solution. *Langmuir* **2002**, *18* (15), 5921-5926.

(121) Binana-Limbele, W.; Zana, R. Fluorescence probing of microdomains in aqueous solutions of polysoaps. 1. Use of pyrene to study the conformational state of polysoaps and their comicellization with cationic surfactants. *Macromolecules* **1987**, *20* (6), 1331-1335.

(122) Hsu, J. L.; Strauss, U. P. Intramolecular micelles in a copolymer of maleic anhydride and hexyl vinyl ether: determination of aggregation number by luminescence quenching. *Journal of Physical Chemistry* **1987**, *91* (24), 6238-6241.

(123) Zhang, H.; Tsenter, E.; Bicho, P.; Doherty, E. A. S.; Riehle, R.; Moran-Mirabal, J.; Pelton, R. H. Carboxylated bleached kraft pulp from maleic anhydride copolymers. *Nordic Pulp & Paper Research Journal* **2021**, *36* (4), 608-617. DOI: 10.1515/npprj-2021-0005.

(124) Zhang, H.; Bicho, P.; Doherty, E. A. S.; Riehle, R. J.; Moran-Mirabal, J.; Pelton, R. H. High-yield grafting of carboxylated polymers to wood pulp fibres. *Cellulose* **2021**, *28* (11), 7311-7326. DOI: 10.1007/s10570-021-04016-0.

(125) Zhang, H.; Bicho, P.; Doherty, E. A. S.; Riehle, R.; Moran-Mirabal, J.; Pelton, R. H. High Yield Poly(ethylene-alt-maleic acid) Grafting to Wood Pulp while Minimizing Fibre/Fibre Wet Adhesion. *Biomacromolecules* **2021**, *22* (7), 3060-3068. DOI: 10.1021/acs.biomac.1c00511.

(126) Zhang, H.; Wang, L.; Bicho, P.; Doherty, E. A. S.; Riehle, R. J.; Borkar, S.; Moran-Mirabal, J.; Pelton, R. H. Grafted maleic acid copolymer giving thermosetting kraft pulp. *Cellulose* **2022**, *29* (7), 3745-3758. DOI: 10.1007/s10570-022-04518-5.

(127) Siró, I.; Plackett, D. Microfibrillated cellulose and new nanocomposite materials: a review. *Cellulose* **2010**, *17*, 459-494.

(128) Kalia, S.; Boufi, S.; Celli, A.; Kango, S. Nanofibrillated cellulose: surface modification and potential applications. *Colloid and Polymer Science* **2013**, *292* (1), 5-31. DOI: 10.1007/s00396-013-3112-9.

(129) Roberts, J. C. *Paper chemistry*; Springer, 1991.

(130) Bottorff, K. J.; Sullivan, M. J. New insights into the AKD sizing mechanism. *Nordic Pulp & Paper Research Journal* **1993**, *8* (1), 86-95.

(131) Lindström, T.; Larsson, P. T. Alkyl ketene dimer (AKD) sizing–A review. *Nordic Pulp & Paper Research Journal* **2008**, *23* (2), 202-209.

(132) Li, H.; Liu, W.; Yu, D.; Song, Z. Anchorage of ASA on cellulose fibres in sizing development. *Nordic Pulp & Paper Research Journal* **2015**, *30* (4), 626-633.

(133) Salajková, M.; Berglund, L. A.; Zhou, Q. Hydrophobic cellulose nanocrystals modified with quaternary ammonium salts. *Journal of Materials Chemistry* **2012**, *22* (37). DOI: 10.1039/c2jm34355j.

(134) Yin, Y.; Hong, Z.; Tian, X.; Zhu, Q.; Jiang, X.; Wang, H.; Gao, W. Cellulose nanocrystals modified with quaternary ammonium salts and its reinforcement of polystyrene. *Polymer Bulletin* **2017**, *75* (5), 2151-2166. DOI: 10.1007/s00289-017-2131-y.

(135) Shimizu, M.; Saito, T.; Fukuzumi, H.; Isogai, A. Hydrophobic, ductile, and transparent nanocellulose films with quaternary alkylammonium carboxylates on nanofibril surfaces. *Biomacromolecules* **2014**, *15* (11), 4320-4325. DOI: 10.1021/bm501329v.

(136) Utsel, S.; Carlmark, A.; Pettersson, T.; Bergström, M.; Malmström, E. E.; Wågberg, L. Synthesis, adsorption and adhesive properties of a cationic amphiphilic block copolymer for use as compatibilizer in composites. *European Polymer Journal* **2012**, *48* (7), 1195-1204. DOI: 10.1016/j.eurpolymj.2012.05.004.

(137) Utsel, S.; Bruce, C.; Pettersson, T.; Fogelström, L.; Carlmark, A.; Malmström, E.; Wågberg, L. Physical Tuning of Cellulose-Polymer Interactions Utilizing Cationic Block Copolymers

Based on PCL and Quaternized PDMAEMA. *ACS Applied Materials & Interfaces* **2012**, *4* (12), 6796-6807. DOI: 10.1021/am301981r.

(138) Sato, A.; Kabusaki, D.; Okumura, H.; Nakatani, T.; Nakatsubo, F.; Yano, H. Surface modification of cellulose nanofibres with alkenyl succinic anhydride for high-density polyethylene reinforcement. *Composites Part A: Applied Science and Manufacturing* **2016**, *83*, 72-79. DOI: 10.1016/j.compositesa.2015.11.009.

(139) Li, W.; Wang, S.; Wang, W.; Qin, C.; Wu, M. Facile preparation of reactive hydrophobic cellulose nanofibril film for reducing water vapor permeability (WVP) in packaging applications. *Cellulose* **2019**, *26*, 3271-3284.

(140) Li, Y.; Zhu, L.; Grishkewich, N.; Tam, K. C.; Yuan, J.; Mao, Z.; Sui, X. CO2-responsive cellulose nanofibres aerogels for switchable oil–water separation. *ACS applied materials & interfaces* **2019**, *11* (9), 9367-9373.

(141) Li, M.; Liu, X.; Liu, N.; Guo, Z.; Singh, P. K.; Fu, S. Effect of surface wettability on the antibacterial activity of nanocellulose-based material with quaternary ammonium groups. *Colloids and Surfaces A: Physicochemical and Engineering Aspects* **2018**, *554*, 122-128.

(142) Auad, M. L.; Contos, V. S.; Nutt, S.; Aranguren, M. I.; Marcovich, N. E. Characterization of nanocellulose- reinforced shape memory polyurethanes. *Polymer International* **2008**, *57* (4), 651-659. DOI: 10.1002/pi.2394.

(143) Abushammala, H. Nano-Brushes of alcohols grafted onto cellulose nanocrystals for reinforcing poly (Butylene succinate): Impact of Alcohol chain length on interfacial adhesion. *Polymers* **2020**, *12* (1), 95.

(144) Oksman, K.; Aitomäki, Y.; Mathew, A. P.; Siqueira, G.; Zhou, Q.; Butylina, S.; Tanpichai, S.; Zhou, X.; Hooshmand, S. Review of the recent developments in cellulose nanocomposite processing. *Composites Part A: Applied Science and Manufacturing* **2016**, *83*, 2-18.

(145) Jeevarathinam, A. S.; Pai, N.; Huang, K.; Hariri, A.; Wang, J.; Bai, Y.; Wang, L.; Hancock, T.; Keys, S.; Penny, W.; et al. A cellulose-based photoacoustic sensor to measure heparin concentration and activity in human blood samples. *Biosens Bioelectron* **2019**, *126*, 831-837. DOI: 10.1016/j.bios.2018.11.052.

(146) Xue, Y.; O'Mara, M. L.; Surawski, P. P.; Trau, M.; Mark, A. E. Effect of poly(ethylene glycol) (PEG) spacers on the conformational properties of small peptides: a molecular dynamics study. *Langmuir* **2011**, *27* (1), 296-303. DOI: 10.1021/la103800h.

(147) Yu, D.; Chen, X.; Pelton, R.; Ghosh, R. Paper-PEG-based membranes for hydrophobic interaction chromatography: Purification of monoclonal antibody. *Biotechnology and bioengineering* **2008**, *99* (6), 1434-1442.

(148) Mathew, A. P.; Oksman, K.; Sain, M. Mechanical properties of biodegradable composites from poly lactic acid (PLA) and microcrystalline cellulose (MCC). *Journal of applied polymer science* **2005**, *97* (5), 2014-2025.

(149) Nordenström, M.; Kaldéus, T.; Erlandsson, J.; Pettersson, T.; Malmström, E.; Wågberg, L. Redispersion Strategies for Dried Cellulose Nanofibrils. *ACS Sustainable Chemistry & Engineering* **2021**, *9* (33), 11003-11010. DOI: 10.1021/acssuschemeng.1c02122.

(150) Yao, K.; Meng, Q.; Bulone, V.; Zhou, Q. Flexible and Responsive Chiral Nematic Cellulose Nanocrystal/Poly(ethylene glycol) Composite Films with Uniform and Tunable Structural Color. *Adv Mater* **2017**, *29* (28). DOI: 10.1002/adma.201701323.

(151) Jiang, G.; Zhang, M.; Feng, J.; Zhang, S.; Wang, X. High Oxygen Barrier Property of Poly(propylene carbonate)/Polyethylene Glycol Nanocomposites with Low Loading of Cellulose Nanocrytals. *ACS Sustainable Chemistry & Engineering* **2017**, *5* (12), 11246-11254. DOI: 10.1021/acssuschemeng.7b01674.

(152) De France, K. J.; Chan, K. J.; Cranston, E. D.; Hoare, T. Enhanced Mechanical Properties in Cellulose Nanocrystal-Poly(oligoethylene glycol methacrylate) Injectable Nanocomposite Hydrogels through Control of Physical and Chemical Cross-Linking. *Biomacromolecules* **2016**, *17* (2), 649-660. DOI: 10.1021/acs.biomac.5b01598.

(153) Hou, K.; Li, Y.; Liu, Y.; Zhang, R.; Hsiao, B. S.; Zhu, M. Continuous fabrication of cellulose nanocrystal/poly(ethylene glycol) diacrylate hydrogel fibre from nanocomposite dispersion: Rheology, preparation and characterization. *Polymer* **2017**, *123*, 55-64. DOI: 10.1016/j.polymer.2017.06.034.

(154) Reid, M. S.; Stimpson, T. C.; Niinivaara, E.; Villalobos, M.; Cranston, E. D. Comparing Soft Semicrystalline Polymer Nanocomposites Reinforced with Cellulose Nanocrystals and Fumed Silica. *Industrial & Engineering Chemistry Research* **2017**, *57* (1), 220-230. DOI: 10.1021/acs.iecr.7b03836.

(155) Guccini, V.; Yu, S.; Agthe, M.; Gordeyeva, K.; Trushkina, Y.; Fall, A.; Schutz, C.; Salazar-Alvarez, G. Inducing nematic ordering of cellulose nanofibres using osmotic dehydration. *Nanoscale* **2018**, *10* (48), 23157-23163. DOI: 10.1039/c8nr08194h.

(156) Guccini, V.; Phiri, J.; Trifol, J.; Rissanen, V.; Mousavi, S. M.; Vapaavuori, J.; Tammelin, T.; Maloney, T.; Kontturi, E. Tuning the Porosity, Water Interaction, and Redispersion of

Nanocellulose Hydrogels by Osmotic Dehydration. *ACS Appl Polym Mater* **2022**, *4* (1), 24-28. DOI: 10.1021/acsapm.1c01430.

Chapter 2

Solution Properties of Hydrophobic Derivatives of Poly (ethylene-*alt*-maleic acid)

Polymer solutions applied for the pulp sheet impregnation are analyzed in this chapter. A series of alkyl-amine molecules were modified on the PEMA, giving comb polymers. The polymer behaviours in water were characterized through dynamic light scattering, pyrene fluorescence probe, potentiometric titration, and imaging. The conformations of the hydrophobically modified polymers with pendant alkyl chains of C6-C10 display a conformational transition from hypercoil to expanded coilin solutions in pH ranging from 4 to 11. PEMA-C10 derivatives with DS of 25-75% exhibit a unimolecular nanogel at pH of 7-9.

The experiment design, data collection and analysis, and first draft writing were completed by me. My summer student Zhen Hu helped me with the sample preparation. Dr. Jose M Moran-Mirabal offered valuable advice on the paper. Dr. Robert Pelton helped me with the data analysis and rewrote parts of the draft as necessary.

This chapter has been published in *European Polymer Journal.*

Solution Properties of Hydrophobic Derivatives of Poly(ethylene-alt-maleic acid)

Xiao Wu,[1] Zhen Hu,[1] Paul Bicho,[2] Erin A.S. Doherty,[3] Richard J. Riehle, [3] Sachin Borkar, [3] Jose Moran-Mirabal,[4] Robert H. Pelton *[1]

1 Department of Chemical Engineering, McMaster University, 1280 Main Street West, Hamilton, Ontario, Canada, L8S 4L7

[2] Canfor Pulp, Unit 138 - 8610 Glenlyon Parkway, Burnaby, BC, Canada, V5J 0B6

[3] Solenis LLC, 2475 Pinnacle Drive, Wilmington, Delaware, United States of America, 19803

[4] Department of Chemistry and Chemical Biology, McMaster University, 1280 Main Street West, Hamilton, Ontario, Canada, L8S 4M1

Pelton: orcid.org/0000-0002-8006-0745

Moran Mirabal: orcid.org/0000-0002-4811-3085

* corresponding author: peltonrh@McMaster.ca

Keywords: polysoap, comb polymers, nanogels,

Graphical Abstract

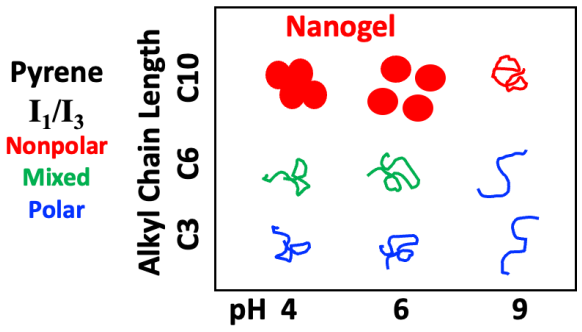

Abstract

A library of hydrophobically modified polyelectrolytes was prepared by reacting linear alkyl amines with poly(ethylene-alt-maleic anhydride), followed by hydrolysis of the residual anhydride groups. Every reacted anhydride gives a pendent alkylamide plus a carboxylic acid group, and the result is a comb architecture. The lengths of the alkyl side chains were 3, 6, 8, or 10 carbons. The density of alkyl side chains was expressed as the fraction of anhydride groups reacted with alkyl amines (25%, 50%, and 75%). The dominant factor influencing the aqueous solution properties is the alkyl chain length. C3 polymers had no pyrene receptive hydrophobic domains. C6 and C8 polymers bound pyrene at pH < 6 and do not give reliable dynamic light scattering (DLS) results. C10 polymers displayed pyrene binding across the pH range and, based on DLS and AFM data, possibly appear as unimolecular nanogel dispersions from pH 7-9. At pH values > 9, our DLS measurements gave low-quality data, whereas at pH<7 both DLS and AFM results indicated nanogel aggregation. The C10 polymer properties were surprisingly insensitive to the degree of hydrophobic substitution over the range of 25-75%. The nanogels with low alkyl contents were slightly more swollen and had high NaCl critical coagulation concentrations compared to the high alkyl content nanogels. These polymers are of particular interest because the non-derivatized maleic moieties in the polymers can form ester linkages to cellulose in an aqueous, catalyst-free process.

Introduction

Presented are the aqueous solution properties of a series of polymers prepared by the reaction of alkylamines with poly(ethylene-alt-maleic anhydride), PEMA, to form a family of hydrophobically modified highly carboxylated polymers designated as HPEMAc – see **Figure 1**. Our interest in these polymers stems from our ongoing efforts to enhance the properties of paper packaging materials as potential replacements for single-use plastic packaging. Previously we have shown that hydrolyzed PEMA can graft onto cellulose surfaces simply by heating the polymer-coated lignocellulose surfaces above 100 °C.[1, 2] Heating regenerates anhydride groups that can form esters with cellulose.[3] This is a convenient route to modified lignocellulose surfaces without catalysts or solvents. There are potential applications for cellulose surfaces with a grafted coating hydrophobically modified PEMA. This contribution describes the synthesis, characterization, and solution properties of a library of HPEMAc polymers, setting the stage for future grafting studies.

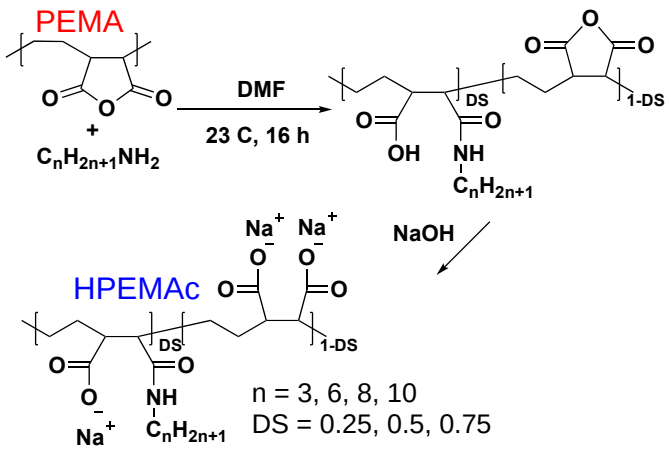

Figure 1 Preparation of hydrophobically modified anionic polyelectrolytes.

Having both ionized carboxylic acid groups and pendent alkyl chains, HPEMAcs are amphiphilic polymers. More specifically, HPEMAc polymers are comb polymers with a variable density of short pendent alkyl chains, an architecture called “polysoap” since the 1950s.[4, 5] Many of the polysoap publications involve alternating copolymers of maleic anhydride (MA) with styrene, olefins, or alkyl vinyl ethers, in some cases yielding structures close to HPEMAc.[6] Described next are some of the critical aspects of MA polysoap behaviors giving context to our work.

Polysoaps are unique in the amphiphilic polymer landscape.[7, 8] Unlike block copolymers that form multimolecular micelles or associative thickeners designed to form macroscopic gels, intramolecular hydrophobic associations dominate polysoap behaviors, particularly at low concentrations.[9] Polysoap characterization in the literature tends to focus on two issues – the association of pendent hydrophobes to form hydrophobic domains and whether or not multiple polymer chains associate. Solution pH and hydrophobic chain length were important parameters in our work. The corresponding literature is now highlighted

Solution pH. The aqueous solution behaviors of MA copolymer polysoaps are dominated by solution pH and the size of the hydrophobic comonomer. At low pH, the backbone charge density is low, and intramolecular hydrophobic association yields dense structures that are often called hypercoils.[10-12] Individual hypercoils can involve one or many polymer chains. And unlike a surfactant micelle, hypercoils contain many hydrophobic domains[13] with a polydisperse size distribution.[6] As pH is raised, the hypercoils often expand, giving a continuum of structures between hypercoils and expanded structures, typical of polyelectrolytes. This process is not a phase transition but an evolution of structures occurring over a broad pH range.

Hydrophobe Size. The influence of linear alkyl chain length on solution properties has been reported. Hydrophobic domains form at low pH when the chain lengths are four carbons and greater.[14] As the hydrophobic chain length grows to 10-12 and greater, the hypercoils persist at high pH where the carboxylic acid groups are fully ionized.[6, 12, 15] At the extreme, C18 seems to be an upper limit above which chain crystallization is a problem.[7] Based on pyrene fluorescence measurements, Anthony and Zana estimated β, the fraction of alkyl pendent chains participating in hydrophobic domains as a function of hydrophobe chain length for poly(MA-alt-vinyl alkyl ether).[16] They found $\beta = 1$ for C16 and $\beta = 0.7$ for C12, with these β values being nearly independent of the extent of ionization. For C10, $\beta = 0.6$ for the uncharged polymer, and the β values decreased with increasing ionization.

Unimolecular vs Multimolecular Hypercoils. The early polysoap research reported very low viscosities for hypercoiled polysoaps [4], leading to the concept of hypercoils consisting of individual polymer molecules. More recently, the paper by Sauvage *et al*. reports light scattering, NMR, and intrinsic viscosity measurements on a range of polysoap structures to determine the extent of polysoap molecule aggregation.[17] Most of their experiments were performed at high pH and intermediate ionic strength. One polymer series was based on poly(maleic anhydride-alt-isobutylene) which was modified using the method shown in **Figure 1**. The hydrophobe chain length seemed to control intra versus intermolecular interactions. Up to the N-octyl derivatives, the structures were unimolecular whereas longer hydrophobes gave aggregates containing about 30 chains.

Other Factors. Backbone charges from ionized carboxylic acids tend to expand polysoap chains, opposing hydrophobic domain and hypercoil formation. Therefore, the tendency to form hydrophobic domains increases with ionic strength, reflecting the screening of electrostatic interactions.[14, 18] Some literature suggests that polysoap behaviors in aqueous solution are not sensitive to the backbone chain length.[9, 14] However an elegant study by Ueda *et al.* showed that low molecular weight polysoaps formed unicore micelles whereas multicore necklaces were formed by high molecular weight polysoaps. [19]

Most of the studies mentioned above involve alternating MA copolymers with one hydrophobe on every repeat unit. A different strategy is needed to vary the average hydrophobe spacing on the MA copolymer platform. McCormick varied the density of 4-butylaniline hydrophobes on 317 kDa poly(MA-alt- ethyl vinyl ether) from 0 to 71 mol% anhydride substitution, using a synthetic approach similar to that shown in **Figure 1**.[20] The polymers were characterized by dynamic light scattering (DLS) and pyrene fluorescence measurements. McCormick's publication appears to be the closest to this contribution; some trends are compared below. Our results build upon the work of McCormick and others by showing the influences on solution properties when varying the hydrophobic chain lengths, the degrees of hydrophobic substitution on the PEMA backbone, and the degree of carboxylic acid ionization.

Experimental

***Materials*.** Poly (ethylene-alt-maleic anhydride), PEMA (MW 100 kDa – 500 kDa), propylamine (≥99%), hexylamine (99%), octylamine (99%), decylamine (99%, GC), pyrene (Puriss, for fluorescence, ≥99.0% (GC)) and anhydrous DMF were purchased from Sigma-Aldrich and used without further purification. Other chemicals were tetrahydrofuran (ACS Reagent Grade, Caledon Laboratories Ltd), poly(diallyl dimethyl ammonium chloride), PDADMAC (BTG Inc. USA), NaCl (Reagent Grade, BioShop Canada Inc.), NaOH and HCl solution (1 M & 0.1 M, LabChem Inc.)

HPEMAc Synthesis. To a solution of 2 g PEMA in 30 mL anhydrous DMF, in a 100 mL round bottom flask was added dropwise, sufficient alkylamine, dissolved in 5 mL of anhydrous DMF to react with either 25%, 50%, or 75% of the PEMA anhydride groups. The reaction mixture was stirred at room temperature for 16 h, after which the reaction mixture was quenched with 10 mL 1 M HCl solution. The product was transferred into a 29 mm diameter dialysis tube (SpectraPor, Spectrum® Labs, 3.5 kDa MWCO), which was submerged in 4 L of pH 1-2 HCl solution. After 3 days and twice a day exchanges of the external solution, the modified polymer was transferred into a glass beaker, and 1 M NaOH solution was added with stirring until the mixture became clear. The solution was transferred into new dialysis tubes. The excess NaOH was removed by exhaustive dialysis against Milli-Q water, and the pH in the dialysis bag was checked every day.

Once the pH was 10, the solution was collected and lyophilized. The degree of substitution (DS) was determined from ^{1}H-NMR and conductometric titration.

Potentiometric titration. The potentiometric titrations were conducted with an auto titrator (MANTECH. Benchtop Titrator Model, MT-10) equipped with a pH probe (PCE-80-PH12000), a temperature probe, and a conductivity meter (Model 4510). 25 mg of HPEMAc was dissolved in 80 mL 0.1 M NaCl solution, and the pH of the solution was lowered to 1.2 by adding 10 M HCl solution. 1 M NaOH standard solution was used as titrant and added in a volume of 10 μL per injection. A 30 s time lag was allowed between two injections to equilibrate the solution. All the titrations were run at 25 ^{o}C from pH 1.2 to 12. A blank titration was performed on the solution in identical salt concentration and pH range but without polymer. The volume of basic solution for ionizing polymer as a function of pH was acquired by subtracting the blank titration curve from the polymer solution titration curves.

Dynamic Light Scattering (DLS) and Electrophoresis. The hydrodynamic diameters and electrophoretic mobilities of hydrophobically modified PEMA were measured with a ZetaSizer Nano ZS, Malvern fitted with a 4 mW He–Ne laser at a scattering angle of 173°. The pH of HPEMAc 0.2 g/L in 1 mM NaCl was adjusted in a range of 9 to 4 by adding 0.1 M HCl. 1 mL sample solutions were placed in polystyrene cuvettes (10 mm, 4.5 mL, SARSTEDT AG & Co. KG, Germany) and equilibrated at 23 ^{o}C for 3 min. The correlation data were analyzed using Zetasizer software (v 7.01) with the CONTIN algorithm, which can provide the size distribution. Electrophoretic mobilities were measured with the same instrument.

Pyrene Fluorescence. HPEMAc stock solutions (40 mM repeating units) were prepared by dissolving HPEMAc sodium salts in 1 mM NaCl solution. A series of polymer solutions were prepared by the dilution of stock solution, and the pH of solutions were adjusted to a range of 4-9 by adding 1 M HCl or 0.1 M HCl. Pyrene as a fluorescence probe was dissolved in THF, giving a solution in a concentration of 100 μM. 80 μL pyrene solution was aliquoted into glass vials, and THF was allowed to evaporate in the dark for 24 h. 4 mL polymer solutions were then added into glass vials yielding a final pyrene concentration of 2 μM, which was within its solubility in water. The mixed solutions were stirred in the dark for 24 h. The fluorescence emission spectra were acquired on a Cary Eclipse Fluorescence Spectrophotometer (Agilent Technologies, Inc. US), using a quartz cuvette with a 10 mm path length (Hellma Analytics). The excitation wavelength was fixed at 337 nm, and the emission spectra were recorded from 360 nm to 410 nm. The slit widths for excitation and emission were 2.5 nm, and the scan speed was set at 200 nm/min. To improve the signal-noise quality, all the scans were performed under Computer Averaging of Transients (CAT) scan mode, which provided the final spectrum after averaging 12 individual scans.

Critical Coagulation Concentrations (CCC). HPEMAc solutions with a repeat unit, RU, concentration of 7.5 mM, were obtained from diluting the stock solutions with 1 mM NaCl solution, and the pH was adjusted to 8. NaCl salts with specific weights targeting ionic strength from 15 mM to 1.5 M were weighed and added into diluted polymer solutions. All the sample solutions were vortexed for 10 sec to dissolve the salts and then transferred into polystyrene cuvettes. Transmittance values at 600 nm relative to 1 mM NaCl solution as a blank were measured from 1 min to 120 h after mixing, employing a spectrophotometer (DU800, Beckman Coulter) with the temperature fixed at 23 ^{o}C. Values for each ionic strength were the means of the results from three independently prepared samples (N = 3), and error bars represent the standard deviations. The CCC values were the salt concentrations at 90% transmittance extrapolated from plots of transmittance versus NaCl concentration.

Atomic Force Microscopy (AFM). To promote the deposition of anionic HPEMAc particles, freshly cleaved mica surfaces (1.5 cm × 1.5 cm, Sigma-Aldrich) were exposed to 10 μL 0.001 N of PDADMAC solution. After 5 min, the excess solution was blotted off, and then mica sheets were rinsed with 1 mM NaCl and blown dry with N_2. 10 μL 0.2 g/L HPEMAc solutions at pH 8 were applied to the treated mica surfaces. The excess polymer solution was blotted off, and the mica surface was dried at room temperature overnight.

AFM height and phase images were collected with a MFP-3D-BIO system (Asylum Research, Oxford Instruments Company, Santa Barbara, CA, USA) in alternating current (AC) mode. Imaging was performed in ambient using high-resolution probes (Hi'Res-C14, μmash) with a tip radius below 1 nm, a typical spring constant of 5.0 N/m, and resonance frequency ranging from 110-220 kHz. The z-maximum height and diameters of the polymer deposits were analyzed by IGOR Pro 6.0 AFM software, and the distribution and average values were determined from a minimum of 100 particles.

Transmission electron microscopy (TEM). 5 μL 0.2 g/L HPEMAc solutions at pH 8 were applied on carbon-coated copper grids (Ultrathin Carbon Film on Lacey Carbon Support Film, TED PELLA, Inc., USA). After 5 min, the excess polymer solution was blotted off, the grids were dried at room temperature overnight and stained by RuO_4 vapor for 30 min. TEM imaging was performed with a JEOL 1200EX TEMSCAN at 80 kV accelerating voltage.

Results and Discussion

HPEMAc, a family of hydrolyzed, hydrophobically modified PEMAs were prepared by reacting linear 1-alkylamines, followed by hydrolysis - **Figure 1**. PEMA is not an ideal starting structure for fundamental studies. High molecular weight, PEMA has a broad molecular distribution typical of maleic anhydride copolymers. [21] Our PEMA was purchased from Sigma-Aldrich, which lists the MW as 100-500 kDa; however, we believe this polymer is equivalent to E400, manufactured by Vertellus. Page 46 in Johnson's Ph.D. thesis is the only published molecular weight distribution of E400 we have found.[22] Based on GPC measurements in water and DMF for E400, hydrolyzed E400, and derivatized E400, he concluded the number average MW for E400 PEMA was 214 kDa, the weight-average was 610 kDa, and the polydispersity index was 2.9. Although it is possible to fractionate the polymer by traditional precipitation methods, [19] we chose not to fractionate because this project was in support of a new cellulose grafting technology employing unfractionated polymer.

HPEMAc Structures. The structures of the HPEMAc polymers are defined by two parameters: 1) DS – the fraction of PEMA anhydrides converted to an alkyl amide plus a carboxylic acid group; and 2) the number of carbon atoms in the pendent alkyl groups – see **Figure 1**. Therefore, specific polymers in this family are designated CxxDSyy, where xx is the number of carbons in the alkyl chain, and yy is the percentual degree of substitution (DS) value. For example, C10DS75 corresponds to a polymer where 75% of the PEMA anhydrides reacted with decylamine. Herein, the concentrations of polymer solutions are expressed as the molarity of repeat units, RU. To convert RU molarity to mass concentrations, we multiply by the average RU molecular weight. The average RU MW depends on the hydrophobic carbon chain lengths and the DS values. Average RU MW values ranging from 193 Da for C3DS25 to 266 Da for C10DS75 are given in **Table S1** in the Supplemental Information.

NMR and conductometric titrations were used to measure the DS. **Table S2** shows that the two techniques gave the same results and that the amide formation reactions were quantitative. ^{1}H NMR spectra of the HPEMAc polymers C3-C10 with DS25-DS75 are shown in **Figure S1** in the Supplemental Information. The yields were very high, and the resulting DS values were close to the feeding ratios.

Solution Properties. The water solubility of the HPEMAc series was measured by transmittance measurements, based on the assumption that polymer solutions with ≥97% transmittance were soluble; the data is in **Figure S2**. C3DS75 was soluble at pH 4 and above. C6, C8, and C10 polymer solutions were turbid at low pH and became soluble over the 6-7 pH range – see **Figure S3**.

The degree of ionization for the HPEMAc series with DS 75%, is plotted as a function of pH in **Figure 2** together with the curve for PEMAc, the unmodified polymer. PEMAc ionization curves have been published [23] and, as shown here, PEMAc ionization increases almost linearly from pH 2 to 10. The C3 HPEMAc curve in **Figure 2** overlaps with the PEMAc curve up to a degree of ionization of 0.5, above which C3DS75 ionizes more readily compared to PEMAc. The C6, C8, and C10 curves are shifted to lower pH values, with the greatest shift corresponding to the longest hydrophobic chain. Based on the optical transmittance values, these polymer solutions are turbid below pH 6, corresponding to 0.8 to 0.9 degrees of ionization. These types of ionization curves have been explained in the literature by hypercoil formation and precipitation at low pH. [10-12]

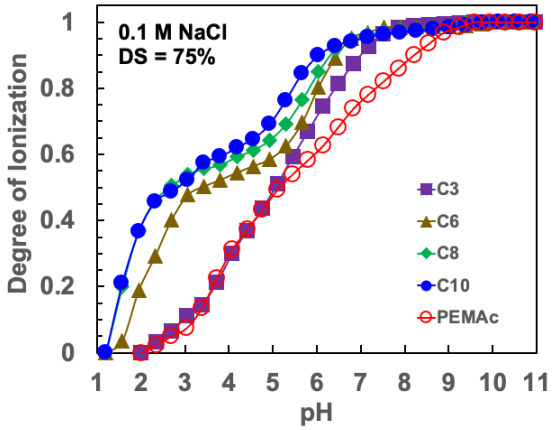

Figure 2 Degree of ionization versus pH for the HPEMAc series with DS =75%.

The HPEMAc solutions were characterized by Dynamic light scattering (DLS). Initial DLS experiments with C3, C6, and C8 solutions did not yield reliable data, whereas C10 polymer did – see example particle size distributions in **Figure S4**. **Figure 3** shows the diameters of the C10 HPEMAc series as a function of the DS and solution pH. The open symbol indicated conditions that did not yield reliable data. Particles were not detected for any of the three C10 polymers at pH values above 9, suggesting the transition to a soluble expanded coil configuration, not characterizable by our DLS instrument. Similarly, below pH 7, the three C10 copolymers underwent aggregation, as evidenced by increasing diameters and breadths of the particle size distributions. Indeed, AFM images of deposited particles from pH 4 suspensions showed large C10DS75 particles – see **Figure S5**.

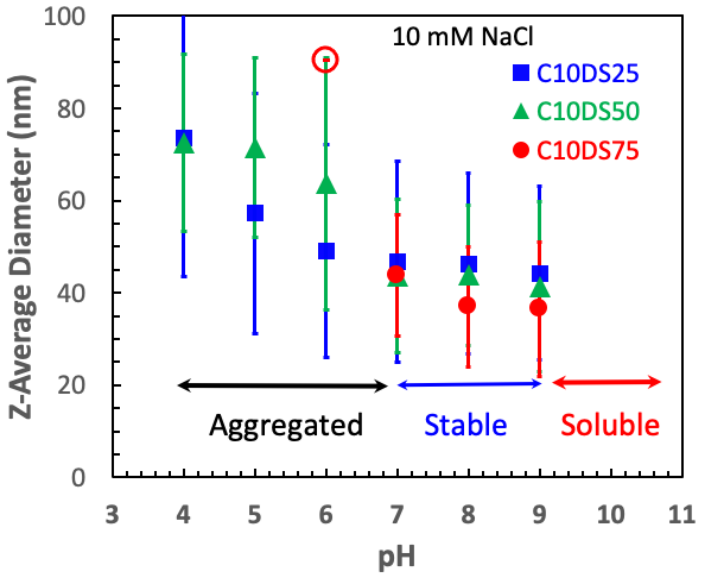

Figure 3 The Z-average hydrodynamic diameters of 0.2 g/L HPEMAc C10 solutions measured by DLS. The error bars portray the standard deviations of the particle size distributions. The open symbol denotes poor data quality.

Over the pH range 7-9, good quality DLS data were obtained for the three C10 polymers with average diameters decreasing slightly with increased hydrophobic substitution. The diameter distributions were monomodal, and the error bars in **Figure 3** portray the standard deviation of the particle size distributions calculated as the product of the PDI (polydispersity index) times the mean diameter. [24] In the next section, we provide limited evidence that the C10 particles were nanogels, with each gel containing an individual HPEMAc chain. The average diameter of C10DS75 at pH 8 is 37 nm (**Figure 3**). Assuming a monomolecular nanogel, based on the number average MW, the mass

fraction of polymer in the nanogel is 0.03, and based on the mass average MW, the mass fraction of polymer is 0.08. The nanogel particles have no covalent crosslinks. However, we propose that C10 chains associate leading to physical crosslinks. In terms of polysoap semantics, the C10 nanogels are hypercoils that are colloidally stable and sufficiently dense to give good DLS and microelectrophoresis results in the pH range 7-9.

McCormick *et al*. reported DLS diameters from pH 4 to 9 for 4-butylaniline modified poly(maleic anhydride-alt-ethyl vinyl ether).[20] Their results showed increased diameter with increasing pH for all their samples, much like one would expect for polycarboxylic polyelectrolytes. We believe our samples also expanded above pH 9, however, our DLS results were too unreliable to include.

Figure 4 shows the particle size distributions for the C10 polymers at pH 7, 8, and 9, as well as TEM images of particles isolated from pH 8 dispersions. Below we propose that in the pH range 7-9, the particles contain a single polymer chain. If correct, the broad particle size distributions at pH 7-9 reflect the polydispersity of the parent PEMA molecular weight distribution which has a PDI of 2.8.

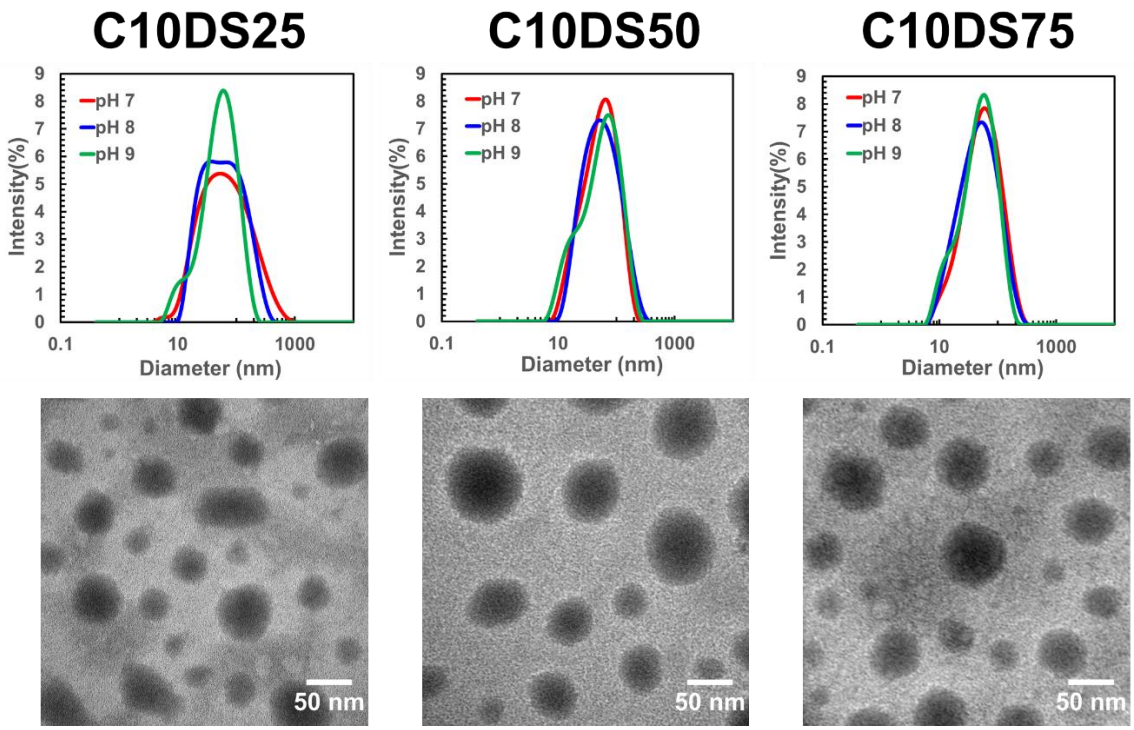

Figure 4 DLS particle size distributions at three pH values and TEM images of dried nanogels deposited from pH 8 dispersions and stained with RuO_4

Yamamoto showed that the aqueous solution properties of hydrophobically modified polymers can depend on sample history.[25] Structures formed under a particular condition

can be locked by hydrophobic interactions and do not respond to changes in solution conditions. They recommended that when solubilizing lyophilized samples, one should start with conditions where the polymer can form an expanded coil. Most of our results correspond to samples that were lyophilized at pH 10 where we believed they were isolated expanded coils. The dried polymers were first dissolved at pH 10 followed by pH adjustment. Lyophilization and re-dissolution at pH 4 or 6 gave larger, multimodal particle size distributions – see **Figure S6**

The electrophoretic mobilities of the C10 HPEMAc series are summarized in **Table 1**. The mobilities increase with pH for the three DS values, reflecting the pH dependence of ionization. Additionally, the higher the DS value, the lower the mobility which is consistent with the loss of a carboxylic acid group for every added hydrophobe.

Table 1 The electrophoretic mobilities of the C10 series as a function of pH in 1 mM NaCl.

	Electrophoretic Mobility (10^{-8} m^2 /V·s)		
pH	C10DS25	C10DS50	C10DS75
4	-2.1±0.11	-1.9±0.1	-1.6±0.1
6	-2.5±0.15	-2.4±0.08	-1.9±0.1
8	-2.8±0.14	-2.6±0.08	-2.5±0.1

Figure 5A shows the influence of salt concentration on the electrophoretic mobilities of the C10 series. Above 100 mM the electrophoretic mobilities decreased with increasing salt concentration and the values were not sensitive to the HPEMAc DS values. The results were more scattered at lower ionic strengths.

Figure 5B shows the corresponding optical transmittance values at 600 nm as a function of the salt concentrations. These measurements were taken after 120 hours of standing time. The plots corresponding to shorter standing times are shown in **Figure S7**. We arbitrarily assigned the critical coagulation concentration, CCC, as the interpolated salt concentrations where the transmittance dropped to 90%, indicating the onset of aggregation.

Figure 5C plots the critical coagulation concentrations (CCC values), taken from **Figure 5B**, as a function of the corresponding electrophoretic mobilities interpolated from **Figure**

5A. Each point in **Figure 5C** represents a different DS value, and therefore a different total charge content. As might be expected, the higher the charge content (i.e., the lower the DS), the higher the CCC. Furthermore, the higher the CCC the more negative the corresponding electrophoretic mobility. Perhaps the most significant observation based on **Figure 5C** is that all the CCC values are high compared to many electrostatically stabilized colloids. For example, in Buscall and Ottewill's review of latex colloidal properties, the NaCl CCCs of many anionic latexes were much less than 200 mM.[26] The high values in **Figure 4** are more reminiscent of microgels where the combined Hamaker constant of water-swollen particles is low. [27]

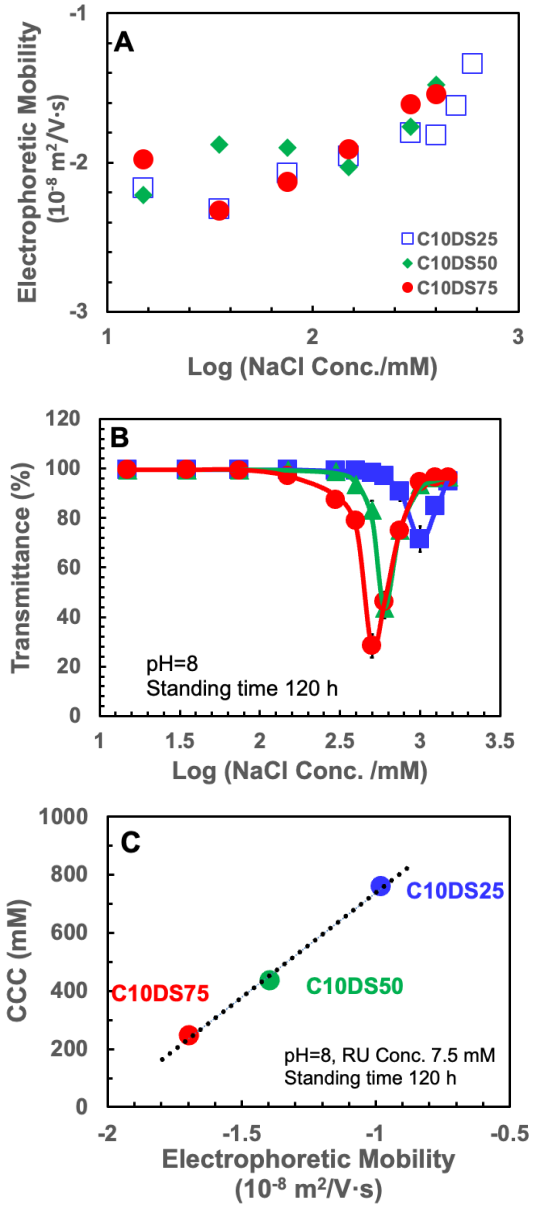

Figure 5 The influence of NaCl concentration on the electrophoretic and colloidal stability properties of the C10 series; A) electrophoretic mobility versus salt concentration; B) optical transmittance (600 nm) versus salt concentration; and C) log CCC versus electrophoretic mobility at the CCC (i.e. combining A&B).

Unimolecular Hydrophobically-Crosslinked Nanogels. The above results suggest that in the pH range 7-9, the C10 series are present as negatively charged colloidally stable particles, below the CCC, with monomodal and approximately log-normal particle size distributions. As summarized in the introduction, the older literature has claimed that polysoaps can exist as "unimolecular micelles". We now present evidence that the C10 nanoparticles at pH 8 have one polymer chain per particle.

Atomic force microscopy was employed to characterize C10 particles. Freshly cleaved mica surfaces, coated with an adsorbed layer of poly(diallyldimethyl ammonium chloride), were exposed to 0.2 g/L C10 solutions at pH 8 and then were rinsed after 5 min and allowed to dry. Example images are shown in **Figure 6**. The top row shows the height images for the three DS values whereas the bottom row shows the phase images. Like the DLS and TEM results, the AFM images suggest a wide range of sizes. **Figure 6** shows representative AFM images and **Figure 7** shows histograms of dried particle heights and diameters based on 100 particles measured per sample.

Our strategy was to estimate the amount of polymer in the dried particles using the measured heights and spot diameters in AFM images. The corresponding mass of dry polymer was estimated assuming dried spots were present as spherical caps and that the density of the dry polymer was 1 g/mL. Dividing dry mass per dried particle by the mass of a C10 chain then gives an estimate of the number of chains per hypercoil in the original suspension.

The 3D height information provided from AFM is relative to the surface of the mica support. Heights for the larger particles will be more accurate since they have the biggest difference compared with the background roughness of the surface. The smallest spots have heights around 1 nm which is the same scale as the roughness of mica. Although we used a very sharp tip with a radius of less than 1 nm, we believe the small particle results were the least reliable.

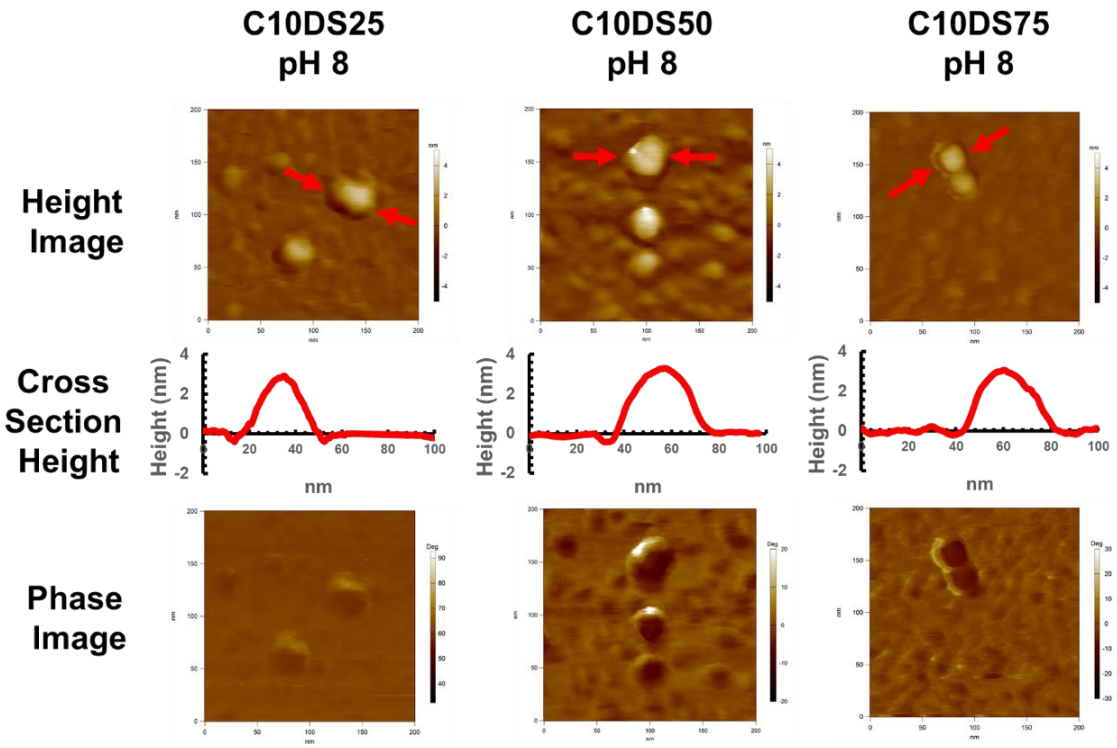

Figure 6 AFM height and phase images (200 nm x 200 nm) of dried C10 polymers deposited on freshly cleaved mica with an adsorbed layer of cationic polymers. The red arrows indicate specific particles whose dimensions are given in **Table 2**.

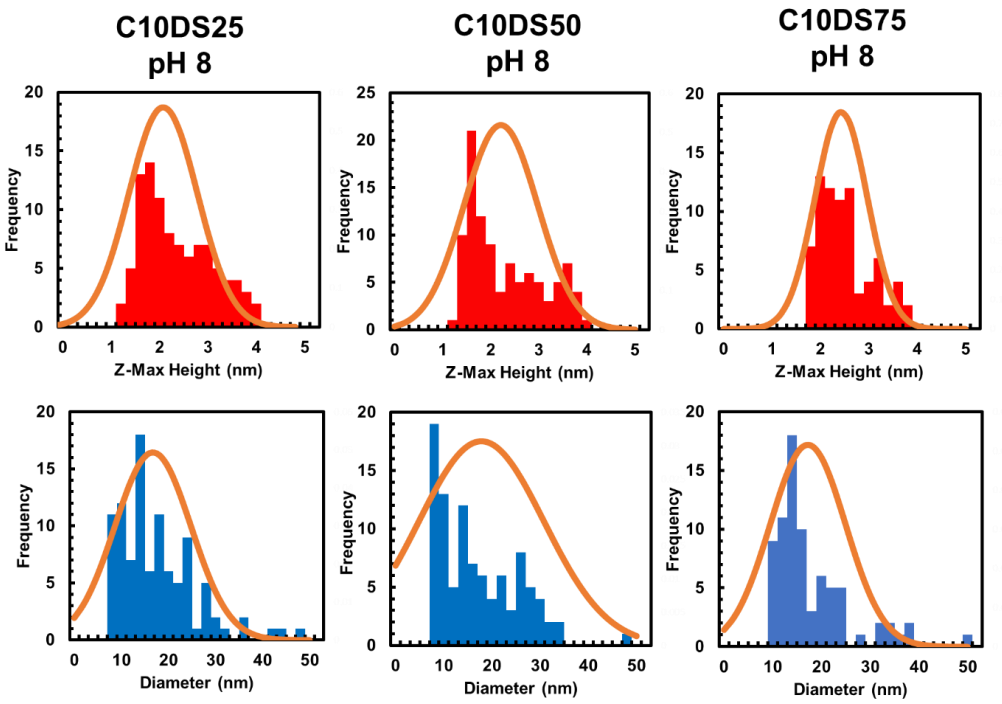

Figure 7 Histograms of dried particle heights and diameters obtained from scans of a 1 μm x 1 μm area.

Table 2 summarizes our AFM and modeling results. The top three rows of AFM heights and diameters were based on the histograms in **Figure 7**. The corresponding volumes were calculated from the diameters and heights assuming the shapes were spherical caps. RU MW were the molecular weights of the average repeat units based on the polymer structures. DPn is the degree of polymerization of the starting PEMA polymer. The value 1697 is based on the number average PEMA MW of 214 kDa. The corresponding number of polymer chains per particle for this group was 0.4. Of course, the lowest number of chains per particle must be ≥ 1. As described above, we think the height distributions were suspect particularly for the small particles.

The second set of results labeled "Individual Red Arrow" refers to measurements of the single large particles indicated by the red arrows in **Figure 6**. Clearly, 1 particle per polymer type is poor statistics, however, the AFM analysis of the largest particles should be the most accurate. Since we have chosen the largest particles, we have also used DPm, the degree of polymerization based on the weight average MW of PEMA of 610 kDa, to reflect the larger end of the molecular weight distribution. These isolated particles appeared to each contain one polymer chain. We acknowledge that these are very rough estimates, however, because the results are so close to one chain per particle, we believe they are useful.

Table 2 Mean dimensions from histograms in **Figure 7** as well as the estimated number of polymer chains per hypercoil.

	Average AFM Spot Size			Polymer Properties		
Mean Values from Histograms	**Height (nm)**	**Diam. (nm)**	**Volume (nm^3)**	**RU MW Da**	**DPn**	**Chains per Particle**
C10DS25	2.27	16.7	255	217	1700	0.415
C10DS50	2.21	17.8	281	247	1700	0.403
C10DS75	2.43	17.2	290	276	1700	0.372
Individual Red Arrows					**DPm**	
C10DS25	2.88	34.3	1343	217	4840	0.768
C10DS50	3.18	40.8	2096	247	4840	1.06
C10DS75	3.07	40.4	1983	276	4840	0.892

Hydrophobic Domains. To gain more insight into HPEMAc solution behaviors, pyrene emission spectra were recorded as a function of pH for the HPEMAc and the spectra for 4 polymers and six pH values are shown in **Figure S8**. The results, summarized in **Figure 8**, show the intensity ratio of the first to the third peak, I_1/I_3 (374 nm/385nm) which is a measure of the polarity of the pyrene environment. A typical I_1/I_3 value for water is 1.7-1.9 [28] and for hexane is 0.6.[29] However, the exact values are very sensitive to the excitation wavelength.[16] The polymer RU concentration for most of the results in **Figure 8** was 7.5 mM, however, the pH 8 results include 37.5 mM data shown as open symbols. Considering first the lower concentration data portrayed by solid symbols. PEMAc is a very hydrophilic polymer. From pH 4-9 the PEMAc I_1/I_3 ratio is close to 1.6, the value for water. At the other extreme, the I_1/I_3 ratio for C10DS75 is below 1 over the entire pH range. C3DS75 is an interesting case because despite being soluble in pH 4-9, the I_1/I_3 ratio is lower than that of PEMAc suggesting some pyrene binding. C6 and C8 show the most pH dependence. At low pH where the chains are collapsed, the I_1/I_3 ratios are low whereas above pH 7 the I_1/I_3 ratios are higher, suggesting a decrease in volume of pyrene-compatible hydrophobic domains and/or an increase in the average polarity of the domains with increasing pH.

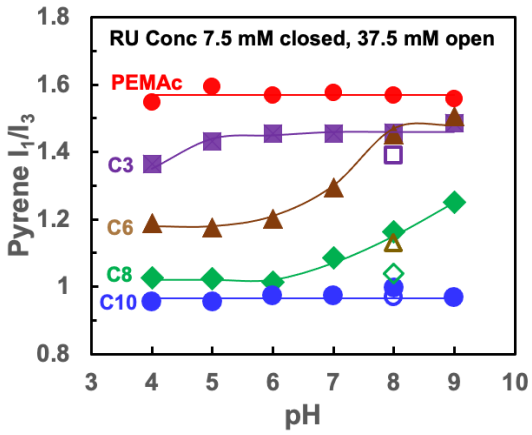

Figure 8 The I_1/I3 (374 nm/385nm) ratios of the pyrene emission spectra for HPEMAc solutions in 1 mM NaCl. The excitation wavelength was 337 nm. The open symbols correspond to a higher RU of 37.5 mM. The DS of all polymers was 75% and the pyrene concentration was 2 μM. The fluorescence spectra are shown in **Figure S8** in the Supplemental Information.

When I_1/I_3 ratios are measured as a function of polysoap concentration at constant pH, sigmoidal shaped curves are obtained where the transition region is stretched over a 3-4 decades of polymer concentration.[16, 18, 30, 31] At the low polymer concentration extreme, the I_1/I_3 ratio is close to that of water since most of the pyrene is in water. At the high polymer concentration limit, most of the pyrene is associated with polymer giving a low I_1/I_3 ratio. For C6DS75 and C8DS75 the I_1/I_3 ratios at pH 8 for 37.5mM copolymer concentration were significantly lower than that observed with 7.5 mM solution. By contrast, the C10DS75 ratio was independent of copolymer concentration suggesting most of the pyrene was bound to hydrophobic domains at both concentrations.

Conclusions

The reaction of amino-terminated alkanes with poly(ethylene-alt-maleic anhydride), followed by hydrolysis of unreacted anhydrides, is a convenient route to HPEMAc, a family of polyelectrolytes bearing pendent, linear alkylamide hydrophobes. The polymer properties can be fine-tuned by two independent parameters, the alkyl chain length, and the DS, the fraction of PEMA anhydride groups converted to an amide plus a carboxylic acid.

The HPEMAc polymers with alkyl chain lengths from C6 to C10 show the classic behaviors of polysoaps, where intramolecular hydrophobic interactions dominate the

behaviors in solution including hypercoil-to-expanded coil transitions when the pH is increased. For example, the C10, the decylamide derivative, was present as an expanded coil at pH 10. Lowering the pH to 7-9 yields colloidally stable small particles that have nano-hydrogel properties that can be measured by dynamic light scattering and electrophoresis. The mass of dried polymer particles was estimated from AFM measurements giving approximate values giving limited support for the proposal that some of the hydrogel particles could be unimolecular. Based on a Z-average hypercoil diameter of 37 nm and the number average molecular weight, the polymer mass fraction in a C10DS75 unimolecular hypercoil nanogel is ~0.03. Comparing the degree of C10 substitution from DS = 25% to DS = 75%, the average hypercoil diameters decreased slightly from 44 to 37 and the electrophoretic mobilities decreased slightly from -2.8 mobility units to -2.5 reflecting the consumption of carboxylic acid groups by the amide substitution. Finally, lowering the pH below 7 induced aggregation, resulting in multiparticle aggregates. The pH corresponding to the onset of aggregation increased with the degree of decyl substitution.

Pyrene I_1/I_3 ratio measurements indicated the presence of hydrophobic domains sufficiently large to lower the polarity around absorbed pyrene. The C10 domains remained sufficiently intact through the hypercoil-to-expanded coil transition, to show a low I_1/I_3 ratio from pH 4 to 9. C6 and C8 polymers had pyrene receptive domains at pH 4 but these disappeared as the chains became expanded coils. The C3 polymer showed evidence of some pyrene binding at pH 4.

In ongoing studies, we are grafting HPEMAc polymers to cellulose surfaces via the unreacted succinic acid moieties. [1, 2] The current results will help us understand the impacts of solution properties on the structures of grafted HPEMAc films on cellulose surfaces. Our primary concern in this study was identifying the solution conditions leading to HPEMAc particle formation or macroscopic phase separation. The extent of unimolecular particle formation remains an open question.

Author Contributions

Xiao Wu: Investigation, Methodology, Writing-Original Draft **Zhen Hu**: Investigation, **Paul Bicho:** Funding acquisition, Conceptualization **Erin A.S. Doherty**: Funding acquisition, Conceptualization, Writing-Review and Editing **Richard J. Riehle**: Writing-Review and Editing **Sachin Borkar**: Writing-Review and Editing **Jose Moran-Mirabal:** Writing-Review and Editing **Robert Pelton:** Conceptualization, Project Administration, Supervision, Writing-Review and Editing, Fund acquisition.

Supplemental Information

The Supplemental Information includes: repeat unit average molecular weights as a function of DS and alkyl chain length; comparison of DS values from NMR vs conductometric titration; proton NMR spectra of the HPEMAc polymers; HPEMAc solution transmittance as a function of pH and polymer concentration; DLS particle size distributions for C3-C8 polymers that did not give high-quality data; AFM images deposited C10DS75 aggregates formed at pH 4; DLS particle size distributions showing the impacts of the freeze-drying pH and dissolution pH; raw optical transmittance values; and, the complete pyrene emission spectra for the HPEMAc series.

Acknowledgments

Ms. Marcia Reid, McMaster Health Sciences is acknowledged for help with electron microscopy. We thank the Natural Sciences and Engineering Research Council of Canada (NSERC) and our industrial partners, Solenis Canada and Canfor for funding this project. R. H. Pelton holds the Canada Research Chair in Interfacial Technologies and J. Moran-Mirabal holds the Canada Research Chair in Micro- and Nanostructured Materials.

References

(1) Zhang, H.; Bicho, P.; Doherty, E. a. S.; Riehle, R. J.; Moran-Mirabal, J.; Pelton, R. H. High-Yield Grafting of Carboxylated Polymers to Wood Pulp Fibres. *Cellulose* **2021,** *28*, 7311–7326. https://doi.org/10.1007/s10570-021-04016-0

(2) Zhang, H.; Bicho, P.; Doherty, E. a. S.; Riehle, R. J.; Moran-Mirabal, J.; Pelton, R. H. High Yield Poly(Ethylene-Alt-Maleic Acid) Grafting to Wood Pulp While Minimizing Fibre/Fibre Wet Adhesion. *Biomacromolecules* **2021,** *22*, 3060–3068. https://doi.org/10.1021/acs.biomac.1c00511

(3) Yang, C. Q.; Wang, X. Formation of Cyclic Anhydride Intermediates and Esterification of Cotton Cellulose by Multifunctional Carboxylic Acids: An Infrared Spectroscopy Study. *Text. Res. J.* **1996,** *66*, 595-603. https://doi.org/10.1177/004051759606600908

(4) Strauss, U. P.; Jackson, E. G. Polysoaps. I. Viscosity and Solubilization Studies on an N-Dodecyl Bromide Addition Compound of Poly-2-Vinylpyridine. *J. Polym. Sci.* **1951,** *6*, 649-659. https://doi.org/10.1002/pol.1951.120060515

(5) Strauss, U. P.; Gershfeld, N. L. The Transition from Typical Polyelectrolyte to Polysoap. I. Viscosity and Solubilization Studies on Copolymers of 4-vinyl-N-Ethylpyridinium Bromide and 4-vinyl-Nn-Dodecylpyridinium Bromide. *J. Phys. Chem.* **1954,** *58*, 747-753. https://doi.org/10.1021/j150519a013

(6) Binana-Limbele, W.; Zana, R. Fluorescence Probing of Microdomains in Aqueous Solutions of Polysoaps. 2. Study of the Size of the Microdomains. *Macromolecules* **1990,** *23*, 2731-2739. https://doi.org/10.1021/ma00212a024

(7) Laschewsky, A., Molecular Concepts, Self-Organisation and Properties of Polysoaps. In *Polysoaps/Stabilizers/Nitrogen-15 Nmr*, Springer Berlin Heidelberg: Berlin, Heidelberg, 1995; pp 1-86.

(8) Tonge, S. R.; Tighe, B. J. Responsive Hydrophobically Associating Polymers: A Review of Structure and Properties. *Adv. Drug Delivery Rev.* **2001,** *53*, 109-122. https://doi.org/10.1016/S0169-409X(01)00223-X

(9) Kramer, M. C.; Steger, J. R.; Hu, Y.; McCormick, C. L. Water-Soluble Copolymers: 66. Phase Transfer Studies of Structural and Environmental Effects on Domain Organization in Aqueous Solutions of Hydrophobically Modified Poly(Sodium Maleate-Alt-Ethyl vinyl Ether)S. *Polymer* **1996,** *37*, 4539-4546. https://doi.org/10.1016/0032-3861(96)00289-3

(10) Dubin, P.; Strauss, U. P. Hydrophobic Hypercoiling in Copolymers of Maleic Acid and Alkyl vinyl Ethers. *J. Phys. Chem.* **1967,** *71*, 2757-2759. https://doi.org/10.1021/j100867a070

(11) Strauss, U. P.; Schlesinger, M. S. Effects of Alkyl Group Size and Counterion Type on the Behavior of Copolymers of Maleic Anhydride and Alkyl vinyl Ethers. 2. Fluorescence of Dansylated Copolymers. *J. Phys. Chem.* **1978,** *82*, 1627-1632. https://doi.org/10.1021/j100503a011

(12) Chu, D. Y.; Thomas, J. Photophysical and Photochemical Studies on a Polymeric Intramolecular Micellar System, Pa-18k2. *Macromolecules* **1987,** *20*, 2133-2138. https://doi.org/10.1021/ma00175a015

(13) Hsu, J. L.; Strauss, U. P. Intramolecular Micelles in a Copolymer of Maleic Anhydride and Hexyl vinyl Ether: Determination of Aggregation Number by Luminescence Quenching. *J. Phys. Chem.* **1987,** *91*, 6238-6241. https://doi.org/10.1021/j100308a033

(14) Dubin, P. L.; Strauss, U. P. Hydrophobic Bonding in Alternating Copolymers of Maleic Acid and Alkyl vinyl Ethers. *J. Phys. Chem.* **1970,** *74*, 2842-2847. https://doi.org/10.1021/j100708a020

(15) Hu, Y.; Smith, G. L.; Richardson, M. F.; McCormick, C. L. Water Soluble Polymers. 74. pH Responsive Microdomains in Labeled N-Octylamide-Substituted Poly(Sodium Maleate-Alt-Ethyl vinyl Ethers): Synthesis, Steady-State Fluorescence, and Nonradiative Energy Transfer Studies. *Macromolecules* **1997,** *30*, 3526-3537. https://doi.org/10.1021/ma9613502

(16) Anthony, O.; Zana, R. Fluorescence Investigation of the Binding of Pyrene to Hydrophobic Microdomains in Aqueous Solutions of Polysoaps. *Macromolecules* **1994,** *27*, 3885-3891. https://doi.org/10.1021/ma00092a031

(17) Sauvage, E.; Plucktaveesak, N.; Colby, R. H.; Amos, D. A.; Antalek, B.; Schroeder, K. M.; Tan, J. S. Amphiphilic Maleic Acid-Containing Alternating Copolymers—2. Dilute Solution Characterization by Light Scattering, Intrinsic Viscosity, and Pgse Nmr Spectroscopy. *J. Polym. Sci., Part B: Polym. Phys.* **2004,** *42*, 3584-3597. https://doi.org/10.1002/polb.20201

(18) Petit-Agnely, F.; Iliopoulos, I.; Zana, R. Hydrophobically Modified Sodium Polyacrylates in Aqueous Solutions: Association Mechanism and Characterization of the Aggregates by Fluorescence Probing. *Langmuir* **2000,** *16*, 9921-9927. https://doi.org/10.1021/la000709j

(19) Ueda, M.; Hashidzume, A.; Sato, T. Unicore−Multicore Transition of the Micelle Formed by an Amphiphilic Alternating Copolymer in Aqueous Media by Changing Molecular Weight. *Macromolecules* **2011,** *44*, 2970-2977. https://doi.org/10.1021/ma102635y

(20) McCormick, C. L.; Hoyle, C. E.; Clark, M. D. Water-Soluble Copolymers: 26. Fluorescence Probe Studies of Hydrophobically Modified Maleic Acid-Ethyl vinyl Ether Copolymers. *Polymer* **1992,** *33*, 243-247. https://doi.org/10.1016/0032-3861(92)90979-7

(21) Reinhardt, S.; Steinert, V.; Werner, K. Investigations on the Dissociation Behaviour of Hydrolyzed Alternating Copolymers of Maleic Anhydride and Propene—I. Potentiometric Titrations. *Eur. Polym. J.* **1996,** *32*, 935-938. https://doi.org/10.1016/0014-3057(96)00028-6

(22) Johnson, D. New Applications for Poly (Ethylene-Alt-Maleic Anhydride). Ph.D. Thesis, Durham University, 2010.

(23) Bianchi, E.; Ciferri, A.; Parodi, R.; Rampone, R.; Tealdi, A. Ethylene-Maleic Anhydride Copolymers and Derivatives. Potentiometric Titrations and Interactions with Polypeptides. *J. Phys. Chem.* **1970,** *74*, 1050-1056. https://doi.org/10.1021/j100700a014

(24) Malvern. Dynamic Light Scattering: An Introduction in 30 Minutes *Technical Note Malvern, MRK656-01* [Online], 2012, p. 1-8. https://warwick.ac.uk/fac/cross_fac/sciencecity/programmes/internal/themes/am2/booking/particlesize/intro_to_dls.pdf.

(25) Yamamoto, H.; Hashidzume, A.; Morishima, Y. Micellization Protocols for Amphiphilic Polyelectrolytes in Water. How Do Polymers Undergo Intrapolymer Associations? *Polym. J. (Tokyo, Jpn.)* **2000,** *32*, 745-752. https://doi.org/10.1295/polymj.32.745

(26) Buscall, R.; Ottewill, R., The Stability of Polymer Latices. In *Polymer Colloids*, Buscall, R.; Corner, T.; Stageman, J. F., Eds. Elsevier: 1985; pp 141-217.

(27) Pelton, R. Temperature-Sensitive Aqueous Microgels. *Adv. Colloid Interface Sci.* **2000,** *85*, 1-33. https://doi.org/10.1016/S0001-8686(99)00023-8

(28) Dong, D. C.; Winnik, M. A. The Py Scale of Solvent Polarities. Solvent Effects on the Vibronic Fine Structure of Pyrene Fluorescence and Empirical Correlations with Et and Y Values. *Photochemistry and Photobiology* **1982,** *35*, 17-21. https://doi.org/10.1111/j.1751-1097.1982.tb03805.x

(29) Kalyanasundaram, K.; Thomas, J. Environmental Effects on Vibronic Band Intensities in Pyrene Monomer Fluorescence and Their Application in Studies of Micellar Systems. *JACS* **1977,** *99*, 2039-2044. https://doi.org/10.1021/ja00449a004

(30) Liang, L.; Yao, P.; Jiang, M. Structural Transformation of Apocytochrome C Induced by Alternating Copolymers of Maleic Acid and Alkene. *Biomacromolecules* **2005,** *6*, 2748-2755. https://doi.org/10.1021/bm050250d

(31) Qiu, Q.; Lou, A.; Somasundaran, P.; Pethica, B. A. Intramolecular Association of Poly(Maleic Acid/Octyl vinyl Ether) in Aqueous Solution. *Langmuir* **2002,** *18*, 5921-5926. https://doi.org/10.1021/la0118356

Supplementary Information

Solution Properties of Hydrophobic Derivatives of Poly(ethylene-alt-maleic acid)

Xiao Wu,[1] Zhen Hu,[1] Paul Bicho,[2] Erin A.S. Doherty,[3] Richard J. Riehle, [3] Sachin Borkar, [3] Jose Moran-Mirabal,[4] Robert H. Pelton *[1]

[1]Department of Chemical Engineering, McMaster University, 1280 Main Street West, Hamilton, Ontario, Canada, L8S 4L7

[2] Canfor Pulp, Unit 138 - 8610 Glenlyon Parkway, Burnaby, BC, Canada, V5J 0B

[3] Solenis LLC, 2475 Pinnacle Drive, Wilmington, Delaware, United States of America, 19803

[4] Department of Chemistry and Chemical Biology, McMaster University, 1280 Main Street West, Hamilton, Ontario, Canada, L8S 4M1

Pelton: orcid.org/0000-0002-8006-0745

Moran Mirabal: orcid.org/0000-0002-4811-3085

* corresponding author: peltonrh@McMaster.ca

Table S1 The average repeat unit, RU, molecular weight (Da) for the sodium salts of the copolymers. The sodium salt of hydrolyzed PEMA has a RU molecular weight of 188 Da.

Degree of Substitution	**RU Molecular Weight (Da) Number of Alkyl Carbons**			
	3	**6**	**8**	**10**
25%	193	203	210	217
50%	198	218	233	247
75%	202	234	255	266

Table S2 COMPARISON of ^{1}H-NMR and conductometric DS values for C10 polymers.

Sample ID	Anhydride:amine mole/mole	DS determined from ^{1}H-NMR (%)	DS determined from conductometric titration (%)
C3DS75	1:0.75	75	74
C6DS75	1:0.75	75	75
C8DS75	1:0.75	75	75
C10DS25	1:0.25	25	25
C10DS50	1:0.50	50	50
C10DS75	1:0.75	75	74

NMR structures. ^{1}H-NMR spectra were recorded to confirm the final structure of PEMAc-*g*-hydrophobes. In the ^{1}H-NMR spectrum shown in **Figure S1**, the characteristic chemical shifts of grafted hydrophobes were labeled and integrated. The chemical shift of 2.8-3.4 ppm (a) is assigned to the CH_2 groups closest to the amide bonds from alkyl side chains. And the chemical shift of 0.5-0.9 ppm (e, f) refers to the protons (-C*H*$_2$C*H*$_3$) on the last two carbon from the end of the alkyl side chain. The other protons attached to the carbons from the middle section of the alkyl chain display chemical shifts merged with the protons from the ethylene domains on the PEMAc backbone as shown from the wide peak of 0.9-1.8 ppm. The chemical shift of 2.0-2.5 ppm (b) is characteristic of the protons (-C*H*(C=O)-C*H*(C=O)-) from succinic units on the PEMAc backbone. The degree of substitution (DS) of the grafted alkyl side chain is calculated from the ratio of the integral of peak (a) to the peak (b), where peak (a) indicates the two protons nearest the amide bonds and peak (b) indicates the two protons in the succinic unit on PEMAc backbone. The total charge of the PEMAc-hydrophobes was also determined from conductometric titration. The DS values calculated from the carboxylate groups contents are also summarized in Table S1. The DS obtained from both ^{1}H-NMR and conductometric titration are nearly identical to the feeding ratio of amine to anhydride.

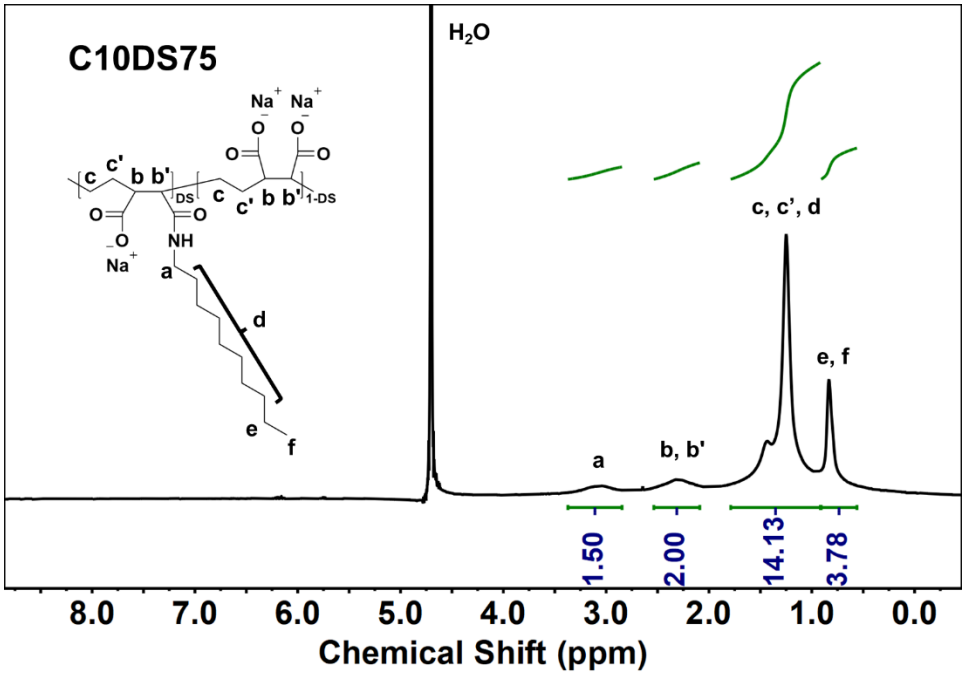

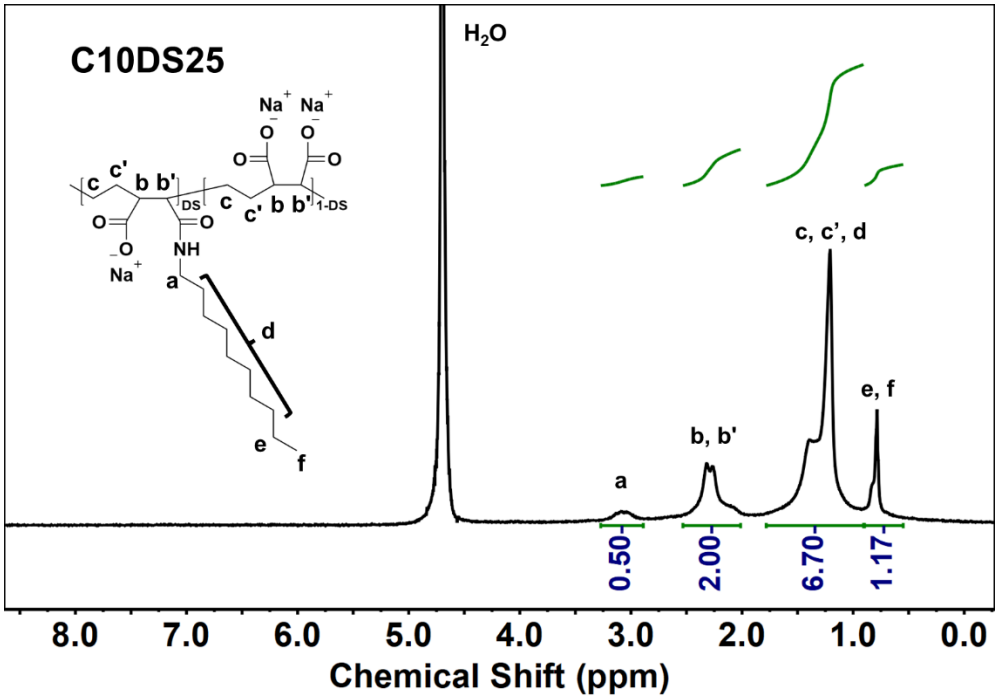
C10DS25
H2O
c, c', d
e, f
b, b'
a
0.50
2.00
6.70
1.17
8.0
7.0
6.0
5.0
4.0
3.0
2.0
1.0
0.0
Chemical Shift (ppm)

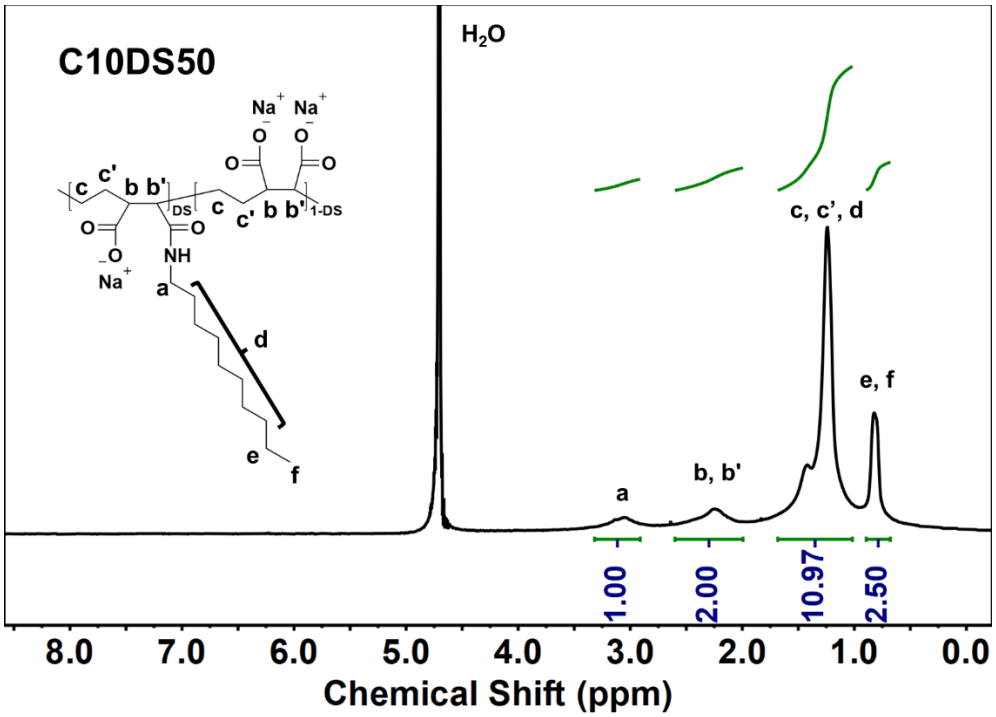
C10DS50
H2O
c, c', d
e, f
b, b'
a
1.00
2.00
10.97
2.50
8.0
7.0
6.0
5.0
4.0
3.0
2.0
1.0
0.0
Chemical Shift (ppm)

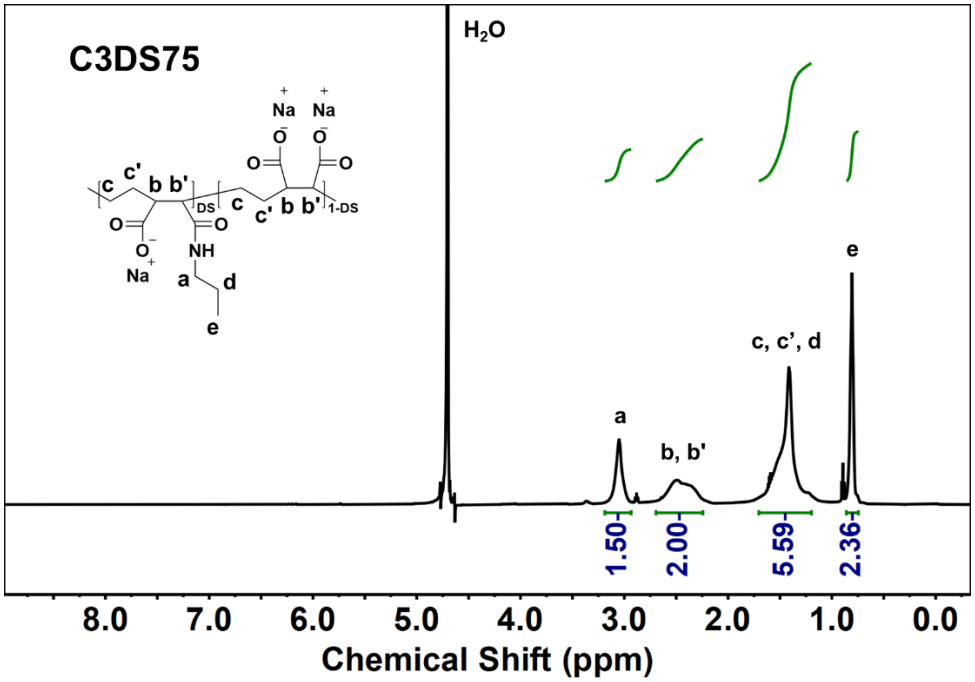
C3DS75
H2O
a
b, b'
c, c', d
e
1.50
2.00
5.59
2.36
8.0
7.0
6.0
5.0
4.0
3.0
2.0
1.0
0.0
Chemical Shift (ppm)

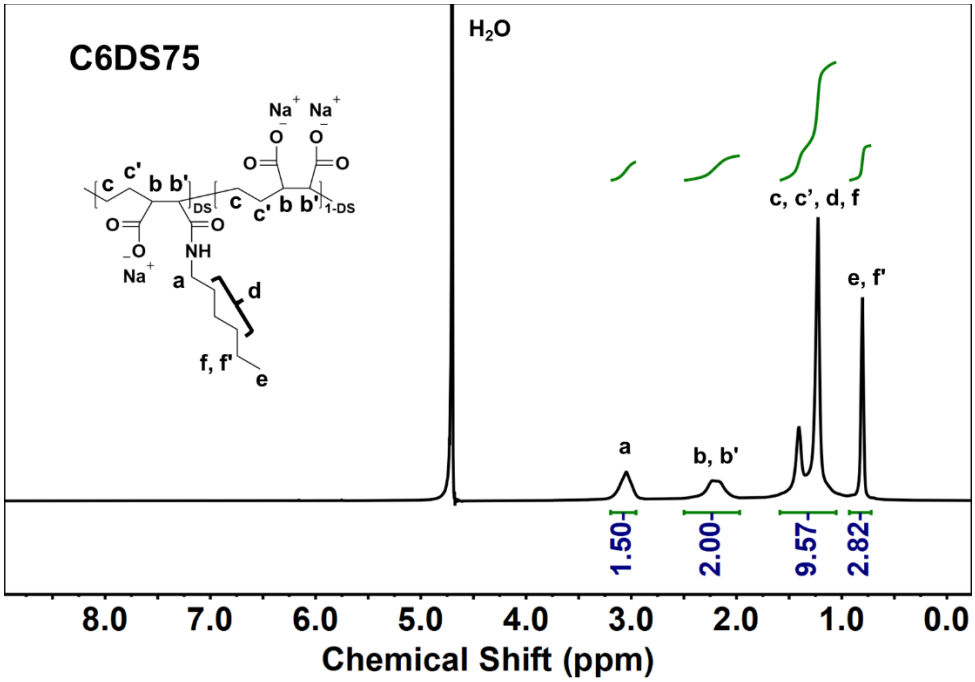
C6DS75
H2O
a
b, b'
c, c', d, f
e, f'
1.50
2.00
9.57
2.82
8.0
7.0
6.0
5.0
4.0
3.0
2.0
1.0
0.0
Chemical Shift (ppm)

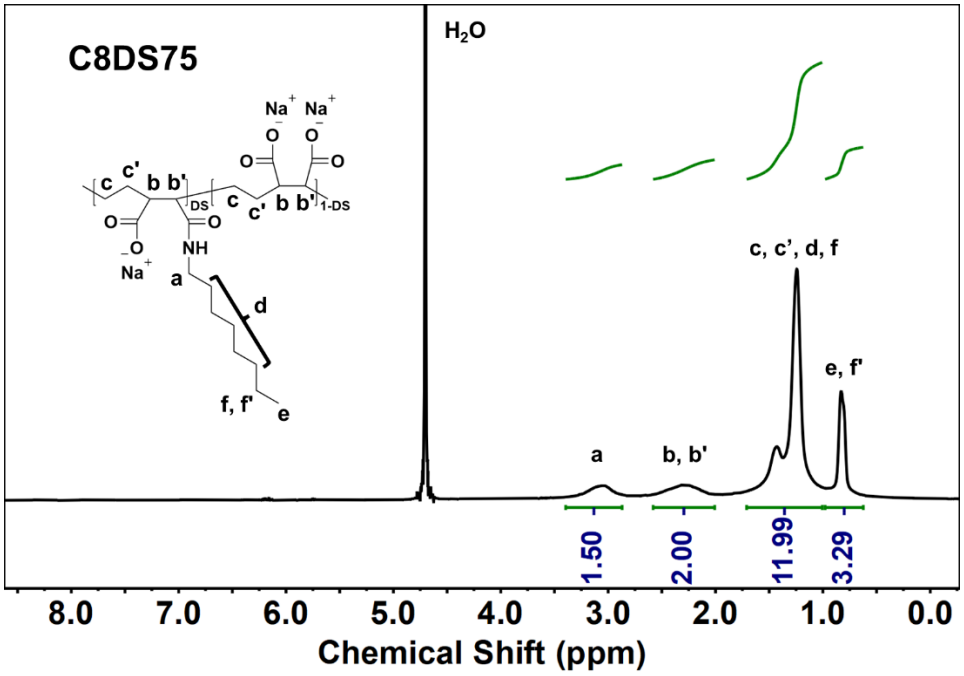

Figure S1 ^{1}H-NMR spectra of the hydrolyzed PEMA derivatizes in D_2O.

HPEMAc Solubility. Hydrolyzed PEMA has the same carboxylic acid content as polyacrylic acid and is water-soluble over the whole pH range whereas the introduction of hydrophobic groups lowers solubility. The optical transmittances of HPEMAc solutions were measured as functions of pH at three concentrations.

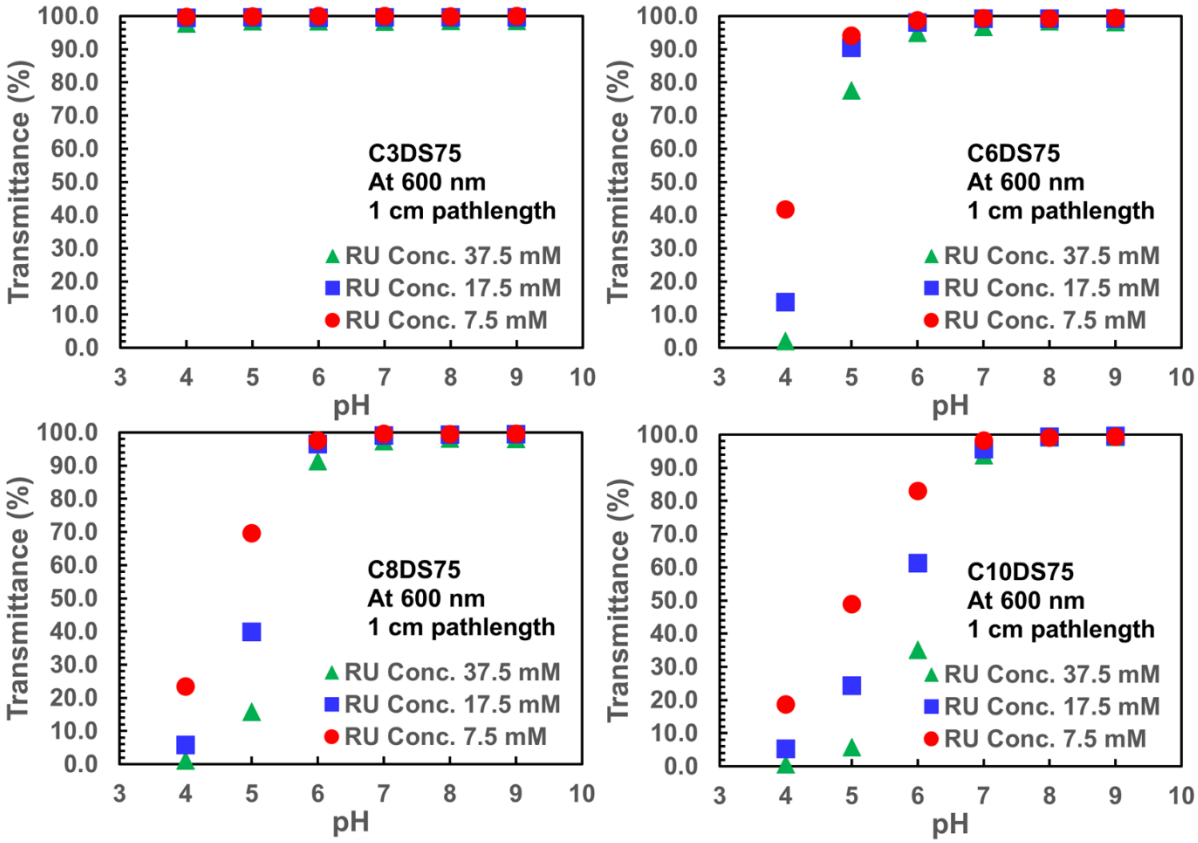

Figure S2 Transmittance at 600nm (1 cm pathlength) versus polymer concentration

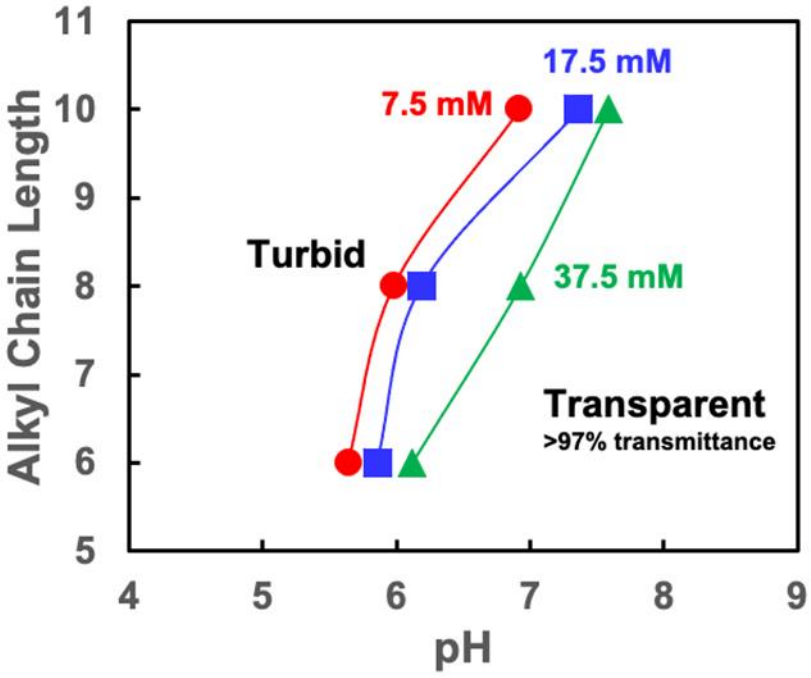

Figure S3 The influence of HPEMAc hydrophobe chain length on the pH at which the transmittance at 600 nm equaled 97% (1 cm pathlength). The labels indicated the HPEMAc RU concentrations in 1 mM NaCl. All the PEMAc DS values were 75%.

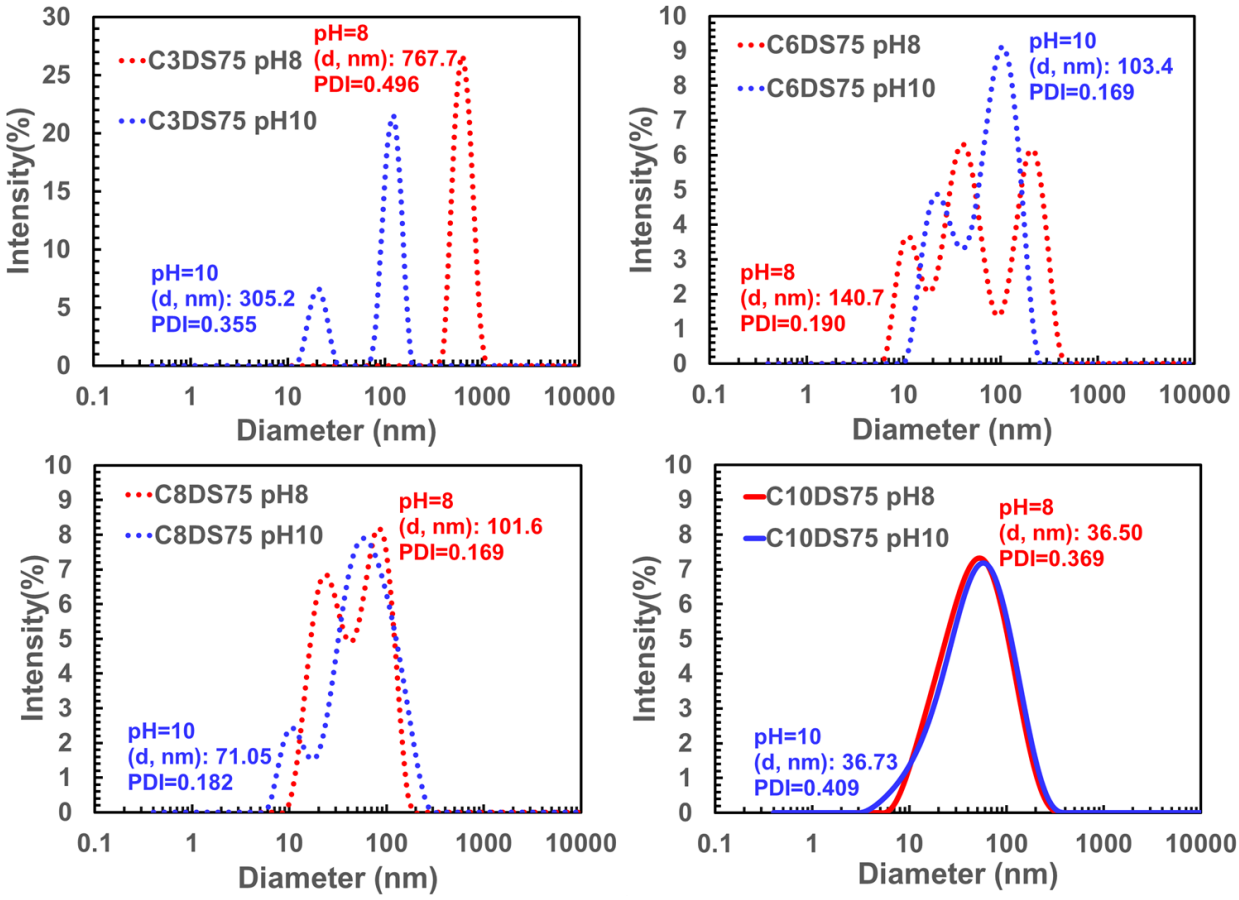

Figure S4 DLS particle size distributions for C3, C6, C8, and C10 polymers at pH 8 and 10. Dash lines indicate bad data quality, while solid lines indicate good data quality.

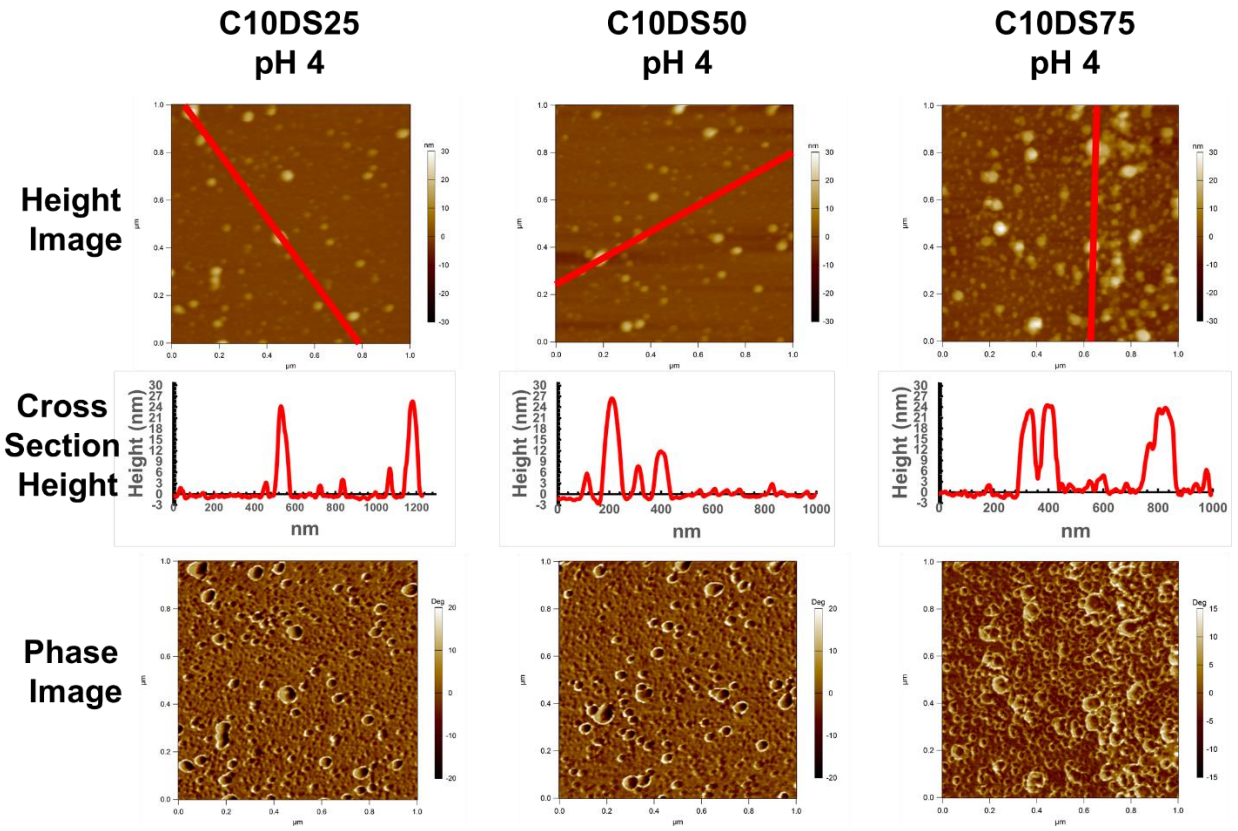

(1 µm × 1 µm)

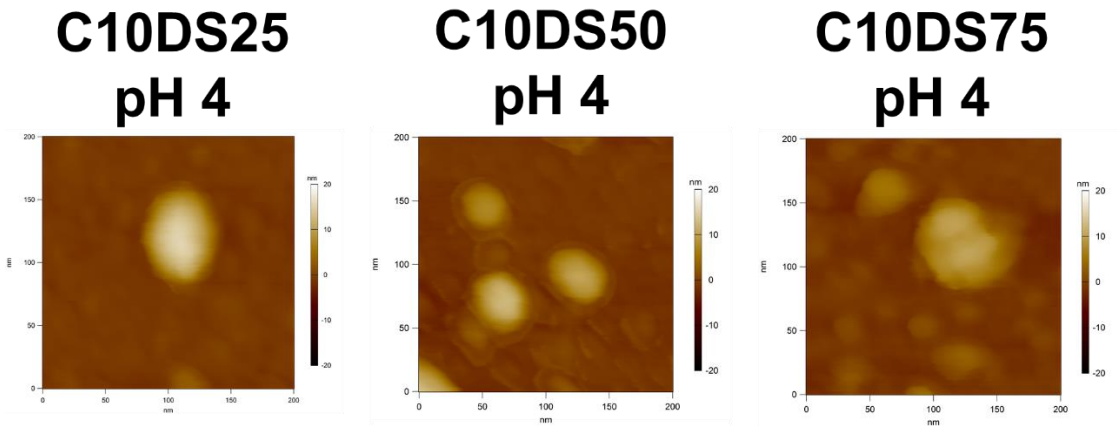

(200 nm × 200 nm)

Figure S5 AFM image of C10DS75 particles deposited from a pH 4 suspension.

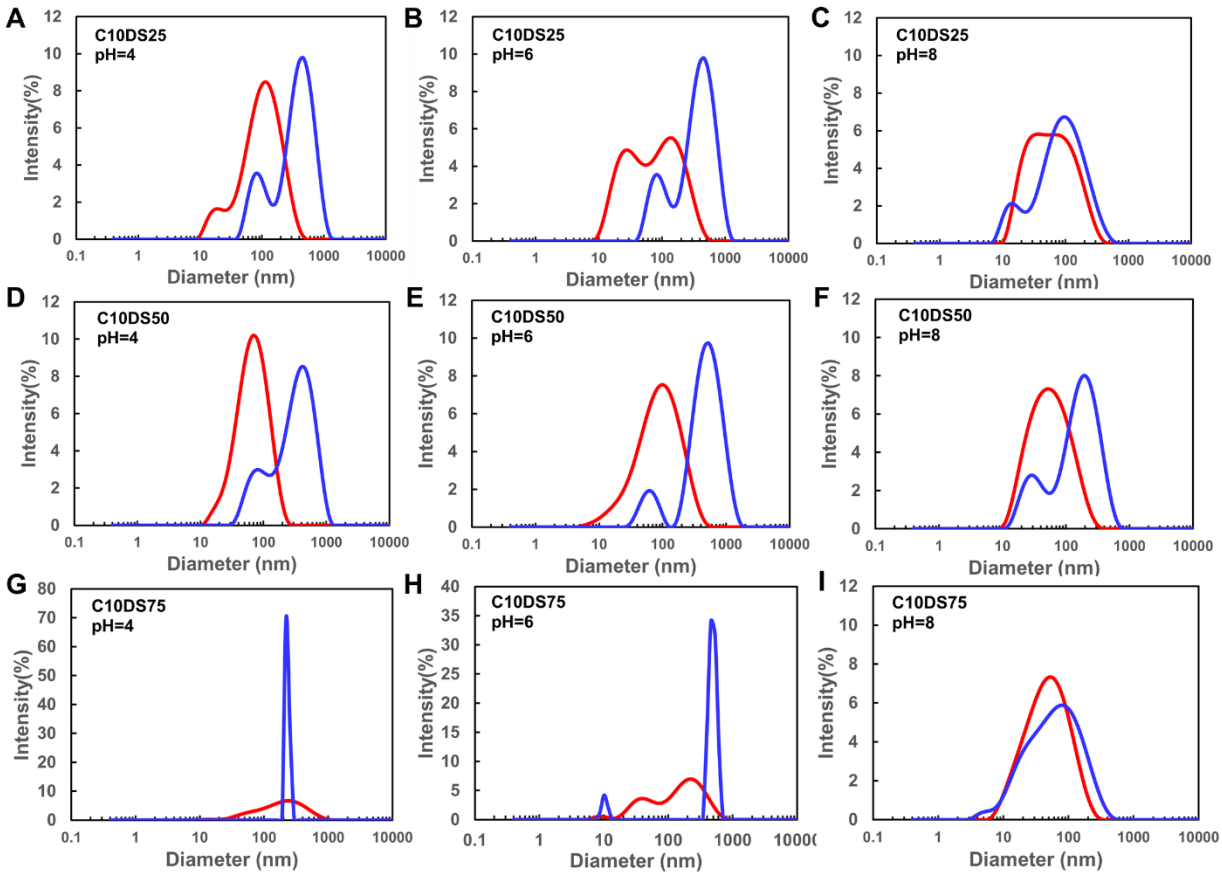

Figure S6 Particle size distributions of C10 polymers as functions of pH. The red curves correspond to samples lyophilized at pH 10, dissolved at pH 10, and then adjusted to pH 4, 6, or 8. The blue curves were for samples that were lyophilized at the same pH value used for the DLS measurements.

Samples lyophilized at pH 4 or 6 and then redispersed at the same pH solution (i.e., the blue curves in Figure S6) had larger particle sizes than those dissolved at pH 10, followed by pH adjustment (the red curves). Lyophilization at low pH can lock in aggregated structures. The pH 8 particle size distributions were much less sensitive to sample history.

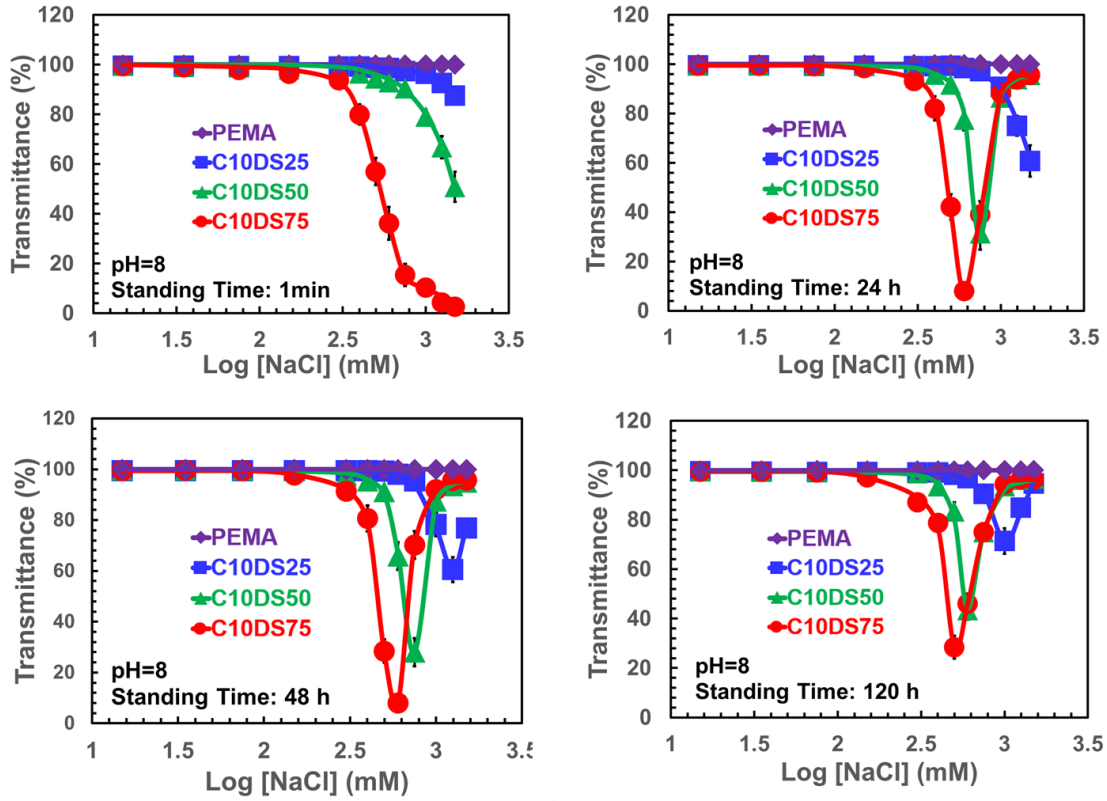

Figure S7 The transmittance at λ = 600 nm of the C10 series as a function of NaCl concentration. The samples were undisturbed for times varying from 1 min to 120 h before measuring transmittance.

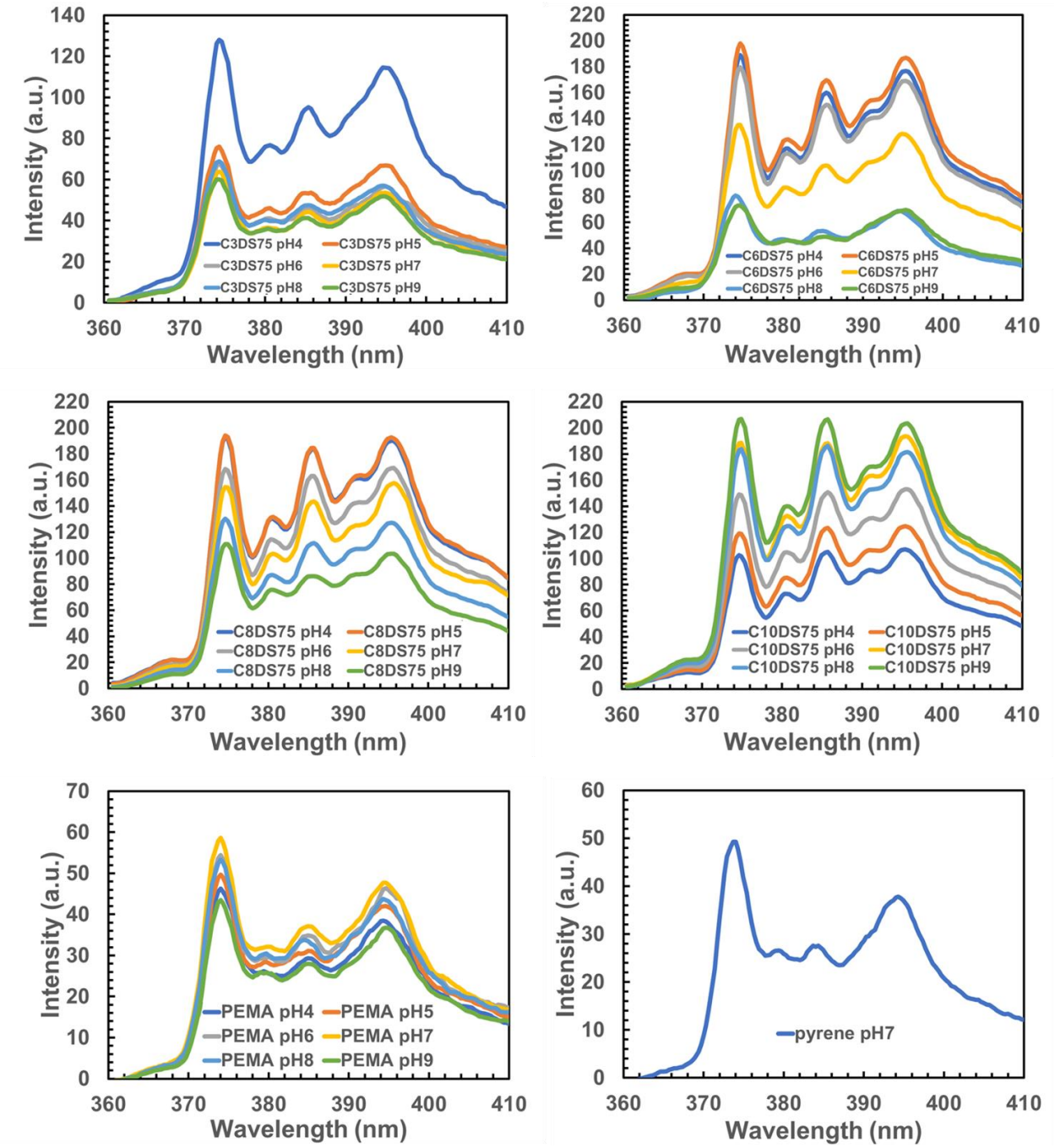

Figure S8 Pyrene emission spectra for HPEMAc polymers in 1 mM NaCl. The excitation wavelength was 337 nm.

Chapter 3

Grafting PEG and Alkyl Comb Polymers onto Bleached Wood Pulp Fibres

In this chapter, alkyl-amines and PEG-amines modified PEMA derivatives, with degrees of substitution (DS) ranging from 25% to 88%, were grafted onto bleached softwood kraft pulp fibres. The grafting process was accomplished through an impregnation approach, where polymer solutions at pH 4 were directly applied to dry pulp sheets, followed by curing at temperatures exceeding 100°C. The grafting yields, wet and dry tensile indices of the cured pulp sheets were tested and analyzed. High yields were achieved with a minimum of 12% succinic acid moieties remaining. The maximum wet tensile indices of all the grafted pulp sheets fit a power-law model.

The experiment design, data collection and analysis, and first draft writing were completed by me. My summer student Annika Culhane and Kashaf Amir helped me with part of the experiments. Dr. Jose M Moran-Mirabal and Dr. William Sampson provided valuable advice on the paper. Dr. Robert Pelton helped me with the data analysis and rewrote parts of the draft as necessary.

This chapter has been published in *The Canadian Journal of Chemical Engineering.*

Grafting PEG and Alkyl Comb Polymers onto Bleached Wood Pulp Fibres

Xiao Wu,[1] Annika Culhane,[1] Kashaf Amir,[1] Paul Bicho,[2] Erin A.S. Doherty,[3] Richard J. Riehle, [3] Sachin Borkar, [3] Jose Moran-Mirabal,[4] Robert H. Pelton *[1]

1 Department of Chemical Engineering, McMaster University, 1280 Main Street West, Hamilton, Ontario, Canada, L8S 4L7

[2] Canfor Pulp, Unit 138 - 8610 Glenlyon Parkway, Burnaby, BC, Canada, V5J 0B6

[3] Solenis LLC, 2475 Pinnacle Drive, Wilmington, Delaware, United States of America, 19803

[4] Department of Chemistry and Chemical Biology, McMaster University, 1280 Main Street West, Hamilton, Ontario, Canada, L8S 4M1

Graphical Abstract

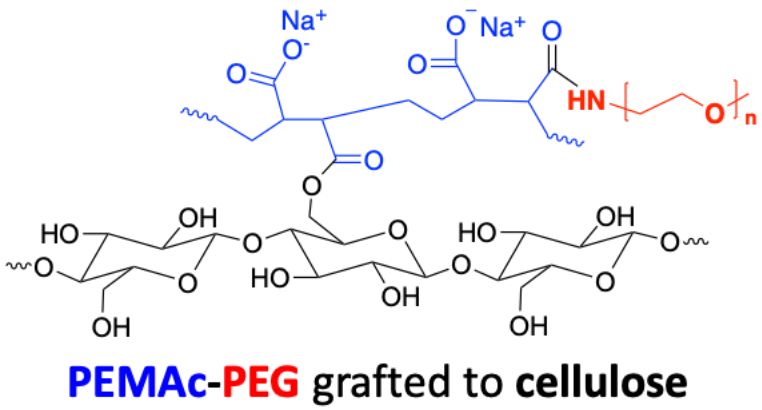

Abstract

Comb polymers were prepared by reacting a poly(ethylene-alt-maleic anhydride) with alkyl amines or PEG amines. The resulting polymers were used to modify bleached softwood kraft pulp fibre surfaces by catalyst-free grafting in a process suitable for pulp mill implementation. Pulp fibres were impregnated with a polymer solution and cured above 100 ^{o}C. High grafting yields were obtained despite having up to 88% of the anhydride groups consumed by amine derivatization. Grafting yields were more than 90% when the polymer dosage was <13 g/kg (dry polymer/dry fibre) for alkyl derivatives and <38 g/kg for PEG derivatives. We propose that the upper dosage limit for efficient grafting reflects the need for direct contact between cellulose and every polymer chain for ester linkage formation. For a given polymer dosage, the cured pulp sheets had a maximum wet tensile index, TI_{max}, when either curing time or temperature was increased. Both the alkyl and PEG derivatives fit the power law for the wet $TI_{max} \sim \beta \Gamma_{ru}^{0.54\text{-}0.62}$ where β values were the estimated conversion of succinic acid moieties to anhydrides when the pulp sheets were cured, and Γ_{ru} is the dimensionless polymer content that is numerically equal to the amount of applied polymer in mmol repeat units/g dry fibre. However, high polymer dosages give experimental TI_{max} values that fall below the power law, irrespective of curing intensity, because the pulp sheets contain unfixed polymer chains that lubricate fibre/fibre joints, lowering wet strength.

Keywords

polymer grafting, repulpability, tensile strength model, pulp wet strength

Introduction

The shift from plastics to more renewable and recyclable materials is an opportunity for renewable products partially or entirely based on wood pulp fibres. The overall goal of our work has been to explore pulp fibre surface modifications that could be implemented at the end of the pulping and bleaching processes that would expand the property space of fibre-based materials. There are several challenges. Bleached wood pulp fibres are mildly reactive materials that only offer hydroxyl and a low density of carboxylic acid groups as reaction sites. Furthermore, pulp mill operations are exclusively aqueous-based and have little tolerance for low molecular weight organics, including solvents and monomers. Based on these limitations, we focused on grafting with reactive polymers. Pulp manufacturers have transformed their bleaching processes to produce products that have essentially no organic chlorine. Therefore, any polymer modification should not include chlorinated polymers. Finally, market pulps are often supplied as large dry bales that must quickly be dispersed, "repulped," in water. Any fibre treatment must not increase fibre-fibre adhesion to the extent that inhibits the repulping process.

In recent publications, we have demonstrated that hydrolyzed poly(ethylene-alt-maleic anhydride), PEMAc, is a suitable grafting candidate – see **Figure 9**. [1, 2] When the water-soluble, highly carboxylated polymer is impregnated into pulp fibres, dried, and cured above 100 ^{o}C, the PEMAc is permanently fixed to the fibres. This contribution describes cellulose grafting studies in which poly(ethylene-alt-maleic anhydride), PEMA, is derivatized by reacting some of the anhydride groups to give pendent alkyl or poly(ethylene glycol), PEG, substituents. Our results demonstrate that derivatizing PEMAc is a general approach for introducing a variety of surface functionalities to cellulose.

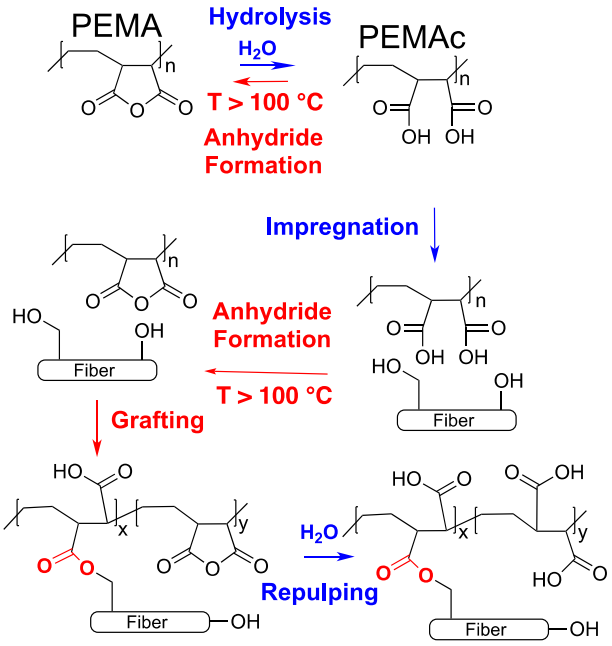

Figure 9 Grafting of PEMAc to cellulose.

Some concepts and approaches from the prior work are employed herein and are now summarized. The proposed grafting mechanism, shown in **Figure 9**, is based on a series of publications in the textile literature. PEMA rapidly hydrolyzes to give highly negatively charged, water-soluble polymer PEMAc which is dried onto the pulp fibre surfaces. Grafting occurs when PEMAc is present as a solid or a melt after water removal. The literature suggests that the formation of anhydride groups (i.e., the conversion of PEMAc back to PEMA) is the intermediate and possibly the rate-determining step in grafting. [3] [4] [5] For an isothermal curing process, the extent of anhydride formation, $0 \leq \beta \leq 1$, during curing was estimated by **Eq 2** where ***t*** is curing time, and the rate constant is given by **Eq 1** with $\boldsymbol{A}$ = 1.24 x 10^3 s^{-1} and $\boldsymbol{E_a}$ = 50 kJ/mol. [6] We emphasized that these equations should have the correct temperature scaling, but the numerical values are estimates based on isothermal thermal gravimetric analysis of PEMAc solutions.

$$k_r = A \cdot exp\left(\frac{-E_a}{RT}\right) \qquad \textbf{Eq 1}$$

$$\beta = 1 - exp(-k_r t) \qquad \textbf{Eq 2}$$

Initial studies involving high contents of impregnated PEMAc followed by aggressive curing produced pulp sheets that could not be repulped because the fibre/fibre adhesion was too high. Therefore, much of our early work on PEMAc grafting focused on identifying curing conditions whereby the yield of fixed polymer was high while ensuring the pulp could be dispersed in water. Following Su *et al.* [7], we used the wet tensile

index (TI) < 2 Nm/g as a measure of repulpability. Note that the TI is the tensile strength divided by the bulk density of the dry pulp sheet.

The TI of wet PEMAc-grafted pulp depends upon the length of the curing time, the curing temperature, and the amount of polymer added to the pulp. To reduce the complexity, we collected the grafting variables into a single parameter, $\beta\Gamma_{ru,}$ where β is given by **Eq 2**, and Γ_{ru} is the dimensionless quantity of added polymer. Γ_{ru} is numerically equal to the polymer content expressed as mmol of polymer repeat units (RU) per g of dry fibre. Note that Γ_{ru} or the corresponding polymer mass dose gives the total polymer content of treated pulp, including fixed and non-fixed polymer.

Because $\beta\Gamma_{ru}$ is a product of two terms, it is not a unique descriptor of impregnation and curing conditions. An infinite number of combinations of β and Γ_{ru} can give the same $\beta\Gamma_{ru}$ value. **Figure 10** shows some of our previously reported tensile strength results plotted as functions of $\beta\Gamma_{ru}$ on a log/log plot. Although the results were widely scattered, reflecting a wide range of experimental conditions, for a given $\beta\Gamma_{ru}$ value, there was a maximum achievable wet tensile index, TI_{max}, above which there was no experimental data – see data on or below the black line **Figure 10**. [6] TI_{max} was related to $\beta\Gamma_{ru}$ by the power law shown in **Eq 3**. For PEMAc on our bleached kraft pulp, ***a*** equals 106.1 Nm/g, and ***b*** equals 0.6. The prefactor ***a*** varies with the type of pulp [6], whereas the exponent ***b*** was independent of pulp type or PEMAc molecular weight.

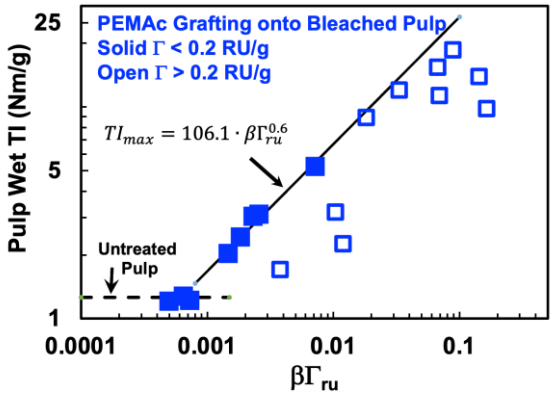

Figure 10 Impregnated pulp wet tensile index as a function of β_{ru} based on tensile data from Zhang *et al.* [6]

$$TI_{max} = a \cdot \beta\Gamma_{ru}^{b} \qquad \textbf{Eq 3}$$

Eq 3 is a powerful tool for designing experiments and, possibly, processes. For example, if one wants to ensure repulpability by keeping the $TI_{max} \leq 2$ Nm/g, for a given quantity of added polymer, one can calculate the corresponding maximum β value.

The new results presented herein show that PEMAc modified with high levels of hydrophilic or hydrophobic constituents can undergo high-yield grafting to bleach pulp fibres and that **Eq 3,** the wet tensile strength model, extends to PEMAc derivatives.

.

Experimental

Materials. Poly(ethylene-alt-maleic anhydride) (Mw 100 kDa -500 kDa), propylamine (⩾99%), decylamine (99%, GC), 2-(2-(2-Methoxyethoxy)ethoxy) ethanamide (⩾95%), poly(ethylene glycol) methyl ether amine (Mn=500) and anhydrous dimethylformamide (DMF) were purchased from Sigma-Aldrich and used without further purification. ECF 90 softwood bleached kraft pulp provided by CANFOR (British Columbia, Canada) was based on a mixture of 40-50% white spruce (*Picea glauca*), 30-40% lodgepole pine (*Pinus contorta*), and 20-30% subalpine fire (*Abies lasiocarpa*). TAPPI standard blotting papers were purchased from Labtech Instruments Inc., Canada.

Polymer Modification. The conversion of PEMAc to hydrophobically modified PEMAc-Cn was described in our previous paper, which focused on the solution properties of PEMAc-Cn. [8] The PEMAc-PEGn series was prepared similarly. 2 g PEMA dissolved in 30 mL anhydrous DMF was placed in a 250 mL round bottom flask. PEG-amine molecules dissolved in 120 mL anhydrous DMF was added dropwise into the PEMA solution. After stirring at room temperature for 16 h, the reaction mixture was quenched with 10 mL 1 M HCl solution. The product was transferred into a 29 mm diameter dialysis tube (SpectraPor, Spectrum® Labs, 12-14 kDa MWCO) and then dialyzed against 4 L pH 1-2 HCl solution for 3 days and pH 10 NaOH solution for 4 days (water was changed twice a day). The solution was collected and lyophilized. The degree of substitution (DS) was determined from ^{1}H-NMR recorded on a Bruker NEO 600 MHz spectrometer using D_2O as solvent. More details and the spectra are in **Figure S1.**

Pulp Sheets Preparation. 25 g ECF 90 dry pulp was soaked in 2 L DI water overnight, followed by disintegration (Model 500-1, Labtech Instrument Inc.) for 30000 revolutions. The disintegrated pulp was filtered, giving a wet pulp cake. The consistency (percentage mass fraction dry fibres) was typically measured 10%. The concentrated wet pulp was stored at 5 ^{o}C in a refrigerator until used.

Pulp sheets with a target basis weight of 60 g/m^2 were prepared using a semi-automatic sheet maker (Model 300-1, Labtech Instrument Inc.). ~12 g of concentrated wet was dispersed in 400 mL 1 mM NaCl solution providing a 0.3% pulp slurry, and the pulp slurry was poured into the sheet maker and further diluted to 0.019% with DI water. After couching under 560 kPa for 5 s, the wet pulp sheet formed on the steel woven mesh was gently peeled off. The wet pulp sheet was placed between two blotting papers and pressed

in a hot press (Standard Auto CH Benchtop Press, Carver, Inc., US) under 635 kPa for 5 min at room temperature. The pressed sheets were restrained in drying rings and dried at 50% relative humidity and 23 ^{o}C for 24 h.

Pulp Impregnation. Individual dry pulp sheets, supported on a plastic woven screen, were wetted with ~ 3 mL of polymer solution applied manually from a pipette. Care was taken to ensure the entire surface was wet. The wet pulp sheet was placed between 2 blotting papers and pressed once with a TAPPI-standard brass couch roller (102 mm diameter and 13 kg) to remove the excess polymer solution. The pressed pulp sheet was placed between two dry blotting papers and dried on a speed dryer (Labtech Instruments Inc.) at 120 ^{o}C or 150 ^{o}C for 2-60 min. Some wet pulp sheets were restrained with drying rings and dried at 50% relative humidity and 23 ^{o}C for 24 h.

The amount of polymer solution imbibed by pulp sheets (*i.e.,* the wet pickup) was calculated by the mass difference between the dry sheet before impregnation and the wet pulp sheet after pressing. Typical wet pickup values were 1.2-1.6 g of polymer solutions per g of dry pulp. The corresponding dry polymer dose (g dry polymer per g dry, untreated fibre) was calculated from the wet pickup and polymer concentration used to treat the sheet. The mass dosages of dry polymer were converted to mmol of repeat units per g of dry fibre by dividing mass dosage by the repeat unit molecular weight given in **Table 3**. For data analysis, we employ the dimensionless dosage $\Gamma_{ru,}$ which is numerically equal to the experimental dosage when expressed in units of mmol repeat units per g of dry fibre.

Grafted Pulp Sheet Wet Strength. The cured pulp sheets were cut into sample specimens of 1.5 cm × 14 cm. The sample specimens were soaked in 1 mM NaCl at neutral pH for 5 min before the tensile test and then placed between two blotting papers to remove excess water. The span between the sample jaws of an Instron 4411 (Instron Corporation, Canton, MA) was 10 cm. The extension rate was 25 mm/min, and forces were measured with a 50 N load cell. The tensile strengths (at break) were expressed as tensile indices (TI), which have units of Nm/g. TI values are obtained by dividing the breaking force per width by the grammage (mass of dry fibre per projected area of pulp handsheet). The tensile index is equivalent to dividing the tensile strength by the dry bulk paper density.

At least four sample strips from the same recipe were measured to get the average wet TI, and the standard deviations (n=4) were used as a measure of error. For the weakest sheets, a typical average wet tensile index was 1.193 Nm/g, with quintuplicate samples covering a typical range of 1.12-1.29 Nm/g. Stronger wet sheets had a typical range of quintuplicate measurements of 11.24 – 12.71 Nm/g. The standard deviations of all wet tensile index measurements are given in **Table S1** in the Supplementary Information file. Dry tensile indices were measured by the same method, using dry strips that had been conditioned at 50% relative humidity at 23 ^{o}C.

Fixation Yield. The amount of polymer firmly fixed to fibres was measured by exhaustive washing followed by conductometric titration. Preliminary tests were performed to determine the extent of washing required to remove unfixed polymer. One cured pulp handsheet was torn into small pieces and added to a beaker containing 1 L of 1 mM NaCl at pH 8. The pulp was agitated with a mechanical stirrer at 500 RPM, and pH was continuously monitored and manually maintained at 8. After 1 h, the pulp was filtered and rinsed once with deionized water. In the supporting information file, washing experiments leading to this protocol are summarized in **Figure S2.**

The charge contents of the washed pulps before and after grafting were measured by conductometric titration. [9] Pulp sheets (~ 0.2 g dry fibre) were dispersed in 80 mL 1 mM NaCl solution, and the pH of the suspension was adjusted below 3 using 1 M HCl solution. 30 μL injections of 0.1 M NaOH solution (LabChem Inc.) occurred with stirring at 30 s intervals. The titrator recorded the conductivity and pH. Typically, 250-300 data points were collected, and the final pH values were 11.5. The titrated fibres were filtered, oven-dried, and weighed. The charge content of the unmodified pulp was 0.062 meq/g, with a standard deviation of 0.003 for triplicate titrations. This low charge content is at the limit of our ability to measure accurate charge contents.

Most numerical results are summarized in **Table S1** in the Supplementary Information file.

Results and Discussion

Most of the samples used to generate the results presented here involved the following processing steps: 1) dilute suspensions of bleached softwood kraft pulp fibres were filtered to form a wet pulp sheet which was dried at 23 ^{o}C giving pulp sheets with the appearance of coarse paper; 2) the pulp sheets were impregnated with known quantities of aqueous polymer solution; 3) the impregnated pulp sheets were dried and cured at elevated temperature; and, 4) the wet strength and grafting yields of the impregnated pulp sheets were measured. We start by describing the polymers.

The Polymers. Comb polymers were prepared by reacting primary amines with PEMA in DMF. **Figure 11** shows the structures of two types of PEMA derivatives, one based on linear alkyl-amines and the other on PEG-amines. Three parameters are required to define the structures of our comb polymers: 1) the type of substituent (alkyl or PEG); 2) the density of substituents given as the DS value between 0 and 1 (maximum of one substituent per repeat unit); and 3) the length of the substituent expressed as the *n* or *m* values. Specific members of the alkyl series (PEMAc-Cn) are named CnDSy, where *n* is the number of carbons in the alkyl chain, and *y* is the DS value. For example, C3DS25 refers to the 1-propylamine derivatized PEMA with DS = 0.25. Specific members of the PEG derivatives, PEMAc-PEGm, are called PEGmDSy, where *m* is the number of ethylene oxide monomers in the PEG chains and *y* is the DS value as before.

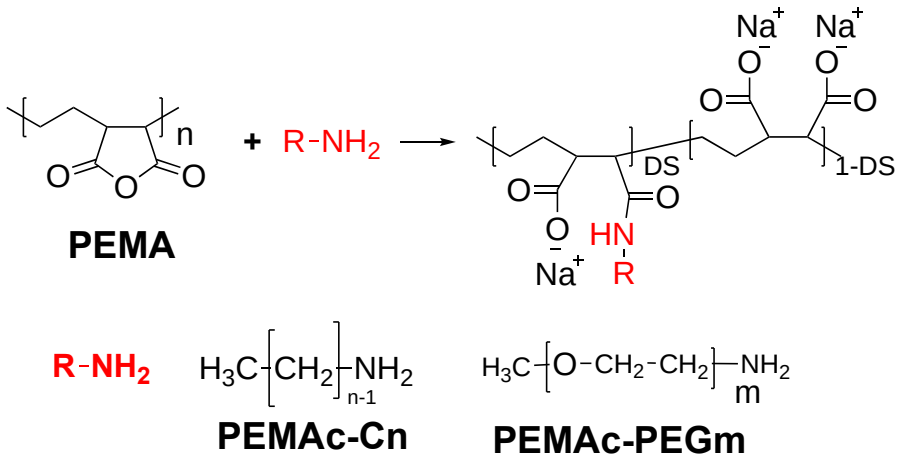

Figure 11 The conversion of PEMA to PEMAc-PEGm and PEMAc-Cn

Table 3 summarizes the properties of three polymer types, the PEMAc starting polymer, the PEMAc-Cn series, and the PEMAc-PEGm series. The RNH_2 Feed (targeted DS), the measured DS, and the polymer modification yield are all related to the PEMA derivatization reactions in **Figure 11**. The quantities of polymer used to impregnate pulp in our experiments are expressed as mmol of repeat units per gram of dry fibre (mmol RU/g). The molecular weight of the RU units in **Table 3** can be used to convert polymer contents in mmol RU/g to mass ratios or mass fractions. The ***a*** and ***b*** values are coefficients for **Eq 3** and will be discussed later.

Table 3 Polymer yields, RU values, Eq 3 parameters, and solubility properties.

Sample ID	RNH_2 Feed [a]	DS [b]	Yield (%)	RU MW (Da) [c]	*a* [d] (Nm/g)	*b* [d]	Solution Properties
PEMAc	-	-	-	188.1	[e] 106.1	[e] 0.6	Soluble
C3DS25	0.25	0.25	100	192.8	85.53	0.62	Soluble
C3DS50	0.50	0.50	100	197.6	72.81	0.63	-
C3DS75	0.75	0.75	100	202.4	72.76	0.61	Soluble with hydrophobic domains
C3DS88	0.95	0.88	93	204.9	65.60	0.59	-
C10DS25	0.25	0.25	100	217.4	85.56	0.57	Aggregated gel particles
PEG3DS24	0.25	0.24	96	217.6	92.23	0.57	Clear solutions
PEG3DS50	0.50	0.50	100	249.7	81.60	0.56	Clear solutions
PEG3DS75	0.75	0.74	99	280.5	81.84	0.58	Clear solutions
PEG3DS88	1	0.88	88	296.5	56.52	0.54	Clear solutions
PEG10DS41	0.5	0.41	82	365.0	82.85	0.56	Cloudy

[a] RNH_2 mol per mol anhydride.

[b] Degree of substitution from NMR.

[c] Repeat unit (RU) molecular weight assuming sodium salt.

[d] Power law coefficients for **Eq 3** based on fits in **Figures S3** and **S4**.

[e] from reference [6]

Most of the pulp impregnation experiments involved polymer solutions at pH 4. Except for PEG10DS41, the PEG derivatives form clear solutions at pH 4 with no dynamic light scattering or UV-Vis evidence of phase separation. In contrast to the PEG derivatives, the alkyl series, PEMAc-Cn, are examples of polysoaps that display complex behaviors in solution. [10] [11] In a preliminary paper, we described alkyl derivatives synthesis, characterization, and solution properties. [8] **Figure 12**A shows the I1/I3 ratio for pyrene fluorescence as a function of pH. PEMA, a very hydrophilic polymer, has a high I1/I3 ratio indicating the absence of hydrophobic domains. The PEMAc-C3 results showed a slightly more hydrophobic character compared to PEMAc. By contrast, with PEMAc-C10, the pyrene probes were concentrated in hydrophobic domains.

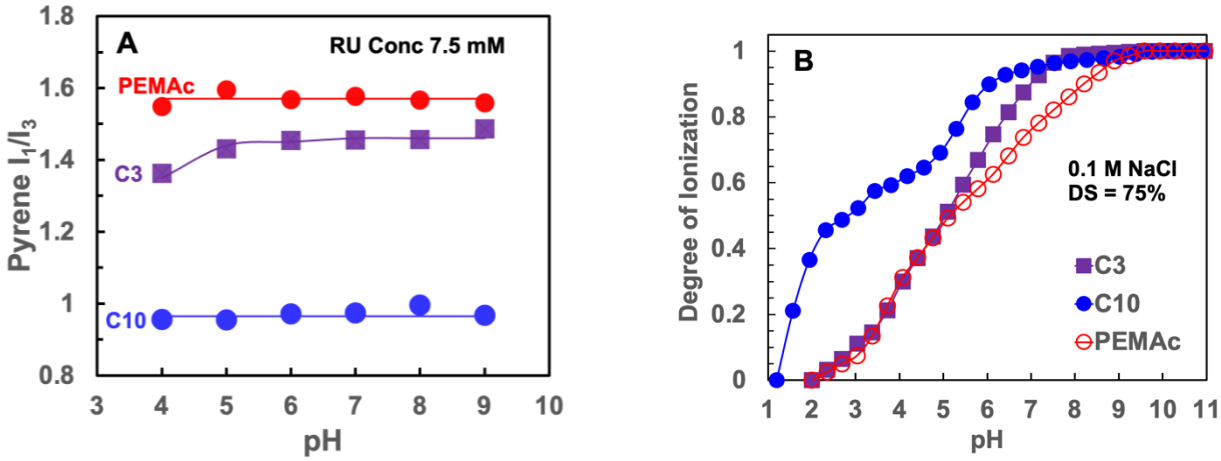

Figure 12 Comparing PEMAc-C10, PEMAc-C3, and PEMAc pyrene binding (A) and ionization (B) as functions of pH. Data extracted from [8].

The potentiometric titration results in **Figure 12**B emphasize the similarity of PEMAc and PEMAc-C3, particularly at pH 4, the impregnation pH. By contrast, the C10 polymer showed the classic behavior of molecules displaying conformational changes as the balance between hydrophobic association and electrostatic repulsion changes with pH. DLS results (not shown here, previously reported in [8]) showed that the C10 polymer formed discrete colloidal-sized hydrogel particles at neutral pH, whereas at pH 4, the gel particles aggregated. In summary, the PEG and the C3 derivatives formed simple aqueous solutions, whereas C10 was a colloidally unstable suspension of microgel particles at pH 4 – the impregnation conditions. The C10 derivatives gave scattered wet tensile results, which we attribute to a poor distribution of the insoluble polymer on the fibre surfaces. The following results do not include the C10 derivatives.

Fixation Yield. High-yield fixation is essential for commercial applications. The fraction of added polymer permanently grafted to the fibres was measured by exhaustively washing the grafted pulp, followed by conductometric titration. **Figure 13A&B** shows the fixation yields and wet tensile indices as a function of dosage for two PEMAc-C3 polymers. Dosages are expressed as Γ_{ru} dimensionless numbers, which are numerically equal to the dose expressed as mmol of repeat units per gram of dry fibre. The scatter in yield and wet tensile strength values reflect a range of curing times and temperatures. The main observations are that above Γ_{ru} of 0.06, there was a significant drop in fixation yield and that the results were insensitive to DS values between 25 and 88%. Note that the yield results for the intermediate cases are shown in **Figure S5**.

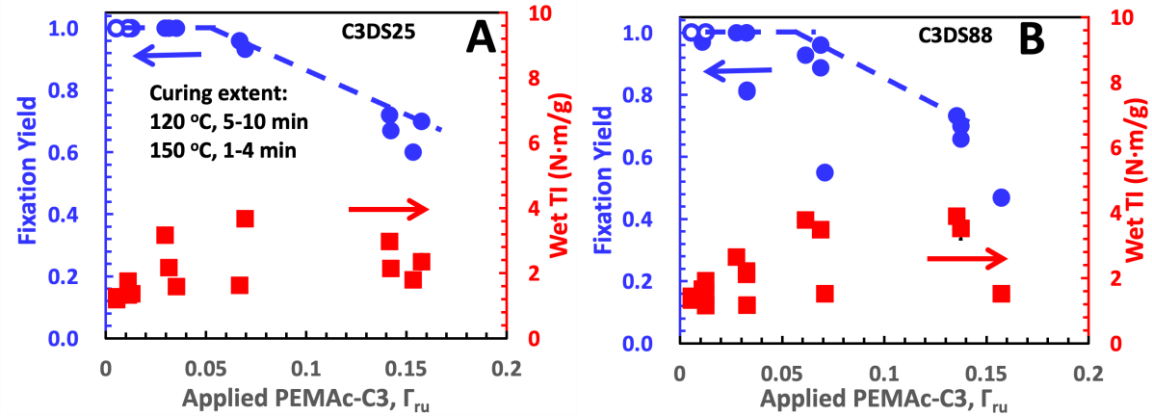

Figure 13 A & B: Fixation yields and wet tensile indices as functions of the PEMAc-C3 contents where Γ_{ru} is a dimensionless number equal to the mmol of repeat units per g of dry fibre.

We propose the following explanation for the 0.06 limit. PEMAc, PEMAc-Cn, or PEMAc-PEGm solutions do not form hydrolytically stable crosslinks with drying and curing. Therefore, the only fixation mechanisms are grafting to the fibres and possibly entanglement with the grafted polymer. With large doses, there is too little cellulose surface available for grafting.

If the goal of grafting is to have a monolayer of grafted polymer on external fibre surfaces, these results predict very high grafting yields. Assuming the external fibre specific surface area is ~ 1 m^2/g and that a monolayer coverage of polymer is ~ $1mg/m^2$, it takes approximately 1g/kg of a high molecular weight polymer to coat the exterior surfaces of a softwood pulp fibre with a high molecular weight polymer. $\Gamma_{ru} = 0.06$ corresponds to 13 g/kg for C3DS25 and 38 g/kg for C3DS88, values far more than 1 g/kg.

Finally, the observation that C3DS88 gave high yield fixation up to $\Gamma_{ru} = 0.06$ means that PEMAc copolymers with only 12% residual anhydride groups can be grafted in high

yields. This suggests many opportunities for employing PEMAc derivatives to fix other functional groups onto fibre surfaces.

Impact of Extreme Curing on Carboxyl Content. Figure 14 shows pulp charge contents measured after extensive washing as a function of curing time at two temperatures. There was a significant loss of carboxylic acid groups with extreme curing at 150 °C, whereas, at 120 °C, there was little change. The applied polymer dosages of Γ_{ru} = 0.12-0.135 (mmol/g) were high. We propose two carboxylic acid-consuming mechanisms for long curing times at 150 °C. With curing, succinic acid moieties can form anhydrides followed by ester formation with cellulose - **Figure 9**. In parallel the amides can cyclize to form imides – see structure **Figure 14**B. Every ester or imide that is formed consumes a carboxylic acid. The open symbols in **Figure 14**B are the theoretical minimum charge contents for two cases. If only ester groups form, *i.e.*, no imide formation, the open, black square gives the minimum charge content. In this case, every repeat unit is an amide or an ester plus a carboxylic acid group, and both copolymers have the same theoretical minimum for the ester-only case. The other open symbols labeled 100% indicate minimum values if every repeat unit reacts to give either an ester or an imide. Comparing the 60 min curing experimental values with theoretical limits suggests that ester formation is the dominant carboxylic acid-consuming reaction. However, there is some evidence for imide formation. **Figure S6** presented FTIR evidence for cyclic imide formation when a solution of PEG3DS88 was dried and cured at 150 °C at various times. Also, extended times resulted in color formation with the PEG amide derivatives - see **Figure S7**, so extreme curing of the amides on bleached pulps is not advised if color and brightness are important.

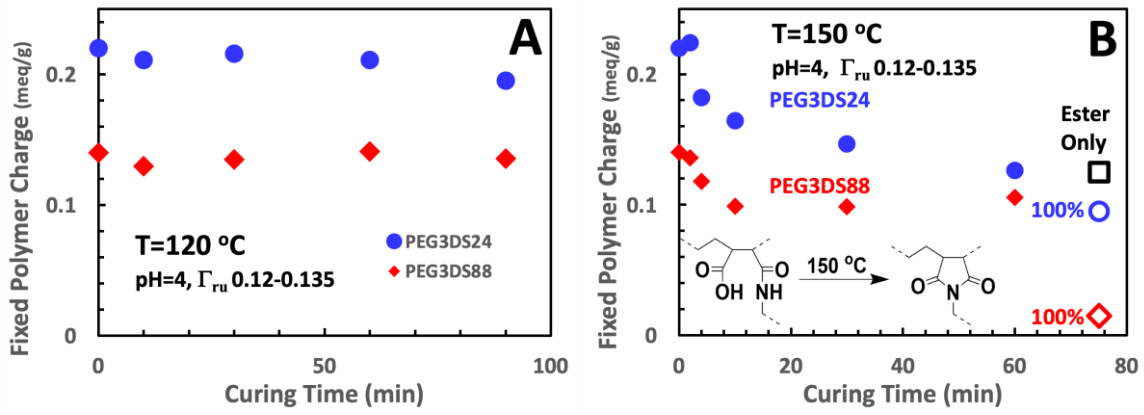

Figure 14 The influence of (A) mild (120 °C) and (B) extreme (150 °C) curing conditions on the fixed carboxylic acid contents. The open symbols are the theoretical charge contents for two cases if Γ_{ru} = 0.125. "Ester Only" is the value when all possible ester linkages are formed. "100%" are the values when every repeat unit reacts to give an imide or ester.

Grafted Pulp Wet Tensile Strength. The impact of grafted polymers on wet tensile strength is significant for two reasons. First, as described in the introduction, a grafted market pulp bale must have a low wet tensile strength to be repulpable by a customer. Second, it might be desirable to have high wet strength in final products such as packaging materials. These appear as conflicting requirements. With PEMAc, we found that mild grafting conditions were sufficient to give a high fixation yield while maintaining a low wet strength. [1] Whereas when the paper was made with PEMAc grafted pulp, high wet strengths could be obtained by aggressive curing. [12]

Figure 15 summarizes all the wet strength results for the C3 and PEG3 series plotted against the product $\beta\Gamma_{ru}$, where Γ_{ru} is the dimensionless quantity of impregnated polymer. β is the estimated conversion of succinic acid moieties to the corresponding anhydrides, calculated with **Eq 2**, employing the same parameters estimated for PEMAc. This assumes that neighboring amide groups do not influence the anhydride formation kinetics curing.

The dashed line in both graphs is the **Eq 3** fit for the PEMAc results from **Figure 10**. For both families of PEMAc derivatives, the various DS polymers are clustered together on nearly linear log/log plots. There are several surprising features in these results. First, the $\beta\Gamma_{ru}$ parameter captures most of the variability in the relationship between the wet tensile index and the impregnation and curing variables. Second, wet strength is rather insensitive to DS, despite the polymers with high DS values having few residual anhydride groups required for grafting. Finally, we hypothesized that PEG copolymers would lubricate wet fibre/ joints, weakening wet strength, whereas hydrophobic substituents might lower the water content in joints, thus strengthening them. We see the opposite. The PEMA-PEG results fall on the PEMAc dashed line (based on **Figure 10**), whereas the PEMA-C3 results are shifted to the right, meaning lower wet tensile strength for a given value of $\beta\Gamma_{ru}$.

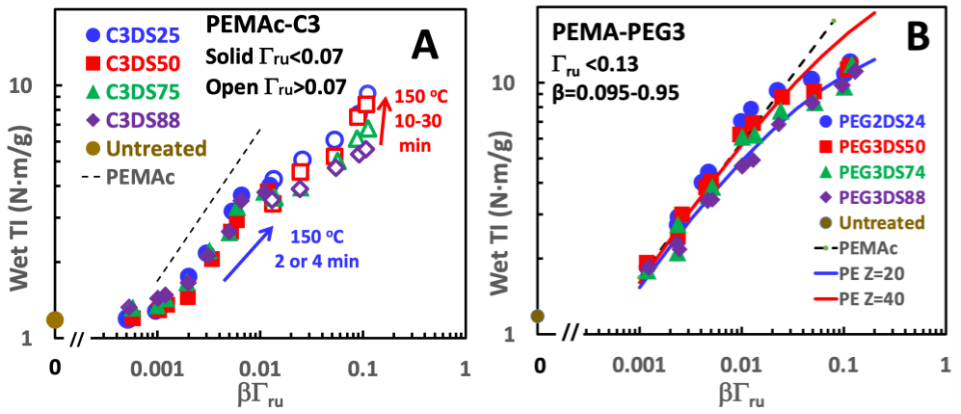

Figure 15 PEMAc-C3 treated pulp wet tensile indices as functions of $\beta\Gamma_{ru}$ where β is the estimated conversion of succinic acid moieties to anhydrides during curing. Γ_{ru} is the dimensionless polymer dose which is numerically equal to the polymer dose expressed as the mmol repeat unit per gram of dry fibre. The black dashed curve denotes the behavior of unmodified PEMAc. The PE solid lines in B show predictions of the modified Page Equation (**Eq 5**), described below. The corresponding dosages and curing conditions for each experiment can be found in **Table S1**.

Looking in more detail at the relationship between DS and wet strength, power law lines were individually fitted to the four PEMAc-PEG3 and the four PEMAc-C3 modified PEMAc polymers (see **Figure S3** and **S4**). The **Eq 3** fit parameters ***a*** and ***b*** are summarized in **Table 3**. To perform these fits, the low $\beta\Gamma$ values that appeared on the linear proportion of the log/log plots were fit with the Excel power law function. The power law fits were used to interpolate the wet TI_{max} values when $\beta\Gamma_{ru}$ = 0.01, and the results are plotted as functions of the DS values in **Figure 16**. For all DS values, the PEMAc-PEG3 wet strengths were greater than those for the corresponding PEMAc-C3 polymers. For both series, increased substitution gave lower wet strength, indicating the importance of succinic acid/anhydride moieties in wet strength development. Note that this plot shows vertical slices at $\beta\Gamma_{ru}$ = 0.01 through the results in **Figure 15A&B**. Slices for other values of $\beta\Gamma_{ru}$ along the powerlaw line show the same trends.

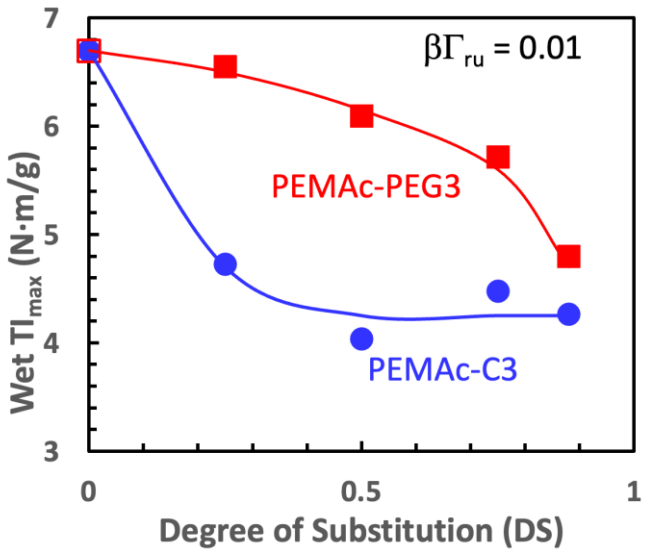

Figure 16 Maximum wet tensile indices, TI_{max}, calculated by applying experimental ***a*** and ***b*** values in **Table 3** to **Eq 3** for the C3 and PEG3 derivatized PEMA. These are vertical slices at $\beta\Gamma_{ru}$ = 0.01 through the results in **Figure 15A&B**.

The empirical power law model, **Eq 3**, is useful as it predicts the maximum achievable wet strength as a function of $\beta\Gamma_{ru}$. However, it describes an upper limit, so it is of interest to understand why some experimental points fall below the log wet TI_{max} versus the log $\beta\Gamma_{ru}$ line. For example, in **Figure 10** we see a few results below the line when $\beta\Gamma_{ru}$ is 0.003-0.01, whereas all the points are below the line when $\beta\Gamma_{ru} > 0.03$. For PEMAc derivatives in **Figure 15**, the experimental points fall on a straight line for $\beta\Gamma_{ru}$ in the range of 0.001 to 0.01, above which they diverge below the line. The power law must fail at very low $\beta\Gamma_{ru}$ values because there is too little curing or too little polymer to contribute to adhesion. We now explore two possible explanations for deviations below the power law line. The first explanation leans upon the classic Page Equation for the tensile strength of paper, and the second explanation involves the role of unfixed polymer in the pulp sheets.

The Page Equation [13, 14] is one of the most widely employed tensile strength models for paper materials. It assumes that a paper sheet fails when either fibres break and/or fibre/fibre joints fail, with the weaker of the joints or the fibres, dictating the tensile strength. The Page Equation is given in **Eq 4** where *TI* is the tensile index, *Z* is the zero-span fibre strength, *S* is the shear strength per area of fibre/fibre joint (note that Page used the symbol "b" instead of "S"), *C* is the fibre coarseness (kg/m), *P* is the perimeter of a fibre cross-section, *L* is fibre length, and *RBA* is the fraction of exterior fibre surface area that is in adhesive contact. The *Z* term gives the contribution of fibre strength to paper strength, whereas the right-hand term gives the contribution of fibre/fibre adhesive joint strength.

$$\frac{1}{TI} = \frac{8}{9Z} + \frac{12C}{P \cdot L \cdot S \cdot RBA} \qquad \textbf{Eq 4}$$

Our empirical power law (**Eq 3**) best fits the data when the wet tensile strengths are low. Therefore, it seems reasonable to replace the fibre/fibre joint strength term in the Page equation with the right-hand side of **Eq 3** to give **Eq 5**. The solid curves in **Figure 15**B were calculated using **Eq 5**. The PEMAc power law parameters, a = 106.1 Nm/g and b = 0.6, were employed as they fit the PEMAc-PEG3 experimental values at low $\beta\Gamma_{ru}$ - see **Figure 15**B. The Z values were arbitrary and lower than the literature values. [15] *Z* for the blue curve was 20 Nm/g, whereas for the red curve, Z = 40 Nm/g. This modeling suggests the deviation of experimental data below the power law line is predicted to occur by the Page Equation as wet strength approaches the wet zero-span strength, *Z*. However, **Eq 5** does not predict deviations at lower tensile strength and lower $\beta\Gamma_{ru}$. The PEMAc-C3 data in **Figure 15**A would not give such a good fit to Eq 5 for unknown reasons.

$$\frac{1}{TI} = \frac{8}{9Z} + \frac{1}{a \cdot \beta\Gamma_{ru}{}^{b}} \qquad \textbf{Eq 5}$$

A qualitative indication of the relative contributions of fibre/fibre joint strength versus the strength of individual fibres comes from examining the fracture line after a tensile test. If fibre strength is the determining factor, a relatively smooth fracture line is obtained, and optical microscopy reveals many severed fibres. If weak fibre/fibre joints dictate wet tensile strength, mainly pulled-out, intact fibres are observed. A qualitative examination of fracture lines from both low and high wet-strength treated pulp sheets suggests that fibre pullout dominated the rupture line. **Figure 17** shows two examples, one for each type of PEMAc derivative. In both cases, the polymer dose was high, and the curing was very aggressive (β = 0.95), which generated wet tensile indices above 10 N·m/g. The images suggest that fibre pullout was the dominant failure mechanism.

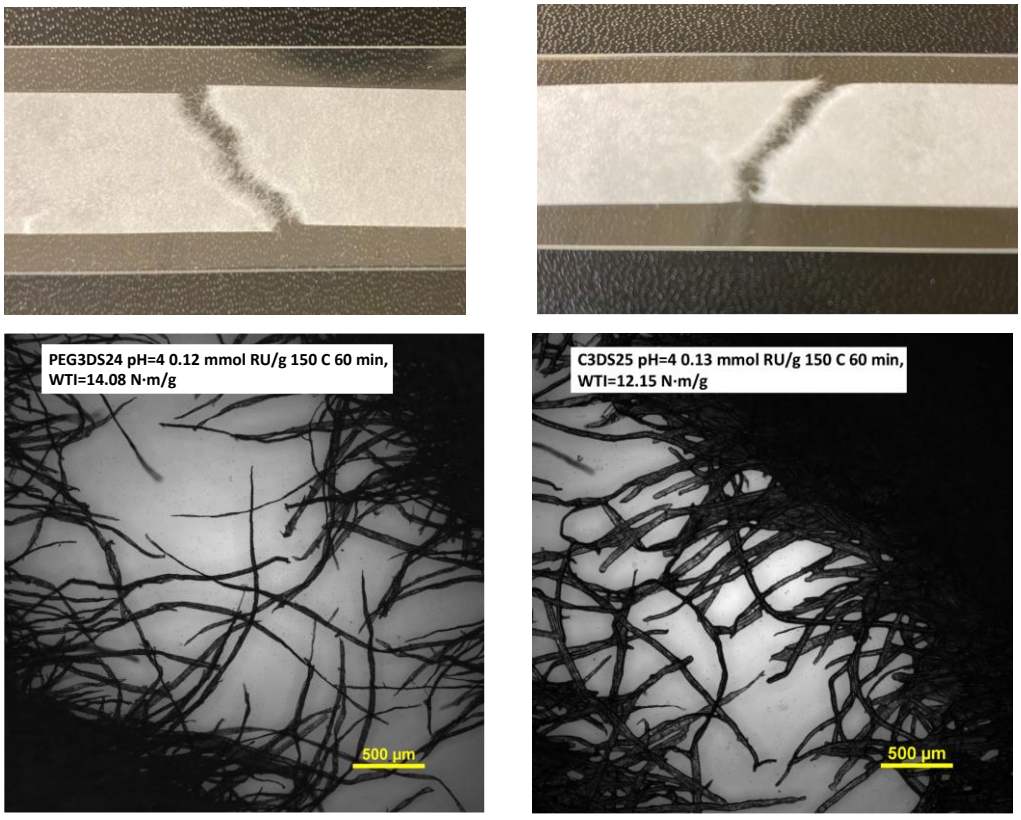

Figure 17 Images of wet tensile failure lines from two grafted pulp sheets.

We now consider the impact of unfixed polymer on the wet tensile index. **Figure 13** and **Figure S5** show many comparisons of fixation yield with the corresponding wet TI of the treated pulp sheets. For both high and low dosages, Γ_{ru}, the lower the fixation yields corresponded to the lower the wet strength values. A more explicit representation of the role of unfixed polymer is shown in **Figure 18**. Each experimental wet tensile index was divided by the corresponding power law prediction (**Eq 3**) and plotted against the experiment fixation yield. The overall trend is clear – the lower the fixation yield, the greater the experimental deviation below the TImax power law prediction. In this analysis, none of the plotted ratios should exceed 1. However, a few points corresponding to low dosages and low wet tensile indices were greater than one. Clearly, fixation yield is not the only factor influencing TI/TImax. The cluster of 6 points with low TI/TImax ratios and fixation yield of around 0.9 are outliers compared to the other results.

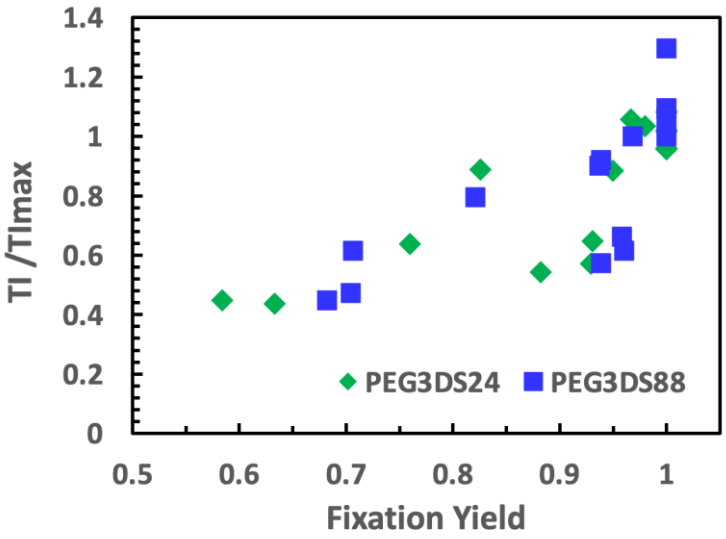

Figure 18 The experimental wet TI divided by the corresponding power law (Eq 3) prediction as functions of the corresponding fixation yields of the grafted pulps. The specific power law coefficients in Table 1 were employed for the two polymers.

Unfixed polymer remains in the pulp sheets during wet tensile testing. We propose that the water-soluble high molecular weight polymer chains that are not grafted act as lubricants instead of adhesives. Indeed we have shown with PEMAc that untreated pulp sheets have higher wet strengths than pulps impregnated with PEMAc but not cured. [6] Summarizing the Page equation, or our modified version (**Eq 5**), predicts that the power law (**Eq 3**) must fail when tensile strength approaches the zero-span fibre strength (Z). However, photographs of the fracture lines suggest that fibre pullout due to weak fibre/fibre joints is the primary failure mechanism. Therefore, we conclude that the main

reason for experimental measurements deviating below the power law line is the presence of unfixed polymer that lubricates the fibre/fibre joints, lowering wet strength.

One of the failure mechanisms for high wet-strengthened papers is the delamination of fibre walls forming fibre/fibre joints. [16] Xu *et al.* compared wet properties of papers impregnated with PEMAc to treatment with BTCA, a small molecule bearing four carboxylic acid groups. [17] They showed, as others before them, that BTCA crosslinked fibre walls making them less likely to delaminate at the cost of making more brittle structures. They argued that high molecular weight PEMAc could not penetrate fibre wall pores and did strengthen the walls. Note that their results involved high PEMAc contents (up to 60 g/kg), high curing extents of 2 min at 170 ^{o}C, and sodium hypophosphite catalyst dosages equal to ½ the PEMAc dose. We believe the importance of fibre wall strengthening by PEMAc is an unresolved question.

Finally, we admit that the mechanism by which PEMAc or its derivatives increases wet strength still needs to be fully elucidated. Paper made in the absence of wet strengthening polymers is very weak when wet because pristine cellulose fibre/fibre joints spontaneously swell and delaminate upon exposure to water. The primary mechanism for most wet-strength resins is to increase wet fibre/fibre joint strength by forming crosslinked polymer networks in the fibre/fibre joint. [18] For example, PAE, a popular wet-strength resin, creates covalent grafts to carboxylic acid groups on fibres and forms covalent crosslinks with other PAE molecules giving a covalent network. By contrast, PEMAc and its derivatives are very hydrophilic polymers with at least one carboxylic acid on every repeat unit providing a large osmotic driving force for water swelling. Covalent linkages to the fibre surfaces and between PEMAc chains are required to limit swelling and thus strengthen the joints. The most significant mechanistic difference with PAE is that pure solutions of PEMAc and its PEG or alkyl derivatives cannot form hydrolytically stable covalent crosslinks within thick PEMAc layers. However, if trace soluble carbohydrates from the pulp are present in thick PEMAc domains, the oligomeric sugars could serve as crosslinking agents by forming ester linkages between polymer chains.

Our experiments involved impregnating dry pulp sheets with non-adsorbing, dilute polymer solutions. With drying, capillary forces will concentrate polymer in cracks formed by overlapping fibres – this was demonstrated by fluorescently labeled dextran solution drops drying on crossed rayon fibres. [19] We propose that the ultimate polymer distribution around a fibre/fibre joint is illustrated in **Figure 19**, which shows a cross-section of 90-degree crossed fibres. Most of the polymer is shown in the junction cracks large formed by the overlapping fibres. Fibre roughness means only a fraction of the overlapping area is in adhesive contact. Exposure to impregnation solution will swell the joint, decreasing the areas in adhesive contact. After drying, we do not know to what extent the high molecular weight PEMAc-based polymers penetrate the overlapping regions of the fibre/fibre joints – we suspect it is small because as polymer concentrates with drying, it will become very viscous. Therefore, we believe there are few instances of grafted single polymer chains bridging between two surfaces, forming a tether. Instead, we propose that the primary strengthening mechanism is the contribution of crosslinked polymer in the fibre-junction cracks (see **Figure 19**) that inhibits crack growth when the sheets are stressed. These hypotheses are speculative and require experimental evaluation.

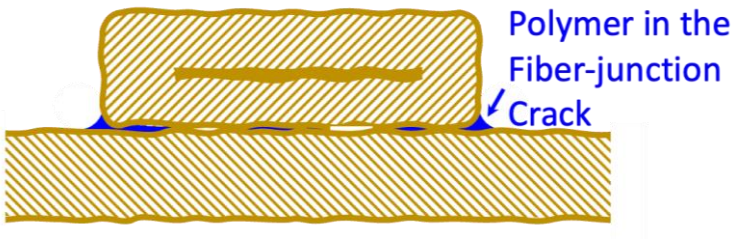

Figure 19 An illustration of a cross section of 90-degree crossed fibres showing the proposed polymer distribution after impregnation and curing. The crosslinked polymer in the fibre-junction crack may inhibit crack growth.

Dry Strength. The dry strength of most paper-based materials is an important property. Previously we have shown that PEMAc grafting does not improve dry strength. This was a surprising result as many publications have documented increases in dry tensile strength by introducing carboxylic acids, particularly on the exterior fibre surfaces – see Barzyk's work and references therein [20, 21]. The results in **Figure 20** show that C3 derivatives had little impact on dry strength until extreme curing at $\beta\Gamma_{ru}$ values above 0.1. The lower DS PEMAc-C3 polymers were slightly stronger, suggesting a role for the anhydride groups formed at high temperatures.

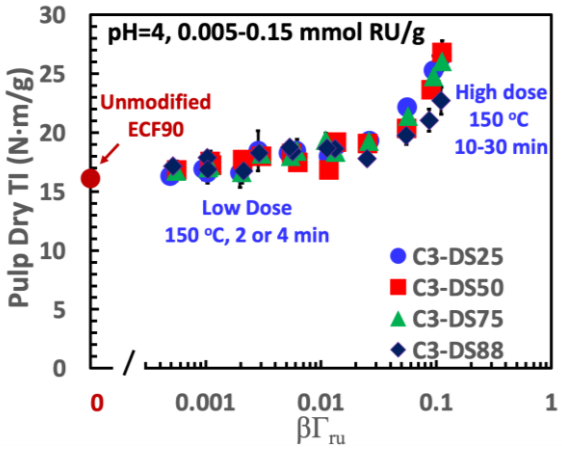

Figure 20 Dry tensile strengths of bleached kraft pulp sheets, made with unbeaten pulps, impregnated with PEMAc-C3, and cured.

Conclusions

This work has shown that poly(ethylene-alt-maleic anhydride), PEMA, can be derivatized in high yields by reaction with hydrophilic polyethylene glycol amines (PEMAc-PEGm) or with hydrophobic alkyl primary amines (PEMAc-Cn). The resulting polymer is easily fixed to cellulose fibre surfaces by drying and heating (curing). Indeed, the grafting could be implemented in a pulp mill after bleaching or after pulping for unbleached products. There are limitations to the types of PEMA derivatives that are practical. Multifunctional amines will crosslink PEMA rendering it useless for fibre modification. Furthermore, the amine derivative must withstand drying and curing during fibre treatment. Specific conclusions include:

1. Although amine derivatization consumes PEMA anhydride groups required for grafting to cellulose, 12% residual anhydrides are sufficient for high-yield grafting to cellulose.

2. Grafting yields of PEMA derivatives showed the same trends as unmodified PEMA. Curing temperatures must exceed 100 ^{o}C, and the pH of the impregnation solution is essential. pH 4 polymer solutions give high fixation yields, whereas pH 6 solutions do not.

3. Because PEMAc or its derivatives are not self-crosslinking, we propose that the only fibre fixation mechanisms are grafting to fibres or mechanical entanglement with grafted polymer. High fixation yields are achieved when most of the added polymer can directly contact cellulose. The upper polymer dose limits to achieving > 90% fixation are 0.12 mmol repeat units per gram of fibre (~ 30 g/kg dry polymer/dry fibre) for PEMAc-PEG3 and 0.06 mmol repeat units per gram (~12 g/kg) for PEMAc-C3.

4. The polymer grafting conditions were characterized by the dimensionless parameter, $\beta\Gamma_{ru,}$ where β values were the estimated conversion of succinic acid moieties to anhydrides when the pulp sheets were cured, and Γ_{ru} is the dimensionless polymer content, that is numerically equal to the amount of applied polymer in repeat unit mmol/g. PEMAc-C3 and PEMAc-PEG3 pulp sheet wet tensile strengths fit the power law $TI_{max} \sim \beta\Gamma_{ru}^{0.54\text{ -}0.62,}$ where TI_{max} is the maximum achievable tensile index for a given value of $\beta\Gamma_{ru}$. The power law seems to be a general relationship since we showed previously low and high molecular weight unmodified PEMAc gave the same scaling with two types of wood pulp. [6] However, high polymer dosages give experimental TI values below the TI_{max} power law line because the pulp sheets contain unfixed polymer chains that lubricate fibre/fibre joints, lowering wet strength.

5. The wet strength decreased modestly with increasing C3 or PEG3 degrees of substitution. The pulp sheets containing the more hydrophobic C3 derivatives were weaker than the corresponding PEG3 sheets. The PEMAc derivatives had little impact

on the dry strengths of treated pulp sheets unless the dosages and curing conditions were extreme.

6. Extended curing at 150 ^{o}C caused a decrease in the carboxylic acid content of PEMAc-PEG polymers. Ester formation seems to be the dominant cause. However, there is evidence of limited imide formation when the amides cyclized with neighboring carboxylic acid groups to form imides.

Acknowledgments

We thank the Natural Sciences and Engineering Research Council of Canada (NSERC) and our industrial partners, Solenis Canada and Canfor, for funding this project. R. H. Pelton holds the Canada Research Chair in Interfacial Technologies, and J. Moran-Mirabal holds the Canada Research Chair in Micro- and Nanostructured Materials. Prof William Sampson, University of Manchester, is acknowledged for advice on applying the Page Equation to our results.

It is a great honor for me (RP) to participate in this special issue dedicated to the memory of Archie Hamielec. Archie recruited me to McMaster, where he was very generous – sharing students, equipment, financial support, and advice. Most of all, I learned from Archie the value of working with industry partners.

References

[1] H. Zhang, P. Bicho, E.A.S. Doherty, R.J. Riehle, J. Moran-Mirabal, R.H. Pelton, High-Yield Grafting of Carboxylated Polymers to Wood Pulp Fibres, Cellulose, 28 (2021) 7311–7326. https://doi.org/10.1007/s10570-021-04016-0

[2] H. Zhang, E. Tsenter, P. Bicho, E.A.S. Doherty, R. Riehle, J. Moran-Mirabal, R.H. Pelton, Carboxylated Bleached Kraft Pulp from Maleic Anhydride Copolymers, Nord. Pulp Pap. Res. J., 36 (2021) 608–617. https://doi.org/10.1515/npprj-2021-0005

[3] C.Q. Yang, Infrared Spectroscopy Studies of the Cyclic Anhydride as the Intermediate for the Ester Crosslinking of Cotton Cellulose by Polycarboxylic Acids. I. Identification of the Cyclic Anhydride Intermediate, J. Polym. Sci., Part A: Polym. Chem., 31 (1993) 1187-1193. https://doi.org/10.1002/pola.1993.080310514

[4] C.Q. Yang, X. Wang, Infrared Spectroscopy Studies of the Cyclic Anhydride as the Intermediate for the Ester Crosslinking of Cotton Cellulose by Polycarboxylic Acids. II. Comparison of Different Polycarboxylic Acids, J. Polym. Sci., Part A: Polym. Chem., 34 (1996) 1573-1580. https://doi.org/10.1002/(SICI)1099-0518(199606)34:8%3C1573::AID-POLA22%3E3.0.CO;2-4

[5] C.Q. Yang, Y. Xu, D. Wang, FT-IR Spectroscopy Study of the Polycarboxylic Acids Used for Paper Wet Strength Improvement, Ind. Eng. Chem. Res., 35 (1996) 4037-4042. https://doi.org/10.1021/ie960207u

[6] H. Zhang, P. Bicho, E.A.S. Doherty, R.J. Riehle, J. Moran-Mirabal, R.H. Pelton, High Yield Poly(Ethylene-Alt-Maleic Acid) Grafting to Wood Pulp While Minimizing Fibre/Fibre Wet Adhesion, Biomacromolecules 22 (2021) 3060–3068. https://doi.org/10.1021/acs.biomac.1c00511

[7] J. Su, W.K. Mosse, S. Sharman, W. Batchelor, G. Garnier, Paper Strength Development and Recyclability with Polyamideamine-Epichlorohydrin (PAE), BioResources, 7 (2012) 0913-0924.

[8] X. Wu, Z. Hu, P. Bicho, E.A.S. Doherty, R.J. Riehle, S. Borkar, J. Moran-Mirabal, R.H. Pelton, Solution Properties of Hydrophobic Derivatives of Poly(Ethylene-Alt-Maleic Acid), Eur. Polym. J., 177 (2022) 111451. https://doi.org/10.1016/j.eurpolymj.2022.111451

[9] S. Katz, A.M. Scallan, The Determination of Strong and Weak Acidic Groups in Sulfite Pulps, Sven. Papperstidn., 87 (1984) 48-54.

[10] A. Laschewsky, Molecular Concepts, Self-Organisation and Properties of Polysoaps, in: Polysoaps/Stabilizers/Nitrogen-15 Nmr, Springer Berlin Heidelberg, Berlin, Heidelberg, 1995, pp. 1-86. https://doi.org/10.1007/BFb0025228

[11] S.R. Tonge, B.J. Tighe, Responsive Hydrophobically Associating Polymers: A Review of Structure and Properties, Adv. Drug Delivery Rev., 53 (2001) 109-122. https://doi.org/10.1016/S0169-409X(01)00223-X

[12] H. Zhang, L. Wang, P. Bicho, E.A.S. Doherty, R.J. Riehle, S. Borkar, J. Moran-Mirabal, R.H. Pelton, Grafted Maleic Acid Copolymer Giving Thermosetting Kraft Pulp, Cellulose, 29 (2022) 3745–3758. https://doi.org/10.1007/s10570-022-04518-5

[13] D.H. Page, A Theory for the Tensile Strength of Paper, TAPPI, 52 (1969) 674.

[14] D.H. Page, A Quantitative Theory of the Strength of Wet Webs, J. Pulp Paper Sci., 19 (1993) 175-176.

[15] N. Gurnagul, D.H. Page, The Difference between Dry and Rewetted Zero-Span Tensile-Strength of Paper, TAPPI, 72 (1989) 164-167.

[16] T. Lindström, L. Wågberg, T. Larsson In On the Nature of Joint Strength in Paper - a Review of Dry and Wet Strength of Paper During Paper Manufacturing, Symposium on "Advances in Paper Science and Technology". Transactions of the 13th Fundamental Research Symposium, Cambridge, UK, The Pulp & Paper Fundamental Research Society: 2005; pp 457-462.

[17] Y.F. Xu, C.Q. Yang, C.M. Chen, Wet Reinforcement of Paper with High-Molecular-Weight Multifunctional Carboxylic Acid, TAPPI, 82 (1999) 150-156.

[18] H.H. Espy, The Mechanism of Wet-Strength Development in Paper: A Review, TAPPI, 78 (1995) 90-99.

[19] R. Pelton, J. Zhang, N. Chen, A. Moghaddamzadeh, The Influence of Dextran Molecular Weight on the Dry Strength of Dextran-Impregnated Paper, TAPPI, 2 (2003) 15-18.

[20] D. Barzyk, D. Page, A. Ragauskas, Acidic Group Topochemistry and Fibre-to-Fibre Specific Bond Strength, J. Pulp Paper Sci., 23 (1997) J59-J61.

[21] D. Barzyk, D. Page, A. Ragauskas In Carboxylic Acid Groups and Fibre Bonding, The Fundamentals of Papermaking Materials: Transactions of the 11th Fundamental Research Symposium, Cambridge, 1997; pp 893-907.

Supplementary Information

Grafting PEG and Alkyl Comb Polymers onto Bleached Wood Pulp Fibres

Xiao Wu,[1] Annika Culhane,[1] Kashaf Amir,[1] Paul Bicho,[2] Erin A.S. Doherty,[3] Richard J. Riehle, [3] Sachin Borkar, [3] Jose Moran-Mirabal,[4] Robert H. Pelton *[1]

1 Department of Chemical Engineering, McMaster University, 1280 Main Street West, Hamilton, Ontario, Canada, L8S 4L7

[2] Canfor Pulp, Unit 138 - 8610 Glenlyon Parkway, Burnaby, BC, Canada, V5J 0B6

[3] Solenis LLC, 2475 Pinnacle Drive, Wilmington, Delaware, United States of America, 19803

[4] Department of Chemistry and Chemical Biology, McMaster University, 1280 Main Street West, Hamilton, Ontario, Canada, L8S 4M1

^{1}H-NMR of PEMAc derivatives. The substituent DS for the PEMAc derivatives was determined by ^{1}H-NMR spectra given below. In the ^{1}H-NMR spectra (**Figure S9**), the PEMAc backbone displays two wide peaks at the chemical shift of 0.9-1.8 ppm (a) and 2.0-2.5 ppm (b) corresponding to the protons from ethylene domains (-C*H*$_2$C*H*$_2$-) and succinic units (-C*H*(C=O)-C*H*(C=O)-) respectively.

For PEMAc-Cn, the pendant hydrophobes show two peaks at the chemical shift of 2.8-3.4 ppm (c) and 0.5-0.9 ppm (d) among which the peak (c) refers to the CH_2 groups closest to the amide bonds (-C=O-NH-C*H*$_2$-) from alkyl side chains and peak (d) refers to the rest of protons (-(C*H*$_2$)$_{n-1}$C*H*$_3$) on the alkyl side chains. The degree of substitution (DS) is calculated based on the integral of the peak (b) and (c), and the equation is given in **EqS1**.

$$DS(Cn) = \frac{I_c}{I_b} \qquad \textbf{Eq S1}$$

For PEMAc-PEGn, the pendant polyethylene glycol chains show peaks (c, d) at the chemical shift ranging from 3.2 ppm to 3.8 ppm which are assigned to all the protons on the PEG side chains. The total number of protons on a single PEG3 molecule is 15 for PEG3 which is given in the specific information from the supplier, while the number for a PEG10 molecule is 46 detected by ^{1}H-NMR. Hence, the degree of substitution (DS) was calculated from equation **EqS2**.

$$DS(PEG3) = \frac{I_c + I_d}{15} \;\&\; DS(PEG10) = \frac{I_c + I_d}{46} \qquad \textbf{Eq S2}$$

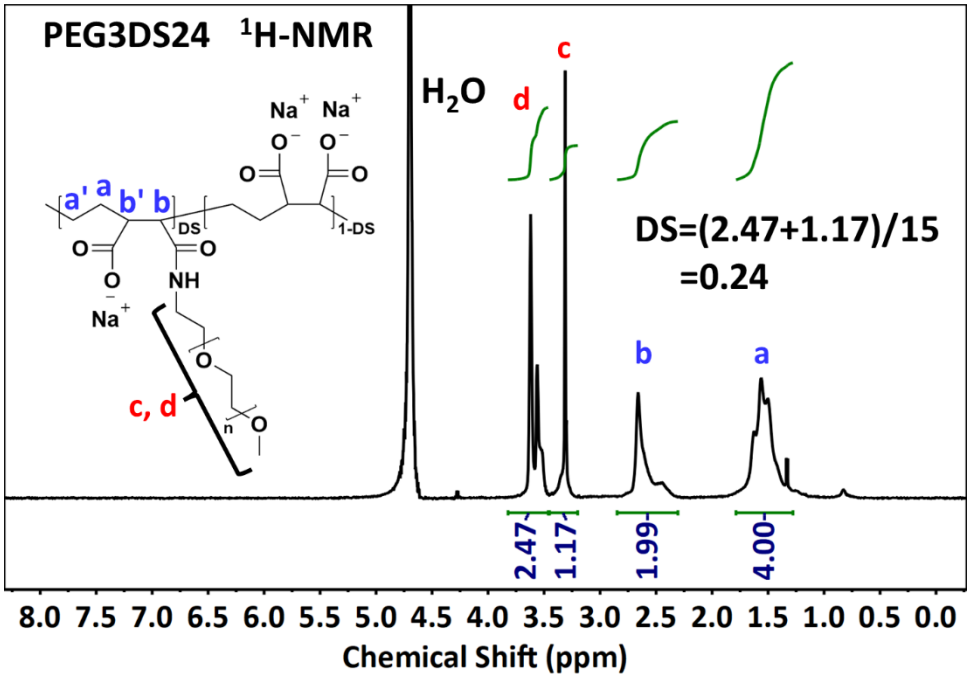
PEG3DS24 ¹H-NMR
H2O
c
d
DS=(2.47+1.17)/15
=0.24
b
a
2.47
1.17
1.99
4.00
8.0 7.5 7.0 6.5 6.0 5.5 5.0 4.5 4.0 3.5 3.0 2.5 2.0 1.5 1.0 0.5 0.0
Chemical Shift (ppm)

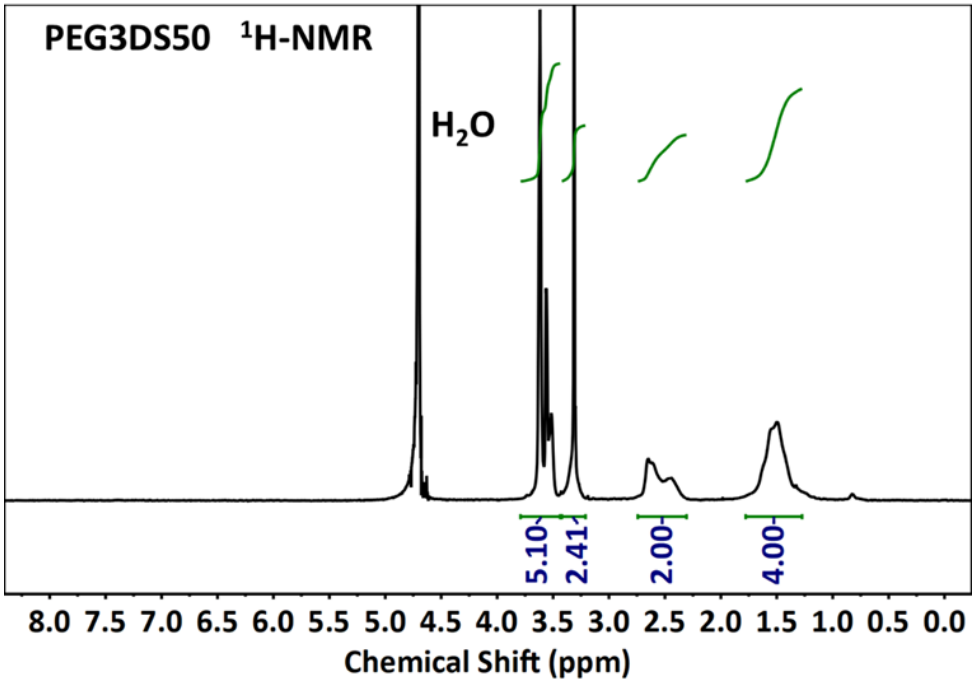
PEG3DS50 ¹H-NMR
H2O
5.10
2.41
2.00
4.00
8.0 7.5 7.0 6.5 6.0 5.5 5.0 4.5 4.0 3.5 3.0 2.5 2.0 1.5 1.0 0.5 0.0
Chemical Shift (ppm)

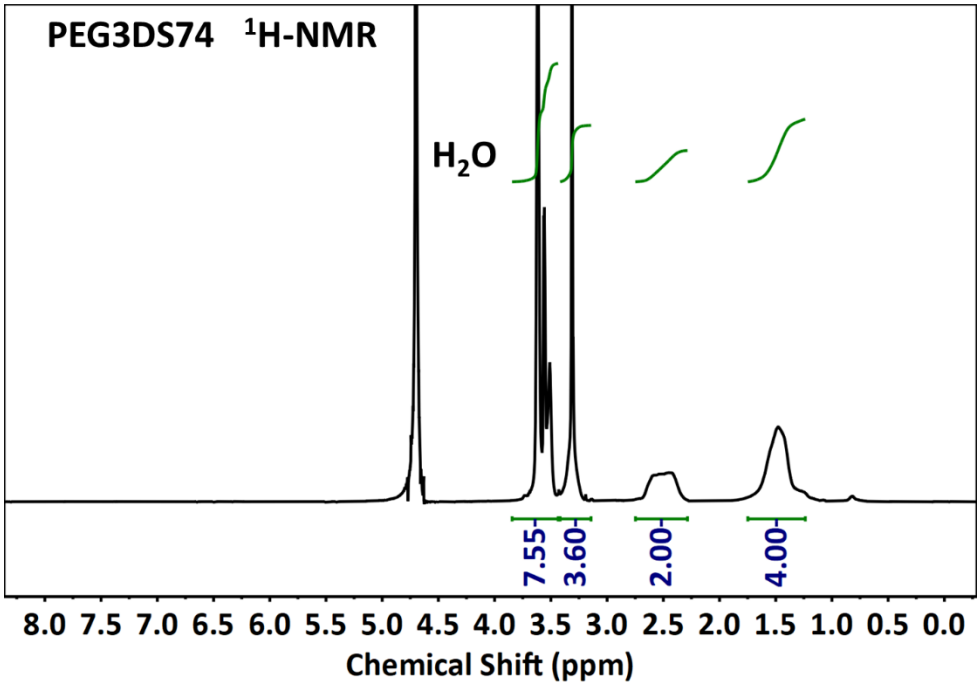
PEG3DS74 ¹H-NMR
H2O
7.55
3.60
2.00
4.00
8.0 7.5 7.0 6.5 6.0 5.5 5.0 4.5 4.0 3.5 3.0 2.5 2.0 1.5 1.0 0.5 0.0
Chemical Shift (ppm)

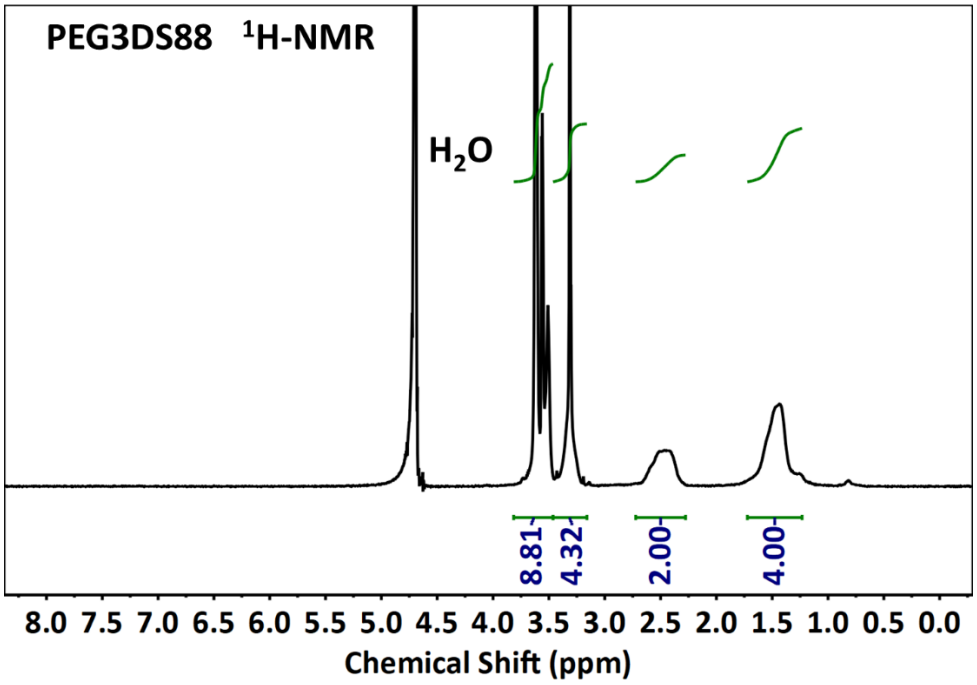
PEG3DS88 ¹H-NMR
H2O
8.81
4.32
2.00
4.00
8.0 7.5 7.0 6.5 6.0 5.5 5.0 4.5 4.0 3.5 3.0 2.5 2.0 1.5 1.0 0.5 0.0
Chemical Shift (ppm)

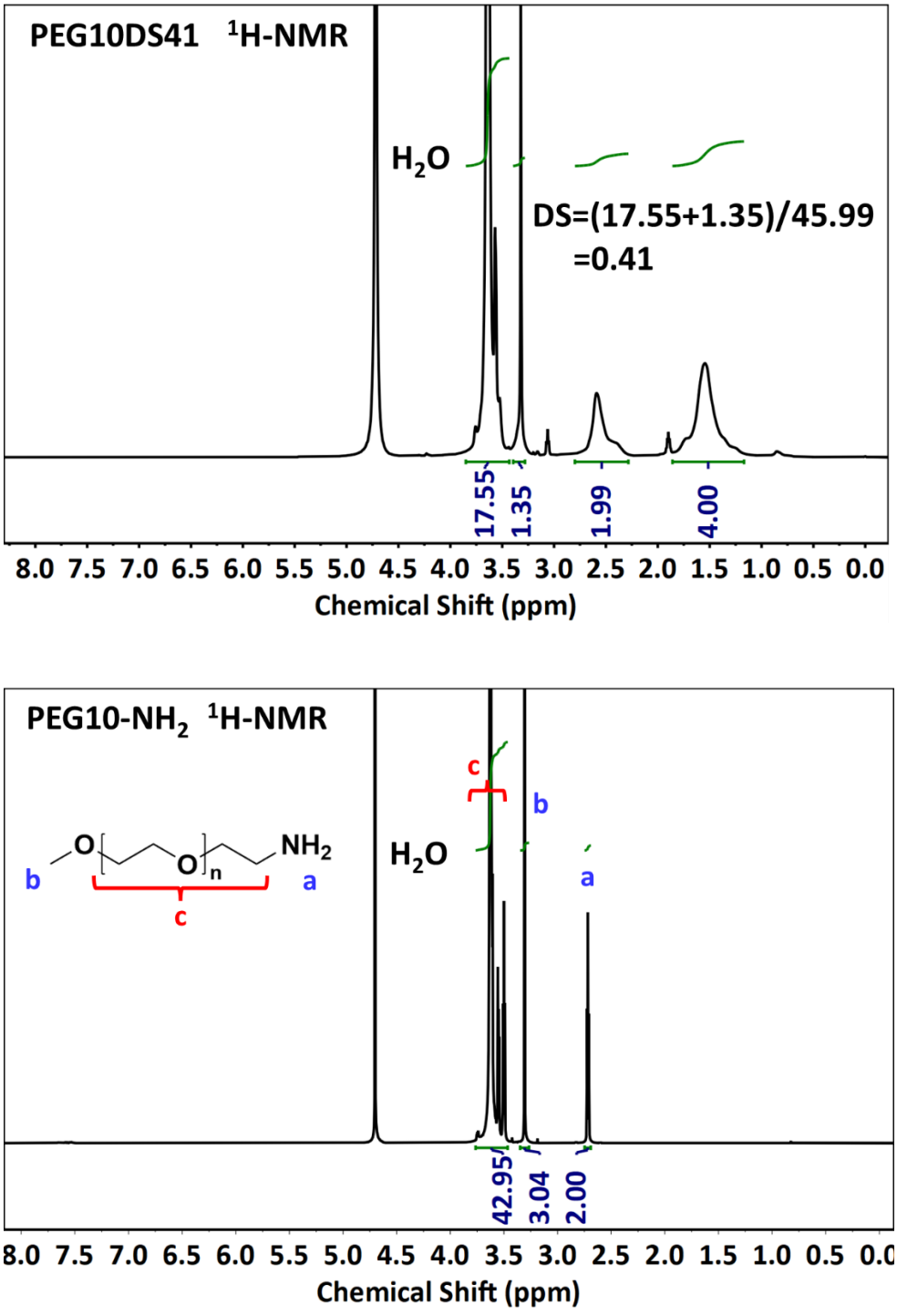

Figure S9 ¹H-NMR spectra of PEMAc-PEGn series.

Developing a Washing Protocol for Measuring Fixation Yield. To measure fixation yield, the unfixed polymer should be completely removed. **Figure S10** shows a series of washing experiments for the PEMAc-Cn series. The x-axis is the number of 5 min washing cycles, and the y-axis is fixation yields. For the high-temperature curing experiments, the fixation yields were approximately constant after 3 washing cycles, which was our standard protocol. However, the room-temperature cured pulps have low fixation yields, as it took many cycles to remove most of the impregnated polymer. Subsequent experiments revealed that a single washing step with a 1 h mixing time gave the same fixation yield as 3 short washing cycles.

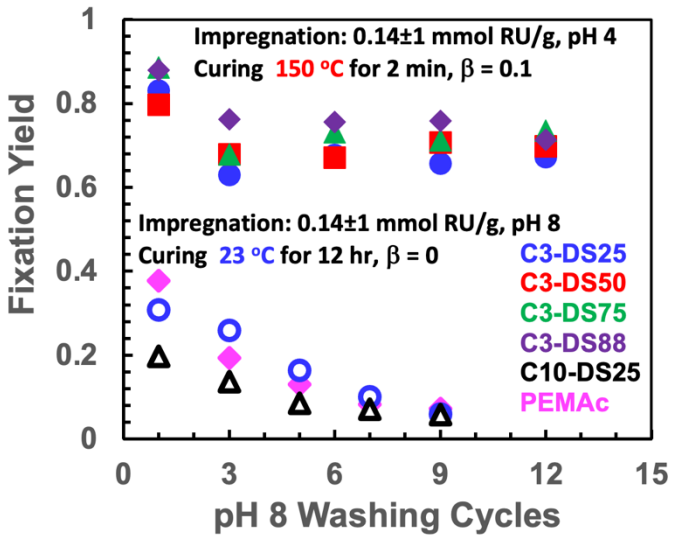

Figure S10 Fixation yield as a function of washing cycles. In each washing cycle, pulp fibres were stirred under 500 rpm in 1 mM NaCl at pH 8 for 5 min.

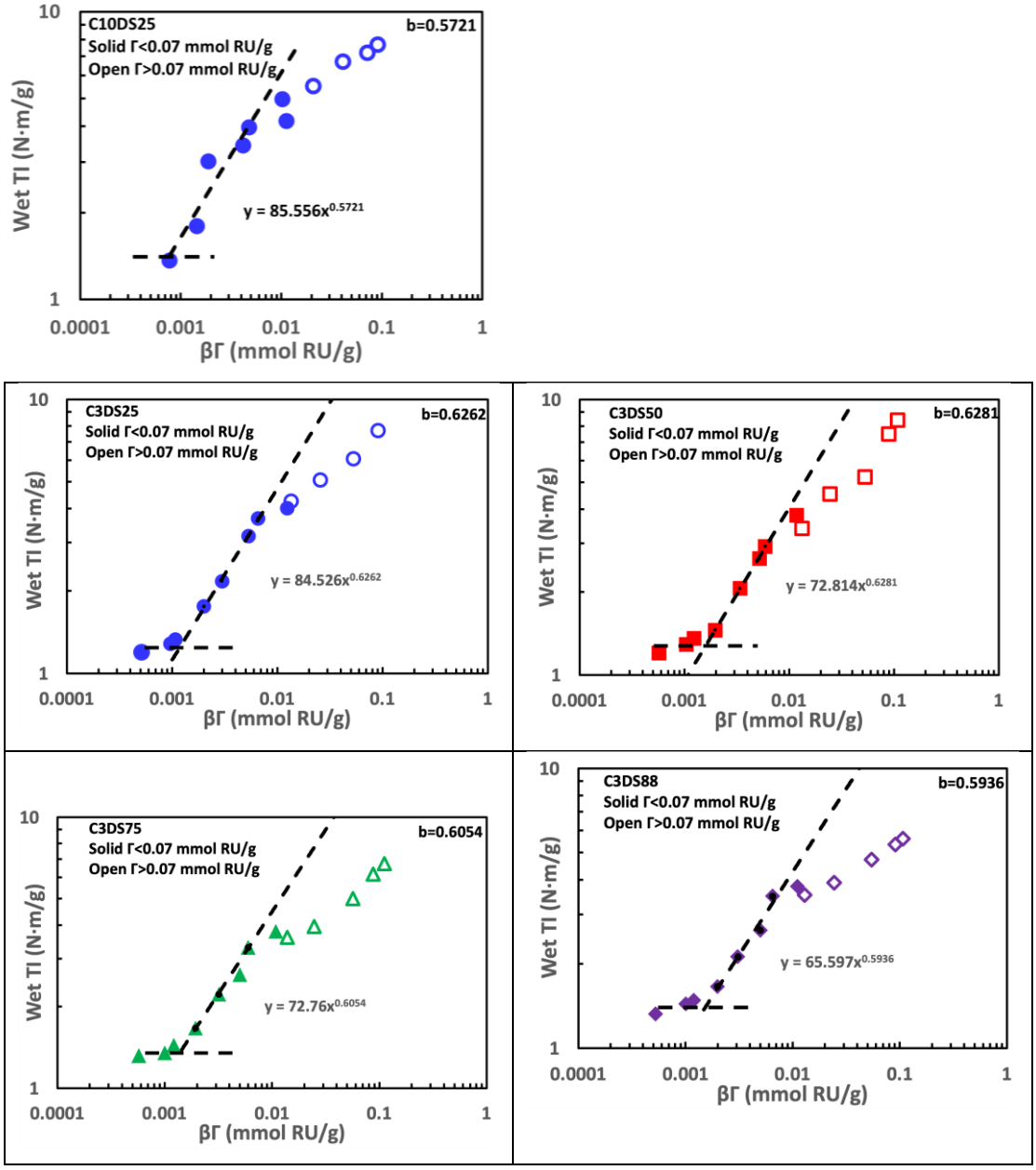

Figure S11 Wet tensile index power law fits for the PEMAc-C series.

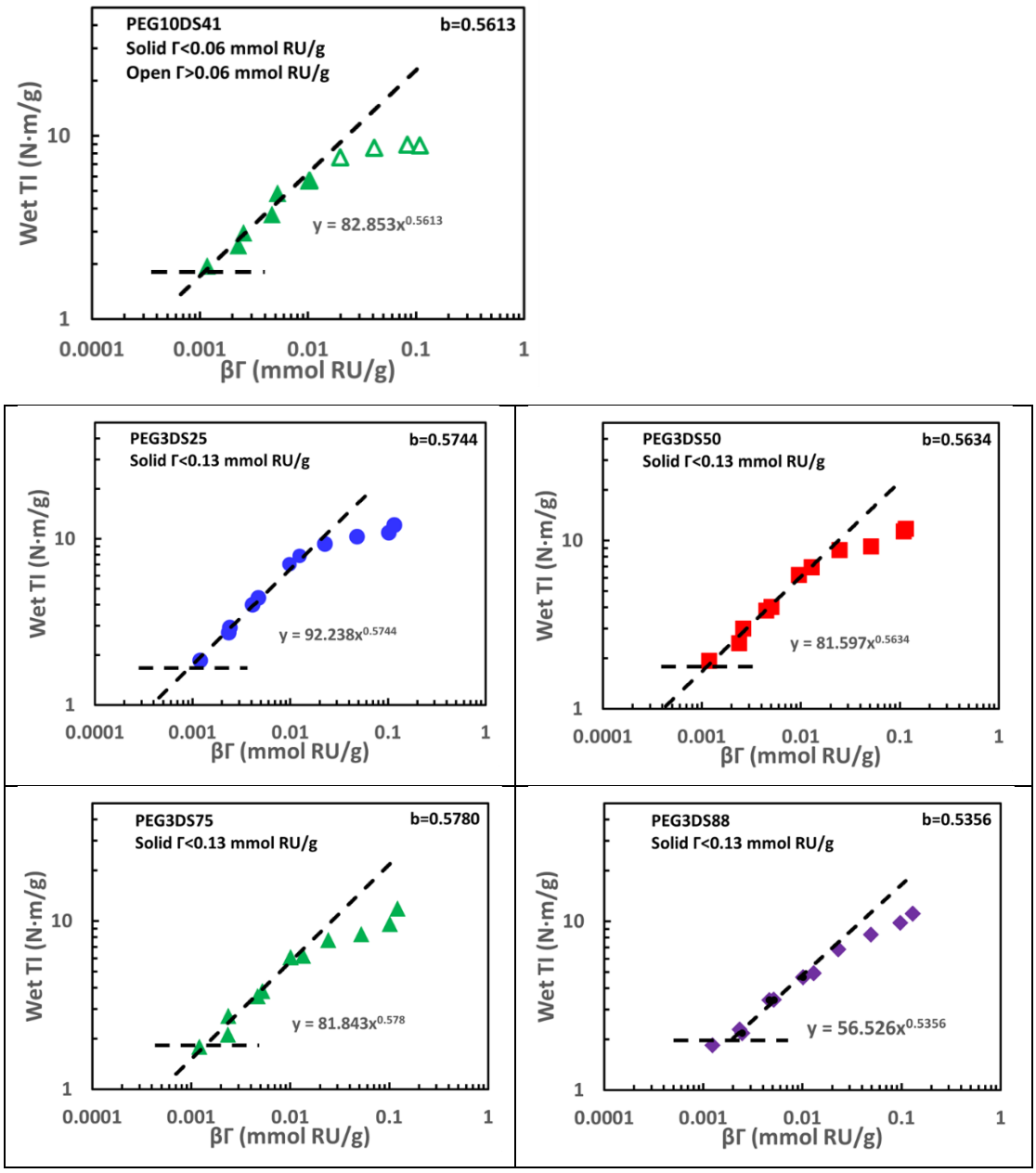

Figure S12 Wet tensile index power law fits for the PEMAc-PEG series.

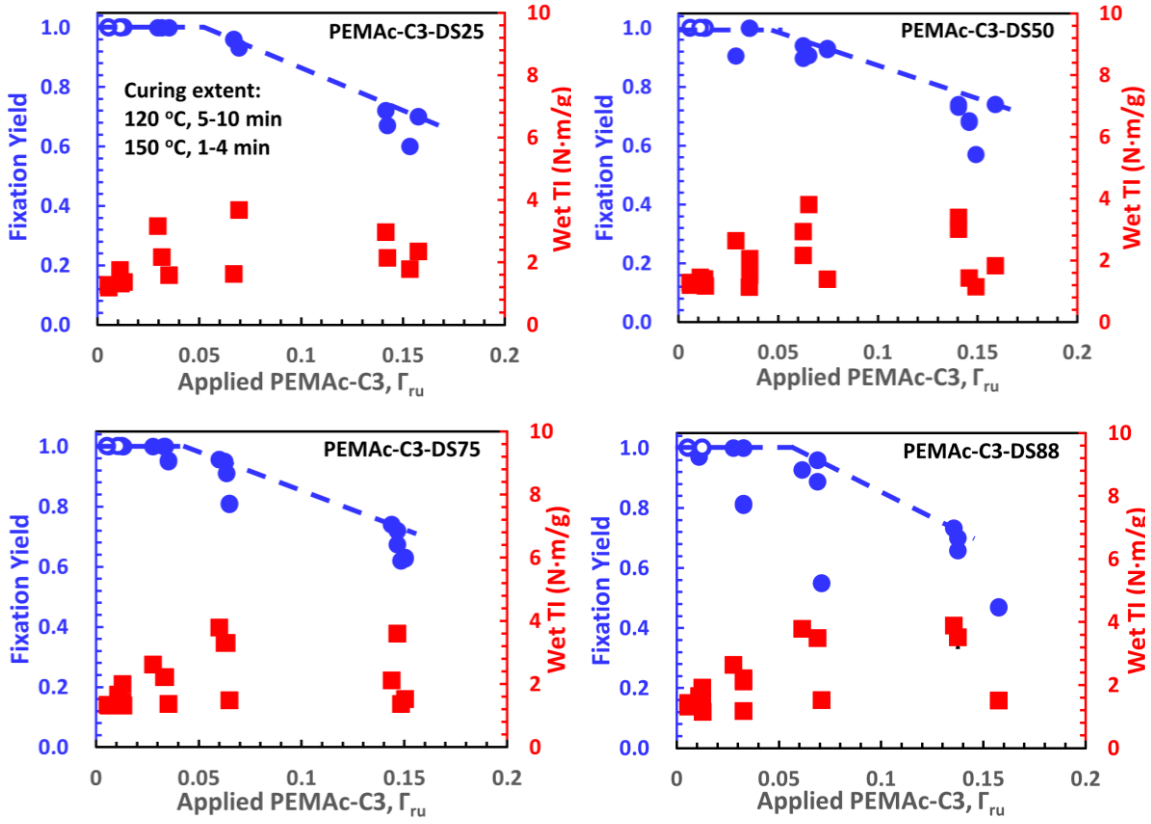

Figure S13 Fixation yields and wet tensile indices as functions of the PEMAc-C3 contents where Γru is a dimensionless number equal to the mmol of repeat units per g of dry fibre. The open symbols portray PEMAc contents that were too low for accurate yield values.

FTIR spectra of PEG3DS88 Cured Films

Experimental. PEG3DS88 solutions were adjusted to pH 4 using 1 N HCl solution and lyophilized. 50 mg lyophilized polymer solid was placed in an aluminum weighing dish and cured in an oven at 150 °C from 2 min to 60 min. 30 mg cured polymer solid was redispersed in 10 mL 0.1 N NaOH solution and stirred for 1 h. After stirring, the suspension was transferred into Amicon® centrifugal filter units (Ultra-15, 10 kDa), then

concentrated to a volume of around 2 mL in a centrifuge equipped with swinging buckets (Beckman Coulter Allegra 64R Series) under 3000g for 20 min. The concentrated polymer suspensions were lyophilized again. The FTIR spectra of cured polymer were collected on an FTIR spectrometer (Thermo Nicolet 6700) under ATR mode.

Interpretation. The carbonyl bands in imides appear at 1778 cm^{-1} for asymmetrical stretching and 1720 cm^{-1} for symmetrical stretching. [1]However, the carbonyl bands in carboxylic acid or ester groups, shown at 1701-1716 $cm^{-1,}$ overlap the symmetrical imide stretching band. To distinguish the carbonyl in carboxylate or imide groups, the carboxylic acid groups were converted to sodium salts by soaking in 0.1 N NaOH solution to shift the carbonyl bands in carboxyl groups to 1582 cm^{-1}. [2] [3] As shown in the FTIR spectra in **Figure S5**, there is no asymmetrical stretching which shows carbonyl bands at 1778 cm^{-1}, and a tiny increased peak at 1720 $cm^{-1,}$ which could be attributed to the carbonyl bands in symmetrical imide-suggesting that only esters and cyclic imide bonds with no intermolecular crosslinking are present. Peaks at 1650 cm^{-1} are characteristic of the carbonyls linked to nitrogen. The increasing intensity of peaks at 1650 cm^{-1} with curing PEMAc-PEG3 suggests imide formation, meaning there were more carbonyls linked with nitrogen after a longer curing time. It is indicated that imides were formed since the only reactive group is the secondary amine (-NH-) in the present amide bonds.

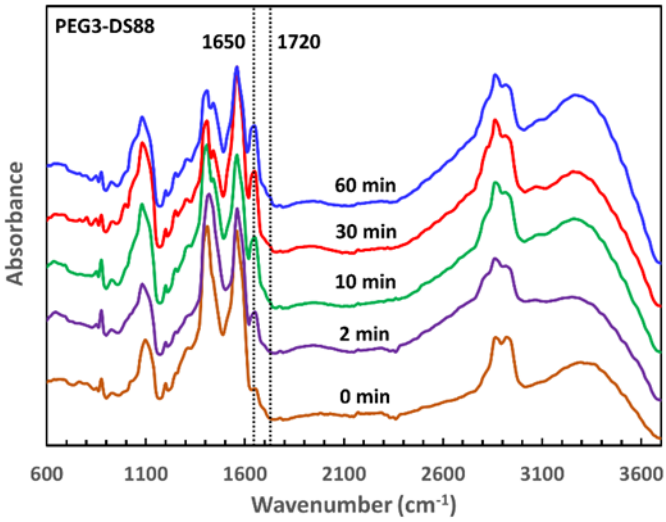

Figure S14 FTIR of a film PEG3DS88 as a function of curing time at 150 °C. Spectra were recorded after NaOH treatment.

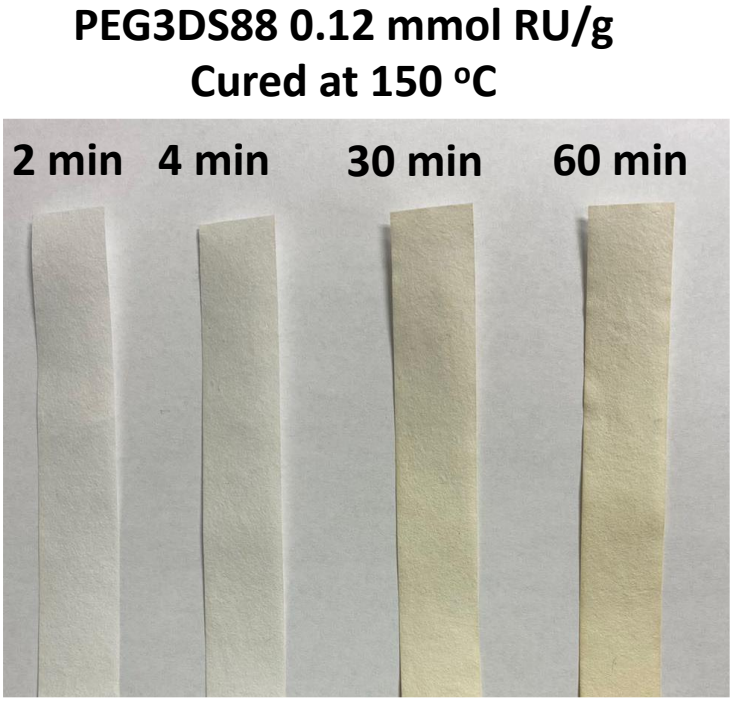

Figure S15 Illustrating the influence of curing time on pulp sheets impregnated with RU/g of PEMAc-PEG3-DS88 cured at 150 °C.

Table S3 Summary of pulp treatment experiments. The titrated charge includes the 0.062 meq/g, the charge content of unmodified fibres.

Row No.	Poly. Type	DS	Dose mmol RU/g	pH	Cure T (°C)	Cure t (min)	β	Titrated Charge (meq/g)	Fixed Poly. (mmol RU/g)	Fix. Yield	TI type	TI (Nm/g)	TI std
1	-	0	0.0000					0.0620			wet	1.180	0.095
2	-	0	0.0000								dry	16.126	0.398
3	C3	25	0.1434	4	150	2	0.09464				dry	18.854	0.814
4	C3	25	0.0648	4	150	2	0.09464				dry	18.480	0.685
5	C3	25	0.0300	4	150	2	0.09464				dry	18.463	1.706
6	C3	25	0.0109	4	150	2	0.09464				dry	16.603	0.901
7	C3	25	0.0052	4	150	2	0.09464				dry	16.295	0.408
8	C3	25	0.1467	4	150	4	0.18032				dry	19.301	0.311
9	C3	25	0.0643	4	150	4	0.18032				dry	18.007	0.268
10	C3	25	0.0290	4	150	4	0.18032				dry	18.281	0.499
11	C3	25	0.0110	4	150	4	0.18032				dry	16.587	1.218
12	C3	25	0.0053	4	150	4	0.18032				dry	16.917	0.922
13	C3	25	0.1425	4	150	10	0.39171				dry	22.133	0.452
14	C3	25	0.1508	4	150	20	0.62998				dry	25.258	1.261
15	C3	25	0.1446	4	150	30	0.77492				dry	26.458	0.980
16	C3	25	0.1415	4	150	1	0.04850	0.2394	0.1014	0.72	wet	2.975	0.155
17	C3	25	0.0668	4	150	1	0.04850	0.1743	0.0642	0.96	wet	1.625	0.114
18	C3	25	0.0352	4	150	1	0.04850	0.1273	0.0373	1.00	wet	1.592	0.049
19	C3	25	0.0129	4	150	1	0.04850				wet	1.367	0.069
20	C3	25	0.1438	4	150	2	0.09464	0.2408	0.1022	0.71	wet	4.245	0.240
21	C3	25	0.0694	4	150	2	0.09464	0.1752	0.0647	0.93	wet	3.679	0.095
22	C3	25	0.0315	4	150	2	0.09464	0.1177	0.0318	1.00	wet	2.168	0.114
23	C3	25	0.0113	4	150	2	0.09464	0.0857	0.0135	1.00	wet	1.327	0.083
24	C3	25	0.0055	4	150	2	0.09464	0.0668	0.0027	1.00	wet	1.193	0.073
25	C3	25	0.1427	4	150	4	0.18032	0.2433	0.1036	0.73	wet	5.073	0.180
26	C3	25	0.0689	4	150	4	0.18032	0.1700	0.0617	0.90	wet	4.010	0.254
27	C3	25	0.0296	4	150	4	0.18032	0.1150	0.0303	1.00	wet	3.170	0.069
28	C3	25	0.0111	4	150	4	0.18032	0.0947	0.0187	1.00	wet	1.755	0.062

Row No.	Poly. Type	DS	Dose mmol RU/g	pH	Cure T (°C)	Cure t (min)	β	Titrated Charge (meq/g)	Fixed Poly. (mmol RU/g)	Fix. Yield	TI type	TI (Nm/g)	TI std
29	C3	25	0.0053	4	150	4	0.18032	0.0735	0.0066	1.00	wet	1.280	0.023
30	C3	25	0.1353	4	150	10	0.39171	0.2365	0.0997	0.74	wet	6.069	0.322
31	C3	25	0.1441	4	150	20	0.62998	0.2378	0.1004	0.70	wet	7.693	0.265
32	C3	25	0.1442	4	150	30	0.77492	0.2605	0.1134	0.79	wet	9.290	0.174
33	C3	25	0.1311	4	150	60	0.94934				wet	11.487	0.361
34	C3	25	0.1294	4	150	90	0.98860				wet	10.826	0.444
35	C3	25	0.1299	4	150	120	0.99743				wet	10.425	0.514
36	C3	25	0.1423	6	150	2	0.99513	0.2283	0.0950	0.67	wet	2.141	0.166
37	C3	25	0.1534	6	120	5	0.99774	0.2234	0.0922	0.60	wet	1.791	0.122
38	C3	25	0.1575	6	120	10	0.99999	0.2554	0.1105	0.70	wet	2.351	0.231
39	C3	50	0.1443	4	150	2	0.09464				dry	19.192	0.385
40	C3	50	0.0665	4	150	2	0.09464				dry	17.456	0.145
41	C3	50	0.0320	4	150	2	0.09464				dry	17.999	0.410
42	C3	50	0.0118	4	150	2	0.09464				dry	17.237	0.708
43	C3	50	0.0059	4	150	2	0.09464				dry	16.847	0.676
44	C3	50	0.1400	4	150	4	0.18032				dry	19.084	0.118
45	C3	50	0.0651	4	150	4	0.18032				dry	16.846	0.625
46	C3	50	0.0308	4	150	4	0.18032				dry	18.222	0.923
47	C3	50	0.0116	4	150	4	0.18032				dry	17.715	0.575
48	C3	50	0.0060	4	150	4	0.18032				dry	17.539	0.880
49	C3	50	0.1408	4	150	10	0.39171				dry	20.342	1.095
50	C3	50	0.1430	4	150	20	0.62998				dry	23.636	0.659
51	C3	50	0.1452	4	150	30	0.77492				dry	26.799	1.016
52	C3	50	0.1458	4	150	1	0.04850	0.2118	0.0999	0.68	wet	1.430	0.056
53	C3	50	0.0746	4	150	1	0.04850	0.1657	0.0691	0.93	wet	1.390	0.045
54	C3	50	0.0356	4	150	1	0.04850	0.1166	0.0364	1.00	wet	1.132	0.025
55	C3	50	0.0134	4	150	1	0.04850				wet	1.174	0.018
56	C3	50	0.1403	4	150	2	0.09464	0.2158	0.1025	0.73	wet	3.399	0.080
57	C3	50	0.0625	4	150	2	0.09464	0.1461	0.0561	0.90	wet	2.928	0.111
58	C3	50	0.0358	4	150	2	0.09464	0.1198	0.0385	1.00	wet	2.058	0.091

Row No.	Poly. Type	DS	Dose mmol RU/g	pH	Cure T (°C)	Cure t (min)	β	Titrated Charge (meq/g)	Fixed Poly. (mmol RU/g)	Fix. Yield	TI type	TI (Nm/g)	TI std
59	C3	50	0.0131	4	150	2	0.09464	0.0776	0.0104	1.00	wet	1.358	0.043
60	C3	50	0.0061	4	150	2	0.09464	0.0640	0.0013	1.00	wet	1.199	0.051
61	C3	50	0.1361	4	150	4	0.18032	0.2048	0.0952	0.70	wet	4.528	0.164
62	C3	50	0.0653	4	150	4	0.18032	0.1507	0.0591	0.91	wet	3.802	0.098
63	C3	50	0.0288	4	150	4	0.18032	0.1011	0.0261	0.90	wet	2.642	0.076
64	C3	50	0.0109	4	150	4	0.18032	0.0816	0.0131	1.00	wet	1.454	0.035
65	C3	50	0.0058	4	150	4	0.18032	0.0729	0.0073	1.00	wet	1.290	0.033
66	C3	50	0.1362	4	150	10	0.39171	0.2107	0.0991	0.73	wet	5.230	0.080
67	C3	50	0.1425	4	150	20	0.62998	0.2164	0.1029	0.72	wet	7.472	0.255
68	C3	50	0.1400	4	150	30	0.77492	0.2082	0.0975	0.70	wet	8.391	0.234
69	C3	50	0.1328	4	150	60	0.94934				wet	8.570	0.308
70	C3	50	0.1492	6	120	5	0.99774	0.1885	0.0843	0.57	wet	1.148	0.108
71	C3	50	0.1589	6	120	10	0.99999	0.2372	0.1168	0.74	wet	1.824	0.194
72	C3	75	0.1417	4	150	2	0.09464				dry	18.326	0.581
73	C3	75	0.0654	4	150	2	0.09464				dry	18.397	1.051
74	C3	75	0.0320	4	150	2	0.09464				dry	18.186	0.455
75	C3	75	0.0115	4	150	2	0.09464				dry	17.187	0.467
76	C3	75	0.0059	4	150	2	0.09464				dry	16.741	0.848
77	C3	75	0.1446	4	150	4	0.18032				dry	19.259	0.535
78	C3	75	0.0608	4	150	4	0.18032				dry	19.353	0.616
79	C3	75	0.0303	4	150	4	0.18032				dry	17.973	0.653
80	C3	75	0.0114	4	150	4	0.18032				dry	16.623	0.921
81	C3	75	0.0058	4	150	4	0.18032				dry	17.020	0.825
82	C3	75	0.1445	4	150	10	0.39171				dry	21.405	0.858
83	C3	75	0.1496	4	150	20	0.62998				dry	24.760	1.193
84	C3	75	0.1444	4	150	30	0.77492				dry	26.051	0.818
85	C3	75	0.1504	4	150	1	0.04850	0.1799	0.0943	0.63	wet	1.519	0.040
86	C3	75	0.0650	4	150	1	0.04850	0.1276	0.0525	0.81	wet	1.483	0.068
87	C3	75	0.0353	4	150	1	0.04850	0.1041	0.0337	0.95	wet	1.376	0.033
88	C3	75	0.0132	4	150	1	0.04850				wet	1.320	0.042

Row No.	Poly. Type	DS	Dose mmol RU/g	pH	Cure T (°C)	Cure t (min)	β	Titrated Charge (meq/g)	Fixed Poly. (mmol RU/g)	Fix. Yield	TI type	TI (Nm/g)	TI std
89	C3	75	0.1466	4	150	2	0.09464	0.1856	0.0989	0.67	wet	3.597	0.175
90	C3	75	0.0634	4	150	2	0.09464	0.1342	0.0578	0.91	wet	3.299	0.095
91	C3	75	0.0336	4	150	2	0.09464	0.1181	0.0449	1.00	wet	2.222	0.093
92	C3	75	0.0129	4	150	2	0.09464	0.0848	0.0182	1.00	wet	1.439	0.070
93	C3	75	0.0061	4	150	2	0.09464	0.0673	0.0042	1.00	wet	1.316	0.037
94	C3	75	0.1375	4	150	4	0.18032	0.1889	0.1015	0.74	wet	3.939	0.167
95	C3	75	0.0600	4	150	4	0.18032	0.1337	0.0574	0.96	wet	3.791	0.098
96	C3	75	0.0277	4	150	4	0.18032	0.0974	0.0283	1.00	wet	2.622	0.031
97	C3	75	0.0108	4	150	4	0.18032	0.0883	0.0210	1.00	wet	1.666	0.069
98	C3	75	0.0055	4	150	4	0.18032	0.0658	0.0030	1.00	wet	1.348	0.045
99	C3	75	0.1449	4	150	10	0.39171	0.1863	0.0994	0.69	wet	5.004	0.111
100	C3	75	0.1395	4	150	20	0.62998	0.1762	0.0914	0.66	wet	6.148	0.103
101	C3	75	0.1444	4	150	30	0.77492	0.1914	0.1035	0.72	wet	6.729	0.096
102	C3	75	0.1397	4	150	60	0.94934				wet	6.667	0.327
103	C3	75	0.1483	6	120	5	0.99774	0.1775	0.0924	0.62	wet	1.367	0.076
104	C3	75	0.1438	6	120	10	0.99999	0.1943	0.1058	0.74	wet	2.113	0.157
105	C3	88	0.1400	4	150	2	0.09464				dry	18.617	0.354
106	C3	88	0.0603	4	150	2	0.09464				dry	18.389	0.146
107	C3	88	0.0308	4	150	2	0.09464				dry	18.259	0.329
108	C3	88	0.0109	4	150	2	0.09464				dry	17.854	0.500
109	C3	88	0.0055	4	150	2	0.09464				dry	17.147	0.374
110	C3	88	0.1387	4	150	4	0.18032				dry	17.793	0.413
111	C3	88	0.0625	4	150	4	0.18032				dry	18.688	1.068
112	C3	88	0.0298	4	150	4	0.18032				dry	18.763	0.361
113	C3	88	0.0118	4	150	4	0.18032				dry	16.742	0.434
114	C3	88	0.0058	4	150	4	0.18032				dry	16.857	0.393
115	C3	88	0.1398	4	150	10	0.39171				dry	19.763	0.777
116	C3	88	0.1375	4	150	20	0.62998				dry	21.055	0.953
117	C3	88	0.1425	4	150	30	0.77492				dry	22.700	1.139
118	C3	88	0.1574	4	150	1	0.04850	0.1451	0.0735	0.47	wet	1.516	0.051

Row No.	Poly. Type	DS	Dose mmol RU/g	pH	Cure T (°C)	Cure t (min)	β	Titrated Charge (meq/g)	Fixed Poly. (mmol RU/g)	Fix. Yield	TI type	TI (Nm/g)	TI std
119	C3	88	0.0708	4	150	1	0.04850	0.1059	0.0388	0.55	wet	1.518	0.083
120	C3	88	0.0327	4	150	1	0.04850	0.0921	0.0266	0.81	wet	1.174	0.022
121	C3	88	0.0126	4	150	1	0.04850				wet	1.155	0.070
122	C3	88	0.1375	4	150	2	0.09464	0.1642	0.0904	0.66	wet	3.518	0.332
123	C3	88	0.0689	4	150	2	0.09464	0.1311	0.0612	0.89	wet	3.488	0.189
124	C3	88	0.0326	4	150	2	0.09464	0.1053	0.0383	1.00	wet	2.117	0.141
125	C3	88	0.0126	4	150	2	0.09464	0.0845	0.0199	1.00	wet	1.484	0.076
126	C3	88	0.0056	4	150	2	0.09464	0.0695	0.0066	1.00	wet	1.322	0.039
127	C3	88	0.1355	4	150	4	0.18032	0.1742	0.0993	0.73	wet	3.892	0.097
128	C3	88	0.0613	4	150	4	0.18032	0.1263	0.0569	0.93	wet	3.782	0.049
129	C3	88	0.0277	4	150	4	0.18032	0.1013	0.0348	1.00	wet	2.639	0.137
130	C3	88	0.0110	4	150	4	0.18032	0.0740	0.0106	0.97	wet	1.658	0.085
131	C3	88	0.0056	4	150	4	0.18032	0.0684	0.0057	1.00	wet	1.439	0.048
132	C3	88	0.1398	4	150	10	0.39171	0.1712	0.0966	0.69	wet	4.715	0.098
133	C3	88	0.1455	4	150	20	0.62998	0.1827	0.1068	0.73	wet	5.327	0.1
134	C3	88	0.1383	4	150	30	0.77492	0.1744	0.0995	0.72	wet	5.589	0.1
135	C3	88	0.1308	4	150	60	0.94934				wet	5.245	0.216
136	C10	25	0.1263	4	150	2	0.09464	0.1783	0.0665	0.53	wet	4.176	0.048
137	C10	25	0.0445	4	150	2	0.09464	0.1407	0.0450	1.00	wet	3.963	0.242
138	C10	25	0.0197	4	150	2	0.09464	0.1003	0.0219	1.00	wet	3.018	0.142
139	C10	25	0.0090	4	150	2	0.09464	0.0866	0.0141	1.00	wet	1.365	0.285
140	C10	25	0.1243	4	150	4	0.18032	0.1955	0.0763	0.61	wet	5.502	0.09
141	C10	25	0.0486	4	150	4	0.18032	0.1365	0.0426	0.88	wet	4.971	0.293
142	C10	25	0.0186	4	150	4	0.18032	0.0980	0.0206	1.00	wet	3.428	0.198
143	C10	25	0.0090	4	150	4	0.18032	0.0754	0.0077	0.85	wet	1.801	0.266
144	C10	25	0.1094	4	150	10	0.39171	0.182	0.0686	0.63	wet	6.696	0.174
145	C10	25	0.1150	4	150	20	0.62998				wet	7.187	0.115
146	C10	25	0.1185	4	150	30	0.77492				wet	7.655	0.208
147	C10	25	0.1258	4	150	60	0.94934				wet	8.285	0.245
148	PEG3	24	0.1317	4	150	2	0.09464	0.2861	0.1273	0.97	wet	7.855	0.437

Row No.	Poly. Type	DS	Dose mmol RU/g	pH	Cure T (°C)	Cure t (min)	β	Titrated Charge (meq/g)	Fixed Poly. (mmol RU/g)	Fix. Yield	TI type	TI (Nm/g)	TI std
149	PEG3	24	0.0500	4	150	2	0.09464	0.1476	0.0486	0.98	wet	4.408	0.327
150	PEG3	24	0.0254	4	150	2	0.09464	0.1102	0.0274	1.00	wet	2.929	0.166
151	PEG3	24	0.0126	4	150	2	0.09464	0.0949	0.0187	1.00	wet	1.854	0.089
152	PEG3	24	0.1254	4	150	4	0.18032	0.2442	0.1035	0.83	wet	9.286	0.333
153	PEG3	24	0.0546	4	150	4	0.18032	0.1577	0.0544	1.00	wet	7.025	0.401
154	PEG3	24	0.0228	4	150	4	0.18032	0.1031	0.0234	1.00	wet	4.018	0.244
155	PEG3	24	0.0130	4	150	4	0.18032	0.1020	0.0227	1.00	wet	2.721	0.132
156	PEG3	24	0.1230	4	150	10	0.39171	0.2264	0.0934	0.76	wet	10.303	0.486
157	PEG3	24	0.1315	4	150	30	0.77492	0.2085	0.0832	0.63	wet	10.853	0.134
158	PEG3	24	0.1229	4	150	60	0.94934	0.1883	0.0718	0.58	wet	12.029	0.626
159	PEG3	24	0.1262	4	120	10	0.15458	0.2729	0.1198	0.95	wet	8.502	0.308
160	PEG3	24	0.1317	4	120	30	0.39575	0.2777	0.1226	0.93	wet	10.930	0.164
161	PEG3	24	0.1290	4	120	60	0.63488	0.2730	0.1199	0.93	wet	12.522	0.393
162	PEG3	24	0.1255	4	120	90	0.77938	0.2569	0.1107	0.88	wet	13.159	0.259
163	PEG3	50	0.1371	4	150	2	0.09464	0.2503	0.1255	0.92	wet	6.908	0.374
164	PEG3	50	0.0533	4	150	2	0.09464	0.1446	0.0551	1.00	wet	4.030	0.144
165	PEG3	50	0.0276	4	150	2	0.09464	0.1077	0.0305	1.00	wet	2.996	0.111
166	PEG3	50	0.0125	4	150	2	0.09464	0.0892	0.0181	1.00	wet	1.925	0.064
167	PEG3	50	0.1377	4	150	4	0.18032	0.2287	0.1111	0.81	wet	8.757	0.402
168	PEG3	50	0.0534	4	150	4	0.18032	0.1339	0.0480	0.90	wet	6.220	0.275
169	PEG3	50	0.0248	4	150	4	0.18032	0.1146	0.0351	1.00	wet	3.833	0.169
170	PEG3	50	0.0132	4	150	4	0.18032	0.0867	0.0165	1.00	wet	2.457	0.102
171	PEG3	50	0.1309	4	150	10	0.39171	0.1992	0.0915	0.70	wet	9.212	0.332
172	PEG3	50	0.1415	4	150	30	0.77492	0.1981	0.0907	0.64	wet	11.306	0.266
173	PEG3	50	0.1219	4	150	60	0.94934	0.1722	0.0735	0.60	wet	11.708	0.532
174	PEG3	74	0.1423	4	150	2	0.09464	0.2160	0.1222	0.86	wet	6.191	0.357
175	PEG3	74	0.0550	4	150	2	0.09464	0.1286	0.0529	0.96	wet	3.835	0.152
176	PEG3	74	0.0250	4	150	2	0.09464	0.0917	0.0236	0.94	wet	2.729	0.153
177	PEG3	74	0.0127	4	150	2	0.09464	0.0809	0.0150	1.00	wet	1.787	0.092
178	PEG3	74	0.1344	4	150	4	0.18032	0.1966	0.1068	0.79	wet	7.705	0.402

Row No.	Poly. Type	DS	Dose mmol RU/g	pH	Cure T (°C)	Cure t (min)	β	Titrated Charge (meq/g)	Fixed Poly. (mmol RU/g)	Fix. Yield	TI type	TI (Nm/g)	TI std
179	PEG3	74	0.0560	4	150	4	0.18032	0.1271	0.0517	0.92	wet	6.075	0.131
180	PEG3	74	0.0260	4	150	4	0.18032	0.0923	0.0241	0.93	wet	3.567	0.172
181	PEG3	74	0.0130	4	150	4	0.18032	0.0907	0.0228	1.00	wet	2.112	0.123
182	PEG3	74	0.1331	4	150	10	0.39171	0.1701	0.0858	0.64	wet	8.353	0.325
183	PEG3	74	0.1311	4	150	30	0.77492	0.1652	0.0819	0.62	wet	9.613	0.153
184	PEG3	74	0.1270	4	150	60	0.94934	0.1490	0.0690	0.54	wet	11.830	0.495
185	PEG3	88	0.1377	4	150	2	0.09464	0.1978	0.1213	0.88	wet	4.908	0.133
186	PEG3	88	0.0547	4	150	2	0.09464	0.1213	0.0529	0.97	wet	3.419	0.081
187	PEG3	88	0.0261	4	150	2	0.09464	0.1053	0.0387	1.00	wet	2.171	0.356
188	PEG3	88	0.0131	4	150	2	0.09464	0.0875	0.0228	1.00	wet	1.843	0.265
189	PEG3	88	0.1281	4	150	4	0.18032	0.1798	0.1052	0.82	wet	6.817	0.155
190	PEG3	88	0.0563	4	150	4	0.18032	0.1211	0.0528	0.94	wet	4.659	0.504
191	PEG3	88	0.0258	4	150	4	0.18032	0.1046	0.0380	1.00	wet	3.409	0.714
192	PEG3	88	0.0129	4	150	4	0.18032	0.0884	0.0236	1.00	wet	2.291	0.320
193	PEG3	88	0.1250	4	150	10	0.39171	0.1609	0.0883	0.71	wet	8.354	0.185
194	PEG3	88	0.1250	4	150	30	0.77492	0.1606	0.0880	0.70	wet	9.774	0.501
195	PEG3	88	0.1369	4	150	60	0.94934	0.1676	0.0943	0.68	wet	11.095	0.381
196	PEG3	88	0.1233	4	120	10	0.15458	0.1916	0.1157	0.94	wet	7.002	0.275
197	PEG3	88	0.1254	4	120	30	0.39575	0.1966	0.1202	0.96	wet	9.064	0.134
198	PEG3	88	0.1309	4	120	60	0.63488	0.2028	0.1257	0.96	wet	11.555	0.471
199	PEG3	88	0.1289	4	120	90	0.77938	0.1975	0.1210	0.94	wet	12.101	0.223
200	PEG10	41	0.1095	4	150	2	0.09464	0.1549	0.0584	0.53	wet	5.694	0.178
201	PEG10	41	0.0556	4	150	2	0.09464	0.1443	0.0518	0.93	wet	4.848	0.169
202	PEG10	41	0.0267	4	150	2	0.09464	0.1027	0.0256	0.96	wet	2.950	0.106
203	PEG10	41	0.0123	4	150	2	0.09464	0.0851	0.0145	1.00	wet	1.946	0.095
204	PEG10	41	0.1112	4	150	4	0.18032	0.1532	0.0574	0.52	wet	7.617	0.429

Row No.	Poly. Type	DS	Dose mmol RU/g	pH	Cure T (°C)	Cure t (min)	β	Titrated Charge (meq/g)	Fixed Poly. (mmol RU/g)	Fix. Yield	TI type	TI (Nm/g)	TI std
205	PEG10	41	0.0567	4	150	4	0.18032	0.1413	0.0499	0.88	wet	5.645	0.275
206	PEG10	41	0.0258	4	150	4	0.18032	0.1132	0.0322	1.00	wet	3.715	0.265
207	PEG10	41	0.0126	4	150	4	0.18032	0.0981	0.0227	1.00	wet	2.516	0.111
208	PEG10	41	0.1056	4	150	10	0.39171	0.1625	0.0632	0.60	wet	8.585	0.349
209	PEG10	41	0.1081	4	150	30	0.77492	0.1375	0.0475	0.44	wet	8.928	0.357
210	PEG10	41	0.1142	4	150	60	0.94934	0.1186	0.0356	0.31	wet	8.835	0.245

References

[1] S.-H. Hsiao, G.-S. Liou, Y.-C. Kung, Y.-J. Lee, Synthesis and Characterization of Electrochromic Poly(Amide–Imide)S Based on the Diimide-Diacid from 4,4′-Diamino-4″-Methoxytriphenylamine and Trimellitic Anhydride, Eur. Polym. J., 46 (2010) 1355-1366. https://doi.org/10.1016/j.eurpolymj.2010.03.016

[2] C.Q. Yang, FT-IR Spectroscopy Study of the Ester Crosslinking Mechanism of Cotton Cellulose, Text. Res. J., 61 (1991) 433-440. https://doi.org/10.1177/004051759106100801

[3] C.Q. Yang, X. Wang, Formation of Five-Membered Cyclic Anhydride Intermediates by Polycarboxylic Acids: Thermal Analysis and Fourier Transform Infrared Spectroscopy, J. Appl. Polym. Sci., 70 (1998) 2711-2718. https://doi.org/10.1002/(SICI)1097-4628(19981226)70:13<2711::AID-APP16>3.0.CO;2-Z

Chapter 4

Polymer Grafting Impacts Aggregated CNF Properties

In this chapter, alkyl-amines and PEG-amines modified PEMA derivatives, with degrees of substitution (DS) ranging from 25% to 86%, were grafted onto cellulose nanofibrils (CNF) via esterification in acetone. The grafting process achieved high yields, even with a minimal 14% succinic acid moiety content remaining. The grafted polymer preserved the aggregated structures in acetone. Through particle size measurements and imaging techniques, the grafted CNF exhibited a composite structure comprising individualized nanofibrils, microribbons assembled by the nanofibrils, and flocs formed through entangled microribbons. Imaging techniques were employed to unveil the PEMAc grafted microribbons in both dry and wet states, showing helical ribbon structures.

The experiment design, data collection and analysis, and first draft writing were completed by me. My summer student Kashaf Amir helped me with part of the experiments. Dr. Mouhanad Babi and Dr. Jose M Moran-Mirabal assisted me with the microscopy imaging. Dr. Robert Pelton rewrote parts of the draft as necessary.

This chapter is in preparation for publication.

Polymer Grafting Impacts Aggregated CNF Properties

Abstract

Poly (ethylene-*alt*-maleic anhydride) (PEMA) was modified with alkyl-amine (C3, C10) and methoxy-PEG-amine (PEG3, PEG10, PEG20) to produce PEMA derivatives with varying degrees of substitution (DS). PEMA and its derivatives were then grafted on mechanically produced cellulose nanofibrils (CNF) through a 4-(dimethylamino pyridine) (DMAP) catalyzed esterification in acetone. The grafting reaction was efficient, showing high yields when the PEMA dosages were below 0.125 g/g. A solvent exchange step was carried out to facilitate the grafting process, transferring the CNF from water to acetone, resulting in the aggregation of nanofibrils. The aggregated structures were crosslinked and preserved by the grafted polymer and further stabilized in water after polymer hydrolysis. The grafted CNF exhibited three structures-fully dispersed nanofibrils, microribbons and flocs. Aligned nanofibrils assembled the microribbons, while the flocs consisted of entangled microribbons. The content of flocs decreased with reduced polymer dosages and increased DS, as indicated by the diameter distributions. The introduction of pendant PEG20 chains effectively improved the dispersibility of the grafted CNF. The microribbon structures were further characterized using imaging techniques, revealing that they were formed from 2-12 layers of nanofibrils, with a thickness ranging from 40-220 nm and a width of approximately 3 μm. The specific structure of PEMA-PEG grafted microribbons was found to be related to the DS values. Microribbons with a DS below 75% exhibited a three-dimensional helical structure, while those with a DS above 75% appeared flat with intermittent twisting. The helical microribbons displayed twisting in both left and right-handed manners, showing the two most common wavelengths of 10.8 μm and 44.6 μm.

Introduction

Nanocelluloses are a class of cellulosic materials having a cross-section in the nanoscale. They are generally classified into three categories-cellulose nanocrystals (CNC), cellulose nanofibrils (CNF) and bacterial celluloses (BMCC).[1] Plant-based cellulose, such as that found in wood, serves as a cost-effective resource for producing CNF and CNC. CNC are derived from the crystalline regions of cellulose, while CNF are derived from disordered and crystalline regions. CNF exhibit a high aspect ratio, making them exceptional materials for reinforcing composites.[2] Plant-derived CNF are created through a defibrillation process that breaks down the hierarchical structure of wood pulp fibres. Pretreatments, such as TEMPO oxidation, carboxymethylation, and enzymatic treatments, can be applied to reduce energy consumption during mechanical homogenization and introduce charged groups that facilitate nanofibril dispersion.[3] In this case, elementary fibrils with a width below 5 nm could be isolated. Nanofibrils produced without pretreatment typically exhibit larger widths ranging from 5 to 100 nm, and they tend to aggregate more easily compared with TEMPO-oxidized and carboxymethylated CNF.[1]

The aggregation of cellulose nanofibrils (CNF) is well-known to occur due to the formation of inter-fibril hydrogen bonds during the removal of water between the CNF.[4] The aggregation is commonly observed during dewatering and drying processes.[5] Dewatering is a step to concentrate CNF slurry at the tail-end of the CNF production process. The most used strategy is centrifugation. Besides other alternative strategies are filtration, pressing, solvent evaporation and shear stress-induced dewatering.[5] When the CNF slurry concentration surpasses 3wt%, it transitions to a gel-like state, forming aggregated bundles. The drying of CNF remains a challenge to date since the dispersibility of CNF is dramatically reduced after full dehydration.[5] Supercritical CO_2 drying, freeze drying, and spray drying are the methods which could suppress the fibril agglomeration. Oven drying typically generates large and entangled aggregates with irreversible dispersibility. Solvent exchange combined with evaporation is another type of dewatering step. Similarly, the solvent exchange to incompatible solvents like ethanol, acetone, toluene, N-methyl pyrrolidone, hexane and pentane also causes the formation of CNF aggregates.[6]

The intermolecular interactions, on the other hand, provide nanocelluloses with the ability to assemble into organized structures and materials through a bottom-up path.[7] The self-assembled nanocelluloses are applied to fabricate nanoparticles, filaments, coating, optical devices, biosensors and membranes.[8] Quick freezing in liquid nitrogen followed by freeze drying resulted in the assembly of CNF into bundles with widths ranging from 30 to 200 nm,[9] while TEMPO-oxidized CNF forms broad ribbons with widths from 125 to 500 nm.[10] Spinning processes encompassing electrospinning, wet spinning and dry spinning convert CNF into micro-scaled filaments in which the internal structures are

affected by CNF self-assembly. Wet spinning, mainly, is an easy-to-operate method due to the inherent self-assembly of CNF. A typical wet spinning process extrudes aqueous CNF gel into a coagulation bath containing water-miscible organic solvents like acetone, tetrahydrofuran, or alcohol.[11] Dehydration rapidly occurs as water is replaced by organic solvents, forming hydrogen bonds that bundle up the nanofibrils. Cellulose-incompatible solvents offer the ability to tune the self-assembly of nanocelluloses. Illustrative examples include the development of films[12] aerogels,[6a, 13] composites[14] and bundles.[15]

In the fabrication of CNF-reinforced polymeric composites, the agglomeration of CNF becomes more pronounced due to the dehydration steps, such as solvent exchange and curing. The solvent exchange process aims to disperse CNF in organic solvents and ensure homogeneous mixing with polymer monomers and crosslinkers. Owing to the utilization of organic solvents, the agglomeration of CNF is akin to the solvent-induced assembly. Acetone, a water-miscible solvent, is extensively employed in blends of CNF with materials such as epoxy resin,[16] poly lactic acid (PLA),[17] poly methyl methacrylate (PMMA),[18] and isocyanates.[19] In these cases, the polymer monomers are not water-soluble, and the presence of water molecules can hinder crosslinking reactions. The process typically involves exchanging CNF from an aqueous slurry to acetone, followed by conducting reactions or transferring them to nonpolar solvents (e.g., chloroform, toluene) for subsequent reactions.

The aggregation of CNF is commonly confirmed using imaging techniques such as AFM, SEM, and TEM, which can magnify objects to the submicron scale. In these images, broad CNF bundles containing multiple nanofibrils can be observed,[20] and some thinner CNF bundles exhibit ribbon or lamella-like structures.[9a, 10] However, due to the consistent entanglement of mechanically prepared CNF, revealing the actual structure of individual CNF aggregates is challenging. The aggregation of CNF is closely related to the inherent self-assembly ability of cellulose. Understanding the structure of aggregated CNF provides valuable insights into the assembly process and the factors driving self-assembly. Furthermore, the structure of cellulosic materials can be designed and altered.

Solvent exchange-induced dehydration offers a potential way to isolate individual CNF aggregates from the entangled large aggregates. A solvent exchange cycle of water - incompatible solvent-water would mimic a dehydration and rehydration process. A suspended CNF system is available for chemical modification and incorporating additives to suppress the entanglement and tune the assembly of aggregates. We have discovered that maleic copolymers, especially poly (ethylene-*alt*-maleic anhydride) (PEMA), are excellent candidates for chemical modification on cellulose because of numerous reactive anhydride groups along the polymer chains.[21] Herein, with a view to revealing the structure of CNF aggregate and the factors affecting the assembly, we isolated individual aggregated CNF microribbon using the solvent exchange to acetone and followed by chemical modification with PEMA. Upon rehydration of the aggregates, unreacted maleic

anhydrides hydrolyzed into maleic acid with carboxylate groups, stabilizing the aggregated structures in water. Alkyl-amine and PEG-amine as hydrophobic and hydrophilic additives are added to alter the assembly. Particle size measurement and imaging techniques, including widefield microscopy, confocal lasering scanning microscopy (CLSM), atomic force microscopy (AFM), and field emission scanning electron microscopy (FESEM), were performed to disclose the aggregated structures of CNF. It is shown that CNF with a high aspect ratio always assembles into microribbon structures which further entangle forming flocs. The factors affecting the structures of aggregated CNF were investigated. Meanwhile, the microribbon structures in both dry and wet states were unravelled.

Experimental

Materials. Never-dried cellulose nanofibre (CNF) aqueous gel (3 wt% solid content, 90% fines grade, lot#U31) was purchased from the University of Maine. Poly (ethylene-alt-maleic anhydride), PEMA (MW 100 kDa – 500 kDa), propylamine (≥99%, C3), decylamine (≥99%, GC, C10), 2-(2-(2-methoxyethoxy)ethoxy) ethanamine (≥95%, MPEG3), Poly(ethylene glycol) methyl ether amine (Mn=500, MPEG10), methoxypolyethylene glycol propyl amine (Mn=1000, MPEG20), 4-(dimethylamino)pyridine (≥99%), (3-aminopropyl)triethoxysilane (APTES,99%), toluene (anhydrous, 99.8%), and methanol (ACS reagent, ≥99.8%) were purchased from Sigma-Aldrich and used without further purification. sulfo-Cyanine5 amine was purchased from Lumiprobe Corp. Acetone (ACS reagent, ⩾99.5%) was purchased from Sigma-Aldrich and pretreated with molecule sieves 3Å to remove water. Other chemicals were $NaHCO_3$ (Reagent Grade, Caledon Lab Ltd), NaOH and HCl solution (1 M & 0.1 M, LabChem Inc.). Ultrapure water was purified from the Barnstead™ Nanopure™ system.

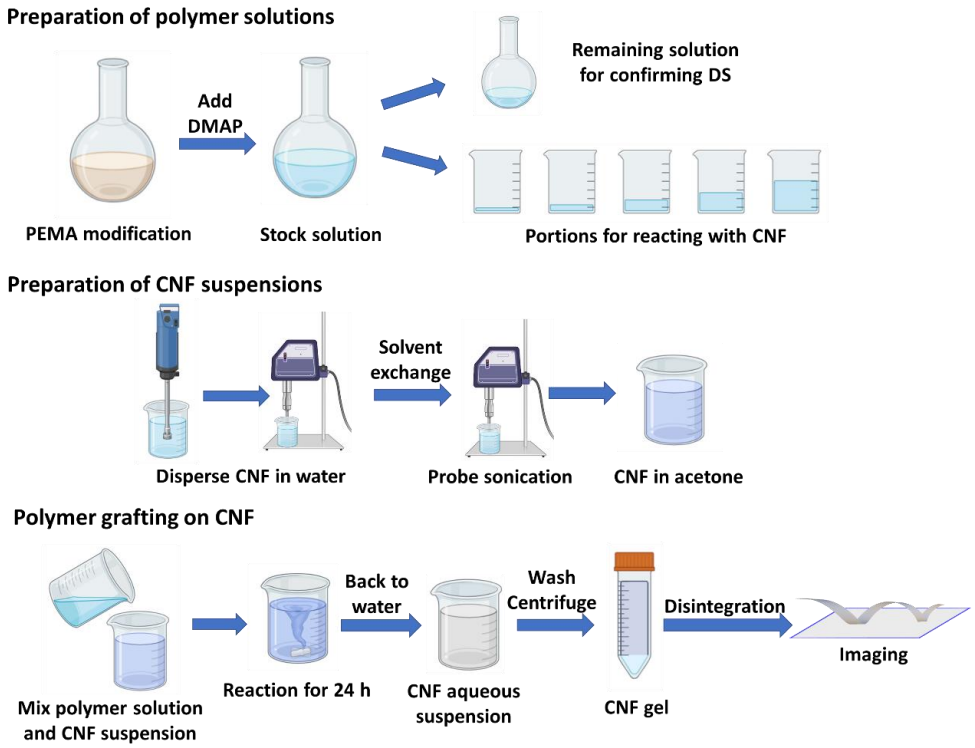

Figure 21. The preparation of polymer solutions and CNF suspensions and the polymer grafting on CNF.

As shown in **Figure 21**, the grafting process includes the preparation of polymer solutions, preparation of CNF suspensions in acetone, and polymer grafting on CNF. The detailed steps are described below.

Preparation of PEMA Derivatives. Alkyl-amines or methoxy terminated PEG-amines molecules were reacted with PEMA backbone substituting 25-86% of anhydride moieties. The modified PEMA derivatives are termed CxDSy (where x is the carbon number, and y is the degree of anhydride substitution in percentage) or MPEGxDSy (where x is the number of ethylene oxide units in the PEG, and y is the DS as before). For example, MPEG3DS86 was prepared as follows. 1 g PEMA powder dissolved in 80 mL acetone was placed in a 250 mL round-bottom flask containing a magnetic stir bar. MPEG3-amines (1.295 g, 100 mol% of PEMA repeating units) dissolved in 15 mL acetone was added dropwise over about 5 min. The solution was mixed for 16 h at room temperature giving the stock solution.

DMAP (4-dimethylamino pyridine) was used as catalyst for the grafting reaction.[22] DMAP (95.0 mg, 10 mol% of PEMA repeating units) in 5 mL acetone was added into the stock solution and allowed to react for 30 min. The polymer concentration in the final stock solutions, expressed as mmol of PEMA repeat units (RU) per liter acetone, was

79.4 mmol RU/L. To minimize further hydrolysis of residual anhydride moieties, the stock solutions were directly used for grafting on CNF in acetone, described in the grafting part. The unused stock solutions were quenched with 10 mL HCl and concentrated in a rotary evaporator and transferred into a 29 mm diameter dialysis tube (SpectraPor, Spectrum® Labs, 12–14 kDa MWCO). After dialyzing against 0.01 N HCl, 20 mM $NaHCO_3$, and ultrapure water, samples were lyophilized for ^{1}H-NMR to determine the DS values.

For unmodified PEMA, 2 g PEMA was directly mixed with 0.19 g DMAP in 200 mL acetone for 30 min at room temperature, giving a stock solution in a concentration of 79.4 mmol RU/L.

Sulfo-Cyanine5 (sulfo-Cy5) Labelled PEMA. In some cases, the PEMA was fluorescently labeled. Sulfo-Cyanine5 amine (1/2000 of PEMA repeating units) was suspended in PEMA acetone solution prior to adding other amine molecules. The mixture was stirred in dark until all the fluorophores dissolved yielding a transparent blue solution.

Preparation of CNF Suspensions. Multiple cellulose nanofibre suspensions for different polymer dosages were prepared simultaneously. In a typical protocol, CNF gel containing 0.2 g dry fibres was first diluted to 200 mL aqueous suspension in a 250 mL glass beaker (PYREX™ Low Form Griffin Beakers) to give a 0.1 wt% suspension. The CNF particles were dispersed by 2 min treatment with a VWR homogenizer (VWR VDI 25 S41) at 13500 rpm for 2 min, followed with a probe sonication (Branson 450 Sonifier w 20kHz, 400Watts, 1/2" horn with a flat tip) under 50% duty cycle and 20% output in an ice bath for 10 min.

The exchange from water to dry acetone involved a few steps. Step 1, the solvent exchange started by adding 100 mL acetone to the suspension in a 400 mL beaker under 500 rpm magnetic stirring, yielding an acetone/water (1:2, v/v) mixture. The liquid phase was immediately removed by centrifugation (swing bucket rotor, 3000×g, 2 min). Step 2, the CNF particles were redispersed in 200 mL acetone/water (2:1, v/v) with 500 rpm magnetic stirring for 5 min. Step 3, after removing the liquid phase, the CNF was redispersed and stirred in 200 mL 100% acetone for another 5 min and followed by centrifugation. Step 4, the CNF were dispersed in acetone, giving suspension comprising 0.2 g dry CNF in 150 mL acetone in a 250 mL beaker. Finally, in step 5, the suspensions were probe-sonicated in an ice bath for 10 min again prior to mixing with polymer solutions.

Polymer Grafting on CNF. The polymer grafting was achieved by mixing the polymer solutions with CNF suspensions in acetone, and the polymer dosage was expressed as in a unit of mmol RU per gram dry CNF. Typically, 1-80 mL DMAP activated stock solutions were added to the CNF suspensions to give the target polymer dosages of 0.4-31.7 mmol

RU/g. Dry acetone was added to the final mixture to give a total volume of 200 mL. The polymer grafting process is performed in a 250 mL beaker covered with polyethylene films to avoid acetone loss and water absorption. The suspension was stirred on a magnetic stirrer (IKA twister) at 500 rpm with a cross-shaped stir bar (VWR® Spinplus®, 25 mm diameter) for 24 h. The reaction was quenched with 10 mL 1 M HCl solution.

Modified CNF were collected through centrifugation (4000×g, 5 min), and then washed with 0.01N HCl (200 mL×3), 20 mM $NaHCO_3$ (200 mL×3), and ultrapure water (200 mL×3). Magnetic stirring (500 rpm for 5 min) and centrifugation (5000×g, 10 min) were performed in between each washing cycle. The final CNF gel was weighed to calculate the dry fibre content using 0.2 g divided by the wet gel weight. The PEG modified CNF have dry fibre contents in range of 1.4-2.5 wt%, and other samples have dry fibre contents in range of 3.1-4.9 wt%.

Conductometric Titration and FTIR. The amount of grafted polymer was determined by a conductometric titrator (Mantech Inc). In a typical titration, the modified CNF gels with 20-40 mg dry fibre content was dispersed in 100 mL 1 mM NaCl and the pH of the suspension was adjusted below 3 using 1 M HCl solution. 0.1 M NaOH solution (LabChem Inc.) was injected through a micro dispenser at 30 s intervals with stirring. The titration was stopped until the pH of the solution reached above 11.7. The conductivity as a function of the injected base solution was plotted to calculate the total charges of modified CNF. The unmodified CNF was titrated as a background. The total grafted polymer in units of mmol repeating unit per gram dry CNF was obtained in triplicates. Modified CNF gel was redispersed in 0.1 N NaOH solution and then filtered through a membrane (hydrophilic PVDF, Durapore®, 0.45 μm) and dried at room temperature overnight. The dried CNF sheets were characterized by FTIR spectroscopy (Nicolet 6700, Thermo Fisher Scientific) under attenuated total reflection (ATR) model.

Particle Size Analysis. The diameter of modified CNF was determined by a Mastersizer 2000[23] particle size analyzer (Malvern, UK) equipped with two laser sources (HeNe gas laser at a wavelength of 633 nm and LED at a wavelength of 466 nm). The detection range of particle size is from 0.02 μm to 2000 μm. CNF was dispersed in 1 mM NaHCO3 solution giving a fibre concentration of 0.02 g/L. In all the measurements, background was blanked with 1 mM $NaHCO_3$, and the CNF suspensions were stirred at 400 rpm with a magnetic stir and circulated into the sample chamber through a peristaltic pump at a 40 mL/min flow rate. All the angular scattering intensities were within the recommended range except for the supernatant samples containing nanofibrils, which had insufficient concentration.

Microribbon Immobilization on Substrates. For the preparation of dry samples. Modified fibres were dispersed in 1 mM $NaHCO_3$ using VWR homogenizer under 9500 rpm for 1

min. Square glass coverslips (22 mm×22 mm, No 1.5, Fisher Scientific), circular glass coverslips (D=22 mm, No 1.5, VWR), silicon wafers ((100), University Wafer, Inc. US) were used as substrates. All the substrates were cleaned in freshly prepared piranha solution (98% H_2SO_4 and 30% H_2O_2, 3:1) for 20 min, washed with ultrapure water thoroughly, and blow-dried with compressed air. The cleaned substrates were immersed in a 1% (v/v) solution of (3-aminopropyl) trimethoxysilane (APTES) in anhydrous toluene. After reacting at 70 ^oC for 20 min, the substrates were rinsed with anhydrous toluene, toluene/methanol (1:1), methanol, and ultrapure water, and dried with compressed air. A drop of the suspension was applied on the positively charged substrate and removed by rinsing with ultrapure water for 5 sec. The substrates were dried with compressed air eventually.

For the preparation of wet samples. Modified fibres were dispersed in 1 mM NaCl (pH=4-6) using VWR homogenizer under 9500 rpm for 1 min. Depression concave glass slides (75 mm×25 mm×1mm, single concave well of diameter 16 mm and depth 0.5 mm, Amscope) and square glass coverslips (22 mm×22 mm, No 1.5, Fisher Scientific) were first rinsed with ultrapure water and ethanol and dried using compressed air. 25 μL suspension (0.001% v/v) was applied to concave well and covered with a bare glass coverslip. Nail polish (clear coat, SinfulColors) was used to seal the edges to prevent any water evaporation or leaking. Subsequently, the glass slides were inverted and placed on petri dishes (60 mm diameter) for 24 h allowing the fibres to settle on the cover glass.

Widefield Microscopy. Dry and wet samples were imaged by upright and inverted light microscopes at the McMaster Centre for Advanced Light Microscopy (CALM)

Upright widefield microscopy was performed on a microscope (Nikon-Eclipse LV100N POL) equipped with 40×/0.65NA objectives and a pco.panda 4.2 sCMOS camera with upto 80% quantum efficiency, providing a maximum resolution of 320 nm. Inverted widefield microscopy was performed on a Nikon inverted Ti2-E equipped with a 60×/1.40NA Plan Apo λ oil-immersion objective and a Hamamatsu Orca Flash 4.0 V3 sCMOS camera with 82% high quantum efficiency, achieving a maximum resolution of 220 nm. All the images were acquired on NIS Elements software (Nikon, Ottawa, Canada) and processed with Fiji imageJ (version 1.54f).

Confocal Laser Scanning Microscopy (CLSM). Images of fluorophore-labeled samples were captured using a Nikon A1R Inverted Confocal Laser Scanning Microscope equipped with a 60×/1.40NA Plan Apo λ oil-immersion objective. The Cy5 filter cube was selected for fluorescence detection. A pinhole size of 1.2 was used, and images were acquired with the galvanometer scanner. To generate 3D images, Z-stacks were obtained with 60-200 steps and a step size of 0.175 μm. The NIKON NIS software (version 5.41.00) was employed for the construction of 3D images. Subsequently, the Z-stack images were imported into Fiji imageJ (version 1.54f) and stacked using the maximum-

intensity Z-projection function. This allowed the projection of 3D structures into 2D images, and the wavelength of the helical structure was measured.

Atomic Force Microscopy (AFM). The topographic images of fibres immobilized on cover glasses were acquired with a Bruker Dimension Icon AFM (Bruker Corporation, Billerica, MA) in ScanAsyst-Air mode (Bruker) using ScanAsyst probes (Bruker) having triangular cantilever with an average spring constant of 0.4 N/m and a tip radius of 2-12 nm. The image processing was conducted using Nanoscope Analysis software (Bruker, version 3.0).

Field Emission Scanning Electron Microscopy (FESEM). Modified fibres are vacuum filtered through a hydrophilic PVDF membrane (Durapore® 0.45 μm) in a Buchner funnel. The gel layer was covered with another PVDF membrane and cured in a hot press (Standard Auto CH Benchtop Press, Carver, Inc., US) under 635 kPa at 120 ^{o}C for 10 min. Prior to the SEM scanning, sheets were coated with 5 nm Chromium. The morphologies were scanned using a Magellan 400-field-emission scanning electron microscope at an acceleration voltage of 1 kV.

Nano-fraction. The solid contents of CNF gels were determined by gravimetric analysis. 100 mg wet gel was heated at 105 ^{o}C in the oven for 6 h and then weighed using a microbalance (Mettler Toledo AX204). For measuring the fraction of nanofibrils, 1 g CNF gels was diluted to 0.1 wt% suspensions in ultrapure water. The suspensions were treated with VWR homogenizer under 13500 rpm for 2 min and probe-sonicated in an ice bath under 50 % duty cycle and 30% output for 10 min. The dispersions were centrifuged (Beckman Coulter Allegra 25R with swing bucket rotor) at 2500×g for 1h.[24] The supernatant and CNF gels were separated and transferred into reweighted bone dry beakers. The water was removed at 105 ^{o}C in the oven for 48 h. The beakers were weighted immediately to give the dry fibre weight. The fractions of nanofibrils were given as means of triplicates.

X-ray diffraction (XRD). The degree of crystallinity of CNF samples was measured by X-ray diffraction. 200 μL CNF suspension (0.5% v/v) was dropped on a freshly cleaned silicon wafer (100, 10 mm ×10 mm). The suspensions were allowed to dry in a room with constant temperature and humidity (50% RH, 23 ^{o}C) for 48 h. The XRD measurements were carried out on the dry films using a Bruker D8 DISCOVER diffractometer (Bruker, USA) equipped with a Eiger2R 500K detector positioned 20 cm from the sample and a CoKα source radiation (λavg = 1.79026 Å) at an anode voltage of 35 kV and a current of 45 mA. Data were recorded from 8^{o} to 48^{o} with 0.02 steps at 1.5s/step. A two-dimensional area detector was used to collect the scattering intensity and integrate the frames creating diffraction patterns. The bare silicon wafer as blank was subtracted from all the diffractograms. The cellulose crystallinities were determined by the deconvolution

method. Peaks for crystalline region in cellulose I and disordered region were inserted and fitted with a pseudo-Voigt function.

Results and Discussion

Polymer Derivatization and Grafting to CNF

PEMA Derivatization

The Polymers. PEMA derivatives were prepared by reacting the amine molecules with PEMA in acetone (**Figure 22**). Two series of substituents were employed, alkyl-amines (Cn-NH_2) and methoxy-terminated polyethylene glycol-amines (MPEGm-NH_2). The variable *n* represents the number of carbons on the alkyl chain, while the value of *m* represents the number of repeat units in the MPEG chain. The substituted succinic acid moieties consist of an amide-linked substituent and a protonated carboxylic acid. **Table 4** summarizes the polymer structures. The polymer names denote the structure. For instance, PEG3DS86 refers to the PEMA with 86% succinic moieties linked with pendant PEG3 chains. The derivatization yields were calculated by dividing the actual DS by the theoretical value obtained from the ratio of amine molecules to the repeat unit of PEMA.

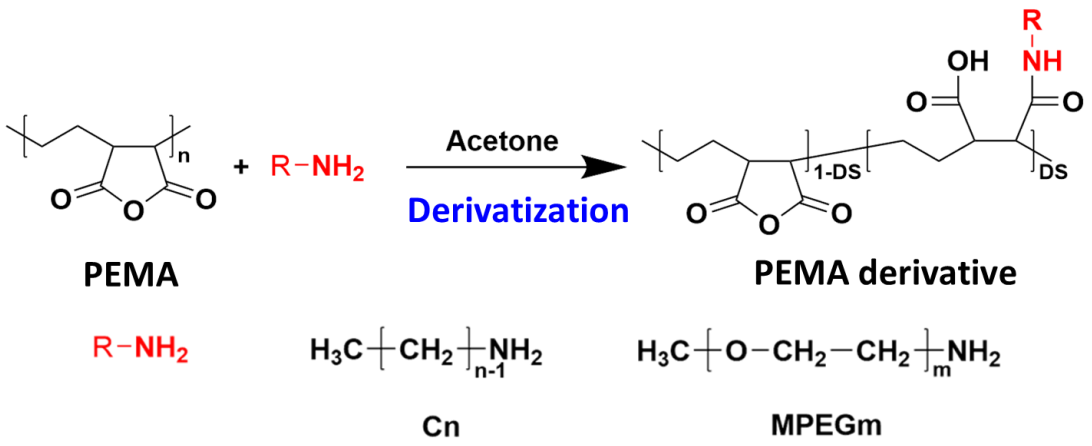

Figure 22. PEMA derivatization.

Table 4 Derivatization yield and the average molecular weight of repeat unit

Sample ID	RNH_2 Feed DS	[b] DS	[a] Amidation Yield (%)	[c] ARU MW (Da)
PEMAc	-	-	-	188.1
PEG3DS25	0.25	25	100	218.9
PEG3DS50	0.50	50	100	249.7
PEG3DS75	0.75	75	100	280.5

PEG3DS86	1.00	86	86	294.0
PEG10DS47	0.50	47	94	390.9
PEG20DS24	0.25	24	96	400.7
C3DS77	1.00	77	77	202.8
C10DS44	0.50	44	88	239.7

[a] DS divided by the feed DS.

[b] determined by ^{1}H-NMR – see **Figure S20** in the SI file.

[c] The average repeat unit, ARU, molecular weight is for the hydrolyzed polymer and assumes all carboxylic acid groups are present as sodium salts.

The amidation reactions in dry acetone were efficient, with yields for both alkyl and PEG derivatives reaching or exceeding 90% when the target DS values are below 75%. However, as the target DS exceeded 75%, the yields declined, particularly in the case of alkyl-modified PEMA. The decreased DS might be attributed to reduced polymer solubility as the alkyl-modified PEMA solutions (C10DS44 and C3DS77) exhibited cloudiness after the reaction.

Polymer Grafting onto CNF. PEMA and PEMA derivatives (**Figure 22**) were reacted with CNF in acetone to give the structures in **Figure 23**. Initially, grafting solvents were screened, including water. The drying and high-temperature curing required with water caused irreversible crosslinking, and the treated CNF could not be dispersed in water. Acetone and DMF both gave grafting without excessive crosslinking. However, dry acetone gave higher grafting yields and was selected as the grafting solvent.

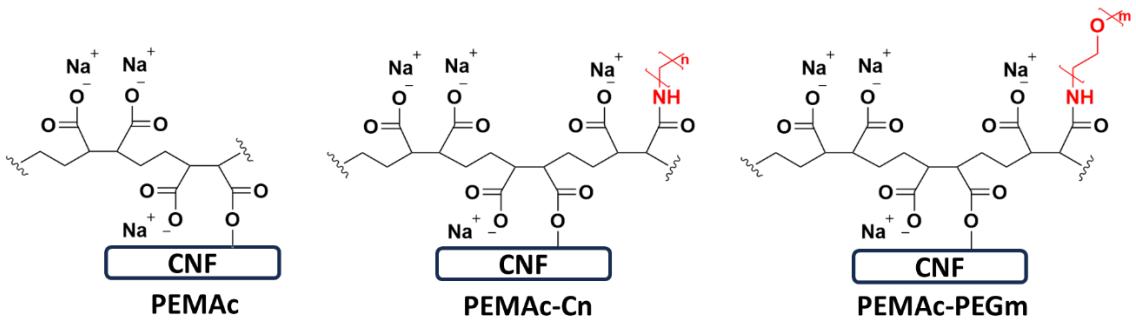

Figure 23 Structures of grafted PEMA and PEMA derivatives after hydrolysis.

Before grafting on cellulose, anhydrides were activated by DMAP (4-dimethylamino pyridine), which is a widely used catalyst to form an acyl-DMAP intermediate that can react with cellulose,[25] and promote esterification with all the hydroxyl groups in the

anhydroglucose units.[22] Following the grafting process, acetone was replaced with water, hydrolyzing residual anhydrides and removing small molecules and ungrafted polymer. Note that PEMA is the starting anhydride polymer (**Figure 22**) whereas the hydrolyzed polymers are PEMAc (**Figure 23**).

Table 5 summarizes the grafting experiments. The grafted CNF charge was determined by conductometric titration. The quantity of grafted was expressed as the grafted repeat unit concentration (grafted RU, mmol/g), and as a mass fraction – both were calculated from the CNF charge. The grafting coverage (mg of polymer per square meter of CNF surface area) was based on the specific surface area of CNF (32 m^2/g) given by the supplier. Finally, the grafting yield is the fraction of added polymer fixed to CNF surfaces.

Table 5 Summary of polymer grafting on CNF.

Row	[a] Polymer Name	RU Dosage (mmol/g)	[b] CNF Charge (meq/g)	Grafted RU (mmol/g)	Grafted Mass Fraction (%)	[c] Grafting Coverage (mg/m^2)	Grafting Yield (%)
1	PEMA	31.8	7.94	3.97	42.8	23.3	12.5
2	PEMA	15.9	7.62	3.81	41.7	22.4	24.0
3	PEMA	7.94	5.85	2.93	35.5	17.2	36.9
4	PEMA	3.97	4.34	2.17	29.0	12.8	54.7
5	PEMA	1.98	3.08	1.54	22.4	9.04	77.5
6	PEMA	0.99	1.92	0.96	15.3	5.65	96.9
7	PEMA	0.40	0.75	0.38	6.60	2.21	94.9
8	PEG3DS25	7.94	5.06	2.89	38.8	19.8	36.4
9	PEG3DS50	7.94	3.35	2.24	35.8	17.4	28.2
10	PEG3DS75	15.9	3.36	2.69	43.0	23.6	16.9
11	PEG3DS86	15.9	3.00	2.63	43.6	24.2	16.6
12	PEG3DS86	7.94	2.15	1.88	35.6	17.3	23.7
13	PEG3DS86	3.97	1.47	1.29	27.4	11.8	32.4
14	PEG3DS86	1.98	1.27	1.11	24.6	10.2	56.0
15	PEG3DS86	0.99	0.76	0.67	16.4	6.15	67.5
16	PEG3DS86	0.40	0.40	0.35	9.40	3.25	89.2
17	PEG10DS47	7.94	1.27	0.83	24.4	10.1	10.4
18	PEG20DS24	15.9	1.39	0.79	24.0	9.89	5.00
19	PEG20DS24	3.97	1.26	0.72	22.3	8.99	18.1
20	PEG20DS24	0.40	0.36	0.20	7.60	2.56	51.5
21	C3DS77	15.9	1.56	1.27	20.5	8.04	8.00

22	C3DS77	3.97	0.42	0.34	6.50	2.18	8.70
23	C3DS77	0.40	0.27	0.22	4.30	1.41	56.0
24	C10DS44	7.94	1.94	1.24	22.9	9.30	15.6

[a] see polymer properties in **Table 4**.
[b] from conductometric titration
[c] assuming CNF specific surface area of 32 m^2/g from the supplier

Table 5 reveals that polymer dosages were high, most of the grafted yields were low, and the charge contents of the resulting CNF were high. Grafted CNF charge ranged from 0.42 to 7.9 meq/g compared to 0.06 meq/g for unmodified CNF. Many factors influence the grafting yields, including the ratio of the dose size to the available CNF surface area, the density of reactive anhydride groups on the polymer chains, the presence of bulky substituents, and the phase behaviors of the polymers in acetone. **Figure 24**A shows the influence of polymer dose on the grafting yields of 4 polymers. PEMA is unmodified and therefore has a reactive anhydride on every repeat unit. PEMA gave the highest grafting yields in **Table 5** when the dose was low. **Figure 24**B shows the PEMA grafting yields versus the coverage (mass of polymer/area of CNF surface). Grafting yield drops linearly when the coverage exceeds ~ 5 mg/m^2.

PEG3DS86 is an interesting polymer as 86% of the anhydride groups on the PEMA backbone were consumed by attaching short PEG3 chains. Despite the loss of grafting anhydride moieties, **Figure 24** shows that PEG3DS86 was only slightly less efficiently grafted compared to PEMA. This suggests that not many anhydrides are required for grafting. PEG20DS24 has 76% of the original anhydrides, however, the pendent PEG chains are long with 20 repeat units. The low grafting yields for PEG20DS24 suggest the pendent chains are blocking grafting sites. The grafting efficiencies of the C3 derivatives were about ½ the corresponding PEG3 polymers. Some DMAP-activated C series acetone solutions were cloudy, suggesting phase separation. Summarizing, Rows 6,7, and 16 in **Table 5** show that high grafting yields can be obtained if dosages do not exceed the capacity of CNF to fix polymer.

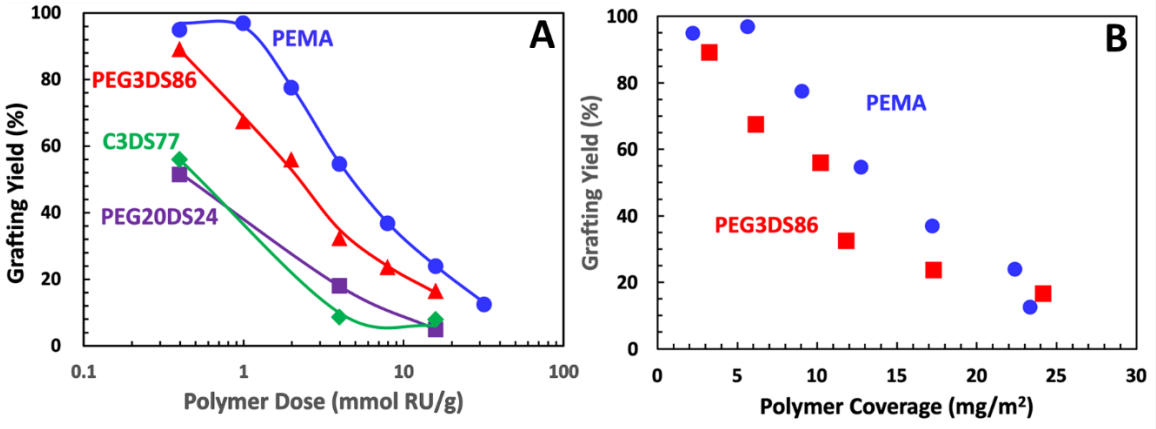

Figure 24 A: grafting yield as a function of polymer dose; B: grafting yield as a function of polymer coverage.

The mass fractions of the fully dispersed nanofibrils for unmodified and modified CNF are given in **Table S4**. The fully dispersed nanofibrils were obtained through probe sonication followed by centrifugation. It is important to note that during the washing steps, some nanofibrils were already removed. The measured nano-fractions represent the combined portion of nanofibrils that were not removed during washing and those produced through ultrasonication. Additionally, the particle size of the nanofibrils in the supernatant was measured to be below 1 μm (**Figure S17**), which is similar to TEMPO-oxidized CNF.[26] The diameter results further confirm the reliability of the nano-fraction procedure.

FTIR analysis of grafted CNF failed to show evidence of ester linkages – see **Figure S18** and associated text. The average number of anhydride groups on an individual PEMA chain is approximately 2380, and only one linkage is required for grafting. Based on the titration of exhaustively washed grafted CNF sample, we know the polymers are firmly attached.

XRD measurements of grafted CNF showed no evidence of a loss of cellulose crystallinity with grafting – see **Figure S19** and associated text in the supporting information.

Grafted CNF Structures

Described in the following sections is the influence of polymer grafting on aggregated CNF structures formed in acetone. Upon redispersion in water, the CNF aggregates could be broken apart to extents depending upon the grafting treatments. We start with the influence of water-to-acetone-to-water exchange on unmodified CNF.

Dispersing and Characterizing Untreated CNF. The CNF used in this paper was obtained from the University of Maine. They are produced from the defibrillation of

Brazilian bleached eucalyptus kraft pulp. The supplier specifications included "nominal" fibre width of 50 nm and length of several hundred microns and BET specific surface area of 31-33 m^2/g.[27]

Figure 25 summarizes a variety of measurements starting with 0.02 g/L never-dried CNF dispersed in 1 mM $NaHCO_3$ and treated with a homogenizer followed by probe sonication. **Figure 25**A is an optical micrograph of dried CNF on APTES treated cover glass. Individualized nanofibres are invisible at this magnification; we presume that the nearly transparent areas are aggregated nanofibrils likely formed in the drying process.

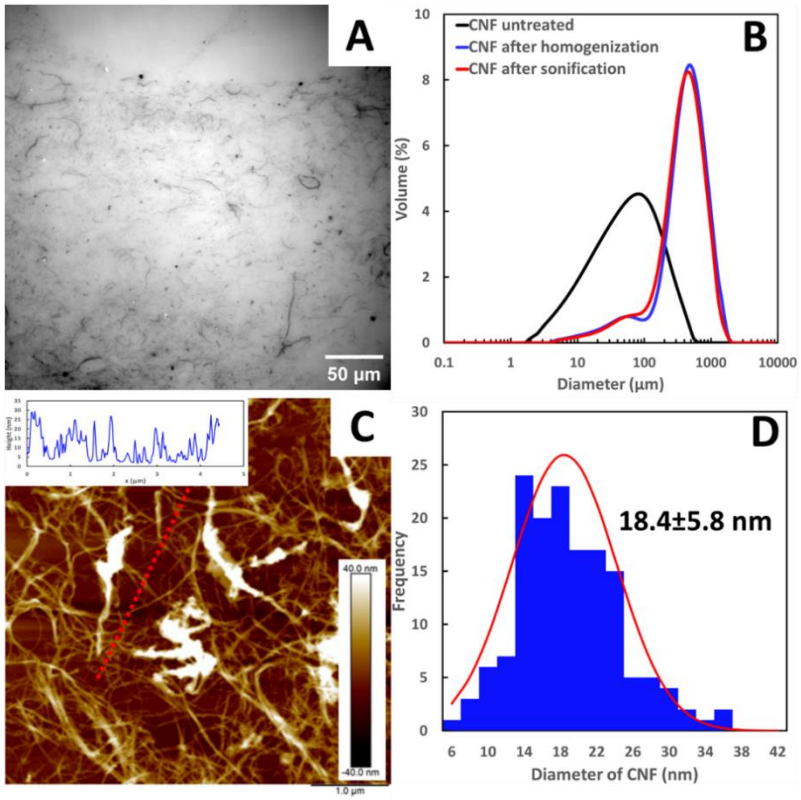

Figure 25 Morphologies of CNF before solvent exchange. Optical (A) and AFM (C) image of CNF settled onto glass surfaces treated with APTES. Samples were dried from 0.02 g/L suspension treated with homogenization and probe sonication. B: Diameter of untreated CNF, CNF after homogenization and after ultrasonication. D: Nanofibril diameter distribution of untreated CNF after counting 200 fibrils. As an example for the measurement, the height profile of the red dash line in Figure (C) is provided.

The size distributions of dispersed CNF were measured by a Mastersizer and the results in **Figure 25**B compare dispersion methods. The result for CNF, gently dispersed by magnetic stirring, is shown as the black curve labeled "untreated". The blue curve

corresponds to a sonicated sample and the red curve was both homogenized and probe sonicated. Fully dispersed nanofibrils do not appear in these distributions because of their very low intensity of scattered and diffracted light. **Figure S17** in the SI file shows Mastersizer distributions of the nanofibrils after larger particles were removed by centrifugation. Nearly monomodal peaks of 100 nm were obtained, however, the software warned that the measurements were outside the acceptable intensity range. The CNF without probe sonication treatment mainly consists of aggregates that can not be dispersed.

Sizes increased by nearly an order of magnitude after homogenization or probe sonication, techniques, compared to the mildly dispersed untreated CNF - **Figure 25**B. This was surprising because these techniques were employed to decrease particle size. Perhaps the untreated CNF dispersion contained relatively compact structures that were opened up but not fractured by sonification. Alternatively, further aggregation was induced by sonification. The literature has a few examples of Mastersizer characterization of CNF.[23, 28] However, none reported sonification-induced aggregation.

Finally, **Figure 25**C&D shows the AFM nanoscale characterization of dry, individualized CNF nanofibrils adhering to glass. The diameter distribution was determined from the height measurements. An 18 nm average diameter is consistent with the literature.[29]

The Effect of Acetone Exchange on Unmodified CNF. Organic solvents induce aggregation of unmodified nano cellulose particles.[30] In our solvent exchange procedures, water was gradually replaced by acetone, inducing aggregation **Figure 26**A shows optical and AFM images of unmodified CNF deposited from acetone and dried. Compared to the starting CNF (**Figure 25**A&C) the acetone treatment produced larger darker aggregated structures. However, when the CNF suspension in acetone was cycled back to water, the optical image in **Figure 26**B suggests that many of the large, dark structures **Figure 26**A disappeared with dispersion in water. In future sections we will show that grafting polymers to the structures in acetone will, in some cases, prevent the disintegration of structures in water.

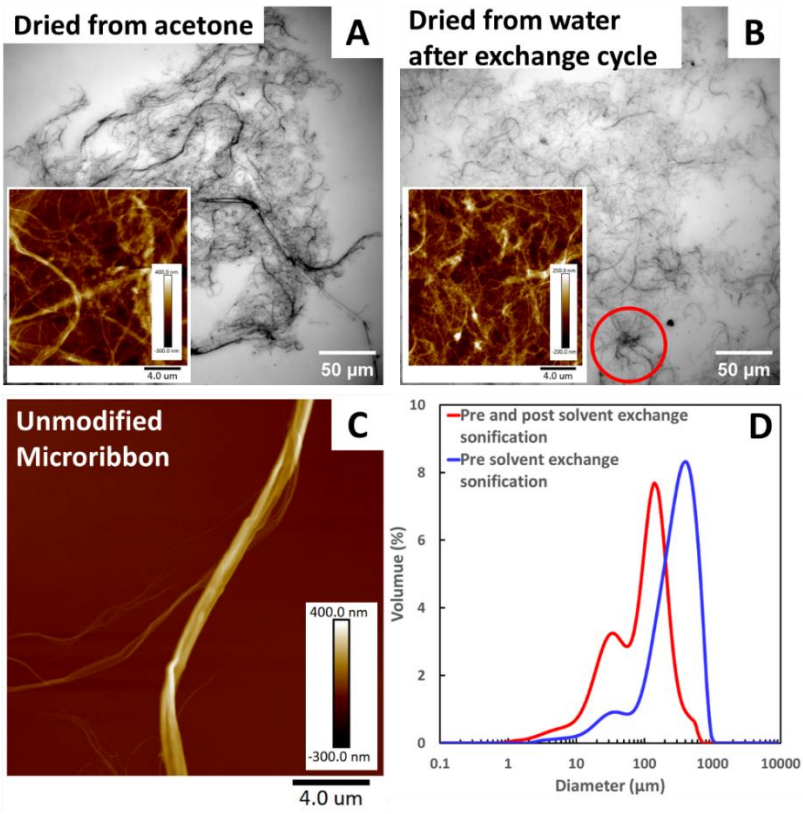

Figure 26. Morphologies of CNF after solvent exchange. Optical and AFM image of CNF settled on cover glass treated with APTES. A: Sample was dried from 0.02 g/L acetone suspension after ultrasonication. B: Sample was dried from 0.02 g/L aqueous suspension after one solvent exchange cycle. C: AFM image of individual microribbon from the sample dried from aqueous suspension. D: Diameter distribution of CNF aqueous suspensions with (red line) or without (blue line) ultrasonication in acetone when doing solvent exchange.

We propose the CNF structures in acetone fall within three groups illustrated in **Figure 27**. The smallest are the individualized nanofibrils. The microribbons formed by the association of 2 to 12 layers of nanofibrils are a few micrometers wide. Finally, large flocs are formed by entangled nanofibrils and microribbons. The fraction of individualized nanofibrils increased after one solvent-exchange cycle and homogenization treatment, likely due to the probe sonication being performed multiple times. **Figure 26**C shows an AFM image of an individual microribbon – we will see more examples with the grafted samples. Finally, **Figure 26**D shows the Mastersizer size distributions of samples gone through the complete cycle of water-to-acetone-to-water. The distributions are bimodal – we propose that the smaller lobe is microribbons and the larger is flocs. Again, the Mastersizer will not register individualized nanofibrils at this concentration.

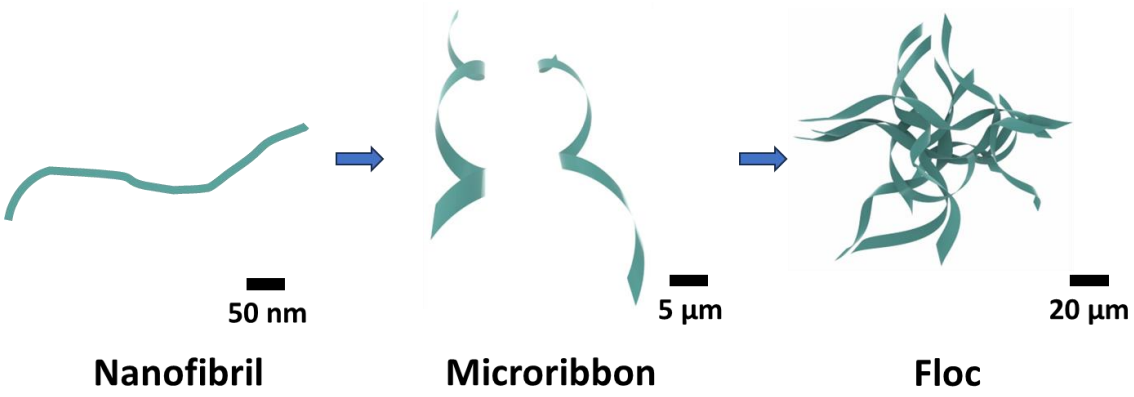

Figure 27. CNF objects span three distance scales.

Effect of PEMA Dosage on Aggregate Structure. The focus of the remaining sections is the influence of polymer grafting on CNF aggregate structure. PEMA was grafted onto CNF in acetone – see polymer structures in **Figure 22** and the grafted, hydrolyzed structures in **Figure 23**. PEMA grafting has two potential effects on CNF structures in acetone. The highly carboxylated polymer coating should inhibit further aggregation in water while reinforcing existing structures by crosslinking and thus inhibiting particle fragmentation in water.

PEMA grafting impacted the aggregated CNF structures. **Figure 28**A shows the particle size distributions in water for three grafting contents. The grafting details correspond to rows R2, R4, and R7 in **Table 5**. The relative areas of the larger diameter peaks, which we call flocs, increased with PEMA dosages suggesting PEMA stabilized the larger structures formed in acetone. The particle size results in A are qualitatively supported by the optical micrographs shown in **Figure 28**B-E. The dispersed ribbons in B and the floc in D, inspired the proposed structures in **Figure 27**. The CNF grafted with PEMAc displayed a low fraction of individualized nanofibrils, and this fraction decreased even further with higher polymer content. It is likely that the nanofibrils agglomerated, forming nanoribbons and flocs, and these structures were fixed by the grafted PEMAc. The presence of a higher polymer content provided strong support for the fixed structure, preventing further defibrillation induced by the probe sonication process.

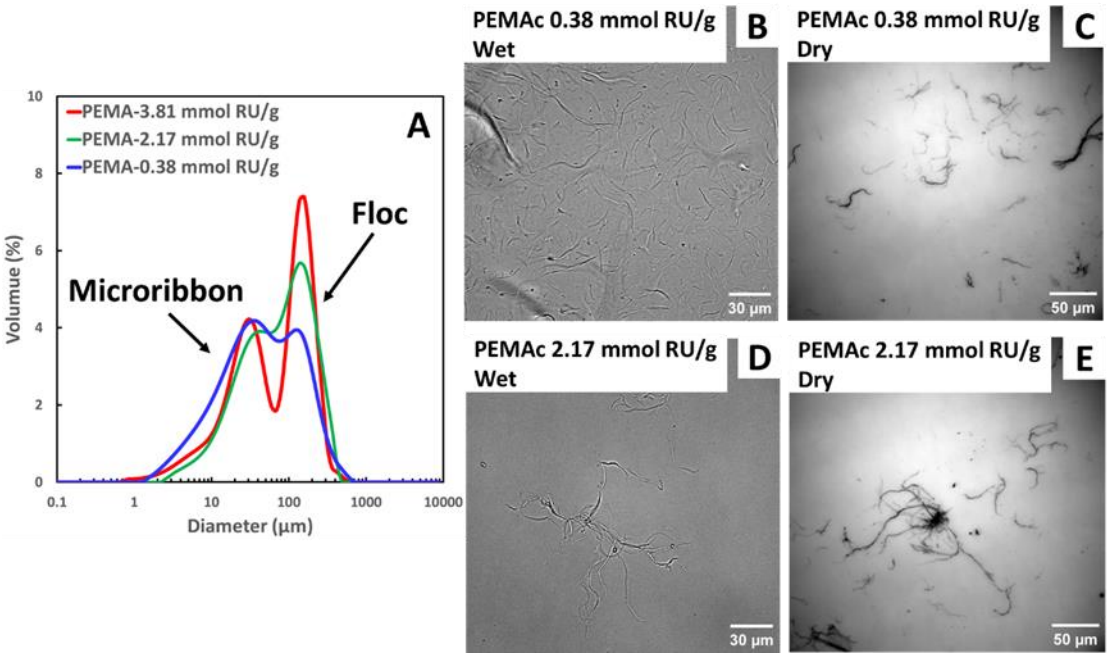

Figure 28 A: The influence PEMAc content on the particle size distributions measured in 1 mM $NaHCO_3$. Optical images of dried PEMAc-modified CNF. The wet samples were dispersed in 1 mM $NaHCO_3$. The dry images were prepared by sedimentation of same suspensions on APTES treated cover glass.

Effect of PEG3 DS. The synthesis of PEMA derivatives consumes reactive anhydride groups – see **Figure 22**. **Figure 29A** shows the influence of PEG3 degree of substitution (DS) on the particle size distribution of grafted CNF. Recall that the last two digits in the polymer names are the DS values as a percentage. The DS 25% and 50% derivatives had similar particle size distributions whereas 75% and 86% DS derivatizes had much lower contents of large flocs.

Figure 29(B, C, D, E), under upright widefield microscopy, the dried microribbons appear dark or alternating dark-bright when the DS of PEG is below 75%. However, when the DS reaches 86%, the microribbons become more transparent. The shift from dark to transparent, under the identical capturing environments, signifies remarkable alternation in the microribbon structure. The opaque structures were folded or tube-shaped microribbons while the transparent segments indicate that the microribbons lay flat on the substrate. The various structures were evidenced by the AFM images which would be provided in discussions of the drying effect. Similarly, C3DS77 modified CNF also exhibited a flat ribbon structure with intermittent sharp twisting as shown in **Figure**

S23. PEGDS86 grafted CNF (R11 in **Table 5**) consisted of high fraction of nanofibrils as given in **Table S4**. It has been previously demonstrated that PEG can affect the inter-fibril bonding of nanocellulose materials. For instance, PEG is mixed with CNC to control the nematic pitch size by intercalating into assembled CNC layers.[31] In addition, PEG is used as an additive mixed with CNF or covalently grafted on CNF to prevent the agglomeration.[32] Therefore, the grafted PEG may contribute to the isolation of nanofibrils.

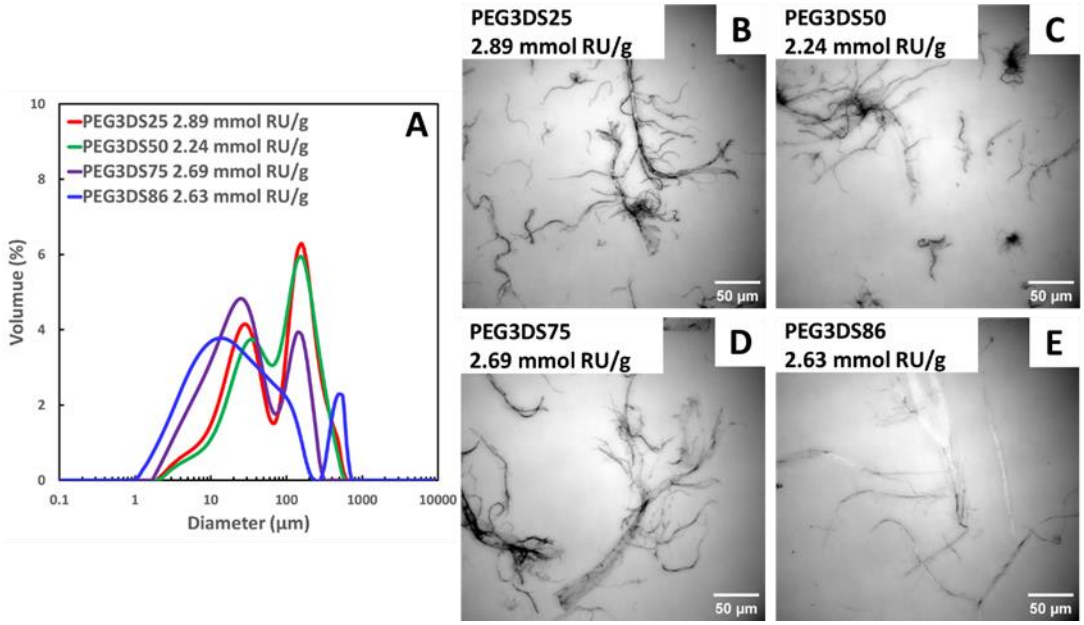

Figure 29 A: Diameter distributions of CNF grafted with PEMAc-PEG3 derivatives. (B, C, D, E) Optical images of CNF grafted with PEMAc-PEG3 with DS of 25% (R8), 50% (R9), 75% (R10), 86% (R11). All the CNF were adsorbed and dried on cover glass treated with APTES.

Effect of PEG Chain Length. The PEG side chains have significant impacts on the aggregated CNF. To explore the influence of PEG chain length, PEG10DS47 and PEG20DS24 were grafted onto CNF resulting in samples R17 and R18 in **Table 5**. The polymer content and the number of ethylene glycol units were kept similar between the two samples. The PEG20DS24 grafted CNF exhibited a broad monomodal distribution (**Figure 30**D), showing a shape and range similar to the CNF without homogenization and polymer grafting. On the other hand, the PEG10DS47 grafted CNF showed a close size distribution to the PEG3DS50 grafted CNF. The morphologies of the grafted CNF adsorbed on cover glass were observed using upright widefield microscopy, as shown in **Figure 30** (A, B). A new structure, marked by the red circle, was observed in the PEG20DS24 grafted CNF. Unlike the dried floc on the substrate, these new areas lacked

branched fibres on the edges and resembled the structure of unmodified CNF layers deposited on the cover glass. The magnified morphology, revealed by AFM in **Figure 30**C, showed entangled fibrils with nano-scaled widths. Therefore, it can be inferred that pendant PEG20 chains could improve the dispersibility of nanofibrils.

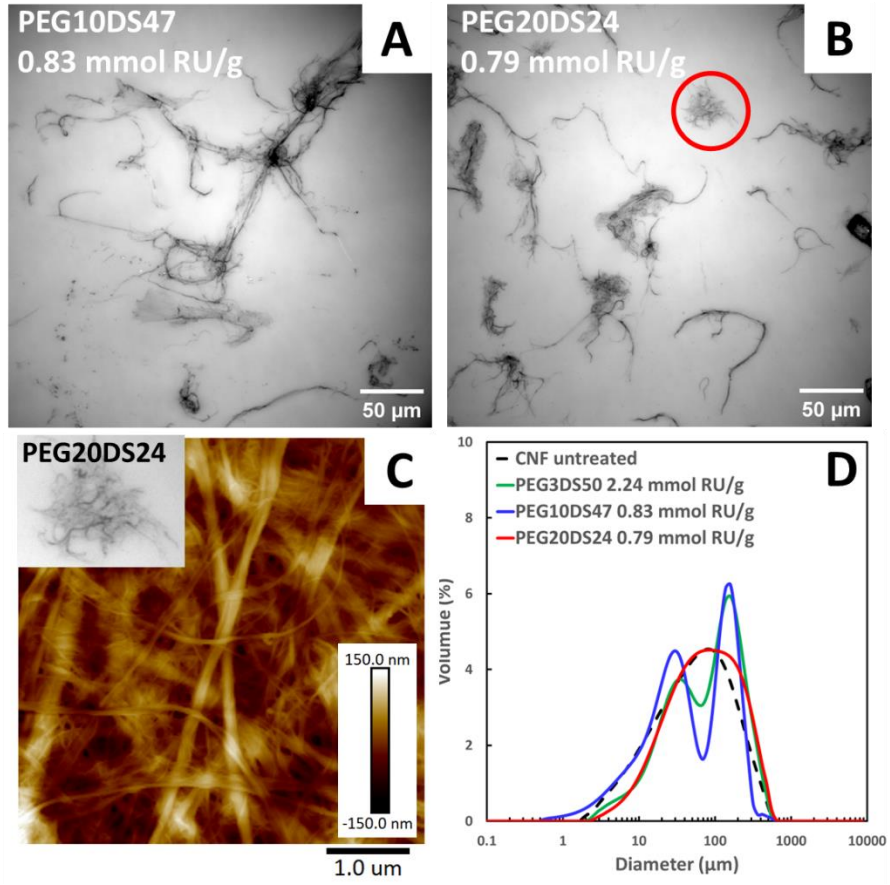

Figure 30 Optical images showing grafted CNF with PEG10DS47 (A) content of 0.83 mmol RU/g and PEG20DS24 (B) content of 0.79 mmol RU/g. (C) AFM height images of areas selected from PEG20DS24 samples. (D) Diameter of CNF samples grafted with PEMAc-PEG derivatives with different PEG chain length. Black dash line represents CNF without homogenization and polymer grafting.

The grafting reaction conducted in acetone is an efficient approach to attach PEMA and its derivatives to the CNF surface. Even with just 14% anhydride units on the PEMA backbone, high yield grafting was achieved. It was shown that the solvent exchange to acetone induced the aggregation of nanofibrils, resulting in different structures in the grafted CNF. The grafted CNF consisted of three main structures: nanofibrils,

microribbons, and flocs, with sizes spanning from nano-scale to micro-scale, as identified by particle size measurements and optical images.

These aggregated structures were preserved by the multiple anhydride groups along the polymer chain. When the anhydride units were converted to acid moieties in water, the water-soluble PEMAc and its derivatives can support the aggregated structures in the aqueous suspensions. The content of flocs in the grafted CNF can be reduced by lowering the polymer dosages and the DS of PEG. Meanwhile, PEG20 grafted CNF show similar morphologies and diameter distributions as the unmodified CNF. Next, we will summarize all the microribbon structures in both dry and wet states.

Drying of Microribbon. Exposure of CNF to acetone promotes aggregation, giving microribbon in floc structures. Since drying is a common step in various applications involving grafted CNF, it is crucial to understand its impact on the morphology and structural integrity of microribbon. We conducted two drying approaches for PEMAc and PEG3DS86 grafted CNF. In the first approach, the aqueous grafted CNF suspension was dropped on positively charged cover glass. Dried structures were fixed on the substrates after rinsing off unabsorbed CNF and drying with compressed air. A paper-making way was applied in the second approach. The grafted CNF were diluted to 0.3wt% suspension in 1 mM NaCl and then filtered through 0.45 μm hydrophilic PVDF membranes to form sheet. The wet CNF sheet was covered with another PVDF membrane, and the sandwich membrane was placed in two blotting paper and dried using a hot press at 120 ^{o}C under 635 kPa pressure for 10 min. The effect of polymer content was minimized by selecting two samples, R3 and R11 in **Table 5**, with similar polymer content.

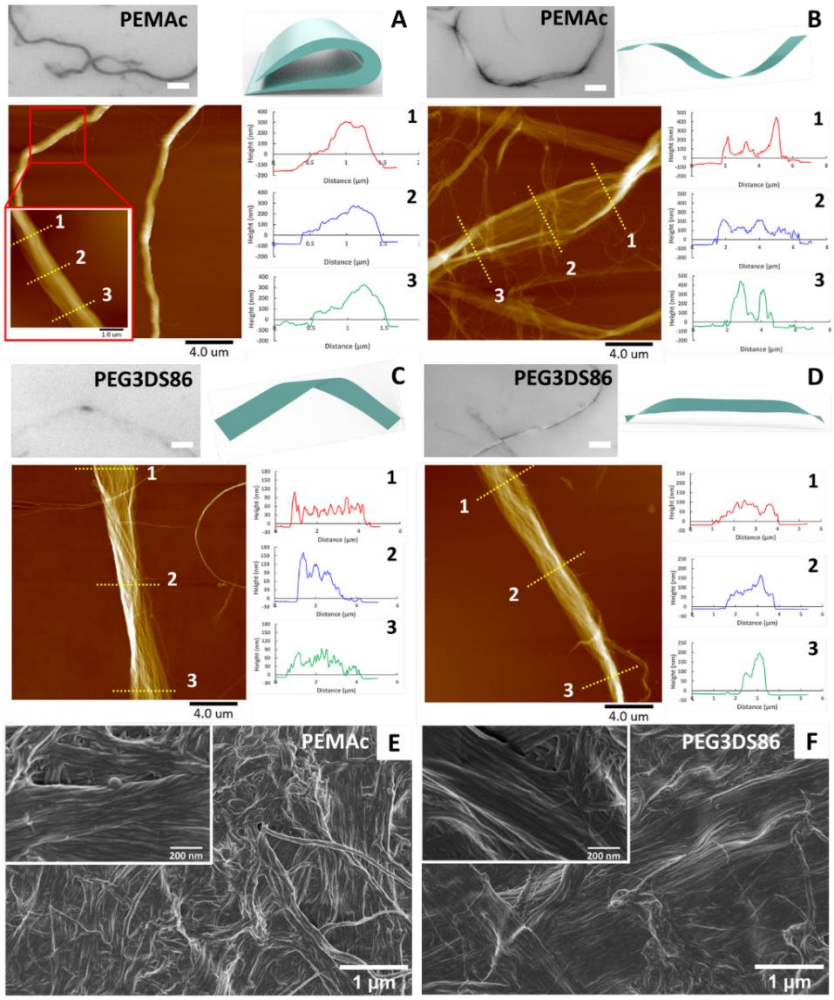

Figure 31 Structures of microribbons with PEMAc content of 2.93 mmol RU/g (A, B) and PEGSDS86 content of 2.63 mmol RU/g (C, D) after adsorbing on amine functionalized cover glass. Structures of microribbons with 2.93 mmol RU/g (E) and PEGSDS86 2.63 mmol RU/g (F) after forming sheets.

Figure 31(A-D) shows optical and AFM images of microribbons dried on cover glass. The optical images are analogous to the previous ones in which the PEMAc grafted microribbons appear as dark and slender structures or intermittent dark-bright structures while the PEG3DS86 grafted microribbons exhibit long transparent segments with short dark segments in the middle or on the two ends.

The AFM height image in **Figure 31**A shows that the dark and slender regions correspond to ribbons folded in half along the width. The three slices in the magnified region show similar height profiles, suggesting the structure as sketched in the 3D model. The helically stacked structure was observed in the PEMAc grafted microribbons as

shown in **Figure 31**B. A helical ribbon structure (given as 3D model) may fit into the structures. The three height profiles at positions marked on the AFM image reveal the twisting direction. Based on the AFM height change along the ribbon, the twisting structure shown in **Figure 31**B is in a left-handed manner.

For the PEG3DS86 grafted microribbons, the transparent segments indicating the flat ribbons were shown in the AFM images (**Figure S24**). The dark segments were unraveled by the AFM images (**Figure 31**C, D). The topologies and height profiles suggest that dark regions are ribbon twisting at 180 degrees as shown in the sketched 3D models. Meanwhile, the twisting areas on PEG3DS86 grafted microribbons are short and non-continuous.

FESEM was utilized to examine the structure of microribbons when packed together to form sheets. In **Figure 31**E, most of the PEMAc grafted microribbons predominantly appear as slender wires, indicating that these ribbons are folded in half along their width. Conversely, in **Figure 31**F, the PEG3DS86 grafted microribbons exhibited a flat structure within the matrix. The microribbons standing in the sheets displayed similar structures to those adsorbed on flat surfaces. In summary, PEMAc grafted microribbons tend to form folded structures in dried state, while PEG3DS86 grafted microribbons tend to adopt flat structures.

Geometry of Microribbon. Geometric descriptions are provided to picture the size and conformation of microribbons. The width and thickness of the dried microribbons were measured using imaging techniques. **Figure 32**A&B display the PEMAc and PEG3DS86 grafted microribbons, respectively, captured with an inverted widefield microscopy. The 60×/1.40NA oil-immersion objective was used providing a maximum resolution of 220 nm. The resolution is sufficient for accurately measuring the width since the widths of microribbons are in the micro-scale range. Over 150 unentangled microribbons were selected, and measurements were taken at three positions - the head, middle, and tail parts of the microribbons.

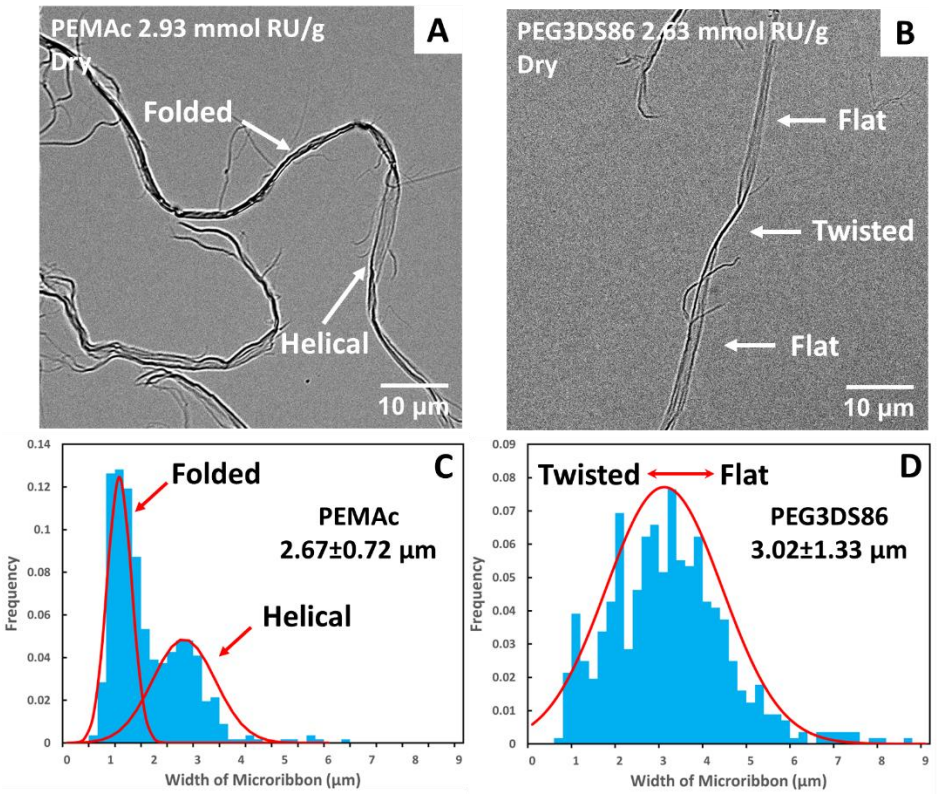

Figure 32 Optical images of microribbons modified with PEMAc (A) and PEG3DS86 (B) captured from inverted widefield microscopy for measurement of width of microribbons. The corresponding width fitted with Gaussian distribution for PEMAc-modified (C) and PEG3DS86-modified (D) after counting 150 microribbons.

The width distributions were fitted into a Gaussian distribution. The PEMAc grafted CNF exhibits a bimodal distribution (**Figure 31**C), with over 2/3 of the counts located near the width of 1.2 µm and a small peak at an average width of 2.67 µm. As seen in **Figure 31**A, the folded structures have a half-width of the helical segments, which explains the two peaks in the distribution corresponding to the folded and helical structures. The dominance of the folded structure is consistent with the morphologies discovered by SEM. The width distribution (**Figure 31**D) for PEG3DS86 grafted microribbons display a broad monomodal, giving an average width of 3.02 µm. The presence of curled microribbons in the PEMAc samples may introduce artifacts when performing the measurement. Hence, the width value obtained from the PEG3DS86 grafted microribbon is considered accurate, as the microribbons stand flat on the substrates.

For the measurements of thickness, over 20 microribbons were scanned with AFM. The images with lowest height and highest height were given in **Figure S24**. The thickness of the flat microribbons ranges from 40-220 nm corresponding to 2-12 layers of nanofibrils.

The microribbon structures, preserved by the grafted polymer, remain stable in suspension because of the water-solubility of the hydrolyzed polymers. **Figure 33**A&B show the microribbon structures in water, where unentangled microribbons grafted with PEMAc display curly conformations expanding in the Z-direction while PEG3DS86 grafted microribbons show flat structures.

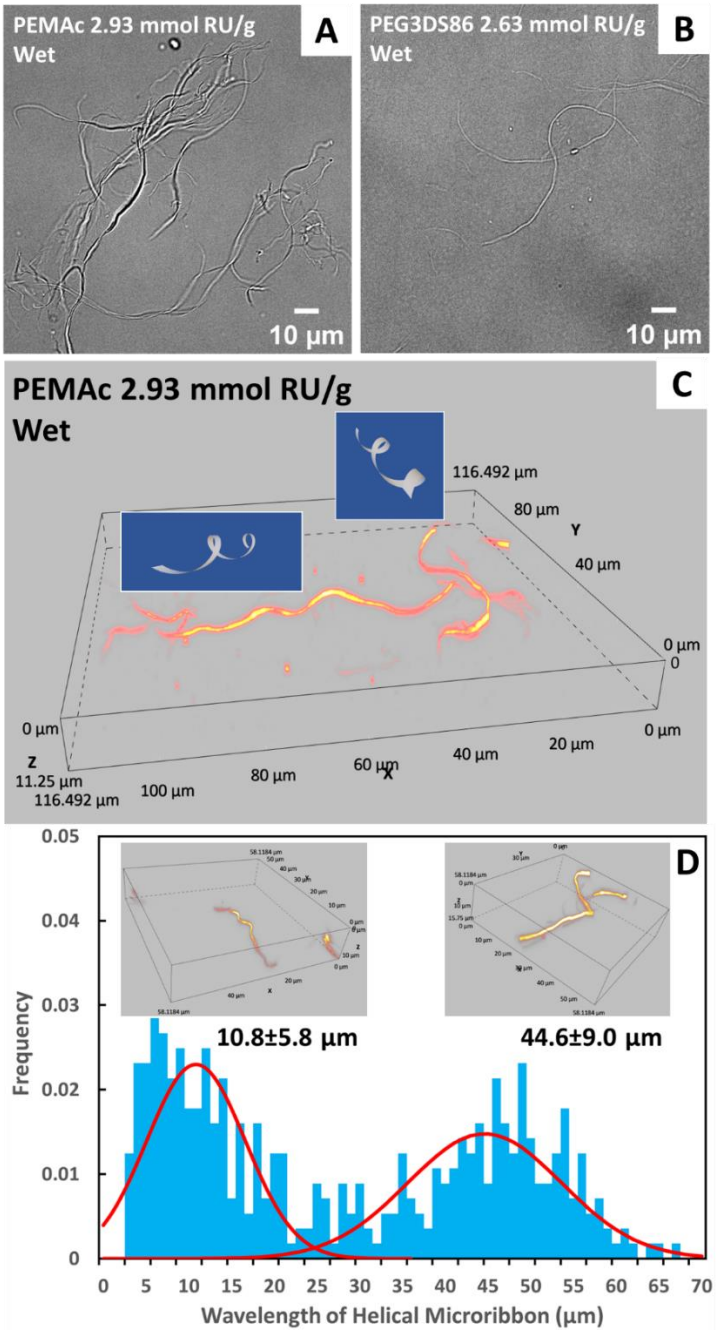

Figure 33 Optical images showing microribbons with PEMAc content of 2.93 mmol RU/g (A) and PEG3DS86 content of 2.63 mmol RU/g (B). Grafted CNF were dispersed in 1 mM $NaHCO_3$. 3D image (C) captured from CLSM showing microribbons with PEMAc content of 2.93 mmol RU/g. (E) The wavelength of helical microribbon measured from Z-projection images after counting over 100 microribbons.

The three-dimensional structures of PEMAc grafted microribbons were visualized using Z-stack imaging with an inverted CLSM, which provided a maximum resolution of 220 nm in the X and Y directions, and 350 nm in the Z-direction. Microribbons were labeled with Sulfo-Cyanine5 through the grafted PEMAc backbone. Diluted suspensions allowed the microribbons to settle horizontally on the substrate. To anchor the microribbons on the cover glass, the pH of the suspension was slightly adjusted to be acidic. **Figure 33**C presents a typical 3D image of PEMAc grafted microribbons, showing a helical ribbon structure in water. Both left- and right-handed twisted helical structures were observed in the PEMAc grafted microribbons. To determine the wavelength of the helical ribbons, more than 100 horizontally lying microribbons were captured to generate 3D images. Subsequently, the helical ribbon structures were projected onto the plane surface to generate 2D images, and the wavelengths of all the complete periods were measured, as exemplified as **Figure S25**A. A bimodal distribution (**Figure 33**D) was obtained with two most frequently appeared wavelengths at 10.8 μm and 44.6 μm. These two types of structures shown in the 3D images in **Figure 33**D and **Figure S25**B correspond to the two wavelengths, indicating the presence of two typical helical ribbon structures formed in the PEMAc grafted microribbons.

Conclusions

1. The application of aqueous, hydrolyzed poly(ethylene-*alt*-maleic anhydride), PEMA, to mechanically produced cellulose nanofibrils (CNF), followed by drying and heating, grafted the polymer to the cellulose. However, the crosslinked CNF could not be redispersed. By contrast grafting from water is effective with much larger wood pulp fibres.

2. PEMA and its derivatives can be grafted onto CNF through DMAP-catalyzed direct esterification in acetone. Grafting yields were >90%, when the PEMA dose was less than 0.125 g/g which ~ 5 mg/m^2 assuming the CNF specific surface area was 32 m^2/g. The grafted product has a high carboxylic acid content of 1.9 meq/g.

3. Derivatizing PEMA, prior to grafting, with amino-terminated polyethylene glycol (PEMA-PEG) improved the aqueous dispersibility of the grafted product. Long PEG

chains with a minimum of 20 ethylene glycol units were essential to achieve this enhanced dispersibility.

4. The solvent exchange cycle of water-to-acetone-to-water removed most of the individualized nanofibrils by forming long microribbons, and much larger aggregates (flocs). The dried microribbons appear to be assembled by 2-12 layers of CNF, with a thickness ranging from 40 to 220 nm and a width of approximately 3 μm. Helical microribbons were observed in water, with the two most appeared wavelengths of 10.8 μm and 44.6 μm.
5. The microribbon structure of PEMA-PEG grafted CNF is influenced by the degree of substitution (DS). When DS is below 75%, microribbons exhibit a helical structure. We proposed that the helices formed in acetone were stabilized by PEMA-PEG crosslinking. Above a DS of 75% the ribbons were flimsy giving flat, and sometimes folded structures when dried and fixed to a surface.

Supplementary Information

CNF Sheet Impregnation with PEMAc Solution. A preliminary experiment was conducted to impregnate the CNF sheets with PEMAc solution akin to the procedure for pulp sheet.

The experimental procedure was described as follow.

1.93 g CNF gel was diluted to 0.1 wt% suspensions and treated with VWR homogenizer at 13500 rpm for 2 min and probe sonciator at 50% duty cycle and 20% output for 10 mins. The suspension was then filtered through a membrane (0.45 μm, hydrophilic PVDF, diameter 35mm) under vacuum. The wet CNF sheets were dried in a room with constant humidity and temperature for 24 h giving a final density of 60 g/m^2.

The dried CNF sheets were soaked in PEMA solution (12.5 mM and 100 mM) for period from 1 min to 24 h. The wet pick-up ratios were plotted as a function of soaking time. The sheets after soaking for 24 h were cured in a speed dryer at 120 ^{o}C for period from 1 min to 10 min. Homogenization (9500 rpm for 1 min) and probe sonication (50% duty cycle and 20% output for 10 mins) were selected for the disintegration of grafted CNF sheets.

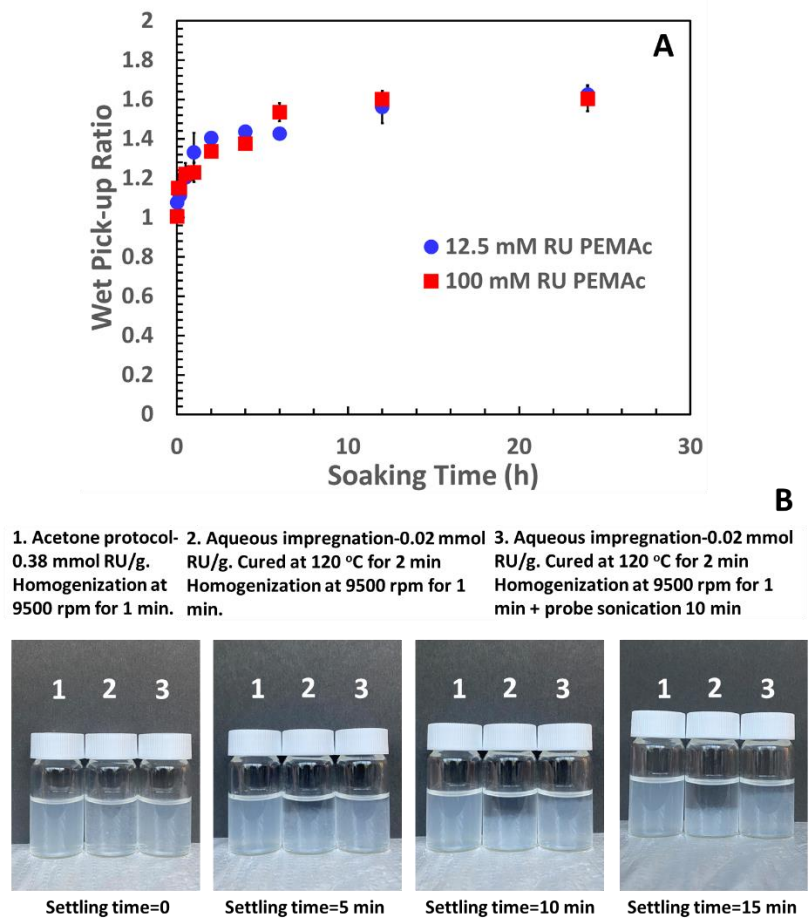

Figure S16 A: Wet pick-up ratio of the CNF sheets after soaking in PEMA solutions (12.5 mM RU and 100 mM RU) for various time. B: Settling images of the redispersed CNF 0.5 g/L in 1 mM $NaHCO_3$ after impregnation and washing.

The reswelling behavior of CNF sheets after room temperature drying was investigated, with a focus on the impact of soaking time in PEMAc solutions at pH 4. The wet pick-up ratio, representing the mass of the solution absorbed by mass of dried CNF, was presented in **Figure S16**A, showing a maximum ratio of 1.6. However, it took at least 12 hours to reach the maximum ratio.

The appearances of redispersed CNF were shown in **Figure S16**B. In the case of the impregnation approach, CNF sheets were soaked in 12.5 mM PEMAc solutions for 24 hours with low polymer dosage (0.02 mmol RU/g) and cured for a short time. After homogenization and probe sonication, the suspensions from impregnated CNF exhibited faster settling compared to CNF modified in acetone. The short settling time observed in CNF after impregnation indicated the presence of large aggregates in the suspension. The

significant aggregation in the CNF suspensions derived from the aqueous impregnation suggests challenges in achieving good dispersibility.

Table S4 Mass fraction of fully dispersed nanofibrils not washed away after solvent exchange.

Sample	Nano-fraction (%)
CNF untreated	2.7±0.8
CNF after one cycle	9.2±3.3
PEMA 2.93 mmol RU/g	3.1±0.9
PEMA 0.38 mmol RU/g	4.4±1.1
PEG3DS86 2.63 mmol RU/g	21.3±8.6
PEG20DS24 0.79 mmol RU/g	9.8±1.6
C3DS77 1.27 mmol RU/g	8.0±3.6

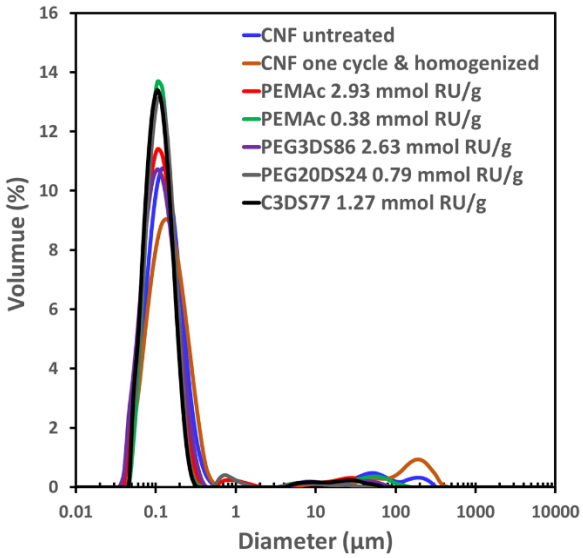

Figure S17 Diameter of nanofibrils in the supernatant after nano-fraction measurements.

FTIR of Grafted CNF. The presence of ester bonds was **not** confirmed by the FTIR spectra in **Figure S18**. To differentiate the peak corresponding to the ester bond, the carboxyl groups were converted into the sodium salt form using 0.1 N NaOH. In this

case, the peaks for the carboxylate groups shifted to 1560 cm^{-1}, additionally, the amide bonds display peak in the range between 1600-1700 cm^{-1}. Therefore, we would expect to observe an ester peak at 1717 cm^{-1}.

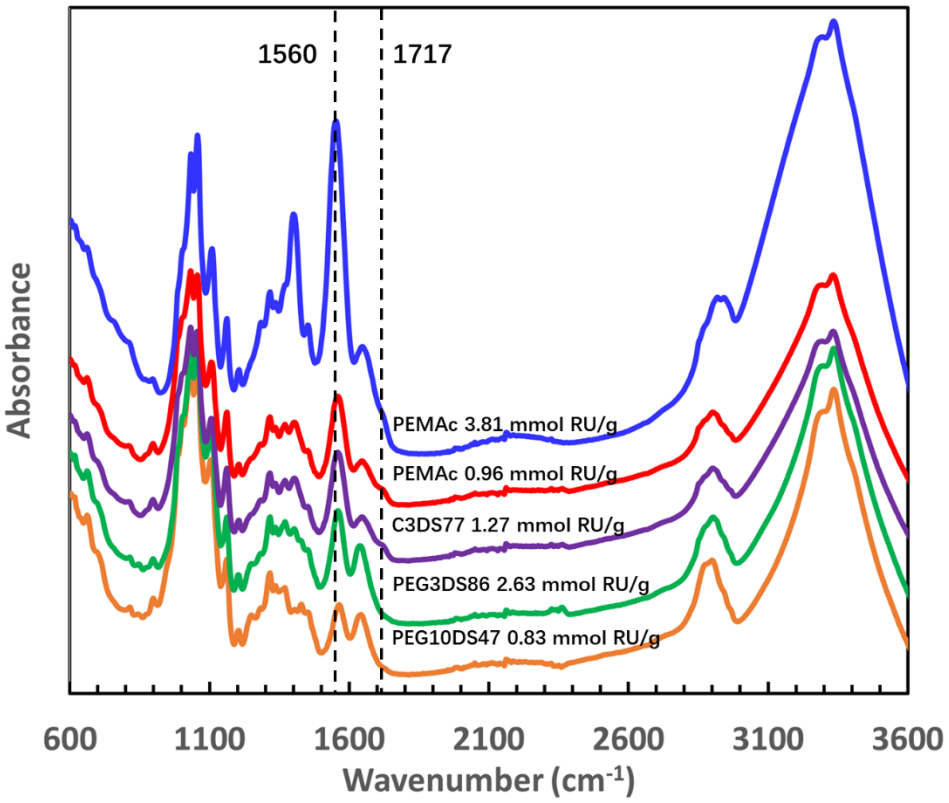

Figure S18 FTIR spectra of grafted CNF

XRD Analysis of Grafted CNF. The X-ray diffraction was conducted to investigate any structural changes in cellulose. A control sample of pristine CNF without any treatment was compared to CNF samples subjected to one solvent exchange cycle and treated with three typical polymer solutions. **Figure S19**A displays the 2θ spectra of all the CNF samples, showing identical patterns. Four peaks at 17.3º, 19.4º, 26.2º, and 40.5° were utilized to identify the crystal planes of (1-10), (110), (200), and (004) within the cellulose-I crystal structure.[33] An additional peak at 24.1° was utilized to characterize disordered regions.[34] The areas under these peaks were determined to quantify the portions corresponding to the crystalline region and disordered region. The degree of crystallinities given in

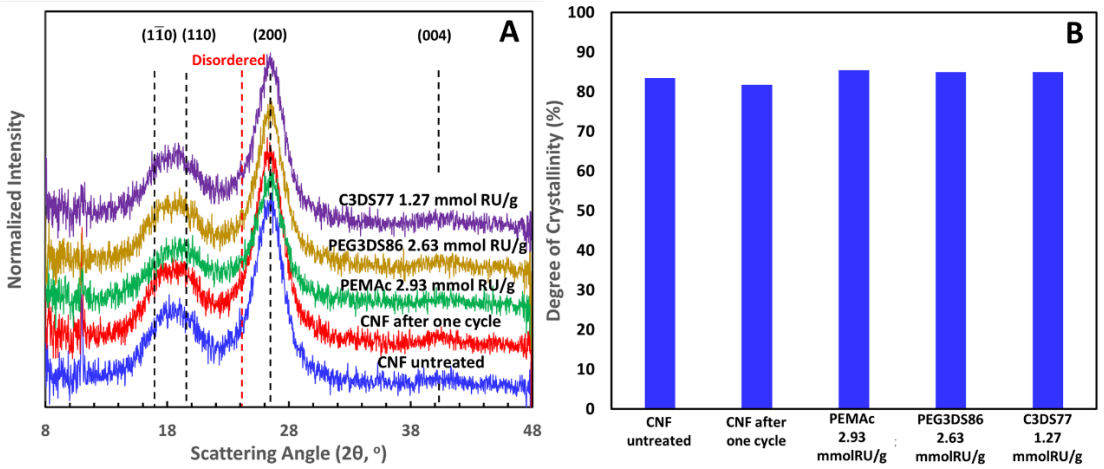

Figure S19 A: XRD 2θ spectra of CNF before and after modifications. B: Degree of crystallinity of CNF before and after modifications determined from XRD 2θ spectra using the peak deconvolution method.

Figure S19B Show similar values for all the samples. It is indicated that both solvent change and polymer grafting do not significantly impact the crystalline structure of the cellulose. Unlike the small molecule grafting, the polymer likely resides on the exterior of the fibril, with limited penetration into the interior of the cellulose structure.

^{1}H-NMR of PEMA derivatives

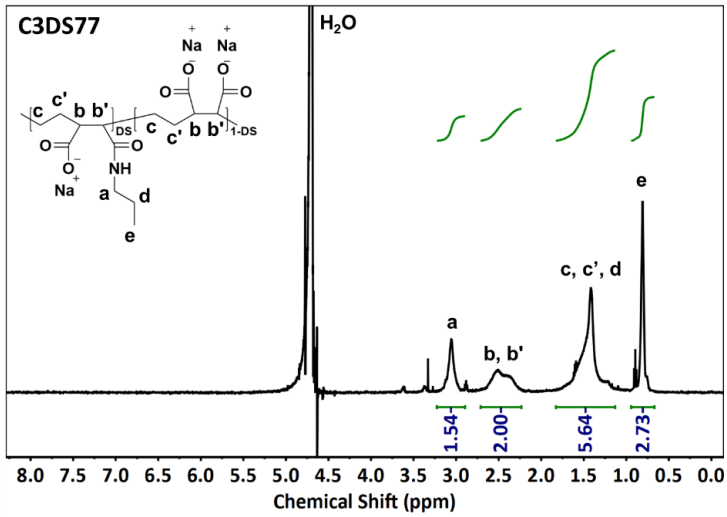

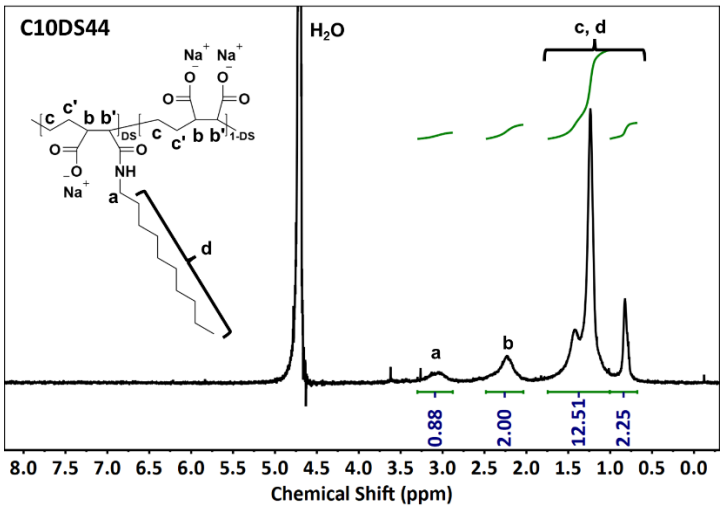

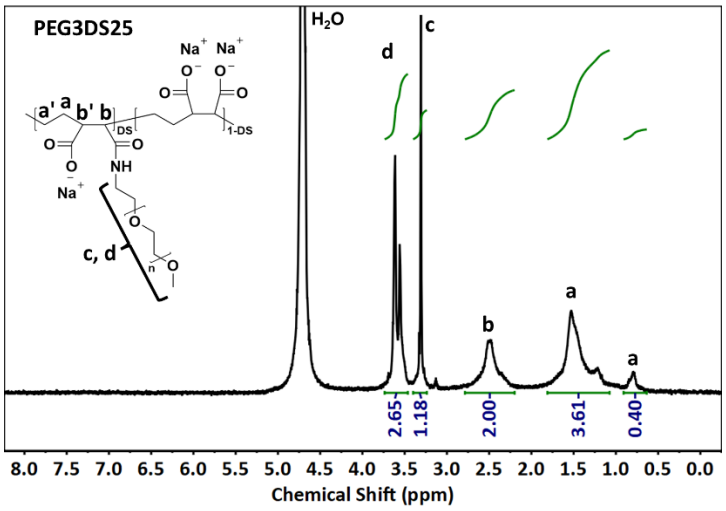
PEG3DS25
H2O
d
c
b
a
a
2.65
1.18
2.00
3.61
0.40
8.0 7.5 7.0 6.5 6.0 5.5 5.0 4.5 4.0 3.5 3.0 2.5 2.0 1.5 1.0 0.5 0.0
Chemical Shift (ppm)

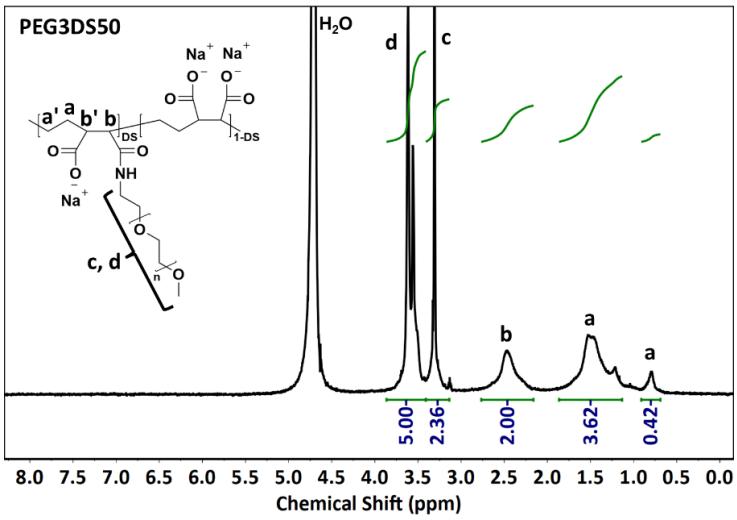
PEG3DS50
H2O
d
c
b
a
a
5.00
2.36
2.00
3.62
0.42
8.0 7.5 7.0 6.5 6.0 5.5 5.0 4.5 4.0 3.5 3.0 2.5 2.0 1.5 1.0 0.5 0.0
Chemical Shift (ppm)

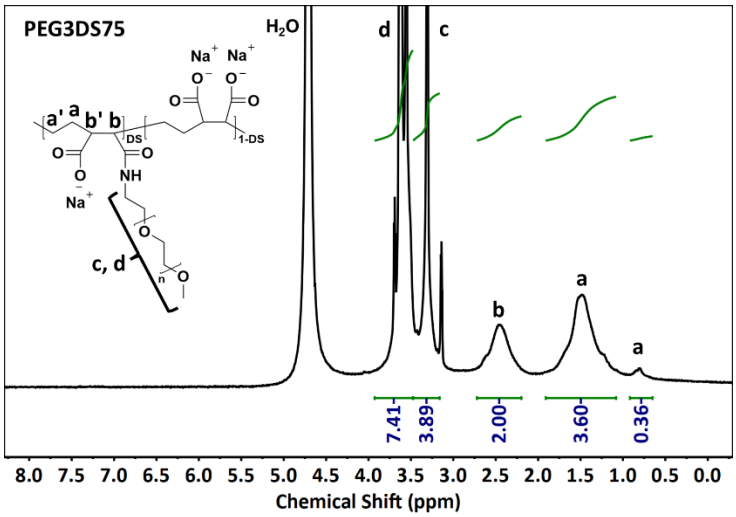
PEG3DS75
H2O
d
c
b
a
a
7.41
3.89
2.00
3.60
0.36
8.0 7.5 7.0 6.5 6.0 5.5 5.0 4.5 4.0 3.5 3.0 2.5 2.0 1.5 1.0 0.5 0.0
Chemical Shift (ppm)

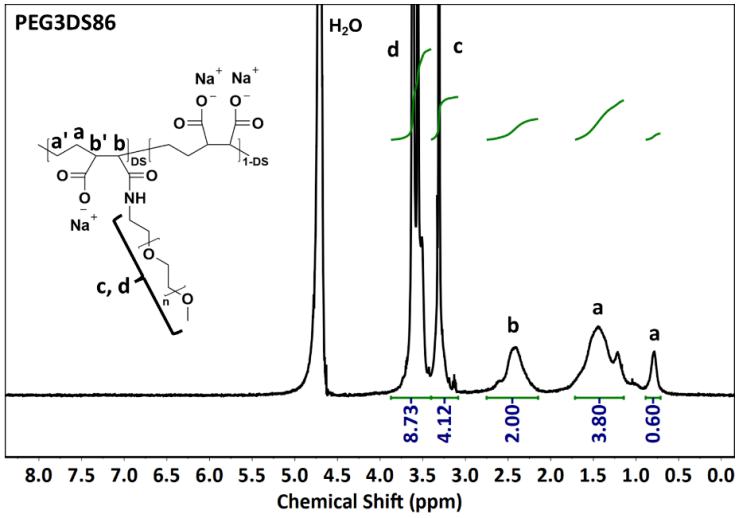
PEG3DS86
H2O
d
c
b
a
a
8.73
4.12
2.00
3.80
0.60
8.0 7.5 7.0 6.5 6.0 5.5 5.0 4.5 4.0 3.5 3.0 2.5 2.0 1.5 1.0 0.5 0.0
Chemical Shift (ppm)

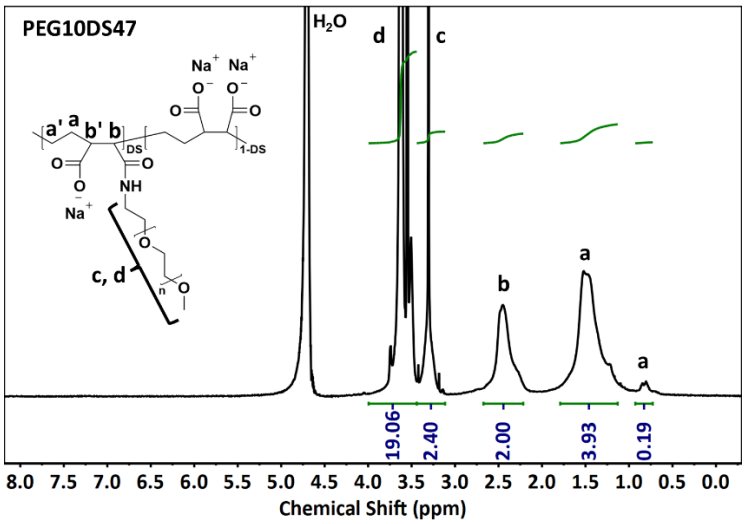
PEG10DS47
H2O
d
c
b
a
a
19.06
2.40
2.00
3.93
0.19
8.0 7.5 7.0 6.5 6.0 5.5 5.0 4.5 4.0 3.5 3.0 2.5 2.0 1.5 1.0 0.5 0.0
Chemical Shift (ppm)

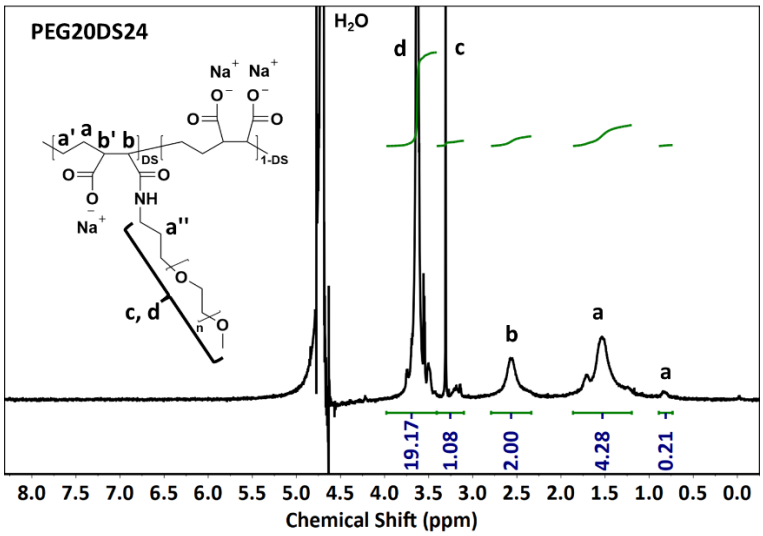
PEG20DS24
H2O
d
c
b
a
a
19.17
1.08
2.00
4.28
0.21
8.0 7.5 7.0 6.5 6.0 5.5 5.0 4.5 4.0 3.5 3.0 2.5 2.0 1.5 1.0 0.5 0.0
Chemical Shift (ppm)

Figure S20 ^{1}H-NMR spectra of PEMAc derivatives

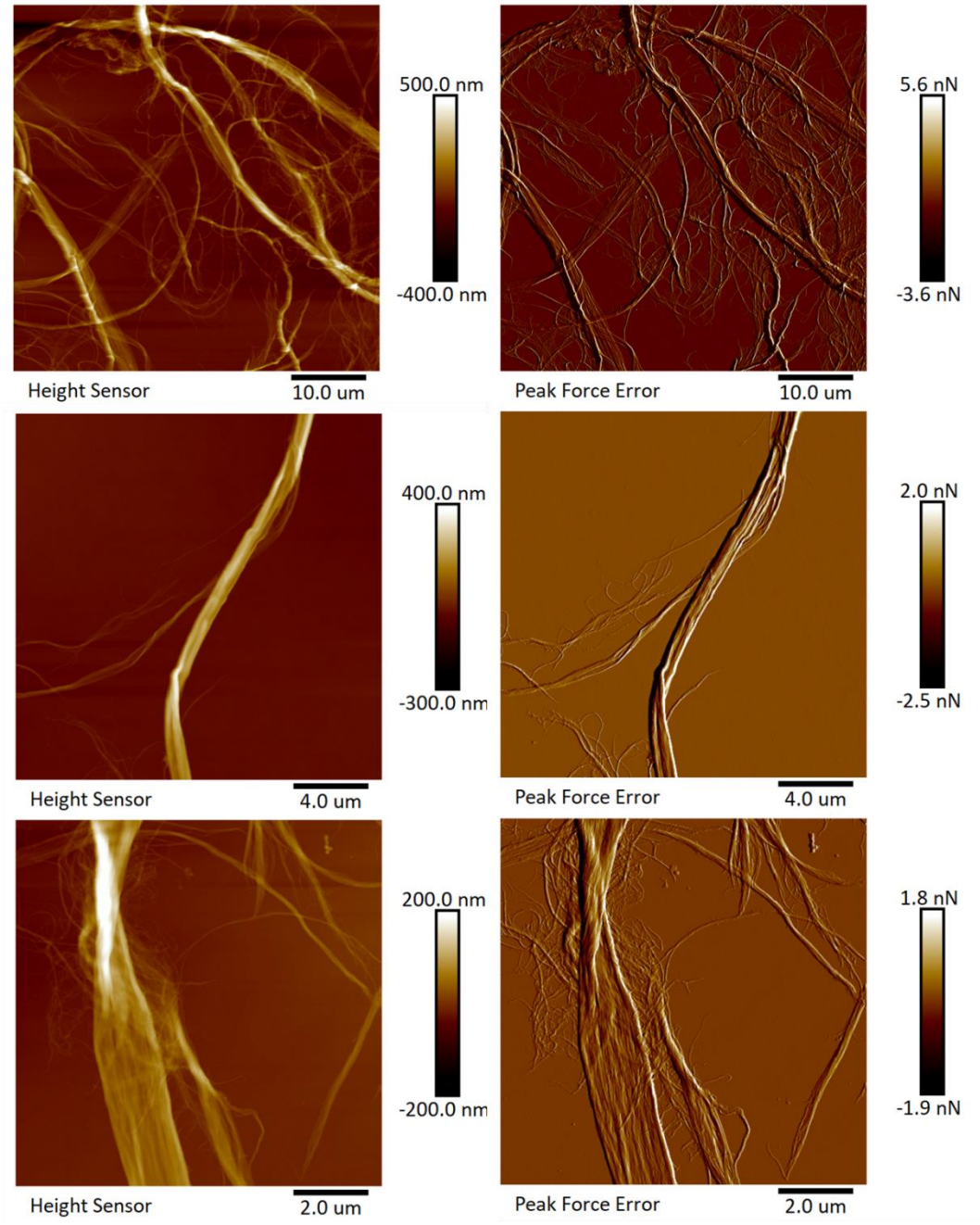

Figure S21 3 random AFM images were taken from CNF aggregates after one solvent exchange cycle (water-acetone-water). The CNF were stirred in acetone for 24 h before rehydration.

Probe sonication has been demonstrated as an efficient method to achieve a colloidal stable CNF dispersion in water. In this work, it was observed that probe sonication also plays a role in suppressing microribbon entanglement in acetone. This is evidenced by samples prepared with different protocols, as illustrated in **Figure S22**. Comparing the samples prepared with and without probe sonication after dispersing CNF in acetone, it is evident that the latter display distribution as dash curves, shifting to a larger particle size area. There are more flocs present in the suspension when probe sonication is skipped in acetone. Therefore, to supress the formation of floc, probe sonication was performed both before and after exchanging fibres in acetone, ensuring a relatively good dispersion of CNF.

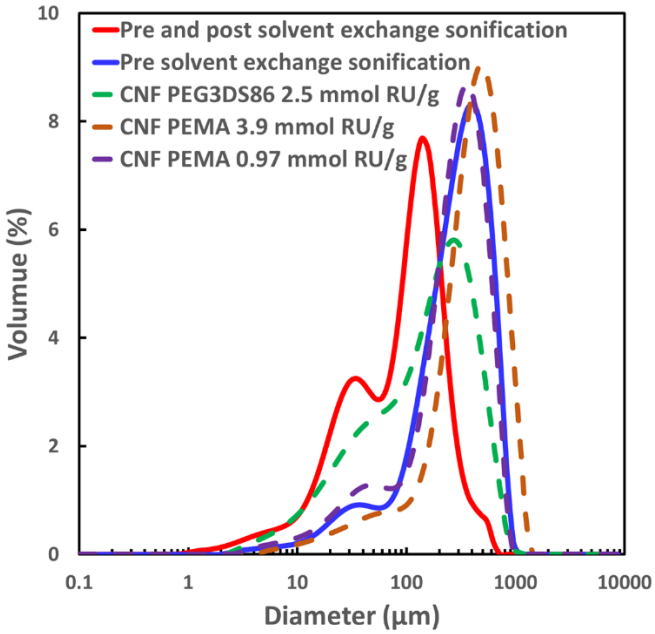

Figure S22 Diameter of the grafted CNF samples prepared without post solvent exchange sonification. Solid lines represent unmodified CNF. Dashed lines represent modified CNF.

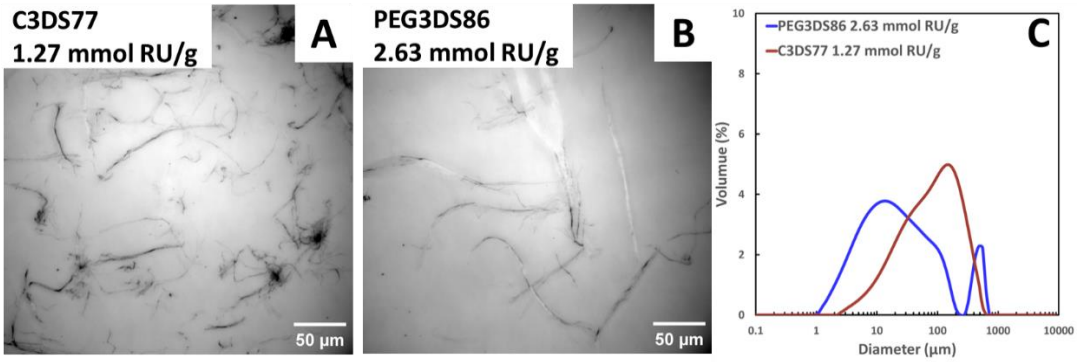

Figure S23 Widefield microscopy images comparing (A) CNF grafted with C3DS77 (R21) and (B) CNF grafted PEG3DS86 (R11). C: Diameter distributions of CNF grafted with PEG3DS86 and C3DS77.

The CNF grafted with C3DS77 (R21) contains more flocs compared to sample R11, as evidenced by the higher intensity of the peak for large particles in **Figure S23**C. The presence of flocs is readily observable in the dried samples, as depicted in **Figure S23**A. It is plausible that the hydrophobic alkyl side chains contribute to the crosslinking of microribbons.

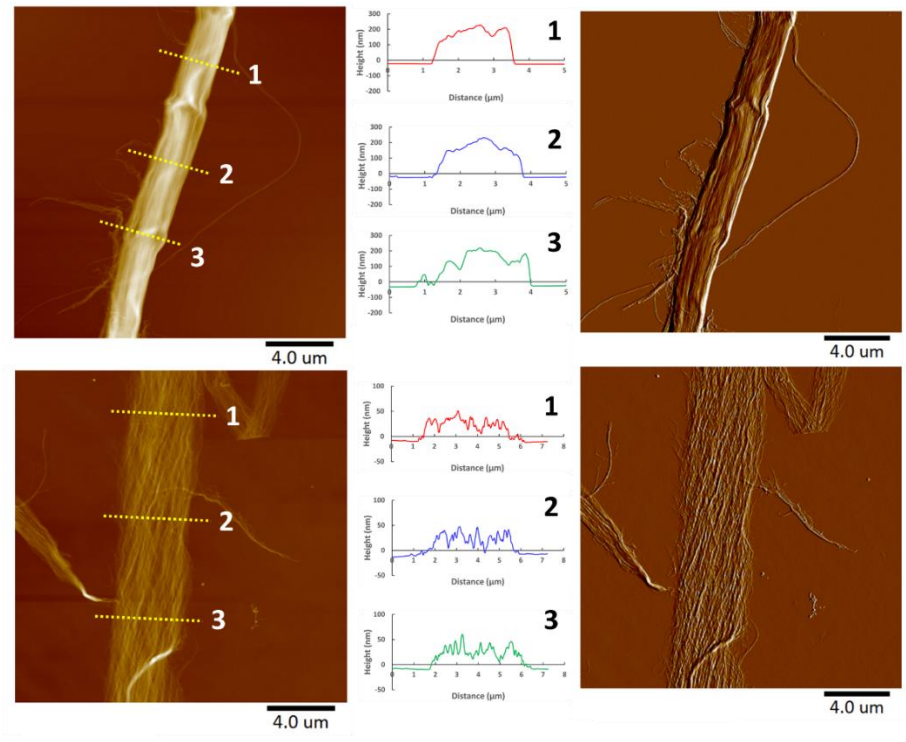

Figure S24 AFM images showing the thickest and thinnest microribbons obtained from 20 randomly selected microribbons with a PEG3DS86 content of 2.63 mmol RU/g.

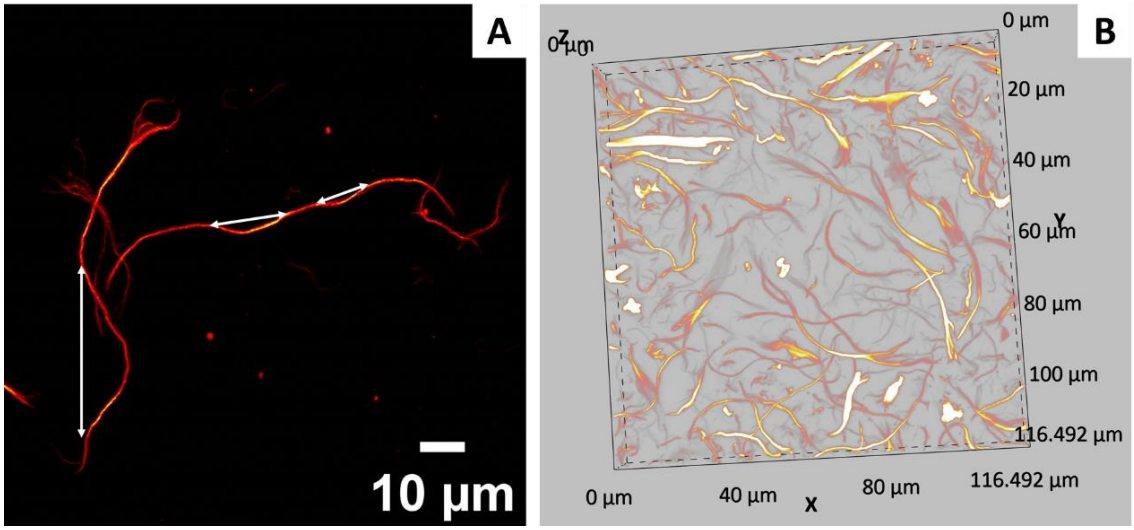

Figure S25 A: Example showing the wavelength measurement of helical microribbons on the image after Z-projection. B: 3D image showing PEMAc grafted CNF (R3 in **Table 5**) suspension (0.05%, v/v)

References

(1) Abdul Khalil, H. P.; Davoudpour, Y.; Islam, M. N.; Mustapha, A.; Sudesh, K.; Dungani, R.; Jawaid, M., Production and modification of nanofibrillated cellulose using various mechanical processes: a review. *Carbohydr Polym* **2014,** *99*, 649-65.

(2) Xu, X.; Liu, F.; Jiang, L.; Zhu, J. Y.; Haagenson, D.; Wiesenborn, D. P., Cellulose nanocrystals vs. cellulose nanofibrils: a comparative study on their microstructures and effects as polymer reinforcing agents. *ACS Appl Mater Interfaces* **2013,** *5* (8), 2999-3009.

(3) Rol, F.; Belgacem, M. N.; Gandini, A.; Bras, J., Recent advances in surface-modified cellulose nanofibrils. *Progress in Polymer Science* **2019,** *88*, 241-264.

(4) Gardner, D. J.; Oporto, G. S.; Mills, R.; Samir, M. A. S. A., Adhesion and Surface Issues in Cellulose and Nanocellulose. *Journal of Adhesion Science and Technology* **2008,** *22* (5-6), 545-567.

(5) Sinquefield, S.; Ciesielski, P. N.; Li, K.; Gardner, D. J.; Ozcan, S., Nanocellulose Dewatering and Drying: Current State and Future Perspectives. *ACS Sustainable Chemistry & Engineering* **2020,** *8* (26), 9601-9615.

(6) (a) Yamasaki, S.; Sakuma, W.; Yasui, H.; Daicho, K.; Saito, T.; Fujisawa, S.; Isogai, A.; Kanamori, K., Nanocellulose Xerogels With High Porosities and Large Specific Surface Areas. *Front Chem* **2019,** *7*, 316; (b) Yano, H.; Omura, H.; Honma, Y.; Okumura, H.; Sano, H.; Nakatsubo, F., Designing cellulose nanofibre surface for high density polyethylene reinforcement. *Cellulose* **2018,** *25* (6), 3351-3362; (c) Sato, A.; Kabusaki, D.; Okumura, H.; Nakatani, T.; Nakatsubo, F.; Yano, H., Surface modification of cellulose nanofibres with alkenyl succinic anhydride for high-density polyethylene reinforcement. *Composites Part A: Applied Science and Manufacturing* **2016,** *83*, 72-79; (d) Sun, Y.; Chu, Y.; Wu, W.; Xiao, H., Nanocellulose-based lightweight porous materials: A review. *Carbohydr Polym* **2021,** *255*, 117489.

(7) Niinivaara, E.; Cranston, E. D., Bottom-up assembly of nanocellulose structures. *Carbohydr Polym* **2020,** *247*, 116664.

(8) Kontturi, E.; Laaksonen, P.; Linder, M. B.; Nonappa; Groschel, A. H.; Rojas, O. J.; Ikkala, O., Advanced Materials through Assembly of Nanocelluloses. *Adv Mater* **2018,** *30* (24), e1703779.

(9) (a) Jiang, F.; Hsieh, Y. L., Chemically and mechanically isolated nanocellulose and their self-assembled structures. *Carbohydr Polym* **2013,** *95* (1), 32-40; (b) Pääkkö, M.; Vapaavuori, J.; Silvennoinen, R.; Kosonen, H.; Ankerfors, M.; Lindström, T.; Berglund, L. A.; Ikkala, O., Long and entangled native cellulose I nanofibres allow flexible aerogels and hierarchically porous templates for functionalities. *Soft Matter* **2008,** *4* (12); (c) Chen, W.; Yu, H.; Li, Q.; Liu, Y.; Li, J., Ultralight and highly flexible aerogels with long cellulose I nanofibres. *Soft Matter* **2011,** *7* (21).

(10) Jiang, F.; Han, S.; Hsieh, Y.-L., Controlled defibrillation of rice straw cellulose and self-assembly of cellulose nanofibrils into highly crystalline fibrous materials. *RSC Advances* **2013,** *3* (30).

(11) (a) Hakansson, K. M.; Fall, A. B.; Lundell, F.; Yu, S.; Krywka, C.; Roth, S. V.; Santoro, G.; Kvick, M.; Prahl Wittberg, L.; Wagberg, L.; Soderberg, L. D., Hydrodynamic alignment and assembly of nanofibrils resulting in strong cellulose filaments. *Nat Commun* **2014,** *5*, 4018; (b) Walther, A.; Timonen, J. V.; Diez, I.; Laukkanen, A.; Ikkala, O., Multifunctional high-performance biofibres based on wet-extrusion of renewable native cellulose nanofibrils. *Adv Mater* **2011,** *23* (26), 2924-8; (c) Li, K.; Clarkson, C. M.; Wang, L.; Liu, Y.; Lamm, M.; Pang, Z.; Zhou, Y.; Qian, J.; Tajvidi, M.; Gardner, D. J.; Tekinalp, H.; Hu, L.; Li, T.; Ragauskas, A. J.; Youngblood, J. P.; Ozcan, S., Alignment of Cellulose Nanofibres: Harnessing Nanoscale Properties to Macroscale Benefits. *ACS Nano* **2021,** *15* (3), 3646-3673.

(12) (a) Zhu, Y.; Guo, Y.; Cao, K.; Zeng, S.; Jiang, G.; Liu, Y.; Cheng, W.; Bai, W.; Weng, X.; Chen, W.; Zhao, D.; Yu, H.; Yu, G., A general strategy for synthesizing biomacromolecular ionogel membranes via solvent-induced self-assembly. *Nature Synthesis* **2023**; (b) Cheung, C. C. Y.; Giese, M.; Kelly, J. A.; Hamad, W. Y.; MacLachlan, M. J., Iridescent Chiral Nematic Cellulose Nanocrystal/Polymer Composites Assembled in Organic Solvents. *ACS Macro Lett* **2013,** *2* (11), 1016-1020; (c) Yuan, Z.; Zhang, J.; Jiang, A.; Lv, W.; Wang, Y.; Geng, H.; Wang, J.; Qin, M., Fabrication of cellulose self-assemblies and high-strength ordered cellulose films. *Carbohydr Polym* **2015,** *117*, 414-421.

(13) (a) Sehaqui, H.; Zhou, Q.; Berglund, L. A., High-porosity aerogels of high specific surface area prepared from nanofibrillated cellulose (NFC). *Composites Science and Technology* **2011,** *71* (13), 1593-1599; (b) Jiang, F.; Hsieh, Y. L., Cellulose Nanofibril Aerogels: Synergistic Improvement of Hydrophobicity, Strength, and Thermal Stability via Cross-Linking with Diisocyanate. *ACS Appl Mater Interfaces* **2017,** *9* (3), 2825-2834; (c) Garemark, J.; Yang, X.; Sheng, X.; Cheung, O.; Sun, L.; Berglund, L. A.; Li, Y., Top-Down Approach Making Anisotropic Cellulose Aerogels as Universal Substrates for Multifunctionalization. *ACS Nano* **2020,** *14* (6), 7111-7120.

(14) Hausmann, M. K.; Siqueira, G.; Libanori, R.; Kokkinis, D.; Neels, A.; Zimmermann, T.; Studart, A. R., Complex‐Shaped Cellulose Composites Made by Wet Densification of 3D Printed Scaffolds. *Advanced Functional Materials* **2019,** *30* (4).

(15) Fittolani, G.; Vargova, D.; Seeberger, P. H.; Ogawa, Y.; Delbianco, M., Bottom-Up Approach to Understand Chirality Transfer across Scales in Cellulose Assemblies. *J Am Chem Soc* **2022,** *144* (27), 12469-12475.

(16) (a) Nair, S. S.; Dartiailh, C.; Levin, D. B.; Yan, N., Highly Toughened and Transparent Biobased Epoxy Composites Reinforced with Cellulose Nanofibrils. *Polymers (Basel)* **2019,** *11* (4); (b) Nair, S. S.; Kuo, P.-Y.; Chen, H.; Yan, N., Investigating the effect of lignin on the mechanical, thermal, and barrier properties of cellulose nanofibril reinforced epoxy composite. *Industrial Crops and Products* **2017,** *100*, 208-217; (c) Lee, K.; Kwon, G.; Jeon, Y.; Jeon, S.; Hong, C.; Choung, J. W.; You, J., Toward millimeter thick cellulose nanofibre/epoxy laminates with good transparency and high flexural strength. *Carbohydr Polym* **2022,** *291*, 119514; (d) Thirunavukarasu, D.; Shimamura, Y.; Tohgo, K.; Fujii, T., Mechanical Characterization on Solvent Treated Cellulose Nanofibre Preforms Using Solution Dipping-Hot Press Technique. *Nanomaterials (Basel)* **2020,** *10* (5).

(17) (a) Jonoobi, M.; Harun, J.; Mathew, A. P.; Oksman, K., Mechanical properties of cellulose nanofibre (CNF) reinforced polylactic acid (PLA) prepared by twin screw extrusion. *Composites Science and Technology* **2010,** *70* (12), 1742-1747; (b) Suryanegara, L.; Nakagaito, A. N.; Yano, H., The effect of crystallization of PLA on the thermal and mechanical properties of microfibrillated cellulose-reinforced PLA composites. *Composites Science and Technology* **2009,** *69* (7-8), 1187-1192; (c) Gazzotti, S.; Rampazzo, R.; Hakkarainen, M.; Bussini, D.; Ortenzi, M. A.; Farina, H.; Lesma, G.; Silvani, A., Cellulose nanofibrils as reinforcing agents for PLA-based nanocomposites: An in situ approach. *Composites Science and Technology* **2019,** *171*, 94-102; (d) Heidarian, P.; Behzad, T.; Karimi, K.; Sain, M., Properties investigation of recycled polylactic acid reinforced by cellulose nanofibrils isolated from bagasse. *Polymer Composites* **2018,** *39* (10), 3740-3749.

(18) (a) Kiziltas, E. E.; Kiziltas, A.; Bollin, S. C.; Gardner, D. J., Preparation and characterization of transparent PMMA-cellulose-based nanocomposites. *Carbohydr Polym* **2015,** *127*, 381-9; (b) Dong, H.; Sliozberg, Y. R.; Snyder, J. F.; Steele, J.; Chantawansri, T. L.; Orlicki, J. A.; Walck, S. D.; Reiner, R. S.; Rudie, A. W., Highly Transparent and Toughened Poly(methyl methacrylate) Nanocomposite Films Containing Networks of Cellulose Nanofibrils. *ACS Appl Mater Interfaces* **2015,** *7* (45), 25464-72.

(19) (a) Chen, H.; Nair, S. S.; Chauhan, P.; Yan, N., Lignin containing cellulose nanofibril application in pMDI wood adhesives for drastically improved gap-filling properties with robust bondline interfaces. *Chemical Engineering Journal*

2019, *360*, 393-401; (b) Niu, X.; Liu, Y.; Fang, G.; Huang, C.; Rojas, O. J.; Pan, H., Highly Transparent, Strong, and Flexible Films with Modified Cellulose Nanofibre Bearing UV Shielding Property. *Biomacromolecules* **2018,** *19* (12), 4565-4575; (c) Wu, T.; Zeng, Z.; Siqueira, G.; De France, K.; Sivaraman, D.; Schreiner, C.; Figi, R.; Zhang, Q.; Nystrom, G., Dual-porous cellulose nanofibril aerogels via modular drying and cross-linking. *Nanoscale* **2020,** *12* (13), 7383-7394.

(20) (a) Krishnamachari, P.; Hashaikeh, R.; Tiner, M., Modified cellulose morphologies and its composites; SEM and TEM analysis. *Micron* **2011,** *42* (8), 751-61; (b) Chen, W.; Li, Q.; Cao, J.; Liu, Y.; Li, J.; Zhang, J.; Luo, S.; Yu, H., Revealing the structures of cellulose nanofibre bundles obtained by mechanical nanofibrillation via TEM observation. *Carbohydr Polym* **2015,** *117*, 950-956.

(21) (a) Zhang, H.; Tsenter, E.; Bicho, P.; Doherty, E. A.; Riehle, R.; Moran-Mirabal, J.; Pelton, R. H., Carboxylated bleached kraft pulp from maleic anhydride copolymers. *Nordic Pulp & Paper Research Journal* **2021,** *36* (4), 608-617; (b) Zhang, H.; Bicho, P.; Doherty, E. A. S.; Riehle, R. J.; Moran-Mirabal, J.; Pelton, R. H., High-yield grafting of carboxylated polymers to wood pulp fibres. *Cellulose* **2021,** *28* (11), 7311-7326.

(22) Scriven, E. F., 4-Dialkylaminopyridines: super acylation and alkylation catalysts. *Chemical Society Reviews* **1983,** *12* (2), 129-161.

(23) (a) Peng, Y.; Gallegos, S. A.; Gardner, D. J.; Han, Y.; Cai, Z., Maleic anhydride polypropylene modified cellulose nanofibril polypropylene nanocomposites with enhanced impact strength. *Polymer composites* **2016,** *37* (3), 782-793; (b) Liu, L.; Kong, F., Influence of nanocellulose on in vitro digestion of whey protein isolate. *Carbohydr Polym* **2019,** *210*, 399-411.

(24) Fall, A. B.; Burman, A.; Wågberg, L., Cellulosic nanofibrils from eucalyptus, acacia and pine fibres. *Nordic Pulp & Paper Research Journal* **2014,** *29* (1), 176-184.

(25) (a) Höfle, G.; Steglich, W.; Vorbrüggen, H., 4-Dialkylaminopyridines as highly active acylation catalysts.[New synthetic method (25)]. *Angewandte Chemie International Edition in English* **1978,** *17* (8), 569-583; (b) Lee, M.-K.; Biermann, C. J., Grafting of maleic anhydride copolymers onto cellulose acetate and methyl cellulose. *Journal of wood chemistry and technology* **1992,** *12* (2), 231-240.

(26) Peng, Y.; Gardner, D. J.; Han, Y., Drying cellulose nanofibrils: in search of a suitable method. *Cellulose* **2011,** *19* (1), 91-102.

(27) Anon. Cellulose nanofibres (CNF) product specification sheet. University of Maine Process Development Center https://umaine.edu/pdc/wp-content/uploads/sites/398/2016/03/Specs-CNF.pdf (accessed 2023 July 20th).

(28) (a) Kim, J.; Bang, J.; Kim, Y.; Kim, J. C.; Hwang, S. W.; Yeo, H.; Choi, I. G.; Kwak, H. W., Eco-friendly alkaline lignin/cellulose nanofibre drying system for efficient redispersion behavior. *Carbohydr Polym* **2022,** *282*, 119122; (b) A, H. T.; Tajvidi, M.; Bousfield, D., Paper-Based Oil Barrier Packaging using Lignin-Containing Cellulose Nanofibrils. *Molecules* **2020,** *25* (6); (c) Amini, E.; Hafez, I.; Tajvidi, M.; Bousfield, D. W., Cellulose and lignocellulose nanofibril suspensions and films: A comparison. *Carbohydr Polym* **2020,** *250*, 117011.

(29) Ballner, D.; Herzele, S.; Keckes, J.; Edler, M.; Griesser, T.; Saake, B.; Liebner, F.; Potthast, A.; Paulik, C.; Gindl-Altmutter, W., Lignocellulose Nanofibre-Reinforced Polystyrene Produced from Composite Microspheres Obtained in Suspension Polymerization Shows Superior Mechanical Performance. *ACS Appl Mater Interfaces* **2016,** *8* (21), 13520-5.

(30) Iwamoto, S.; Isogai, A.; Iwata, T., Structure and mechanical properties of wet-spun fibres made from natural cellulose nanofibres. *Biomacromolecules* **2011,** *12* (3), 831-6.

(31) Yao, K.; Meng, Q.; Bulone, V.; Zhou, Q., Flexible and Responsive Chiral Nematic Cellulose Nanocrystal/Poly(ethylene glycol) Composite Films with Uniform and Tunable Structural Color. *Adv Mater* **2017,** *29* (28).

(32) (a) Qu, P.; Gao, Y.; Wu, G.-f.; Zhang, L.-p., Nanocomposites of poly (lactic acid) reinforced with cellulose nanofibrils. *BioResources* **2010,** *5* (3); (b) Tang, H.; Butchosa, N.; Zhou, Q., A transparent, hazy, and strong macroscopic ribbon of oriented cellulose nanofibrils bearing poly(ethylene glycol). *Adv Mater* **2015,** *27* (12), 2070-6.

(33) (a) Terinte, N.; Ibbett, R.; Schuster, K. C., Overview on native cellulose and microcrystalline cellulose I structure studied by X-ray diffraction (WAXD): Comparison between measurement techniques. *Lenzinger Berichte* **2011,** *89* (1), 118-131; (b) Hu, Z.; Berry, R. M.; Pelton, R.; Cranston, E. D., One-Pot Water-Based Hydrophobic Surface Modification of Cellulose Nanocrystals Using Plant Polyphenols. *ACS Sustainable Chemistry & Engineering* **2017,** *5* (6), 5018-5026.

(34) Chen, F.; Xiang, W.; Sawada, D.; Bai, L.; Hummel, M.; Sixta, H.; Budtova, T., Exploring Large Ductility in Cellulose Nanopaper Combining High Toughness and Strength. *ACS Nano* **2020,** *14* (9), 11150-11159.

Chapter 5

My Contributions

The thesis investigates the potential of using poly (ethylene-alt-maleic anhydride) (PEMA) for grafting alkyl-amine and PEG-amine onto cellulosic fibres. The major contributions of the work are as follows:

1. The research achieves the grafting of PEMAc derivatives modified with alkane and PEG, encompassing a range of degrees of substitution (DS). These derivatives are efficiently grafted onto bleached softwood kraft pulp through an aqueous impregnation process and onto mechanically produced cellulose nanofibrils (CNF) using direct esterification in acetone. High grafting yields can be achieved with as little as 12-14% succinic or anhydride moieties remaining along the PEMA backbone.
2. The research delves into the conformation of hydrophobically modified PEMA in aqueous solutions. It systematically explores the impact of alkyl chain length and the degree of substitutions on conformational transitions in response to changes in solution pH.
3. The examined power-law model ($WTI_{max} \sim \beta \Gamma_{ru}^{0.54–0.62}$), correlating the maximum wet tensile indices with anhydride moieties conversion and polymer dosages, is validated for both alkane- and PEG-modified PEMAc derivatives. The model predicts optimum pulp curing conditions for grafting PEMAc derivatives onto pulp to achieve high yields and maintain good repulpability.
4. PEMAc grafted helical microribbons were produced from the grafting reaction in acetone. The approach inspires a way by taking advantage of the reactivity and hydrolysis of cyclic anhydride moieties to transform the nanocellulose structures from organic solvent environments to aqueous suspensions.